

AD-A286 165



NAVAL POSTGRADUATE SCHOOL

Monterey, California

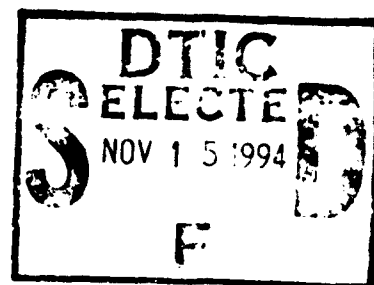


94-35104



2168

THESIS



DTIC SELECTE 3

EFFECT OF JUNCTURE FILLETS ON DOUBLE-DELTA WINGS
UNDERGOING SIDESLIP AT HIGH ANGLES OF ATTACK

BY

CHANG, WEN-HUAN

September, 1994

Thesis Advisor :

S. K. Hebbar

CO-Advisor :

M. F. Platzer

Approved for public release : distribution is unlimited.

94

7

REPORT DOCUMENT PAGE

Form Approved
OMB No. 0704-0188

Public reporting burden for this collection of information is estimated to average 1 hour per response, including the time for reviewing instructions, searching existing data sources, gathering and maintaining the data needed, and completing and reviewing the collection of information. Send comments regarding this burden estimate or any other aspect of this collection of information, including suggestions for reducing this burden, to Washington Headquarters Services, Directorate for Information Operations and Reports, 1215 Jefferson Davis Highway, Suite 1204, Arlington, VA 22202-4302, and to the Office of Management and Budget, Paperwork Reduction Project (0704-0188), Washington, DC 20503

1. AGENCY USE ONLY (Leave Blank)		2. REPORT DATE SEP. 1994	3. REPORT TYPE AND DATES COVERED Master's Thesis	
4. TITLE AND SUBTITLE EFFECT OF JUNCTURE FILLETS ON DOUBLE DELTA WINGS UNDERGOING SIDESLIP AT HIGH ANGLES OF ATTACK			5. FUNDING NUMBERS	
6. AUTHORS CHANG, WEN-HUAN				
7. PERFORMING ORGANIZATION NAME(S) AND ADDRESS(ES) Naval Postgraduate School Monterey, CA 93943-5000			8. PERFORMING ORGANIZATION REPORT NUMBER	
9. SPONSORING / MONITORING AGENCY NAME(S) AND ADDRESS(ES)			10. SPONSORING / MONITORING AGENCY REPORT NUMBER	
11. SUPPLEMENTARY NOTES The views expressed in this thesis are those of the author and do not reflect the official policy or position of the Department of Defense or the U. S. Government.				
12a. DISTRIBUTION / AVAILABILITY STATEMENT Approved for public release; distribution is unlimited.			12b. DISTRIBUTION CODE	
13. ABSTRACT (Maximum 200 words) A flow visualization study of the vortical flow over a baseline double-delta wing model and a diamond-fillet double-delta wing model both with sharp leading edges was conducted in the Naval Postgraduate School water tunnel using the dye-injection technique. The main focus of this study was to observe the effect of juncture fillet on the vortex core trajectory, and vortex burst location on the wing surface at high angles of attack with sideslip angles. The data reported in this thesis is believed to be the first of its kind on the effect of juncture fillets on double-delta wings undergoing sideslip at high angles of attack. The results indicate that the strake vortex burst point moves upstream with increasing angle of attack at zero sideslip angle; but at constant angle of attack the windward side strake vortex burst location moves upstream and inboard while the leeward side vortex burst point moves downstream and outboard with increasing sideslip angle. Comparison of test results between the baseline model and the diamond-fillet model indicates a clear delay for the latter model in terms of both vortex core trajectory and breakdown location at high angles of attack with and without sideslip angle. The vortex breakdown data for the diamond-fillet model implies lift augmentation during sideslip motion, thus supporting the concept of flow control using fillets.				
14. SUBJECT TERMS Effect of fillets on vortex core trajectories and vortex breakdown, effect of sideslip, double-delta wing at high angle of attack, water tunnel flow visualization, dye-injection technique			15. NUMBER OF PAGES 217	
			16. PRICE CODE	
17. SECURITY CLASSIFICATION OF REPORT UNCLASSIFIED	18. SECURITY CLASSIFICATION OF THIS PAGE UNCLASSIFIED	19. SECURITY CLASSIFICATION OF ABSTRACT UNCLASSIFIED	20. LIMITATION OF ABSTRACT UL	

Approved for public release; distribution is unlimited.

**EFFECT OF JUNCTURE FILLETS ON DOUBLE-DELTA WINGS UNDERGOING
SIDESLIP AT HIGH ANGLES OF ATTACK**

by

Chang, Wen-Huan

Lieutenant Colonel, Chinese Air Force (Republic Of China)

B.S., Chinese Air Force Academy, 1979

Submitted in partial fulfillment of the requirements for
the degree of

MASTER OF SCIENCE IN AERONAUTICAL ENGINEERING

from the

NAVAL POSTGRADUATE SCHOOL

September 1994

Author:

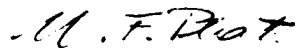


Chang , Wen-Huan

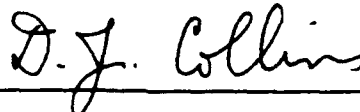
Approved by :



S. K. Hebbar, Thesis Advisor



M. F. Plazer, Co - Advisor



D. Collins, Chairman

Department of Aeronautics and Astronautics

ABSTRACT

A flow visualization study of the vortical flow over a baseline double-delta wing model and a diamond fillet double-delta wing model, both with sharp leading edges, was conducted in the Naval Postgraduate School water tunnel using the dye-injection technique. The diamond fillet increased the wing area of the baseline model by 1%. The main focus of this study was to observe the effect of juncture fillet on the vortex core trajectory and vortex burst location on the wing surface at high angles of attack with sideslip angles. The data reported in this thesis is believed to be the first of its kind on the effect of juncture fillets on double-delta wings undergoing sideslip at high angles of attack. The results indicate that the strake vortex burst point moves upstream with increasing angle of attack at zero sideslip angle; but at constant angle of attack the windward side strake vortex burst location moves upstream and inboard while the leeward side vortex burst point moves downstream and outboard with increasing sideslip angle. Comparison of test results between the baseline model and the diamond-fillet model indicates a clear delay for the latter model in terms of both vortex core trajectory and breakdown location at high angles of attack with and without sideslip angle. The vortex breakdown data for the diamond-fillet model implies lift augmentation during sideslip motion, thus supporting the concept of flow control using fillets.

Accession For		
NTIS	CRA&I	<input checked="" type="checkbox"/>
DTIC	TAB	<input type="checkbox"/>
Unannounced		<input type="checkbox"/>
Justification		
By		
Distribution/		
Availability Codes		
Dist	Avail and/or Special	
A-1		

TABLE OF CONTENTS

I. INTRODUCTION	1
A. GENERAL DESCRIPTION	1
B. AERODYNAMICS OF DOUBLE-DELTA WINGS	5
C. FILLET AERODYNAMICS	8
D. GOAL OF THE THESIS	8
II. EXPERIMENTAL FACILITIES & EQUIPMENT	10
A. THE NPS WATER TUNNEL	10
B. TEST MODELS	13
C. DYE TUBE INSTALLATION	14
D. MODEL MOUNTING	16
III. EXPERIMENTAL PROCEDURE	17
A. EXPERIMENTAL PROGRAM AND TEST CONDITIONS	
.....	17
B. TEST PROCEDURES	17
C. DATA ACQUISITION AND REDUCTION	18
D. METHOD OF PHOTOGRAPHY	19
IV. TEST RESULTS & DISCUSSION	21
A. EFFECT OF AOA ON VORTEX CORE BREAKDOWN	
AT ZERO SIDESLIP	
.....	22
1. BASELINE MODEL :	22
2. DIAMOND-FILLET MODEL	23
3. COMPARISON OF THE TWO MODELS	24

B.	EFFECT OF ANGLE OF SIDESLIP ON VORTEX CORE BREAKDOWN	25
1.	BASELINE MODEL	25
2.	DIAMOND-FILLET MODEL	26
3.	COMPARISON OF THE TWO MODELS	26
C.	EFFECT OF AOA ON THE VORTEX CORE TRAJECTORY AT ZERO SIDESLIP	27
1.	BASELINE MODEL	27
2.	DIAMOND-FILLET MODEL	28
3.	COMPARISON OF THE TWO MODELS	30
D.	EFFECT OF ANGLE OF SIDESLIP ON VORTEX CORE TRAJECTORY	30
1.	BASELINE MODEL	30
2.	DIAMOND-FILLET MODEL	31
3.	COMPARISON OF THE TWO MODELS	32
E.	OPERATIONAL ENVELOPE FOR MANEUVERING .	33
V.	CONCLUSIONS AND RECOMMENDATIONS	35
	LIST OF REFERENCES	37
	APPENDIX A: EXPERIMENTAL RESULTS (TABLES)	39
	APPENDIX B: EXPERIMENTAL RESULTS (PHOTOGRAPHS AND PLOTS)	129
	INITIAL DISTRIBUTION LIST	209

ACKNOWLEDGEMENT

This thesis was a part of a research program on double-delta wings supported by the Naval Postgraduate School. My gratitude goes to my thesis advisor, Professor S. K. Hebbar, and co-advisor Professor M. F. Platzler, for their guidance, encouragement and patience throughout the course of this research.

I would like to thank my sponsor (Republic of China Government) for the opportunity to study at U. S Naval Postgraduate School. I would also like to thank the many people at the School who provided the service and expertise necessary for this research. In particular :

Mr. Ron Ramaker, Aeronautics model Shop.

Mr. Jack King, Aeronautics Lab .

Mr. Andy Sarakon, Photo Lab .

Mr. Frank Cardoza and Mr. Harry Thomas , Video Lab.

Finally, I would like to express my deepest gratitude and appreciation to my wife, Tzung-Wei, and my sons, Ming-Hao and Ming-Han, for their encouragement in support of my efforts.

I. INTRODUCTION

A. GENERAL DESCRIPTION

Modern high performance fighters require high maneuverability, agility, excellent stall and poststall characteristics. These requirements call for new designs for aerodynamic configurations that can provide superior aerodynamic characteristics, excellent flying and handling qualities and maneuvering capabilities over a wide range of Mach numbers and angles of attack to achieve the goal of airborne tactical superiority.

In the 1930's, German engineers developed the idea of sweepback, the wing planform that could reduce drag at supersonic speeds. After World War II, the Soviet Union built the first swept wing jet fighter in 1946, called MIG-15 "Fagot" (Fig. 1). In the 1950's, further studies showed that the delta shaped wing may effectively control the air flow over the wing surface to high angle of attack beyond the usual stall angle and provide additional lift. Since then, a series of delta winged fighter aircraft such as the Soviet Mig-21 "Fishbed" (Fig 2), Swedish SAAB-210, United States F-102 "Dagger" (Fig.3), and French Mirage III fighter, had been designed and built heralding the delta wing era [Ref.1]. The most significant design advantage of the delta-wing is that the leading edge vortex flows are effective in reducing pre-stall buffet levels to give a mild loss of lift above the angle of attack for maximum lift coefficient [Ref. 2]. The major disadvantages of the delta-wing planform are its sluggish maneuverability and its low wing loading.

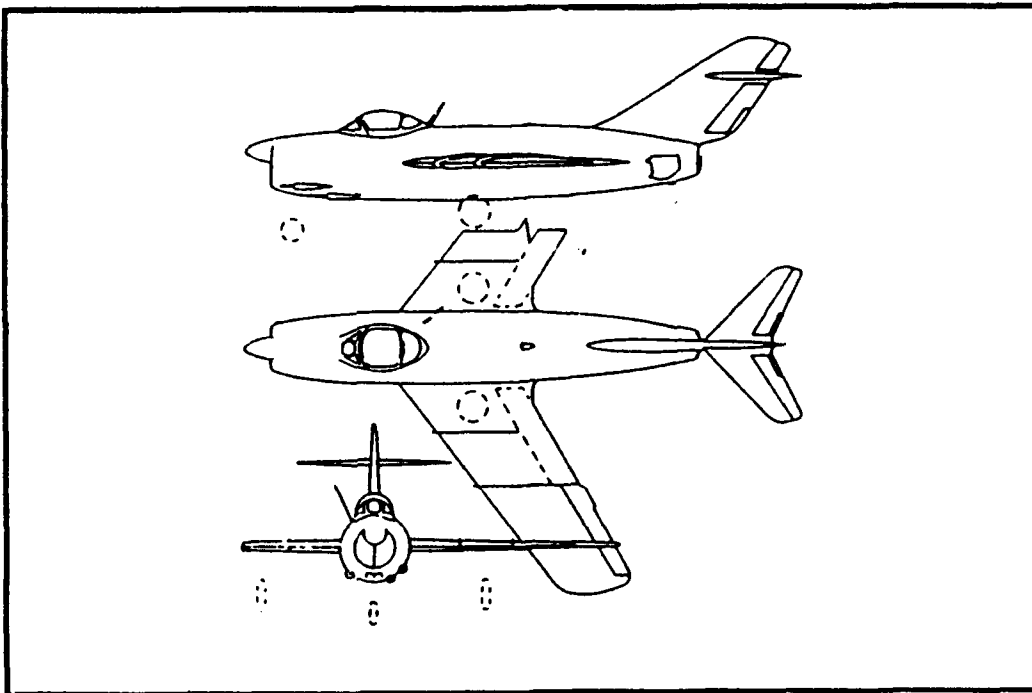


Figure 1 : Soviet MIG - 15 "Fagot" configuration.

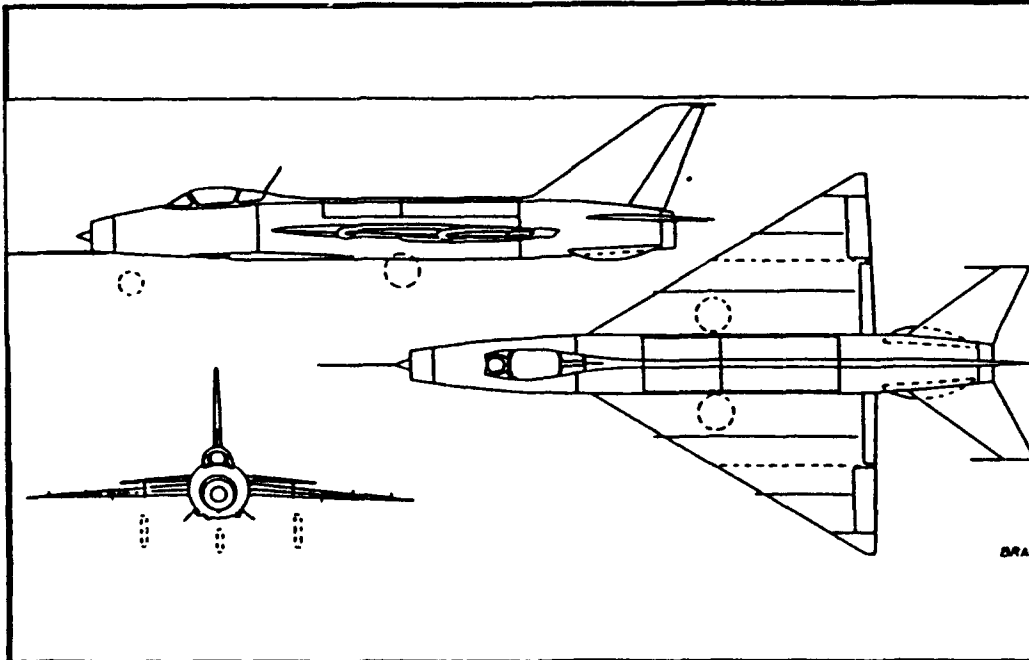


Figure 2 : Soviet Mig-21 "Fishbed" configuration.

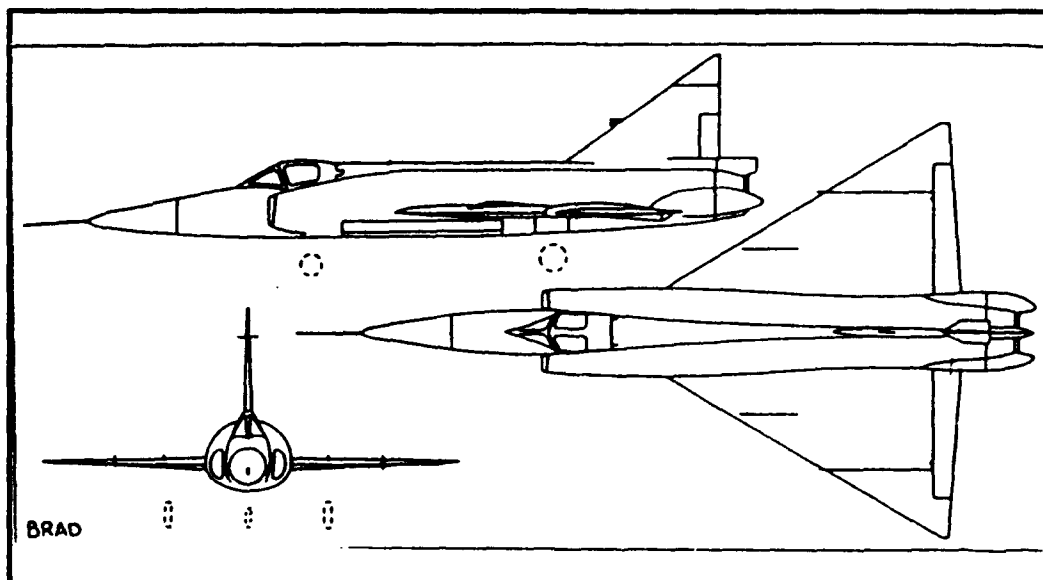


Figure 3 : United States F -102 "Dagger" configuration.

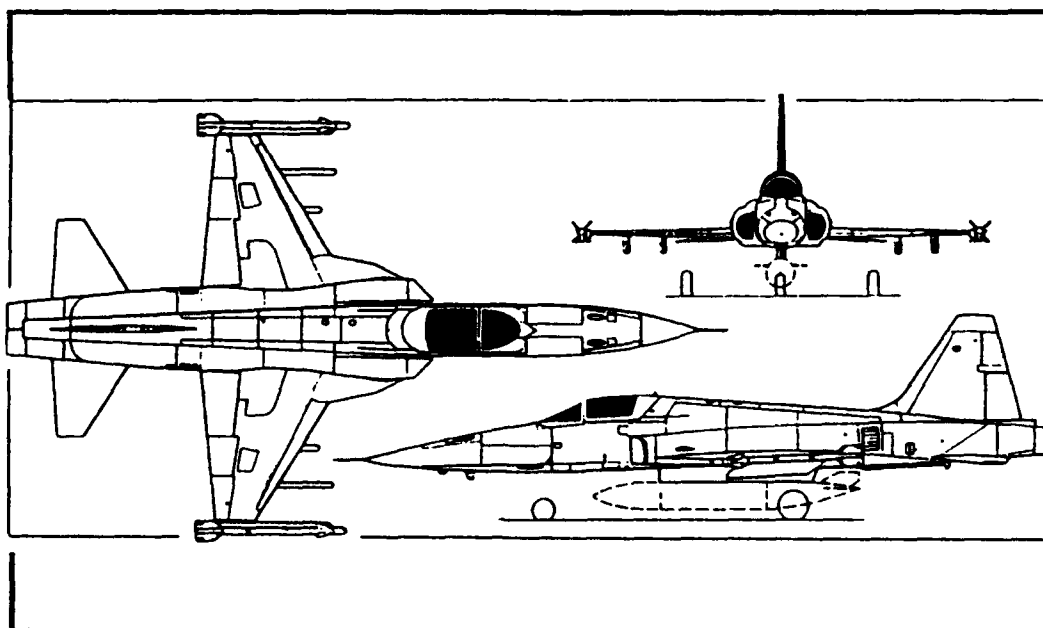


Figure 4 : United States F-5E/F "Tiger Shark" configuration.

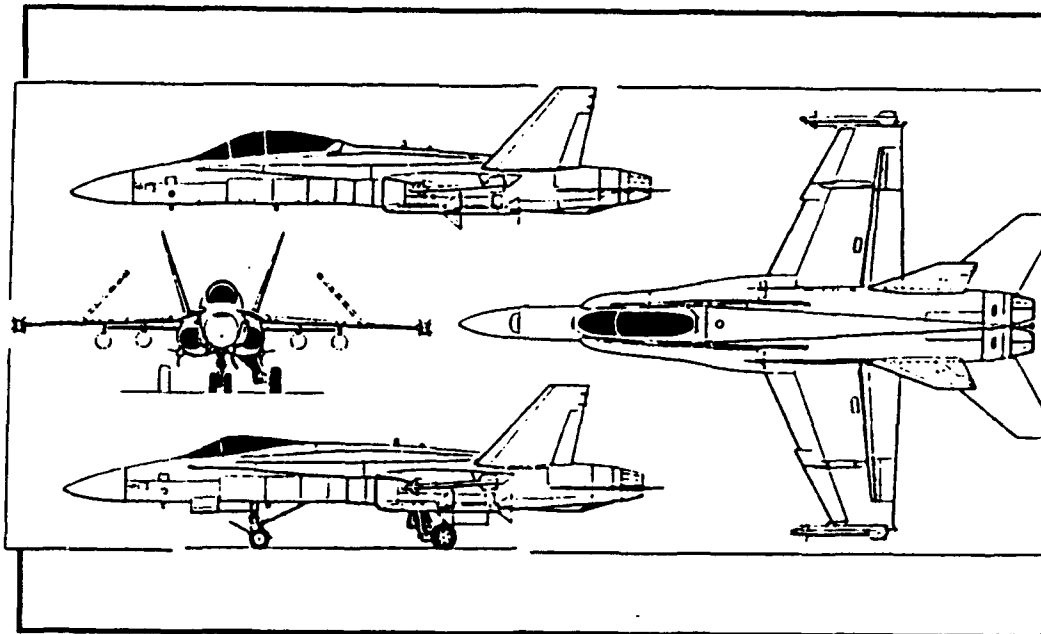


Figure 5 : United States F/A-18 "Hornet"

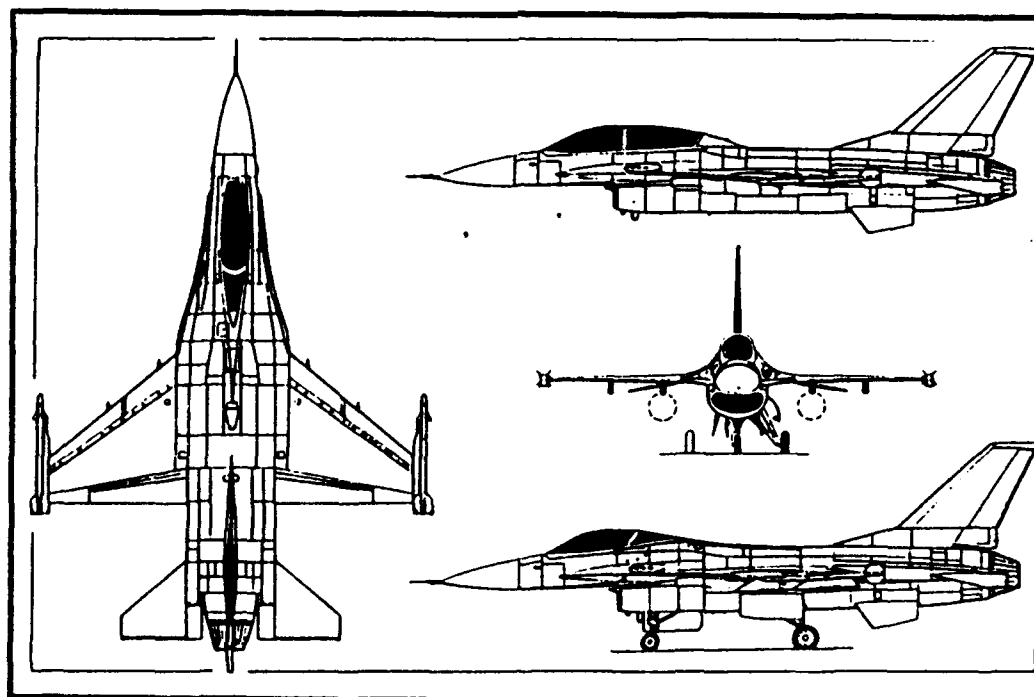


Figure 6 : United States F-16 "Falcon" configuration.

Because of the disadvantages of the single delta wing planform, the subsequent design and research efforts focussed on providing new design concepts and guidelines for vortex control on advanced, highly maneuvering aircraft at extremely high angles of attack. The first idea related to flow control through vortex manipulation started in the 1950's, with the use of asymmetric edge shape effects to achieve lateral control of low aspect ratio aircraft at low speeds and at high angles of attack. [Ref. 3] The use of double-delta wing planforms was ultimately developed in the 1970's. These planforms are currently applied on the F-5E/F "Tiger Shark"(Fig.4), F/A-18 "Hornet" (Fig. 5) and F-16 "Falcon" (Fig.6). [Refs. 1, 4 - 7]

B. AERODYNAMICS OF DOUBLE-DELTA WINGS

The challenge for the advanced fighter designer is to design an aircraft capable of cruising supersonically and maneuvering transonically with good handling qualities in the high angle of attack regime. As pointed out before, the concept of a double-delta wing planform provides an excellent technology for vortex control and manipulation. The McDonnell Douglas F/A-18E/F strake modification is a successful demonstration of vortex control at high angles of attack.

The basic aerodynamic phenomenon of a delta wing includes formation of leading edge vortices and their development and subsequent breakdown (burst).[Refs. 8 and 9] Two symmetric leading edge vortices are generated on wings with sweep angles greater than 45 degrees as the wing pitches up (Fig.7) [Ref. 10]; the vortices accelerate the flow over the wing surface, generating more lift (called vortex lift). The core flow of the vortex suddenly stagnates and

expands in size at high angles of attack. This is called vortex breakdown or bursting whose location is affected by wing sweep, angle of attack and the leading edge shape.[Ref. 11]

A combination of a wing and a leading edge extension(also called strake) forms a double-delta wing planform whose geometric characteristics are similar to a delta wing but for a discontinuity or kink in its leading edge. The flow pattern over a double-delta wing is similar to that over a delta wing but is much more complicated. The vortical flow over a double-delta wing at high angles of attack consists of a strake vortex or inner vortex generated at the apex and a wing vortex or outer vortex generated at the kink. (Fig. 8) These two vortices interact over the wing surface, coiling-up at low angles of attack. At high angles of attack, bursting may occur even before the interaction. The vortex breakdown phenomenon is influenced by various factors similar to the case of a single delta wing. The significant contribution of the strakes of a double-delta wing planform is that they not only increase the lifting area of the wing planform, but also create strake vortices which help to stabilize the flow field of the wing planform.

Recent studies of double-delta wings have generally focussed attention on the static conditions of the model, with emphasis on understanding the effects of angle of attack on the complicated phenomena of vortex interaction and bursting. [Refs. 4,12 - 14] A recent low speed wind tunnel investigation [Ref.15] deals with the effects of sideslip on double-delta wings. Reference 16 discusses the results of a water tunnel flow visualization study on a sideslipping, canard-configured, X-31A-like fighter aircraft model. In general, the data relating to sideslip effects on double-delta wings are extremely limited even for static conditions. A brief review of these studies appears in Ref. 12.

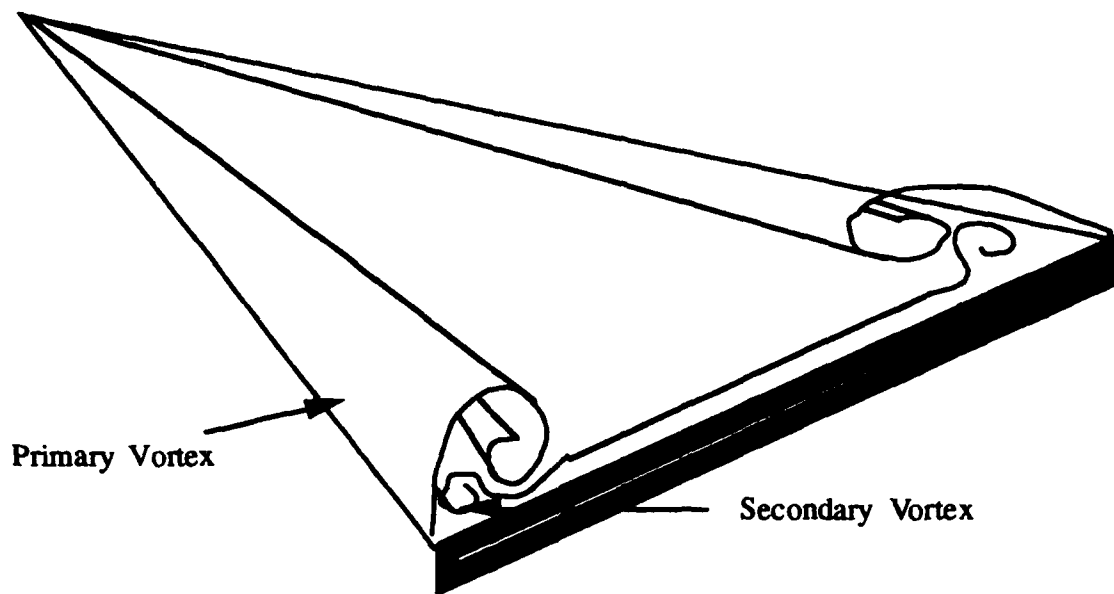


Figure 7 : Typical vortex pattern over a Delta Wing at high AOA

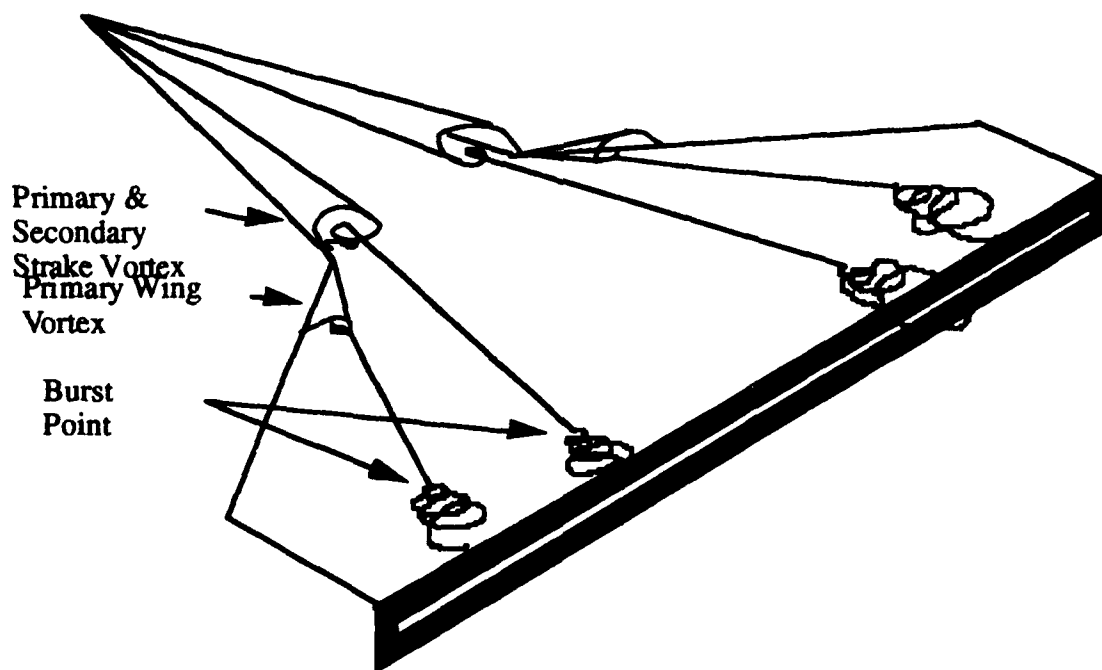


Figure 8 : Typical Vortex Structure over a Cropped Double-Delta Wing at High AOA.

C. FILLET AERODYNAMICS

A number of studies have been reported in the literature that are related to vortex manipulations for control purposes and to enhance the aircraft flying qualities and maneuverability. In a recent paper by Kern[Ref. 10], it is suggested that small geometry modifications (fillets) at the strake/wing junction of a cropped double-delta wing could enhance the lift by 13.6 % at low angles of attack and 17.9% at high angles of attack with a slight improvement in lift-to-drag ratio. It also suggested that the fillets may be deployed as lateral and directional control devices.

Alkhozam [Ref.11] carried out a detailed experimental investigation on the interaction, bursting, and control of vortices of a cropped double-delta wing at high angles of attack. The vortex breakdown data reported in Ref. 11 and 12 imply lift augmentation for both the static and dynamic case, with the static data correlating well with the numerical results of Kern. [Ref. 10] Again these data refer to the effect of angle of attack only and there is no data available on the effect of juncture fillets in the presence of sideslip .

D. GOAL OF THE THESIS

The effects of sideslip can be important for the stability and control of aircraft in the high angle of attack flight condition during takeoff, landing and maneuvering. However, as pointed out before, the experimental data available on the influence of sideslip on double-delta wings at high angles of attack is very limited. In particular, there is no data available on the influence of juncture

fillets on double-delta wings undergoing sideslip at high angles of attack.

The objective of this thesis, therefore, was to better understand the physics of vortical flows, with and without juncture fillets, over sharp-edged double-delta wings undergoing sideslip at high angles of attack. It consisted of extensive flow visualization studies in the Naval Postgraduate School (NPS) water tunnel facility with the dye-injection technique and focussed on vortex core trajectories and breakdown characteristics on the leeward surface at high angles of attack with and without sideslip. The models included a 76/40 degree cropped double-delta wing baseline model and its derivative with a small diamond-shaped fillet at the juncture of the strake and the wing leading edge. The model and fillet geometries were identical to the ones reported in Refs. 11 and 12.

II. EXPERIMENTAL FACILITIES & EQUIPMENT

A. THE NPS WATER TUNNEL

The experiments were performed in the Naval Postgraduate School flow visualization water tunnel facility. [Ref. 17] It is a closed circuit facility suitable for studying a wide range of aerodynamic and fluid dynamic phenomena. This tunnel was the first one designed by Eidetics International Inc., Torrance, California, and was installed in late 1988. The layout of the water tunnel is shown in Figure 9.

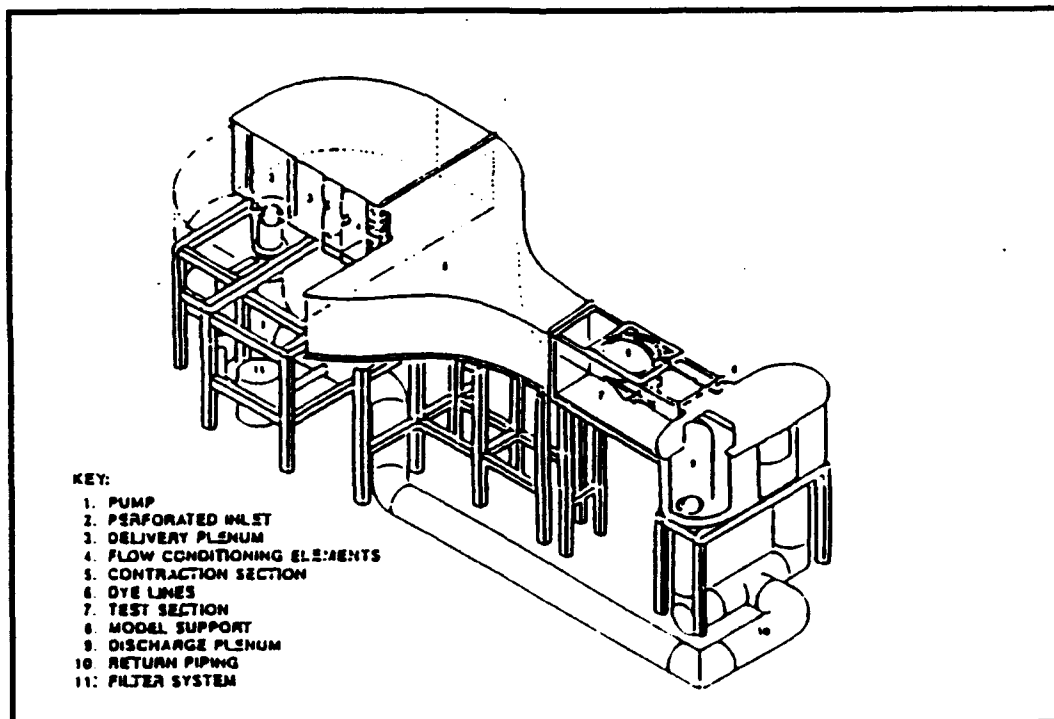


Figure 9 : The NPS Flow Visualization Water Tunnel Facility

The key design features of the NPS water tunnel are high flow quality,

horizontal orientation and continuous operation. The flow rate of circulation of water is up to 900 gallons per minute to provide up to 1 ft/sec flow rate in the test section. The horizontal orientation facilitates access, and enables the test models to be readily changed without draining the water from the tunnel. The top of the water tunnel is removable for easy access to the model while the tunnel is operating. The water tunnel is operated as a continuous flow channel, and the water level is adjusted to be approximately 2 inches below the top of the test section.

The test section is constructed primarily of tempered glass to provide thermal stability, scratch resistance and maximum viewing of the model. The size of the water tunnel is 15 inches wide, 20 inches high and 60 inches long. In order to compensate for boundary layer growth and to maintain uniform flow velocity throughout, the side walls of the test section have slight divergence. In addition, the transparent test section and the discharge plenum allow simultaneous viewing of the model from the bottom, from both sides and from the rear. The level of flow quality (measured outside the boundary layer) over the range of test section velocities is shown in Table 1.

Table 1: The flow quality in the test section.

Mean flow angularity	$< \pm 1.0^\circ$ in pitch and yaw
Turbulence intensity level (RMS)	$< \pm 1.0\%$
Velocity uniformity	$< \pm 2.0\%$

Six pressurized dye canisters using water soluble food coloring are used for

flow visualization. Each canister is pressurized with air from a small compressor and is connected to the model port through an individually routed line. The pressurized system controls and regulates the dye emission and provides a means of blowing air out of the dye lines going to the model.

The model support system shown in Figure 10 is mounted on the top of the test section and the model is usually sting-mounted upside down in the test section. The system is designed for high angle of attack aerodynamic research studies. It utilizes a C-strut to change the pitch angle from -10 degrees to +110 degrees, and a turntable to change the yaw angle through ± 20 degrees. The attitude control system uses two servo motors to control the model pitch and yaw independently, with separate actuation switches and high/low rate control switches.

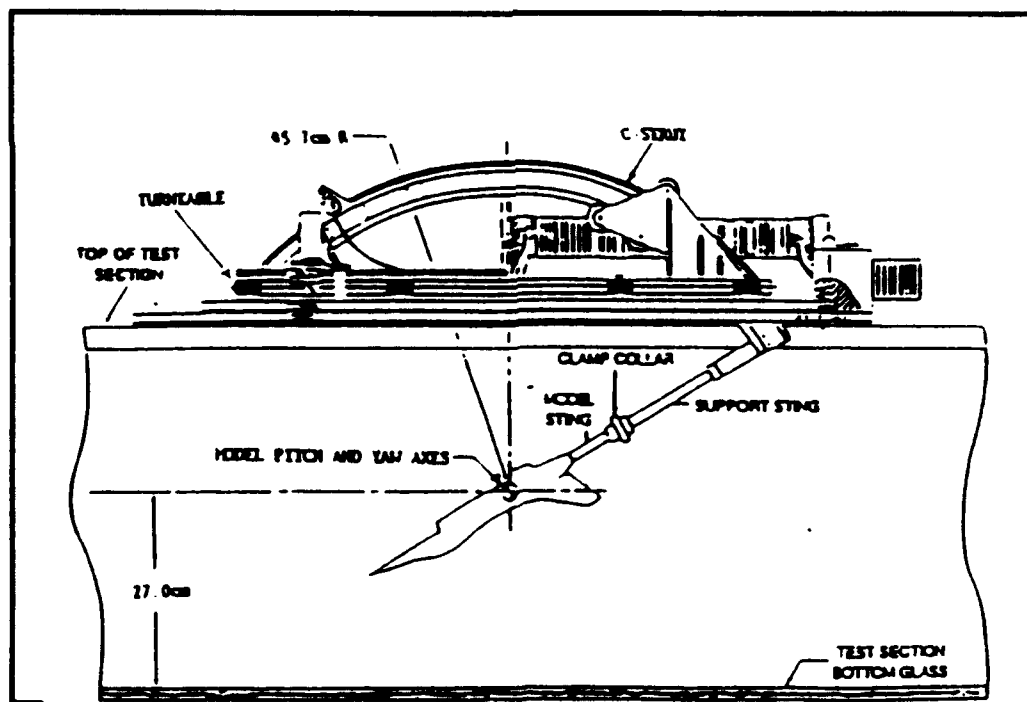


Figure 10 : Model Support System of the NPS Water Tunnel.

B. TEST MODELS

Two types of double-delta wing models were used in the experiments: a baseline model and its derivative with a diamond fillet at the junction.

The baseline model shown in figure 11 is made of 0.25 inch thick plexiglass ; it has a 76-degree sweep strake and a 40-degree sweep wing, both with sharp, 20-degree bevelled leading edges and flat top surfaces. The centerline chord of the baseline model is 9.375 inches, the wing span is 9.5 inches and the planform area is 39.9 square inches.

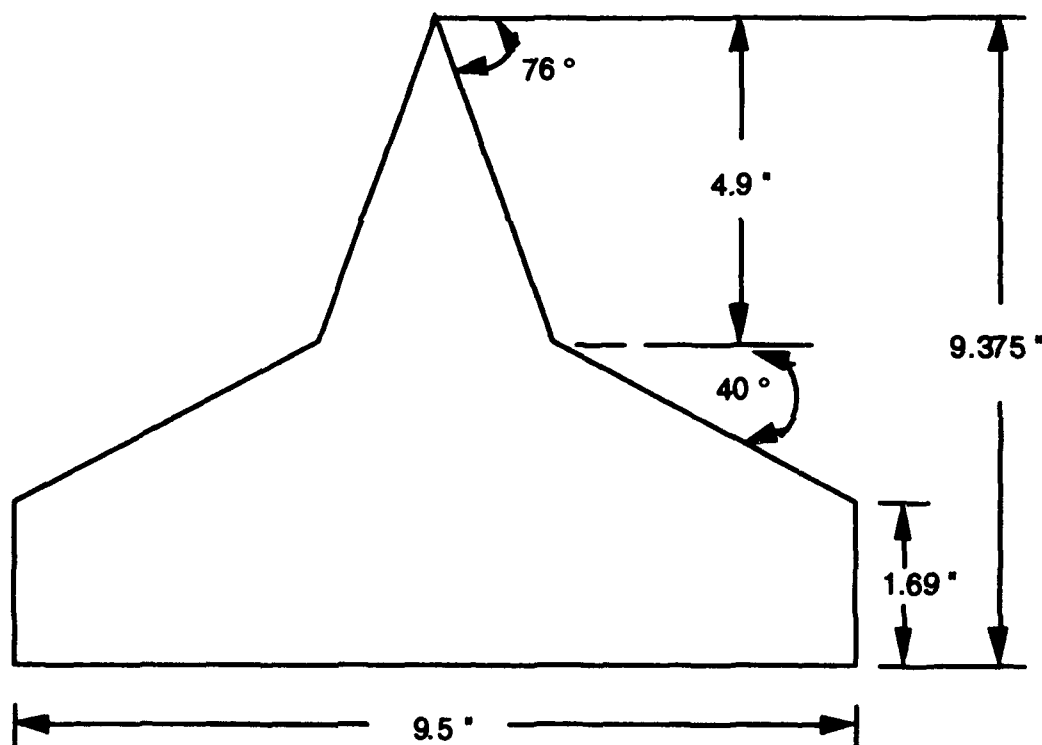


Figure 11 : Double -Delta Wing Baseline Model.

The diamond-fillet model (shown in Fig. 12) is made of the same material as the baseline model but with a little geometry modification (fillet) at the intersection (juncture or kink) of the strake and wing leading edges. The fillet increases the planform area of the baseline model by about 1%. The two models were used in the previous investigation.(Ref. 11) Both models are marked with 0.25 X 0.25-inch grid lines on the upper surface to help identify the vortex burst point location and core trajectory.

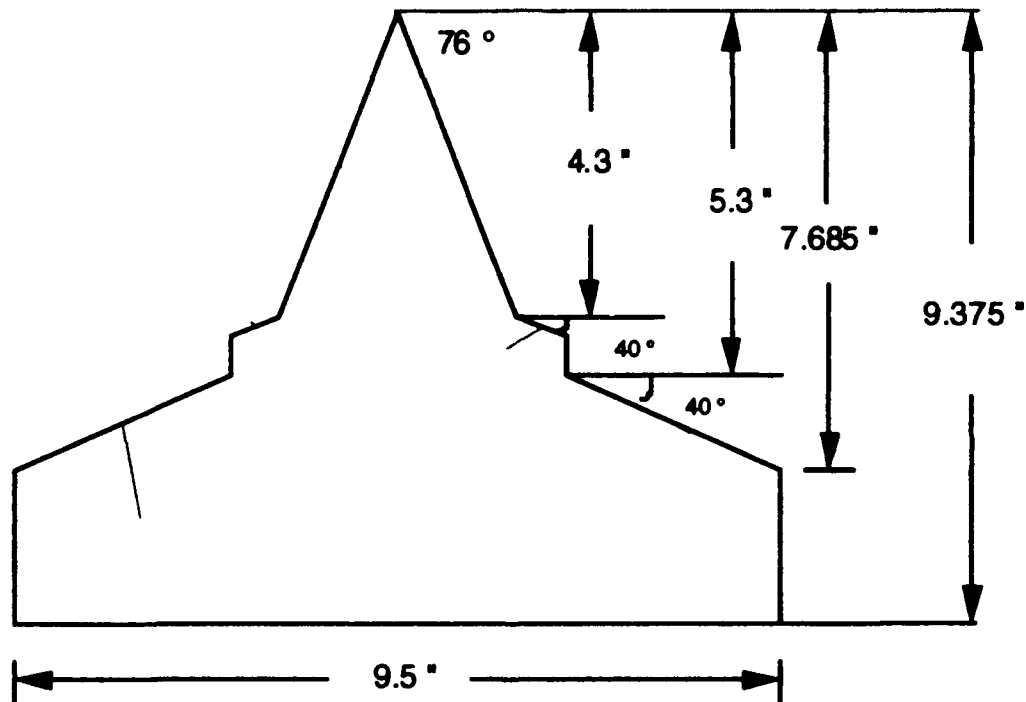


Figure 12 : The Diamond-fillet Double-Delta wing model.

C. DYE TUBE INSTALLATION

The configuration of brass dye tubes installed on the lower surface of each

model is shown in Fig. 13. For convenience of direct visualization, different color dyes were used for different locations.

The exact location of the tip of the dye tube was determined by moving around the tube and observing the dye line at different attitudes of the model. Both the location of the dye injection and the injection rate are crucial in obtaining a good flow visualization of the model flow field. The pressurized dye system helped to control the injection rate. In configuration #1, four brass tubes were installed on the lower surface of the model, two of the tips close to the apex and the other two close to the juncture or kink, all the tips sitting squarely on the flat surface. In configuration #2 six brass tubes were installed on the lower surface of the model, two of the tips close to the apex, two close to the beginning of the fillet and the remaining two close to the end of the fillet.

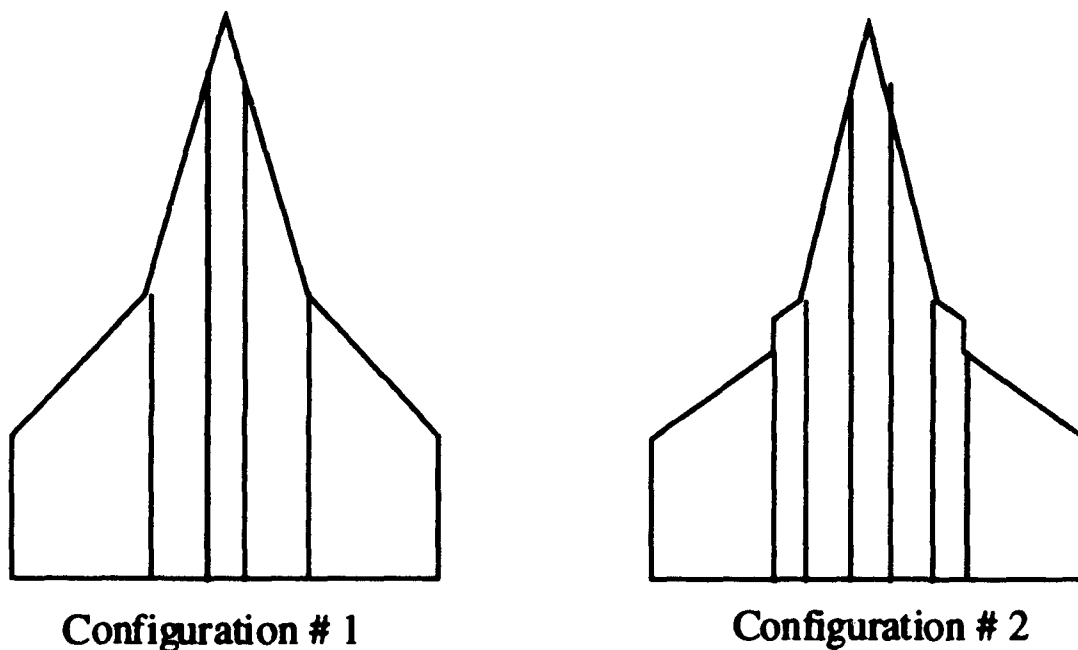


Figure 13 : The configuration of dye tubes.

D. MODEL MOUNTING

In order to have a good symmetry of the vortex core and the vortex burst data, it is extremely important to mount the model horizontally in the water tunnel with zero pitch, zero yaw and zero roll. Details of model mounting are given in [Ref. 17]. The model sting was secured to the sting holder of the model support system and then introduced into the test section. The centerline of the model was aligned with the freestream (tunnel centerline) for ensuring zero pitch angle. To ensure zero yaw, the model apex was set at equal distance from either sidewall of the test section. To ensure zero roll angle, the left and right wing tip were located at the same height from the bottom of the test section. To confirm the model was mounted correctly, three parallel lines were drawn on test section and discharge plenum glass walls to make sure that the model reference line was parallel to these lines. The model pitch and yaw axis were located at about 5.25 inches aft of the apex (56% of the centerline chord).

III. EXPERIMENTAL PROCEDURE

A. EXPERIMENTAL PROGRAM AND TEST CONDITIONS

The goal of this investigation was to study the vortical flow past two sharp-edged double-delta wings, one with a simple baseline geometry and the other with a geometric modification at the junction. (see Fig. 11 & Fig. 12) The experimental program included flow visualization of the two models with and without sideslip over a range of angles of attack in the static condition. The angle of attack range varied from 10 degrees to 50 degrees and the angle of sideslip range varied from 0 degree to 15 degrees, both in 5-degree increments. Both still-picture photography and videotape recording were used for documentation of the flow visualization of the model in topview and sideview. The flow velocity in the test section was kept nearly constant at 0.25 ft/sec which corresponded to a nominal Reynolds number of 24160/ft or 18876 based on the centerline chord.

B. TEST PROCEDURE

The test procedure is outlined below:

- 1) Mount the model in the test section, connect the dye tubes to dye lines and check the reference mark to ensure the model is mounted symmetrically in the horizontal plane.
- 2) Set up the lighting arrangement, adjust the lamp position to get the best lighting on the model.
- 3) Set up the 35-mm cameras and video cameras for recording flow visualization data.
- 4) Turn on the water tunnel and run it at 0.25 ft/sec.

- 5) Fill the canisters with the food coloring dye of different colors, establish the air pressure (10 psi) to the canisters and check out the dye lines to the model.
- 6) Operate the pitch and yaw switches to set up the model test condition.
- 7) Turn on each dye control knob and fine tune it to get the optimum dye injection for flow visualization purpose.
- 8) Observe the vortical flow patterns for the model test condition.
- 9) Record the flow visualization data on video tapes and take the pictures in both sideview and topview.
- 10) Turn off the dye control knob and set up the next test condition for the model.
- 11) Repeat items 7) to 10) as required to the end of the test.

C. DATA ACQUISITION AND REDUCTION

The data acquisition system included two video cameras and two 35-mm cameras. The data was collected by operating the system simultaneously to record the sideview and topview of the vortical flow field of the strake and the wing or fillet vortex cores generated by the two models for different sideslip angles in the high angle of attack range.

The data reduction was accomplished by measuring the vortex core location along the model centerline from the apex (X -coordinate) and outboard from the centerline (Y-coordinate) and measuring the burst location of the vortices shed off the leading edge of the model. The vortex core trajectories were constructed by plotting the Y coordinate versus the X coordinate and the burst location plots were constructed by plotting the burst location X_b versus angle of attack. When a yaw angle is imposed on the model, the side opposite the yaw input is called the

windward side and the side in the same direction as the yaw input is called the leeward side. For this study, both the windward and the leeward side data were collected for data analysis purposes. The vortex core location and burst location data were visually determined from direct observation / videotape playback / photographs. The measurements of the vortex core and burst locations were made with utmost care and consistency, and scaled for non-dimensionalization using the centerline chord length C . There may be some degree of imprecision in the data due to the difficulty in locating the trajectory and burst points, especially at high angles of attack. The vortices from the wing and the fillet were extremely difficult to read when the angle of attack was higher than 25 degrees, so there was no data for the wing and fillet vortices above 30 degrees. In addition, it should be noted that during the experiments, the vortex burst location fluctuated up to ± 0.75 inches (about $\pm 8\%$ of the centerline chord).

D. METHOD OF PHOTOGRAPHY

The equipment used for the data acquisition consisted of two 35-mm automatic cameras, one U-matic Sony video camera, one Panasonic video camera, 3 Smith-Victor 600 watt photographic lights and a fixed flood light installed below the test section. For the sideview photographs two of the lights were placed at a distance of 1 - 3 feet at 45 degrees angle from the test section. and the third one was moved around to compensate the shadow on the model. The lighting set-up is shown in figure 14.

A Minolta 5000i Maxima camera positioned in front of the test section for the sideview used 35-mm black & white Kodak ASA-400 film. A Nikon 2050 camera positioned at the bottom of the test section for the top view, also used 35-

mm black & white Kodak ASA -400 film and was operated with a remote shutter release. Both cameras were focussed manually each time before clicking. The Sony video camera was placed at the bottom of the test section whereas the Panasonic video camera was set up in front of the test section for the sideview. Both sideview and topview of the model photographs and videos were taken simultaneously at all test conditions.



Figure 14 : Photographic equipment and lighting set-up

IV. TEST RESULTS & DISCUSSION

The flow visualization data has been collected using several hours of videotapes and several rolls of 35 mm black and white film. The reduced experimental data on vortex core trajectory and bursting point are shown in Appendix A (Tables 2 - 125). Several selected photographs are presented in Appendix B (Figs. 15 - 30) to highlight the flow characteristics and the effect of the diamond-fillet. Each figure shows two views of the flow field, one in topview (taken from the bottom of the test section) and the other in sideview (taken from the side of the test section). It should be pointed out that the angle-of-attack(AOA) reading in these photographs is not necessarily the true angle of attack since the sideview camera was not always focussed exactly at the model centerline. The true angle of attack was read off from the AOA indicator on the model motion control box. The vortex burst point plots and the vortex trajectory plots derived from the test data are shown in Appendix B (Figs. 31 - 90).

It is important to mention the factors that would affect the data quality here. First , the vortex burst location which fluctuated almost all the time; second, the AOA and angle-of-sideslip(AOS) indicator readings on the control panel, which fluctuated occasionally; third, the parallax error from the video camera. It is suspected that these factors have affected the data quality to a small extent.

The results of the experimental data are discussed below. First the data is analyzed for the effects of angle of attack and sideslip on vortex burst location and vortex core trajectory on each model and then the effects on two models are

compared. Finally, the data is interpreted to provide an AOA - AOS operational envelope for maneuvering.

A. EFFECT OF AOA ON VORTEX CORE BREAKDOWN AT ZERO SIDESLIP

1. BASELINE MODEL

The strake vortex core burst location for the baseline model as a function of angle of attack at different sideslip angles is shown for windward and leeward sides in Figures 31 and 32, respectively. Note that for the zero sideslip case there is no difference between the windward and leeward sides, and the plots corresponding to $\beta = 0^\circ$ in these figures are identical. The plots show that the farthest burst location for the symmetric condition ($\beta = 0^\circ$) occurs at 10° AOA, at about 92% of the centerline chord. The strake burst point moves forward as the angle of attack increases, the most forward burst point occurring at 50° AOA, at less than 10% of the centerline chord. The slope of the curve is steep in the AOA range of 15° to 30° , implying faster upstream movement of the burst in this range. Figure 33 compares the present data with the data of Ref. [11] for the same model in the same AOA range at zero sideslip. The present data indicate slightly higher values of burst locations in the AOA range of 15° to 28° , the maximum difference being about 5% at 25° AOA. Considering the experimental uncertainty associated with these data sets, the agreement between them is excellent.

The wing vortex core burst location for the baseline model as a function of angle of attack at different sideslips is shown in Figures 34 and 35. The data are

limited to 25° AOA because of the difficulties in visualizing and reading burst locations at high angles of attack. As before, the plots for $\beta = 0^\circ$ represent zero sideslip and are identical in these figures. The slopes of these curves imply small upstream movements of burst locations. Figure 36 compares the present data with that of Ref. [11] for which the data start at AOA = 16° . The present data indicate a slightly lower value of burst location compared to Ref. [11] for AOAs lower than 22° , the maximum difference being 8% at 16° AOA. The two curves cross at 22° AOA with the present data indicating slightly higher values, the maximum difference being about 5% at 25° AOA. In view of the experimental uncertainty, the agreement between the data sets is considered excellent.

2. DIAMOND-FILLET MODEL

Figures 37 and 38 show the strake vortex core burst location for diamond-fillet model as a function of AOA at different sideslip angles. As before, the zero sideslip case corresponds to symmetric flow and the plots representing $\beta = 0^\circ$ in these figures are identical for the windward side and the leeward side. These plots show a steeper slope between 15° and 30° AOA. The farthest burst point occurs at 10° AOA at about 95% of the centerline chord, the most upstream burst location occurring at 50° AOA at about 18% of the centerline chord. Figure 39 compares the present data with the data of Ref. [11] for zero sideslip. The overall agreement between the data sets is excellent, the indicated maximum difference of about 5%(at 22° AOA) being well within the experimental uncertainty.

The diamond-fillet model had two dye tubes near the fillet, one close to the beginning of the fillet and the other close to the end of the fillet. The beginning-

of-fillet vortex core burst location data are shown in Figures 40 and 41. For reasons mentioned before, the AOA range is limited to 30° . The slope of the plot for zero sideslip case ($\beta = 0^\circ$) suggests small upstream movements of the burst location. Figure 42 shows a comparison of the present data with the data of Reference 11. A maximum difference of about 15% is observed between the two sets at 26° AOA.

The end-of-fillet vortex core burst location data are shown in Figures 43 and 44. The data are limited to 25° AOA. The zero sideslip plot ($\beta = 0^\circ$) shows very small upstream movements of the burst location. This plot is compared with the data of Reference 11 in Figure 45. A maximum difference of 6% is observed between the two data sets at 23° AOA.

3. COMPARISON OF THE TWO MODELS

Comparison of the strake vortex core burst location data for the baseline and the diamond-fillet models is shown in Figures 46 and 47. For the zero sideslip case ($\beta = 0^\circ$), the slopes of the curves are pretty much the same but the burst locations for the diamond-fillet model lag those for the baseline model throughout the AOA range tested by about 8%. These plots therefore imply a vortex burst delay for the diamond-fillet model.

The wing vortex core burst location data for the two models are compared in Figures 48 to 51. A careful examination of the plots for the zero sideslip case ($\beta = 0^\circ$) indicates that the plots for the wing vortex and the beginning-of-fillet vortex practically coincide, suggesting no delay in breakdown. On the other hand, the end-of-fillet vortex core burst locations indicate an early bursting

compared to wing vortex core bursting.

B. EFFECT OF ANGLE OF SIDESLIP ON VORTEX CORE BREAKDOWN

1. BASELINE MODEL

The effect of sideslip on strake vortex core burst location for the windward and leeward sides of the baseline model is illustrated graphically in Figures 31 and 32, respectively. These plots clearly demonstrate the differential effect of small sideslip angles on the burst location at any given AOA; namely the forward(upstream) movement of the burst location on the windward side and the rearward(downstream) movement on the leeward side. Large burst movements are observed in the 20° to 35° AOA range on both sides, the leeward side showing relatively greater sideslip effect. Maximum sideslip effect on the burst movement is seen around $AOA = 30^\circ$ on both sides. Furthermore, the sideslip effect on the burst movement is pronounced at small sideslip angles($\beta < 10^\circ$), but diminishes at higher sideslip angles ($\beta > 10^\circ$). Note that the influence of sideslip can be explained in terms of the effective sweep angle for the windward side and the leeward side [Ref. 16] .

The effect of sideslip on wing vortex core burst location for the windward and leeward sides of the baseline model is illustrated graphically in Figures 34 and 35, respectively. The sideslip effects observed in the 10° to 25° AOA range on the burst location of the wing vortex core on the windward and leeward sides are qualitatively similar to those on the strake vortex core discussed above. Of

particular interest on the leeward side is the fact that the plot for $\beta = 15^\circ$ (Fig. 35) has a zero slope, the burst locations move downstream of the trailing edge with increase of AOA, and there is no burst on the wing surface (see Figure 26)

2. DIAMOND-FILLET MODEL

The effect of the sideslip on strake vortex core burst location for the windward and leeward sides of the diamond-fillet model is illustrated graphically in Figures 37 and 38, respectively. The sideslip effects observed here on the burst location of the strake vortex core on the windward and leeward sides of the diamond-fillet model are qualitatively similar to those observed on the baseline model. As before, sideslip effects are more pronounced on the leeward side. In fact, at a sideslip of $\beta = 15^\circ$, the burst locations on the leeward side for AOA less than 20° occur outside the model, downstream of the trailing edge. (Fig. 38)

Figures 40 to 41 and 43 to 44 illustrate the effect of sideslip on the burst location of the beginning-of-fillet vortex core and the end-of-fillet vortex core, respectively, for the windward and leeward sides of the diamond-fillet model. The sideslip effects observed in the 10° to 30° range on the burst location of the beginning-of-fillet vortex core on the windward and leeward sides (Figs. 40 and 41) are qualitatively similar to those observed on the wing vortex core of the baseline model (Figs. 34 and 35), with one exception namely that even at $\beta = 15^\circ$, the bursting occurs on the diamond-fillet model surface, upstream of the trailing edge. (see Figure 30A) Similar qualitative trends are observed in the plots for the end-of-fillet vortex core burst location. (Figs. 43 and 44)

3. COMPARISON OF THE TWO MODELS

Figures 46 and 47 compare the strake vortex burst locations at different sideslip angles for the baseline and diamond-fillet models, respectively. It is clear from these plots that , over the AOA range tested, the major effect of sideslip is to delay the vortex bursting on the leeward side and advance it on the windward side. It is also very clearly seen that in comparison to the baseline model, the effect on the diamond-fillet model is more pronounced on the leeward side but less pronounced on the windward side. In other words, the fillet is seen to enhance the sideslip effect on the leeward side but reduce it on the windward side.

Figures 48 to 49 and 50 to 51 compare the wing / fillet vortex burst locations at different sideslip angles for the baseline and diamond-fillet models, respectively. On the windward side, the burst location of the beginning-of-fillet vortex is generally aft of the wing vortex burst location. However, on the leeward side this is reversed on few occasions as seen in Figure 49. These general features are also seen in the behavior of the end-of-fillet vortex burst location (Fig. 50 and 51)

C. EFFECT OF AOA ON THE VORTEX CORE TRAJECTORY AT ZERO SIDESLIP

1. BASELINE MODEL

The non-dimensional X-Y plots of the strake vortex core trajectories for the windward and leeward sides of the baseline model at different sideslip angles are shown in Figures 52 to 55 for AOAs of 10°, 20°, 30°, and 40°, respectively. For all practical purposes, the end of the trajectory in all these plots signifies the

vortex burst location. For the zero sideslip case, there is no difference between the windward and leeward sides and the plots corresponding to $\beta = 0^\circ$ in these figures are essentially symmetrical with respect to the centerline chord. They clearly indicate that, as the AOA increases at zero sideslip, the strake vortex core length decreases (the burst location moves upstream) and the vortex core moves inboard toward the centerline chord. Figures 56 to 58 compare the present trajectory data with that of Ref.[11] for the same model in the same AOA range at zero sideslip. The maximum deviation between the two trajectory data is about 5%, which is well within the experimental uncertainty of the data. It should be pointed out here that unlike in the present data, the last data point of the vortex core in Ref.[11] was measured a little ahead of the visual burst location, and therefore the end points for the two sets of data are slightly different in Figures 57 and 58.

Figures 59 and 60 show the non-dimensional X-Y plots of the wing vortex core trajectories for the windward and leeward sides of the baseline model at different sideslip angles for AOAs of 10° and 20° , respectively. As before, the plots for $\beta = 0^\circ$ represent the zero sideslip case and are practically symmetrical in these figures. With increase in AOA, the core length decreases and the vortex cores move inboard. Figures 61 and 62 compare the wing vortex trajectory data with the data of Ref.[11] at zero sideslip. Small differences are seen between the data sets in the tail region of the vortex core, but in the light of the experimental uncertainty, the overall agreement between the trajectory data is very good.

2. DIAMOND-FILLET MODEL

The non-dimensional X-Y plots of the strake vortex core trajectories for the

windward and leeward sides of the diamond-fillet model at different sideslip angles are shown in Figures 63 to 66 for AOAs of 10° , 20° , 30° and 40° , respectively. As before, the zero sideslip case corresponds to symmetric flow and the plots for $\beta = 0^\circ$ in these figures are symmetrical with respect to the centerline chord. The trends observed in these plots are essentially similar to those in the baseline model discussed above, namely reduction in core length and inboard movement of the vortex core with increase in AOA at zero sideslip. Figures 67 and 68 compare the present trajectory data with that of Ref. [11] for zero sideslip and the agreement between the data sets is within the experimental uncertainty.

Figures 69 and 70 show the non-dimensional X-Y plots of the beginning-of-fillet vortex core trajectories for the windward and leeward sides of the diamond-fillet model at different sideslip angles for AOAs of 10° and 20° , respectively. As before, the plots for $\beta = 0^\circ$ represent the zero sideslip case and are practically symmetrical in these figures. The AOA influence on these trajectories is very much similar to its influence on the wing vortex trajectory of the baseline model. Figures 71 and 72 compare the beginning-of-fillet vortex trajectory data with the data of Ref. [11] at zero sideslip. The agreement at 10° AOA (Fig. 71) is excellent. Figures 73 and 74 show the non-dimensional X-Y plots of the end-of-fillet vortex core trajectories for the windward and leeward sides of the diamond-fillet model at different sideslip angles for AOAs of 10° and 20° , respectively. The present data is compared with that of Ref. [11] in Figures 75 and 76. The trends observed in these figures are very similar to those for the beginning-of-fillet vortex core trajectories, except the fact that the end-of-fillet vortex core lengths are much shorter.

3. COMPARISON OF THE TWO MODELS

Figures 77 to 80 compare the strake vortex trajectory data for the baseline and the diamond-fillet models at different sideslip angles, for AOAs of 10° , 20° , 30° and 40° , respectively. An examination of the plots for zero sideslip angle ($\beta=0^\circ$) indicates that the strake vortex trajectory of the baseline model is closer to the centerline chord at low AOA (Fig. 77), but moves outboard with increasing AOA. Note that in all the cases, the strake vortex core of the diamond-fillet model bursts later and therefore has a longer core length.

The vortex trajectory data for the wing vortex core of the baseline model and the beginning-of-fillet vortex core of the diamond-fillet model at different sideslip angles are compared in Figures 81 and 82, for AOAs of 10° and 20° , respectively. The plots corresponding to zero sideslip case ($\beta = 0^\circ$) show that the trajectories for the two models stay close to each other at 10° AOA, but the fillet vortex trajectory has moved outboard at 20° AOA. The vortex core lengths for the two models are equal. Similar trends can also be observed in the zero sideslip plots ($\beta=0^\circ$) shown in Figures 83 and 84, which compare the wing vortex core trajectory data for the baseline model and the end-of-fillet vortex core trajectory data for the diamond-fillet model at AOA = 10° and AOA = 20° , respectively. However, in this case the fillet vortex has a slightly shorter core length.

D. EFFECT OF ANGLE OF SIDESLIP ON VORTEX CORE TRAJECTORY

1. BASELINE MODEL

Figures 52 to 55 illustrate the sideslip effect on the strake vortex core trajectories on the windward and leeward sides of the baseline model. These plots clearly demonstrate that with increasing sideslip input, at any given angle of attack, the windward / leeward vortex core length decreases / increases and the trajectory moves inboard / outboard. Note that the core length is a strong decreasing function of angle of attack.

Figures 59 and 60 show the sideslip effect on the wing vortex core trajectories on the windward and leeward sides of the baseline model. At both the AOAs shown here, the general effect of sideslip input on the wing vortex trajectories is qualitatively very similar to that observed on the strake vortex trajectory.

The combined trajectory patterns for the baseline model are shown in Figures 85 and 86 for AOAs of 10° and 20° , respectively. These help to visualize the vortex interaction phenomenon in the X-Y plane.

2. DIAMOND-FILLET MODEL

The sideslip effects on the strake vortex core trajectories on the windward and leeward sides of the diamond-fillet model are shown in Figures 63 to 66. The data trend in these plots is similar to that for the baseline model, the notable difference being that the diamond-fillet model has a longer vortex core and its windward vortex core trajectory even moves over to the leeward side at high AOA and high AOS. (Fig. 66)

Figures 69 and 70 show the sideslip effect on the beginning-of-fillet vortex core trajectories on the windward and leeward sides of the diamond-fillet model,

whereas Figures 73 and 74 depict the sideslip effect on the end-of-fillet vortex core trajectories. The general trend in these plots is similar to that for the wing vortex core trajectory for the baseline model.

The combined trajectory patterns for the diamond-fillet model shown in Figures 87 to 90 help visualize the vortex interaction phenomenon in the X-Y plane.

3. COMPARISON OF THE TWO MODELS

Figures 77 to 80 compare the strake vortex trajectory data at different sideslip angles for the baseline and diamond-fillet models. A general feature in all these plots is the fact that the leeward strake vortex core lengths for the diamond-fillet model are usually longer than their counterparts for the baseline model and the vortex trajectories tend to remain farther outboard at high AOA and AOS(Fig. 80).

Figures 81 to 84 compare the wing and fillet-vortex trajectory data at different sideslip angles for the baseline and diamond-fillet models. There is some crossing-over of the plots in these figures and it is difficult to see the trend here.

The combined trajectory patterns for 10° and 20° AOA are shown in Figures 85 and 86 for the baseline model and in Figures 87 to 90 for the diamond-fillet model. These patterns clearly indicate that the vortex interaction points on the windward side / leeward side move upstream and inboard / downstream and outboard with sideslip input.

E. OPERATIONAL ENVELOPE FOR MANEUVERING

The results of the comparison of present data for zero sideslip case with that of Ref.[11] clearly indicates that, within the limits of experimental uncertainty, the test data are reproducible and reliable. The burst location is a function of both AOA and sideslip. With increasing AOA, the burst locations move upstream implying loss of lift. However, the rate of burst movement is not uniform, being maximum in the AOA range of 15° to 30° . With sideslip input at any AOA, both the strake vortex core burst location and the vortex interaction point move upstream and inboard on the windward side, but downstream and outboard on the leeward side. These movements imply a vortex trajectory with a shorter core length that is closer to the centerline chord on the windward side, but a vortex trajectory with a longer core length that is farther from the centerline chord on the leeward side. As both of these movements have an adverse effect on lift generation, loss of lift increases with sideslip. At 15° sideslip angle, the lift loss increases considerably for AOAs greater than 30° .

Based on the result of the flow visualization data , an operational envelope for maneuvering can be visualized for each model. Maneuvers at high AOA and appreciable sideslip angles provide more agility and are therefore desirable. Assuming that the angle of sideslip is limited to 15° (for lack of test data at higher angles), and stipulating that the minimum operating AOA is 20° and the burst point moves no closer than $X_b/C = 0.4$ (this assumes there is still sufficient lift developed to carry out the maneuver), operational envelopes can be constructed as shown in Figures 91 and 92, for the baseline model and the diamond-fillet model, respectively. The two envelopes are compared in Figure 93, which

clearly demonstrates that the diamond-fillet model has a better operational envelope.

V. CONCLUSIONS AND RECOMMENDATIONS

A flow visualization study of the vortical flow over a baseline double-delta wing model and a diamond-fillet double-delta wing model, both with sharp leading edges, was conducted in the NPS water tunnel using the dye-injection technique. The diamond-fillet increased the wing area of the baseline model by 1%. The main focus of this study was to evaluate the effect of the diamond-fillet on the vortex core trajectory and vortex burst location on the wing surface at high angles of attack with sideslip. The water tunnel visualization data reported here is believed to be the first of its kind on the effect of juncture fillets on a double-delta wing undergoing sideslip at high angles of attack. Based on the results, the following conclusions are drawn:

1. At zero sideslip, the vortex trajectories and burst locations are symmetric over the AOA range tested. With increase in the AOA, the vortex burst point moves upstream and the vortex core length decreases, indicating that the separated flow region increases at higher AOAs. These findings are in agreement with those of earlier investigations.
2. Both vortex core trajectory and burst location are functions of sideslip angle. At a constant AOA, as angle of sideslip increases, the windward-side strake vortex trajectory moves inboard with its burst point moving upstream while the leeward-side strake vortex trajectory moves outboard with its burst point moving downstream.
3. Comparison of the test results between the baseline model and the diamond-

fillet model indicates that the strake vortex burst locations on both windward and leeward sides of the diamond-fillet model are delayed at high AOA with sideslip. The vortex breakdown data for the diamond-fillet model therefore implies lift augmentation during sideslip motion, thus supporting the concept of flow control using fillets.

The following recommendations are made based on this study :

1. Quantitative measurements of the flow field should be undertaken with a laser Doppler velocimetry(LDV) to correlate the present flow visualization data.
2. The wind tunnel study of the baseline & diamond-fillet shapes using a force balance is recommended to further assess quantitatively the suitability of the diamond-fillet as a control device.
3. Further flow visualization experiments are suggested to continue the present study to include dynamic sideslip effects.
4. Other fillet shapes should be studied for their suitability as flow control devices.

LIST OF REFERENCES

1. Janes "All The World Aircraft", 1950 - 1956
2. R. Whitford, "Design for Air Combat", Janes Publishing Company Ltd, London, 1987.
3. G.E Barlett, R. J. Vidal, "Experimental Investigation of influence of Edge Shape on the Aerodynamic Characteristics of Low Aspect Ratio Wing at low Speeds". Journal of the Aeronautical Science, Volume 22, Number 8, Aug. 1955.
4. S. K Hebbar, M. F Platzer, F.H Li, "A Visualization study of the Vortical flow over a double-delta wing in dynamic motion" AIAA 93-3425, Aug. 1993.
5. D. F. Fisher, J. H. Del Frate, F. A. Zuniga, "In-Flight flow Visualization of the NASA F-18 High Alpha Research Vehicle at High Angle of Attack", NASA TM-4130, May 1990.
6. D. F. Fisher, J. H. Del Frate, F. A. Zuniga, "Summary of In-Flight Flow Visualization obtained from the NASA F-18 High Alpha Research Vehicle", NASA TM-101734, January 1991.
7. D. F. Fisher, J. H. Del Frate, F. A. Zuniga, "In-Flight flow Visualization with Pressure Measurements at low Speeds on the NASA F-18 High Alpha Research Vehicle", NASA TM-101726, October, 1990.
8. John J. Bertin, Michael L. Smith, "Aerodynamics for Engineers" Prentice Hall, Second Edition, 1989.
9. M. Lee, M. C. Ho, "Vortex Dynamics of Delta Wings", Springer Verlag,

1989.

10. S. B. Kern, " Vortex Flow Control Using Fillets on a Double-Delta Wing,"
Journal of Aircraft, Vol. 30, No. 6, 1993, P. 818. Also see AIAA paper
92-0411.
11. Abdullah. M. Alkhozam, " Interaction, Bursting and control of vortices of a
Cropped Double-Delta Wing at High Angle of Attack", M.S Thesis, Naval
Postgraduate School, March, 1994.
12. S. K. Hebbar, M. Platzer, A. Khozam, " Investigation Into The Effects of
Juncture Fillets on the Vortical Flow over a Cropped, Double-Delta Wing",
AIAA 94-0602.
13. P. Olsen, R. Nelson, "Vortex Interaction over Double-Delta Wings at High
Angle of Attack", AIAA 89-2191.
14. Feng-Hsi Li, " Static and Dynamic FLOW Visualization Studies of
Double-Delta Wing Models at High Angle of Attack", M.S Thesis, Naval
Postgraduate School, March 1992.
15. D. Grismer, R. Nelson, " The Aerodynamic Effect of Sideslip on
Double-Delta Wings", AIAA 93-0053.
16. S. K. Hebbar, M. F. Platzer, C. H. Kim, " Experimental Investigation of
Vortex Breakdown over a Sideslipping Canard-Configured Aircraft Model, "
Journal of Aircraft, Vol. 31, No. 4, 1994, PP. 998-1001.
17. User's Manual, Flow Visualization Water Tunnel Operation Manual for
Model 1520, Eidetic International Inc., Torrance, CA, 1988.

APPENDIX A

Tables (2 - 125)

Table 2 : Strake vortex core trajectory of the baseline model . $\alpha = 10^\circ$, $\beta = 0^\circ$,
Chord (C) = 9.375 inches .

Point No.	X / C	Y / C (Windward)	Y / C (Leeward)
1	0.0539	0.003	0.003
2	0.1078	0.013	0.013
3	0.1617	0.027	0.026
4	0.2156	0.032	0.032
5	0.2695	0.054	0.054
6	0.3234	0.060	0.060
7	0.3773	0.065	0.065
8	0.4312	0.067	0.067
9	0.4852	0.081	0.081
10	0.5391	0.086	0.086
11	0.5930	0.094	0.094
12	0.6469	0.108	0.108
13	0.7008	0.121	0.122
14	0.7547	0.135	0.135
15	0.8086	0.148	0.148
16	0.8625	0.162	0.162
17	0.9164	0.189	0.188

Table 3 : Strake vortex core trajectory of the baseline model. $\alpha = 10^\circ$, $\beta = 5^\circ$,
Chord (C) = 9.375 inches .

Point No.	X / C	Y / C (Windward)	Y / C (Leeward)
1	0.0539	0.003	0.003
2	0.1078	0.013	0.013
3	0.1617	0.021	0.027
4	0.2156	0.027	0.040
5	0.2695	0.040	0.059
6	0.3234	0.054	0.062
7	0.3773	0.054	0.065
8	0.4312	0.059	0.081
9	0.4852	0.070	0.094
10	0.5391	0.081	0.108
11	0.5930	0.081	0.121
12	0.6469	0.081	0.135
13	0.7008	0.081	0.162
14	0.7547	0.094	0.175
15	0.8086	0.127	0.210
16	0.8625	0.135	0.248
17	0.9164		0.269
18	0.9434		0.269

Table 4 : Strake vortex core trajectory of the baseline model . $\alpha = 10^\circ$, $\beta = 10^\circ$,
Chord (C) = 9.375 inches

Point No.	X / C	Y / C (Windward)	Y / C (Leeward)
1	0.0539	0.003	0.003
2	0.1078	0.011	0.013
3	0.1617	0.016	0.032
4	0.2156	0.027	0.054
5	0.2695	0.032	0.065
6	0.3234	0.040	0.067
7	0.3773	0.049	0.081
8	0.4312	0.054	0.089
9	0.4852	0.062	0.102
10	0.5391	0.062	0.121
11	0.5930	0.067	0.135
12	0.6469	0.067	0.151
13	0.7008	0.054	0.183
14	0.7547	0.067	0.194
15	0.8086	0.081	0.243
16	0.8625		0.337
17	0.9164		0.350
18	0.9704		0.364

Table 5 : Strake vortex core trajectory of the baseline model . $\alpha = 10^\circ$, $\beta = 15^\circ$,
Chord (C) = 9.375 inches

Point No.	X / C	Y / C (Windward)	Y / C (Leeward)
1	0.0539	0.000	0.013
2	0.1078	0.000	0.028
3	0.1617	0.011	0.038
4	0.2156	0.022	0.043
5	0.2695	0.027	0.070
6	0.3234	0.032	0.075
7	0.3773	0.035	0.081
8	0.4312	0.049	0.108
9	0.4852	0.049	0.108
10	0.5391	0.049	0.135
11	0.5930	0.049	0.135
12	0.6469	0.054	0.162
13	0.7008	0.054	0.189
14	0.7547	0.059	0.377
15	0.8086		0.270
16	0.8625		0.350
17	0.9164		0.377
18	0.9434		0.431
19	0.997		0.458

Table 6 : Strake vortex core trajectory of the baseline model . $\alpha = 15^\circ$, $\beta = 0^\circ$,
Chord (C) = 9.375 inches

Point No.	X / C	Y / C (Windward)	Y / C (Leeward)
1	0.0539	0.005	0.005
2	0.1078	0.013	0.013
3	0.1617	0.027	0.027
4	0.2156	0.032	0.032
5	0.2695	0.040	0.040
6	0.3234	0.054	0.054
7	0.3773	0.059	0.059
8	0.4312	0.067	0.073
9	0.4852	0.081	0.081
10	0.5391	0.086	0.094
11	0.5930	0.094	0.108
12	0.6469	0.108	0.121
13	0.7008	0.108	0.135
14	0.7547	0.108	0.148
15	0.8086	0.135	0.162
16	0.8625	0.162	0.175

Table 7 : Strake vortex core trajectory of the baseline model . $\alpha = 15^\circ$, $\beta = 5^\circ$,
Chord (C) = 9.375 inches

Point No.	X / C	Y / C (Windward)	Y / C (Leeward)
1	0.0539	0.005	0.005
2	0.1078	0.013	0.013
3	0.1617	0.027	0.027
4	0.2156	0.032	0.032
5	0.2695	0.040	0.040
6	0.3234	0.049	0.054
7	0.3773	0.054	0.059
8	0.4312	0.054	0.073
9	0.4852	0.067	0.081
10	0.5391	0.081	0.094
11	0.5930	0.081	0.108
12	0.6469	0.094	0.121
13	0.7008	0.094	0.135
14	0.7547	0.102	0.148
15	0.8086	0.108	0.162
16	0.8356	0.108	0.175
17	0.8625		0.264
18	0.9029		0.283

Table 8 : Strake vortex core trajectory of the baseline model . $\alpha = 15^\circ$, $\beta = 10^\circ$,
Chord (C) = 9.375 inches

Point No.	X / C	Y / C (Windward)	Y / C (Leeward)
1	0.0539	0.005	0.005
2	0.1078	0.013	0.013
3	0.1617	0.022	0.027
4	0.2156	0.027	0.032
5	0.2695	0.032	0.040
6	0.3234	0.040	0.054
7	0.3773	0.054	0.059
8	0.4312	0.054	0.073
9	0.4852	0.054	0.081
10	0.5391	0.054	0.094
11	0.5930	0.054	0.108
12	0.6469	0.054	0.121
13	0.7008	0.054	0.135
14	0.7547	0.067	0.148
15	0.7817	0.081	0.162
16	0.8086		0.175
17	0.8625		0.297
18	0.9164		0.377
19	0.9434		0.391

Table 9 : Strake vortex core trajectory of the baseline model . $\alpha = 15^\circ$, $\beta = 15^\circ$,
Chord (C) = 9.375 inches

Point No.	X / C	Y / C (Windward)	Y / C (Leeward)
1	0.0539	0.000	0.022
2	0.1078	0.000	0.027
3	0.1617	0.013	0.035
4	0.2156	0.027	0.049
5	0.2695	0.027	0.059
6	0.3234	0.027	0.067
7	0.3773	0.027	0.081
8	0.4312	0.027	0.102
9	0.4852	0.032	0.108
10	0.5391	0.027	0.135
11	0.5930	0.022	0.148
12	0.6469	0.022	0.162
13	0.7008	0.027	0.189
14	0.7278	0.040	0.210
15	0.7547		0.216
16	0.8086		0.243
17	0.8625		0.324
18	0.9164		0.391
19	0.9434		0.431
20	0.9704		0.445

Table 10 : Strake vortex core trajectory of the baseline model . $\alpha = 20^\circ$, $\beta = 0^\circ$,
Chord (C) = 9.375 inches

Point No.	X / C	Y / C (Windward)	Y / C (Leeward)
1	0.0539	0.005	0.005
2	0.1078	0.013	0.013
3	0.1617	0.027	0.027
4	0.2156	0.032	0.032
5	0.2695	0.040	0.040
6	0.3234	0.054	0.054
7	0.3773	0.059	0.059
8	0.4312	0.067	0.073
9	0.4852	0.081	0.081
10	0.5391	0.094	0.094
11	0.5930	0.089	0.108
12	0.6469	0.121	0.121
13	0.7008	0.127	0.127
14	0.7143	0.135	0.135

Table 11 : Strake vortex core trajectory of the baseline model . $\alpha = 20^\circ$, $\beta = 5^\circ$,
Chord (C) = 9.375 inches

Point No.	X / C	Y / C (Windward)	Y / C (Leeward)
1	0.0539	0.005	0.005
2	0.1078	0.013	0.013
3	0.1617	0.021	0.032
4	0.2156	0.027	0.032
5	0.2695	0.040	0.054
6	0.3234	0.049	0.059
7	0.3773	0.054	0.067
8	0.4312	0.059	0.081
9	0.4852	0.062	0.097
10	0.5391	0.062	0.108
11	0.5930	0.067	0.130
12	0.6469	0.081	0.140
13	0.7008		0.162
14	0.7547		0.189
15	0.8086		0.216
16	0.8490		0.270

Table 12 : Strake vortex core trajectory of the baseline model . $\alpha = 20^\circ$, $\beta = 10^\circ$,
Chord (C) = 9.375 inches

Point No.	X / C	Y / C (Windward)	Y / C (Leeward)
1	0.0539	0.000	0.008
2	0.1078	0.005	0.013
3	0.1617	0.013	0.040
4	0.2156	0.027	0.040
5	0.2695	0.032	0.054
6	0.3234	0.040	0.067
7	0.3773	0.049	0.075
8	0.4312	0.054	0.086
9	0.4852	0.054	0.108
10	0.5391	0.054	0.116
11	0.5660	0.054	0.135
12	0.5930		0.140
13	0.6469		0.162
14	0.7008		0.189
15	0.7547		0.210
16	0.8086		0.243
17	0.8625		0.296
18	0.9164		0.350

Table 13 : Strake vortex core trajectory of the baseline model . $\alpha = 20^\circ$, $\beta = 15^\circ$,
Chord (C) = 9.375 inches

Point No.	X / C	Y / C (Windward)	Y / C (Leeward)
1	0.0539	0.000	0.008
2	0.1078	0.000	0.013
3	0.1617	0.013	0.040
4	0.2156	0.022	0.040
5	0.2695	0.027	0.054
6	0.3234	0.032	0.067
7	0.3773	0.032	0.081
8	0.4312	0.032	0.102
9	0.4852	0.040	0.113
10	0.5391		0.130
11	0.5930		0.135
12	0.6469		0.175
13	0.7008		0.189
14	0.7547		0.243
15	0.8086		0.264
16	0.8625		0.324
17	0.9164		0.377
18	0.9434		0.431

Table 14 : Strake vortex core trajectory of the baseline model . $\alpha = 25^\circ$, $\beta = 0^\circ$,
Chord (C) = 9.375 inches

Point No.	X / C	Y / C (Windward)	Y / C (Leeward)
1	0.0539	0.005	0.005
2	0.1078	0.013	0.013
3	0.1617	0.027	0.027
4	0.2156	0.032	0.032
5	0.2695	0.040	0.040
6	0.3234	0.054	0.054
7	0.3773	0.059	0.067
8	0.4312	0.067	0.073
9	0.4852	0.081	0.081
10	0.5391	0.086	0.086

Table 15 : Strake vortex core trajectory of the baseline model. $\alpha = 25^\circ$, $\beta = 5^\circ$,
Chord (C) = 9.375 inches

Point No.	X / C	Y / C (Windward)	Y / C (Leeward)
1	0.0539	0.005	0.008
2	0.1078	0.008	0.022
3	0.1617	0.022	0.027
4	0.2156	0.027	0.032
5	0.2695	0.032	0.054
6	0.3234	0.040	0.067
7	0.3773	0.067	0.081
8	0.4312	0.075	0.086
9	0.4852		0.102
10	0.5391		0.113
11	0.5930		0.135
12	0.6469		0.151
13	0.7008		0.167
14	0.7278		0.189

Table 16 : Strake vortex core trajectory of the baseline model . $\alpha = 25^\circ$, $\beta = 10^\circ$,
Chord (C) = 9.375 inches

Point No.	X / C	Y / C (Windward)	Y / C (Leeward)
1	0.0539	0.000	0.008
2	0.1078	0.005	0.013
3	0.1617	0.013	0.027
4	0.2156	0.022	0.040
5	0.2695	0.027	0.054
6	0.3234	0.032	0.067
7	0.3773		0.081
8	0.4312		0.102
9	0.4852		0.108
10	0.5391		0.135
11	0.5930		0.140
12	0.6469		0.162
13	0.7008		0.189
14	0.7547		0.216
15	0.8086		0.237
16	0.8625		0.283

Table 17 : Strake vortex core trajectory of the baseline model . $\alpha = 25^\circ$, $\beta = 15^\circ$,
Chord (C) = 9.375 inches

Point No.	X / C	Y / C (Windward)	Y / C (Leeward)
1	0.0539	0.000	0.013
2	0.1078	0.000	0.022
3	0.1617	0.013	0.035
4	0.2156	0.022	0.043
5	0.2695	0.027	0.054
6	0.3234		0.060
7	0.3773		0.081
8	0.4312		0.102
9	0.4852		0.121
10	0.5391		0.135
11	0.5930		0.162
12	0.6469		0.189
13	0.7008		0.216
14	0.7547		0.243
15	0.8086		0.270
16	0.8625		0.297
17	0.9164		0.324

Table 18 : Strake vortex core trajectory of the baseline model . $\alpha = 30^\circ$, $\beta = 0^\circ$,
Chord (C) = 9.375 inches

Point No.	X / C	Y / C (Windward)	Y / C (Leeward)
1	0.0539	0.005	0.005
2	0.1078	0.013	0.013
3	0.1617	0.027	0.026
4	0.2156	0.032	0.032
5	0.2695	0.040	0.040
6	0.3234	0.054	0.054
7	0.3773	0.067	0.067

Table 19 : Strake vortex core trajectory of the baseline model . $\alpha = 30^\circ$, $\beta = 5^\circ$,
Chord (C) = 9.375 inches

Point No.	X / C	Y / C (Windward)	Y / C (Leeward)
1	0.0539	0.005	0.008
2	0.1078	0.008	0.016
3	0.1617	0.013	0.027
4	0.2156	0.022	0.040
5	0.2695	0.027	0.054
6	0.3234		0.067
7	0.3773		0.081
8	0.4312		0.086
9	0.4852		0.075
10	0.5391		0.108
11	0.5660		0.113

Table 20 : Strake vortex core trajectory of the baseline model . $\alpha = 30^\circ$, $\beta = 10^\circ$,
Chord (C) = 9.375 inches

Point No.	X / C	Y / C (Windward)	Y / C (Leeward)
1	0.0539	0.000	0.008
2	0.1078	0.005	0.022
3	0.1617	0.008	0.032
4	0.2156	0.016	0.049
5	0.2695		0.054
6	0.3234		0.075
7	0.3773		0.081
8	0.4312		0.102
9	0.4852		0.113
10	0.5391		0.124
11	0.5930		0.135
12	0.6469		0.162
13	0.7008		0.189

Table 21 : Strake vortex core trajectory of the baseline model . $\alpha = 30^\circ$, $\beta = 15^\circ$,
Chord (C) = 9.375 inches

Point No.	X / C	Y / C (Windward)	Y / C (Leeward)
1	0.0539	0.000	0.013
2	0.1078	0.000	0.027
3	0.1617	0.000	0.040
4	0.2156		0.054
5	0.2695		0.059
6	0.3234		0.067
7	0.3773		0.086
8	0.4312		0.108
9	0.4852		0.121
10	0.5391		0.135
11	0.5930		0.162
12	0.6469		0.189
13	0.7008		0.202
14	0.7547		0.216
15	0.8086		0.243

Table 22 : Strake vortex core trajectory of the baseline model . $\alpha = 35^\circ$, $\beta = 0^\circ$,
Chord (C) = 9.375 inches

Point No.	X / C	Y / C (Windward)	Y / C (Leeward)
1	0.0539	0.005	0.005
2	0.1078	0.013	0.013
3	0.1617	0.022	0.022
4	0.2156	0.027	0.027
5	0.2695	0.032	0.032

Table 23 : Strake vortex core trajectory of the baseline model . $\alpha = 35^\circ$, $\beta = 5^\circ$,
Chord (C) = 9.375 inches

Point No.	X / C	Y / C (Windward)	Y / C (Leeward)
1	0.0539	0.005	0.011
2	0.1078	0.008	0.022
3	0.1617	0.016	0.026
4	0.2156	0.022	0.040
5	0.2695		0.054
6	0.3234		0.060
7	0.3504		0.067

Table 24 : Strake vortex core trajectory of the baseline model . $\alpha = 35^\circ$, $\beta = 10^\circ$,
Chord (C) = 9.375 inches

Point No.	X / C	Y / C (Windward)	Y / C (Leeward)
1	0.0539	0.000	0.013
2	0.1078	0.008	0.025
3	0.1617	0.011	0.032
4	0.2156		0.040
5	0.2695		0.054
6	0.3234		0.075
7	0.3773		0.081
8	0.4312		0.102
9	0.4582		0.113

Table 25 : Strake vortex core trajectory of the baseline model . $\alpha = 35^\circ$, $\beta = 15^\circ$,
Chord (C) = 9.375 inches

Point No.	X / C	Y / C (Windward)	Y / C (Leeward)
1	0.0539	0.000	0.022
2	0.1078	-0.005	0.027
3	0.1210	-0.013	0.040
4	0.1617		0.049
5	0.2156		0.054
6	0.2695		0.062
7	0.3234		0.073
8	0.3773		0.086
9	0.4312		0.108
10	0.4852		0.121

Table 26 : Strake vortex core trajectory of the baseline model . $\alpha = 40^\circ$, $\beta = 0^\circ$,
Chord (C) = 9.375 inches

Point No.	X / C	Y / C (Windward)	Y / C (Leeward)
1	0.0539	0.005	0.005
2	0.1078	0.013	0.013
3	0.1617	0.022	0.022
4	0.1887	0.027	0.027

Table 27 : Strake vortex core trajectory of the baseline model . $\alpha = 40^\circ$, $\beta = 5^\circ$,
Chord (C) = 9.375 inches

Point No.	X / C	Y / C (Windward)	Y / C (Leeward)
1	0.0539	0.005	0.005
2	0.1078	0.008	0.013
3	0.1348	0.013	0.016
4	0.1617	0.016	0.026
5	0.2156		0.040
6	0.2695		0.049

Table 28 : Strake vortex core trajectory of the baseline model . $\alpha = 40^\circ$, $\beta = 10^\circ$,
Chord (C) = 9.375 inches

Point No.	X / C	Y / C (Windward)	Y / C (Leeward)
1	0.0539	0.000	0.013
2	0.1078	0.003	0.022
3	0.1348	0.003	0.022
4	0.1617		0.032
5	0.2156		0.049
6	0.2695		0.054
7	0.3234		0.060

Table 29 : Strake vortex core trajectory of the baseline model . $\alpha = 40^\circ$, $\beta = 15^\circ$,
Chord (C) = 9.375 inches

Point No.	X / C	Y / C (Windward)	Y / C (Leeward)
1	0.0539	0.000	0.016
2	0.1078	-0.027	0.027
3	0.1617		0.040
4	0.2156		0.059
5	0.2695		0.067
6	0.3234		0.075
7	0.3773		0.086

Table 30 : Strake vortex core trajectory of the baseline model . $\alpha = 45^\circ$, $\beta = 0^\circ$,
Chord (C) = 9.375 inches

Point No.	X / C	Y / C (Windward)	Y / C (Leeward)
1	0.0539	0.005	0.005
2	0.0809	0.008	0.008
3	0.1078	0.008	0.008
4	0.1617	0.016	0.016

Table 31 : Strake vortex core trajectory of the baseline model . $\alpha = 45^\circ$, $\beta = 5^\circ$,
Chord (C) = 9.375 inches

Point No.	X / C	Y / C (Windward)	Y / C (Leeward)
1	0.0539	0.000	0.000
2	0.0809	0.003	0.011
3	0.1348	0.005	0.016
4	0.1617		0.027
5	0.2156		0.043

Table 32 : Strake vortex core trajectory of the baseline model . $\alpha = 45^\circ$, $\beta = 10^\circ$,
Chord (C) = 9.375 inches

Point No.	X / C	Y / C (Windward)	Y / C (Leeward)
1	0.0539	0.000	0.013
2	0.0809	0.003	0.022
3	0.1210	-0.005	0.027
4	0.1617		0.032
5	0.2156		0.040
6	0.2695		0.054

Table 33 : Strake vortex core trajectory of the baseline model . $\alpha = 45^\circ$, $\beta = 15^\circ$,
Chord (C) = 9.375 inches

Point No.	X / C	Y / C (Windward)	Y / C (Leeward)
1	0.0539	0.003	0.022
2	0.0809	-0.008	0.027
3	0.1078	-0.013	0.032
4	0.1617		0.038
5	0.2156		0.054
6	0.2695		0.059
7	0.3234		0.065

Table 34 : Strake vortex core trajectory of the baseline model . $\alpha = 50^\circ$, $\beta = 0^\circ$,
Chord (C) = 9.375 inches

Point No.	X / C	Y / C (Windward)	Y / C (Leeward)
1	0.0539	0.000	0.000
2	0.0809	0.000	0.000
3	0.1078	0.000	0.000
4	0.1210	0.000	0.000

Table 35 : Strake vortex core trajectory of the baseline model . $\alpha = 50^\circ$, $\beta = 5^\circ$,
Chord (C) = 9.375 inches

Point No.	X / C	Y / C (Windward)	Y / C (Leeward)
1	0.0539	0.000	0.013
2	0.0809	0.000	0.016
3	0.1078	0.000	0.022
4	0.1617		0.027

Table 36 : Strake vortex core trajectory of the baseline model . $\alpha = 50^\circ$, $\beta = 10^\circ$,
Chord (C) = 9.375 inches

Point No.	X / C	Y / C (Windward)	Y / C (Leeward)
1	0.0270	0.000	0.000
2	0.0539	0.000	0.000
3	0.0809	0.000	0.000
4	0.1078		0.027
5	0.1617		0.032
6	0.2156		0.040
7	0.2426		0.054

Table 37 : Strake vortex core trajectory of the baseline model . $\alpha = 50^\circ$, $\beta = 15^\circ$,
Chord (C) = 9.375 inches

Point No.	X / C	Y / C (Windward)	Y / C (Leeward)
1	0.0270	0.000	0.022
2	0.0539	-0.022	0.027
3	0.0809		0.040
4	0.1348		0.054
5	0.1887		0.067
6	0.2426		0.081
7	0.2965		0.086

Table 38 : Wing vortex core trajectory of the baseline model . $\alpha = 10^\circ$, $\beta = 0^\circ$,
Chord (C) = 9.375 inches

Point No.	X / C	Y / C (Windward)	Y / C (Leeward)
1	0.5391	0.148	0.022
2	0.5930	0.102	0.032
3	0.6469	0.086	0.038
4	0.7008	0.108	0.054
5	0.7574	0.143	0.143
6	0.8086	0.162	0.162
7	0.8625	0.162	0.162
8	0.9164	0.148	0.148
9	0.9434	0.135	0.135

Table 39 : Wing vortex core trajectory of the baseline model . $\alpha = 10^\circ$, $\beta = 5^\circ$,
Chord (C) = 9.375 inches

Point No.	X / C	Y / C (Windward)	Y / C (Leeward)
1	0.5391	0.148	0.148
2	0.5930	0.121	0.135
3	0.6469	0.094	0.121
4	0.7008	0.067	0.148
5	0.7574	0.054	0.194
6	0.8086	0.054	0.216
7	0.8356	0.054	0.216
8	0.8625		0.210
9	0.9164		0.221
10	0.9434		0.237
11	0.9704		0.297

Table 40 : Wing vortex core trajectory of the baseline model . $\alpha = 10^\circ$, $\beta = 10^\circ$,
Chord (C) = 9.375 inches

Point No.	X / C	Y / C (Windward)	Y / C (Leeward)
1	0.5391	0.148	0.148
2	0.5930	0.130	0.143
3	0.6469	0.108	0.135
4	0.6736	0.108	0.143
5	0.7008	0.108	0.156
6	0.7547		0.189
7	0.8086		0.256
8	0.8625		0.310
9	0.9164		0.302
10	0.9704		0.324
11	1.0000		0.135

Table 41 : Wing vortex core trajectory of the baseline model . $\alpha = 10^\circ$, $\beta = 15^\circ$,
Chord (C) = 9.375 inches

Point No.	X / C	Y / C (Windward)	Y / C (Leeward)
1	0.5391	0.148	0.148
2	0.5930	0.116	0.146
3	0.6469	0.108	0.151
4	0.7008		0.162
5	0.7574		0.202
6	0.8086		0.216
7	0.8625		0.278
8	0.9164		0.350
9	0.9704		0.372
10	1.0000		0.391

Table 42 : Wing vortex core trajectory of the baseline model . $\alpha = 15^\circ$, $\beta = 0^\circ$,
Chord (C) = 9.375 inches

Point No.	X / C	Y / C (Windward)	Y / C (Leeward)
1	0.5391	0.148	0.148
2	0.5930	0.108	0.108
3	0.6469	0.081	0.081
4	0.7008	0.094	0.094
5	0.7574	0.135	0.135
6	0.8086	0.162	0.162
7	0.8356	0.167	0.167

Table 43 : Wing vortex core trajectory of the baseline model . $\alpha = 15^\circ$, $\beta = 5^\circ$,
Chord (C) = 9.375 inches

Point No.	X / C	Y / C (Windward)	Y / C (Leeward)
1	0.5391	0.148	0.148
2	0.5930	0.130	0.140
3	0.6469	0.108	0.130
4	0.7008	0.094	0.135
5	0.7574		0.189
6	0.8086		0.216
7	0.8625		0.216
8	0.8895		0.216

Table 44 : Wing vortex core trajectory of the baseline model . $\alpha = 15^\circ$, $\beta = 10^\circ$,
Chord (C) = 9.375 inches

Point No.	X / C	Y / C (Windward)	Y / C (Leeward)
1	0.5391	0.148	0.148
2	0.5930	0.121	0.140
3	0.6200	0.102	0.135
4	0.6469		0.135
5	0.7008		0.143
6	0.7547		0.189
7	0.8086		0.264
8	0.8625		0.283
9	0.9164		0.297

Table 45 : Wing vortex core trajectory of the baseline model . $\alpha = 15^\circ$, $\beta = 15^\circ$,
Chord (C) = 9.375 inches

Point No.	X / C	Y / C (Windward)	Y / C (Leeward)
1	0.5391	0.148	0.148
2	0.5930	0.108	0.162
3	0.6469		0.162
4	0.7008		0.162
5	0.7574		0.175
6	0.8086		0.216
7	0.8625		0.305
8	0.9164		0.350
9	0.9704		0.377
10	1.0000		0.404

Table 46 : Wing vortex core trajectory of the baseline model . $\alpha = 20^\circ$, $\beta = 0^\circ$,
Chord (C) = 9.375 inches

Point No.	X / C	Y / C (Windward)	Y / C (Leeward)
1	0.5391	0.148	0.148
2	0.5930	0.121	0.121
3	0.6200	0.086	0.086
4	0.6469	0.054	0.054
5	0.6739	0.049	0.049
6	0.7008	0.054	0.054
7	0.7278	0.094	0.094
8	0.7574	0.108	0.108
9	0.7817	0.081	0.081

Table 47 : Wing vortex core trajectory of the baseline model . $\alpha = 20^\circ$, $\beta = 5^\circ$,
Chord (C) = 9.375 inches

Point No.	X / C	Y / C (Windward)	Y / C (Leeward)
1	0.5391	0.148	0.148
2	0.5930	0.116	0.135
3	0.6469	0.049	0.081
4	0.6739	0.043	0.067
5	0.7008	0.049	0.081
6	0.7278		0.108
7	0.7547		0.135
8	0.8086		0.216
9	0.8625		0.243

Table 48 : Wing vortex core trajectory of the baseline model . $\alpha = 20^\circ$, $\beta = 10^\circ$,
Chord (C) = 9.375 inches

Point No.	X / C	Y / C (Windward)	Y / C (Leeward)
1	0.5391	0.148	0.480
2	0.5930	0.108	0.140
3	0.6200	0.067	0.135
4	0.6469		0.135
5	0.6739		0.135
6	0.7008		0.148
7	0.7278		0.162
8	0.7547		0.189
9	0.8086		0.243
10	0.8625		0.283
11	0.9164		0.297

Table 49 : Wing vortex core trajectory of the baseline model . $\alpha = 20^\circ$, $\beta = 15^\circ$,
Chord (C) = 9.375 inches

Point No.	X / C	Y / C (Windward)	Y / C (Leeward)
1	0.5391	0.148	0.148
2	0.5930	0.081	0.148
3	0.6469		0.135
4	0.7008		0.162
5	0.7547		0.189
6	0.8086		0.270
7	0.8625		0.324
8	0.9164		0.350
9	0.9704		0.364
10	1.0000		0.364

Table 50 : Wing vortex core trajectory of the baseline model . $\alpha = 25^\circ$, $\beta = 0^\circ$,
Chord (C) = 9.375 inches

Point No.	X / C	Y / C (Windward)	Y / C (Leeward)
1	0.5391	0.148	0.148
2	0.5930	0.121	0.121
3	0.6469	0.121	0.121
4	0.6739	0.086	0.086
5	0.7008	0.108	0.108

Table 51 : Wing vortex core trajectory of the baseline model . $\alpha = 25^\circ$, $\beta = .5^\circ$,
Chord (C) = 9.375 inches

Point No.	X / C	Y / C (Windward)	Y / C (Leeward)
1	0.5391	0.148	0.148
2	0.5930	0.162	0.135
3	0.6200	0.162	0.108
4	0.6469		0.102
5	0.7008		0.094
6	0.7547		0.094
7	0.8086		0.108

Table 52 : Wing vortex core trajectory of the baseline model . $\alpha = 25^\circ$, $\beta = 10^\circ$,
Chord (C) = 9.375 inches

Point No.	X / C	Y / C (Windward)	Y / C (Leeward)
1	0.5391	0.148	0.148
2	0.5660	0.148	0.202
3	0.5930		0.202
4	0.6469		0.243
5	0.7008		0.264
6	0.7547		0.270
7	0.8086		0.270
8	0.8625		0.283

Table 53 : Wing vortex core trajectory of the baseline model . $\alpha = 25^\circ$, $\beta = 15^\circ$,
Chord (C) = 9.375 inches

Point No.	X / C	Y / C (Windward)	Y / C (Leeward)
1	0.5391	0.148	0.148
2	0.5930		0.210
3	0.6469		0.243
4	0.7008		0.297
5	0.7574		0.324
6	0.8086		0.324
7	0.8625		0.350
8	0.9164		0.377
9	0.9704		0.391
10	1.0000		0.391

Table 54 : Strake vortex core trajectory of the diamond-fillet model . $\alpha = 10^\circ$, $\beta = 0^\circ$,
Chord (C) = 9.375 inches

Point No.	X / C	Y / C (Windward)	Y / C (Leeward)
1	0.0539	0.003	0.003
2	0.1078	0.005	0.005
3	0.1617	0.013	0.013
4	0.2156	0.027	0.027
5	0.2695	0.040	0.040
6	0.3235	0.054	0.054
7	0.3774	0.059	0.059
8	0.4313	0.067	0.067
9	0.4852	0.081	0.081
10	0.5391	0.094	0.094
11	0.5930	0.108	0.108
12	0.6469	0.121	0.121
13	0.7008	0.135	0.135
14	0.7547	0.162	0.162
15	0.8086	0.175	0.175
16	0.8625	0.189	0.189
17	0.9164	0.202	0.202
18	0.9704	0.216	0.216

Table 55 : Strake vortex core trajectory of the diamond-fillet model. $\alpha = 10^\circ$, $\beta = 5^\circ$,
Chord (C) = 9.375 inches

Point No.	X / C	Y / C (Windward)	Y / C (Leeward)
1	0.0539	0.003	0.003
2	0.1078	0.005	0.005
3	0.1617	0.013	0.013
4	0.2156	0.027	0.040
5	0.2695	0.040	0.040
6	0.3235	0.054	0.054
7	0.3774	0.054	0.067
8	0.4313	0.059	0.081
9	0.4852	0.081	0.102
10	0.5391	0.086	0.108
11	0.5930	0.094	0.130
12	0.6469	0.108	0.135
13	0.7008	0.121	0.162
14	0.7547	0.135	0.189
15	0.8086	0.140	0.202
16	0.8625	0.148	0.216
17	0.9164	0.162	0.229
18	0.9434	0.162	0.243
19	1.0000		0.297

Table 56 : Strake vortex core trajectory of the diamond-fillet model. $\alpha = 10^\circ$, $\beta = 10^\circ$,
Chord (C) = 9.375 inches

Point No.	X / C	Y / C (Windward)	Y / C (Leeward)
1	0.0539	0.003	0.005
2	0.1078	0.005	0.013
3	0.1617	0.013	0.027
4	0.2156	0.027	0.049
5	0.2695	0.032	0.054
6	0.3235	0.049	0.067
7	0.3774	0.054	0.067
8	0.4313	0.054	0.081
9	0.4852	0.054	0.108
10	0.5391	0.059	0.113
11	0.5930	0.059	0.135
12	0.6469	0.067	0.162
13	0.7008	0.081	0.189
14	0.7547	0.081	0.202
15	0.8086	0.094	0.216
16	0.8625	0.108	0.243
17	0.9164	0.108	0.297
18	0.9704		0.310
19	1.0000		0.324

Table 57 : Strake vortex core trajectory of the diamond-fillet model. $\alpha = 10^\circ$, $\beta = 15^\circ$,
Chord (C) = 9.375 inches

Point No.	X / C	Y / C (Windward)	Y , C (Leeward)
1	0.0539	0.000	0.013
2	0.1078	0.003	0.022
3	0.1617	0.005	0.027
4	0.2156	0.022	0.054
5	0.2695	0.027	0.059
6	0.3235	0.032	0.075
7	0.3774	0.049	0.081
8	0.4313	0.049	0.094
9	0.4852	0.054	0.108
10	0.5391	0.054	0.121
11	0.5930	0.054	0.135
12	0.6469	0.054	0.175
13	0.7008	0.054	0.189
14	0.7547	0.054	0.216
15	0.8086	0.054	0.243
16	0.8625	0.054	0.270
17	0.8895	0.054	0.270
18	0.9164		0.324
19	0.9704		0.337
20	1.0000		0.350

Table 58 : Strake vortex core trajectory of the diamond-fillet model. $\alpha = 15^\circ$, $\beta = 0^\circ$,
Chord (C) = 9.375 inches

Point No.	X / C	Y / C (Windward)	Y / C (Leeward)
1	0.0539	0.003	0.003
2	0.1078	0.005	0.005
3	0.1617	0.013	0.013
4	0.2156	0.027	0.027
5	0.2695	0.054	0.054
6	0.3235	0.054	0.054
7	0.3774	0.067	0.067
8	0.4313	0.067	0.067
9	0.4852	0.081	0.081
10	0.5391	0.081	0.081
11	0.5930	0.108	0.108
12	0.6469	0.108	0.108
13	0.7008	0.135	0.135
14	0.7547	0.162	0.162
15	0.8086	0.189	0.189
16	0.8625	0.216	0.216
17	0.9164	0.229	0.229

Table 59 : Strake vortex core trajectory of the diamond-fillet model. $\alpha = 15^\circ$, $\beta = 5^\circ$,
Chord (C) = 9.375 inches

Point No.	X / C	Y / C (Windward)	Y / C (Leeward)
1	0.0539	0.003	0.003
2	0.1078	0.005	0.005
3	0.1617	0.013	0.013
4	0.2156	0.022	0.040
5	0.2695	0.040	0.049
6	0.3235	0.054	0.059
7	0.3774	0.054	0.067
8	0.4313	0.067	0.081
9	0.4852	0.067	0.081
10	0.5391	0.081	0.108
11	0.5930	0.081	0.113
12	0.6469	0.102	0.135
13	0.7008	0.108	0.162
14	0.7547	0.121	0.175
15	0.8086	0.135	0.189
16	0.8625	0.162	0.270
17	0.9164		0.297
18	0.9434		0.310

Table 60 : Strake vortex core trajectory of the diamond-fillet model. $\alpha = 15^\circ$, $\beta = 10^\circ$,
Chord (C) = 9.375 inches

Point No.	X / C	Y / C (Windward)	Y / C (Leeward)
1	0.0539	0.003	0.003
2	0.1078	0.005	0.013
3	0.1617	0.013	0.027
4	0.2156	0.022	0.040
5	0.2695	0.027	0.040
6	0.3235	0.040	0.054
7	0.3774	0.054	0.067
8	0.4313	0.054	0.081
9	0.4852	0.059	0.086
10	0.5391	0.059	0.108
11	0.5930	0.067	0.135
12	0.6469	0.075	0.148
13	0.7008	0.081	0.189
14	0.7547	0.094	0.216
15	0.8086	0.102	0.216
16	0.8625		0.270
17	0.9164		0.324
18	0.9704		0.324

Table 61 : Strake vortex core trajectory of the diamond-fillet model. $\alpha = 15^\circ$, $\beta = 15^\circ$,
Chord (C) = 9.375 inches

Point No.	X / C	Y / C (Windward)	Y / C (Leeward)
1	0.0539	0.000	0.013
2	0.1078	0.003	0.022
3	0.1617	0.005	0.027
4	0.2156	0.013	0.049
5	0.2695	0.027	0.049
6	0.3235	0.049	0.065
7	0.3774	0.054	0.075
8	0.4313	0.054	0.086
9	0.4852	0.054	0.102
10	0.5391	0.054	0.113
11	0.5930	0.054	0.135
12	0.6469	0.054	0.162
13	0.7008	0.067	0.189
14	0.7547	0.081	0.243
15	0.7817	0.081	0.243
16	0.8086		0.297
17	0.8625		0.350
18	0.9164		0.350
19	0.9704		0.350
20	1.0000		0.350

Table 62 : Strake vortex core trajectory of the diamond-fillet model. $\alpha = 20^\circ$, $\beta = 0^\circ$,
Chord (C) = 9.375 inches

Point No.	X / C	Y / C (Windward)	Y / C (Leeward)
1	0.0539	0.005	0.005
2	0.1078	0.013	0.013
3	0.1617	0.027	0.027
4	0.2156	0.040	0.040
5	0.2695	0.054	0.054
6	0.3235	0.059	0.059
7	0.3774	0.067	0.067
8	0.4313	0.081	0.081
9	0.4852	0.086	0.086
10	0.5391	0.094	0.094
11	0.5930	0.108	0.108
12	0.6469	0.116	0.116
13	0.7008	0.143	0.143
14	0.7547	0.148	0.148
15	0.7817	0.156	0.156

Table 63 : Strake vortex core trajectory of the diamond-fillet model. $\alpha = 20^\circ$, $\beta = 5^\circ$,
Chord (C) = 9.375 inches

Point No.	X / C	Y / C (Windward)	Y / C (Leeward)
1	0.0539	0.003	0.003
2	0.1078	0.005	0.013
3	0.1617	0.022	0.027
4	0.2156	0.032	0.040
5	0.2695	0.040	0.054
6	0.3235	0.049	0.059
7	0.3774	0.059	0.070
8	0.4313	0.067	0.081
9	0.4852	0.067	0.089
10	0.5391	0.081	0.102
11	0.5930	0.081	0.108
12	0.6469	0.086	0.135
13	0.7008	0.094	0.162
14	0.7547		0.197
15	0.8086		0.202
16	0.8625		0.243

Table 64 : Strake vortex core trajectory of the diamond-fillet model. $\alpha = 20^\circ$, $\beta = 10^\circ$,
Chord (C) = 9.375 inches

Point No.	X / C	Y / C (Windward)	Y / C (Leeward)
1	0.0539	0.003	0.003
2	0.1078	0.005	0.013
3	0.1617	0.013	0.027
4	0.2156	0.022	0.040
5	0.2695	0.040	0.054
6	0.3235	0.049	0.067
7	0.3774	0.054	0.075
8	0.4313	0.054	0.086
9	0.4852	0.054	0.108
10	0.5391	0.054	0.113
11	0.5930	0.059	0.135
12	0.6469	0.067	0.162
13	0.7008		0.175
14	0.7547		0.216
15	0.8086		0.243
16	0.8625		0.297
17	0.9164		0.324

Table 65 : Strake vortex core trajectory of the diamond-fillet model. $\alpha = 20^\circ$, $\beta = 15^\circ$,
Chord (C) = 9.375 inches

Point No.	X / C	Y / C (Windward)	Y / C (Leeward)
1	0.0539	0.000	0.013
2	0.1078	0.003	0.022
3	0.1617	0.008	0.032
4	0.2156	0.019	0.040
5	0.2695	0.027	0.054
6	0.3235	0.032	0.067
7	0.3774	0.040	0.081
8	0.4313	0.049	0.094
9	0.4852	0.049	0.121
10	0.5391	0.054	0.135
11	0.5930		0.148
12	0.6469		0.162
13	0.7008		0.202
14	0.7547		0.229
15	0.8086		0.256
16	0.8625		0.297
17	0.9164		0.337
18	0.9704		0.377
19	1.0000		0.391

Table 66 : Strake vortex core trajectory of the diamond-fillet model. $\alpha = 25^\circ$, $\beta = 0^\circ$,
Chord (C) = 9.375 inches

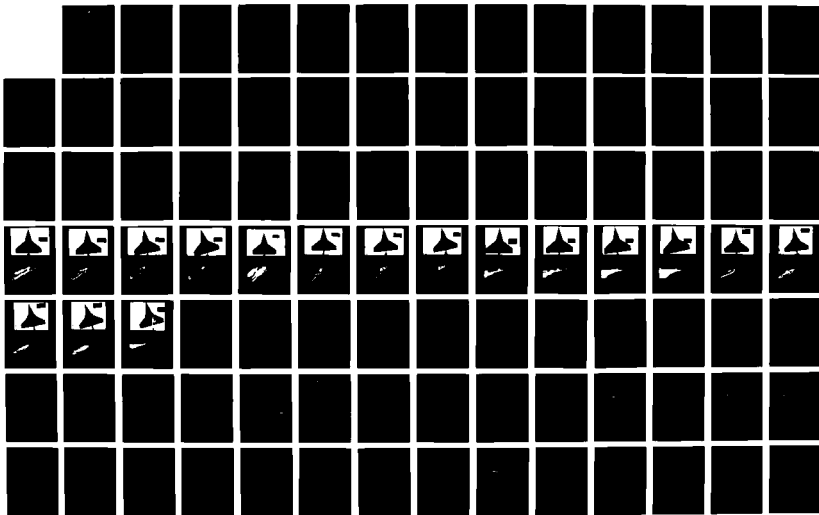
Point No.	X / C	Y / C (Windward)	Y / C (Leeward)
1	0.0539	0.005	0.005
2	0.1078	0.013	0.013
3	0.1617	0.027	0.027
4	0.2156	0.032	0.032
5	0.2695	0.049	0.049
6	0.3235	0.059	0.059
7	0.3774	0.067	0.067
8	0.4313	0.075	0.075
9	0.4852	0.081	0.081
10	0.5391	0.086	0.086
11	0.5930	0.094	0.102

AD-A286 185

EFFECT OF JUNCTURE FILLETS ON DOUBLE-DELTA WINGS
UNDERGOING SIDESLIP AT HIGH ANGLES OF ATTACK(U) NAVAL
POSTGRADUATE SCHOOL MONTEREY CA W CHANG SEP 94 X8-NPS

UNCLASSIFIED

NL



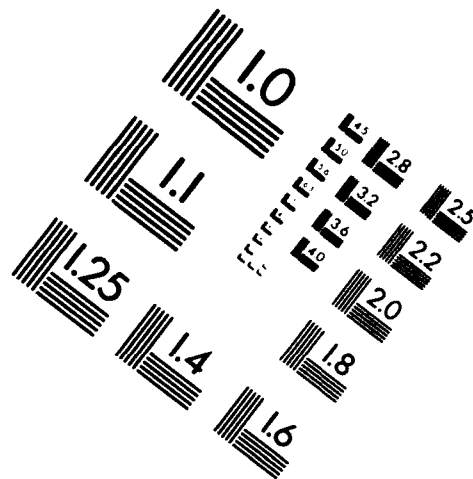
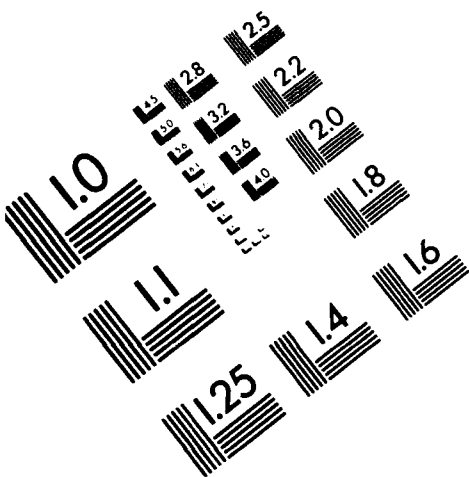


AIM

Association for Information and Image Management

1100 Wayne Avenue, Suite 1100
Silver Spring, Maryland 20910

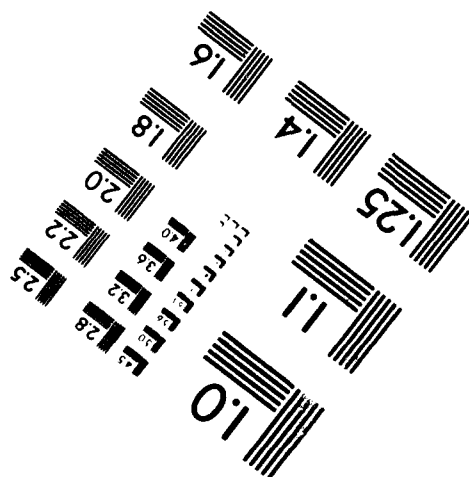
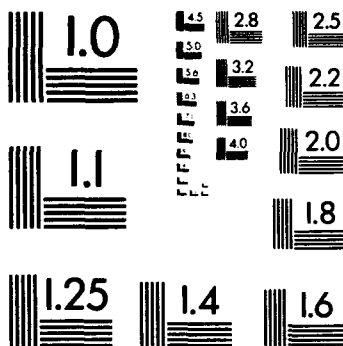
301/587-8202



Centimeter



Inches



MANUFACTURED TO AIM STANDARDS
BY APPLIED IMAGE, INC.

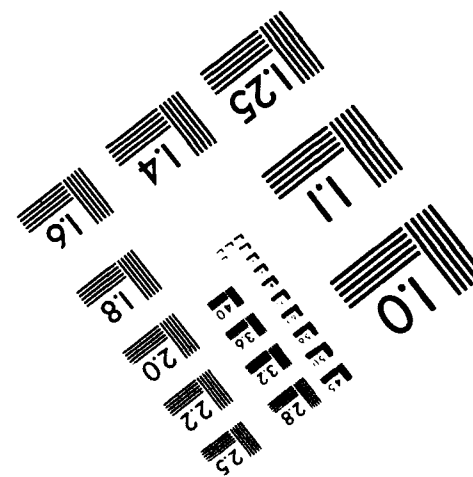


Table 67 : Strake vortex core trajectory of the diamond-fillet model. $\alpha = 25^\circ$, $\beta = 5^\circ$,
Chord (C) = 9.375 inches

Point No.	X / C	Y / C (Windward)	Y / C (Leeward)
1	0.0539	0.003	0.003
2	0.1078	0.005	0.013
3	0.1617	0.013	0.027
4	0.2156	0.022	0.032
5	0.2695	0.027	0.040
6	0.3235	0.027	0.054
7	0.3774	0.043	0.070
8	0.4313	0.054	0.081
9	0.4852	0.054	0.094
10	0.5391		0.102
11	0.5930		0.121
12	0.6469		0.135
13	0.7008		0.162
14	0.7547		0.175

Table 68 : Strake vortex core trajectory of the diamond-fillet model. $\alpha = 25^\circ$, $\beta = 10^\circ$,
Chord (C) = 9.375 inches

Point No.	X / C	Y / C (Windward)	Y / C (Leeward)
1	0.0539	0.003	0.008
2	0.1078	0.005	0.022
3	0.1617	0.013	0.032
4	0.2156	0.016	0.040
5	0.2695	0.027	0.054
6	0.3235	0.027	0.054
7	0.3774	0.032	0.081
8	0.4313	0.032	0.094
9	0.4852		0.108
10	0.5391		0.135
11	0.5930		0.148
12	0.6469		0.162
13	0.7008		0.189
14	0.7547		0.216
15	0.8086		0.229
16	0.8625		0.270

Table 69 : Strake vortex core trajectory of the diamond-fillet model. $\alpha = 25^\circ$, $\beta = 15^\circ$,
Chord (C) = 9.375 inches

Point No.	X / C	Y / C (Windward)	Y / C (Leeward)
1	0.0539	0.000	0.013
2	0.1078	0.003	0.022
3	0.1617	0.005	0.032
4	0.2156	0.013	0.040
5	0.2695	0.027	0.040
6	0.3235	0.027	0.067
7	0.3774	0.032	0.081
8	0.4313		0.094
9	0.4852		0.108
10	0.5391		0.135
11	0.5930		0.135
12	0.6469		0.162
13	0.7008		0.189
14	0.7547		0.216
15	0.8086		0.243
16	0.8625		0.267
17	0.9164		0.297

Table 70 : Strake vortex core trajectory of the diamond-fillet model. $\alpha = 30^\circ$, $\beta = 0^\circ$,
Chord (C) = 9.375 inches

Point No.	X / C	Y / C (Windward)	Y / C (Leeward)
1	0.0539	0.005	0.005
2	0.1078	0.013	0.013
3	0.1617	0.027	0.027
4	0.2156	0.032	0.032
5	0.2695	0.043	0.043
6	0.3235	0.049	0.049
7	0.3774	0.054	0.054
8	0.4313	0.054	0.054

Table 71 : Strake vortex core trajectory of the diamond-fillet model. $\alpha = 30^\circ$, $\beta = 5^\circ$,
Chord (C) = 9.375 inches

Point No.	X / C	Y / C (Windward)	Y / C (Leeward)
1	0.0539	0.005	0.013
2	0.1078	0.013	0.022
3	0.1617	0.022	0.032
4	0.2156	0.027	0.040
5	0.2695	0.032	0.049
6	0.3235	0.038	0.054
7	0.3504	0.040	0.067
8	0.3774		0.067
9	0.4313		0.075
10	0.4852		0.081
11	0.5391		0.086
12	0.5930		0.094

Table 72 : Strake vortex core trajectory of the diamond-fillet model. $\alpha = 30^\circ$, $\beta = 10^\circ$,
Chord (C) = 9.375 inches

Point No.	X / C	Y / C (Windward)	Y / C (Leeward)
1	0.0539	0.003	0.008
2	0.1078	0.005	0.022
3	0.1617	0.013	0.032
4	0.2156	0.022	0.040
5	0.2695	0.022	0.054
6	0.3235		0.059
7	0.3774		0.081
8	0.4313		0.094
9	0.4852		0.108
10	0.5391		0.121
11	0.5930		0.135
12	0.6469		0.148
13	0.7008		0.162
14	0.7278		0.167

Table 73 : Strake vortex core trajectory of the diamond-fillet model. $\alpha = 30^\circ$, $\beta = 15^\circ$,
Chord (C) = 9.375 inches

Point No.	X / C	Y / C (Windward)	Y / C (Leeward)
1	0.0539	0.000	0.013
2	0.1078	0.000	0.022
3	0.1617	0.000	0.032
4	0.2156	0.000	0.040
5	0.2426	0.000	0.049
6	0.2695		0.054
7	0.3235		0.067
8	0.3774		0.086
9	0.4313		0.102
10	0.4852		0.108
11	0.5391		0.135
12	0.5930		0.148
13	0.6469		0.162
14	0.7008		0.175
15	0.7547		0.189
16	0.8086		0.202
17	0.8356		0.216

Table 74 : Strake vortex core trajectory of the diamond-fillet model. $\alpha = 35^\circ$, $\beta = 0^\circ$,
Chord (C) = 9.375 inches

Point No.	X / C	Y / C (Windward)	Y / C (Leeward)
1	0.0539	0.003	0.003
2	0.1078	0.008	0.008
3	0.1617	0.016	0.016
4	0.2156	0.027	0.027
5	0.2695	0.032	0.032
6	0.3235	0.032	0.032

Table 75 : Strake vortex core trajectory of the diamond-fillet model . $\alpha = 35^\circ$, $\beta = 5^\circ$,
Chord (C) = 9.375 inches

Point No.	X / C	Y / C (Windward)	Y / C (Leeward)
1	0.0539	0.003	0.013
2	0.1078	0.005	0.022
3	0.1617	0.013	0.027
4	0.2156	0.022	0.032
5	0.2426	0.022	0.040
6	0.2695		0.049
7	0.3235		0.054
8	0.3774		0.067

Table 76 : Strake vortex core trajectory of the diamond-fillet model. $\alpha = 35^\circ$, $\beta = 10^\circ$,
Chord (C) = 9.375 inches

Point No.	X / C	Y / C (Windward)	Y / C (Leeward)
1	0.0539	0.000	0.013
2	0.1078	0.000	0.022
3	0.1617	0.000	0.027
4	0.1887	0.000	0.027
5	0.2156		0.040
6	0.2695		0.054
7	0.3235		0.067
8	0.3774		0.081
9	0.4313		0.086
10	0.4852		0.092

Table 77 : Strake vortex core trajectory of the diamond-fillet model. $\alpha = 35^\circ$, $\beta = 15^\circ$,
Chord (C) = 9.375 inches

Point No.	X / C	Y / C (Windward)	Y / C (Leeward)
1	0.0539	0.000	0.013
2	0.1078	0.000	0.022
3	0.1617	-0.013	0.027
4	0.2156		0.054
5	0.2695		0.059
6	0.3235		0.075
7	0.3774		0.086
8	0.4313		0.094
9	0.4852		0.108
10	0.5391		0.121

Table 78 : Strake vortex core trajectory of the diamond-fillet model . $\alpha = 40^\circ$, $\beta = 0^\circ$,
Chord (C) = 9.375 inches

Point No.	X / C	Y / C (Windward)	Y / C (Leeward)
1	0.0539	0.008	0.008
2	0.1078	0.013	0.013
3	0.1617	0.016	0.016
4	0.2156	0.027	0.027
5	0.2426	0.032	0.032

Table 79 : Strake vortex core trajectory of the diamond-fillet model . $\alpha = 40^\circ$, $\beta = 5^\circ$,
Chord (C) = 9.375 inches

Point No.	X / C	Y / C (Windward)	Y / C (Leeward)
1	0.0539	0.005	0.011
2	0.1078	0.008	0.016
3	0.1617	0.011	0.022
4	0.1887	0.013	0.032
5	0.2156		0.040
6	0.2695		0.040
7	0.2965		0.046

Table 80 : Strake vortex core trajectory of the diamond-fillet model. $\alpha = 40^\circ$, $\beta = 10^\circ$,
Chord (C) = 9.375 inches

Point No.	X / C	Y / C (Windward)	Y / C (Leeward)
1	0.0539	0.003	0.013
2	0.1078	0.005	0.022
3	0.1348	0.005	0.022
4	0.1480	0.008	0.027
5	0.1617		0.027
6	0.2156		0.040
7	0.2695		0.054
8	0.3235		0.059
9	0.3504		0.065

Table 81 : Strake vortex core trajectory of the diamond-fillet model. $\alpha = 40^\circ$, $\beta = 15^\circ$,
Chord (C) = 9.375 inches

Point No.	X / C	Y / C (Windward)	Y / C (Leeward)
1	0.0539	0.000	0.016
2	0.1078	- 0.003	0.027
3	0.1348	-0.005	0.035
4	0.1617		0.035
5	0.2156		0.049
6	0.2695		0.065
7	0.3235		0.081
8	0.3774		0.094
9	0.4313		0.102

Table 82 : Strake vortex core trajectory of the diamond-fillet model. $\alpha = 45^\circ$, $\beta = 0^\circ$,
Chord (C) = 9.375 inches

Point No.	X / C	Y / C (Windward)	Y / C (Leeward)
1	0.0539	0.003	0.003
2	0.1078	0.005	0.005
3	0.1617	0.008	0.008
4	0.1887	0.008	0.008

Table 83 : Strake vortex core trajectory of the diamond-fillet model. $\alpha = 45^\circ$, $\beta = 5^\circ$,
Chord (C) = 9.375 inches

Point No.	X / C	Y / C (Windward)	Y / C (Leeward)
1	0.0539	0.000	0.013
2	0.1078	0.003	0.022
3	0.1480	0.005	0.027
4	0.1617		0.027
5	0.2156		0.032
6	0.2426		0.040

Table 84 : Strake vortex core trajectory of the diamond-fillet model. $\alpha = 45^\circ$, $\beta = 10^\circ$,
Chord (C) = 9.375 inches

Point No.	X / C	Y / C (Windward)	Y / C (Leeward)
1	0.0539	0.000	0.013
2	0.1078	0.000	0.022
3	0.1210	0.000	0.027
4	0.1617		0.032
5	0.2156		0.040
6	0.2695		0.049
7	0.2965		0.054

Table 85 : Strake vortex core trajectory of the diamond-fillet model. $\alpha = 45^\circ$, $\beta = 15^\circ$,
Chord (C) = 9.375 inches

Point No.	X / C	Y / C (Windward)	Y / C (Leeward)
1	0.0539	0.000	0.016
2	0.1078	-0.005	0.027
3	0.1617		0.032
4	0.2156		0.054
5	0.2695		0.067
6	0.3235		0.075

Table 86 : Strake vortex core trajectory of the diamond-fillet model. $\alpha = 50^\circ$, $\beta = 0^\circ$,
Chord (C) = 9.375 inches

Point No.	X / C	Y / C (Windward)	Y / C (Leeward)
1	0.0539	0.000	0.000
2	0.1078	0.005	0.005
3	0.1617	0.000	0.000

Table 87 : Strake vortex core trajectory of the diamond-fillet model. $\alpha = 50^\circ$, $\beta = 5^\circ$,
Chord (C) = 9.375 inches

Point No.	X / C	Y / C (Windward)	Y / C (Leeward)
1	0.0539	0.000	0.000
2	0.1078	0.000	0.000
3	0.1348	0.000	0.000
4	0.1617		0.013
5	0.2156		0.013

Table 88 : Strake vortex core trajectory of the diamond-fillet model. $\alpha = 50^\circ$, $\beta = 10^\circ$,
Chord (C) = 9.375 inches

Point No.	X / C	Y / C (Windward)	Y / C (Leeward)
1	0.0539	0.000	0.013
2	0.1078	-0.005	0.022
3	0.1617	0.000	0.027
4	0.2156		0.032
5	0.2426		0.032
6	0.2695		0.054

**Table 89 : Strake vortex core trajectory of the diamond-fillet model. $\alpha = 50^\circ$, $\beta = 15^\circ$.
Chord (C) = 9.375 inches**

Point No.	X / C	Y / C (Windward)	Y / C (Leeward)
1	0.0539	- 0.005	0.016
2	0.1078	- 0.013	0.027
3	0.1617		0.040
4	0.2156		0.049
5	0.2695		0.054
6	0.2965		0.067

**Table 90 : Beginning of fillet vortex core trajectory of the diamond-fillet model .
 $\alpha = 10^\circ$, $\beta = 0^\circ$, Chord (C) = 9.375 inches**

Point No.	X / C	Y / C (Windward)	Y / C (Leeward)
1	0.4717	0.121	0.121
2	0.5121	0.108	0.108
3	0.5391	0.094	0.094
4	0.5930	0.081	0.081
5	0.6469	0.108	0.108
6	0.6739	0.162	0.162
7	0.7008	0.162	0.162
8	0.7547	0.175	0.175
9	0.8086	0.162	0.162
10	0.8356	0.162	0.162
11	0.8895	0.189	0.189
12	0.9434	0.216	0.216

Table 91 : Beginning of fillet vortex core trajectory of the diamond-fillet model.
 $\alpha = 10^\circ$, $\beta = 5^\circ$. Chord (C) = 9.375 inches

Point No.	X / C	Y / C (Windward)	Y / C (Leeward)
1	0.4717	0.121	0.121
2	0.5121	0.108	0.102
3	0.5391	0.086	0.094
4	0.5660	0.075	0.108
5	0.5930	0.081	0.108
6	0.6469	0.094	0.162
7	0.7008	0.108	0.189
8	0.7547	0.108	0.189
9	0.8086	0.162	0.216
10	0.8625	0.148	0.243
11	0.8895	0.135	0.243
12	0.9164		0.243
13	0.9704		0.270

Table 92 : Beginning of fillet vortex core trajectory of the diamond-fillet model .
 $\alpha = 10^\circ$, $\beta = 10^\circ$, Chord (C) = 9.375 inches

Point No.	X / C	Y / C (Windward)	Y / C (Leeward)
1	0.4717	0.121	0.121
2	0.5121	0.108	0.108
3	0.5391	0.081	0.121
4	0.5930	0.067	0.108
5	0.6469	0.081	0.135
6	0.7008	0.121	0.189
7	0.7547	0.121	0.189
8	0.8086		0.216
9	0.8625		0.243
10	0.9164		0.270
11	0.9704		0.297
12	1.0000		∞

Table 93 : Beginning of fillet vortex core trajectory of the diamond-fillet model .
 $\alpha = 10^\circ$, $\beta = 15^\circ$, Chord (C) = 9.375 inches

Point No.	X / C	Y / C (Windward)	Y / C (Leeward)
1	0.4717	0.121	0.121
2	0.5121	0.102	0.135
3	0.5391	0.081	0.121
4	0.5930	0.067	0.121
5	0.6469	0.067	0.135
6	0.7008	0.108	0.216
7	0.7547		0.216
8	0.8086		0.216
9	0.8625		0.256
10	0.9164		0.297
11	0.9704		0.377
12	1.0000		0.404

Table 94 : Beginning of fillet vortex core trajectory of the diamond-fillet model .
 $\alpha = 15^\circ$, $\beta = 0^\circ$, Chord (C) = 9.375 inches

Point No.	X / C	Y / C (Windward)	Y / C (Leeward)
1	0.4717	0.121	0.121
2	0.5121	0.108	0.108
3	0.5391	0.094	0.086
4	0.5660	0.067	0.067
5	0.5930	0.081	0.081
6	0.6200	0.108	0.108
7	0.6469	0.148	0.140
8	0.7008	0.148	0.140
9	0.7547	0.162	0.167
10	0.8086	0.189	0.189
11	0.8356	0.189	0.189

Table 95 : Beginning of fillet vortex core trajectory of the diamond-fillet model .
 $\alpha = 15^\circ$, $\beta = 5^\circ$, Chord (C) = 9.375 inches

Point No.	X / C	Y / C (Windward)	Y / C (Leeward)
1	0.4717	0.121	0.121
2	0.5121	0.108	0.135
3	0.5391	0.081	0.121
4	0.5930	0.081	0.108
5	0.6469	0.081	0.094
6	0.7008	0.162	0.108
7	0.7547	0.216	0.202
8	0.8086		0.243
9	0.8356		0.270
10	0.8895		0.270

Table 96 : Beginning of fillet vortex core trajectory of the diamond-fillet model .
 $\alpha = 15^\circ$, $\beta = 10^\circ$, Chord (C) = 9.375 inches

Point No.	X / C	Y / C (Windward)	Y / C (Leeward)
1	0.4717	0.121	0.121
2	0.5121	0.108	0.135
3	0.5391	0.094	0.108
4	0.5930	0.067	0.121
5	0.6469	0.054	0.189
6	0.7008	0.054	0.189
7	0.7547		0.189
8	0.8086		0.243
9	0.8625		0.297
10	0.9164		0.324
11	0.9704		0.350
12	1.0000		0.350

Table 97 : Beginning of fillet vortex core trajectory of the diamond-fillet model .
 $\alpha = 15^\circ$, $\beta = 15^\circ$, Chord (C) = 9.375 inches

Point No.	X / C	Y / C (Windward)	Y / C (Leeward)
1	0.4717	0.121	0.121
2	0.5121	0.094	0.135
3	0.5391	0.081	0.121
4	0.5660	0.054	0.108
5	0.5930	0.027	0.121
6	0.6469		0.162
7	0.7008		0.215
8	0.7547		0.215
9	0.8086		0.215
10	0.8625		0.243
11	0.9164		0.323
12	0.9704		0.377
13	1.0000		0.404

Table 98 : Beginning of fillet vortex core trajectory of the diamond-fillet model .
 $\alpha = 20^\circ$, $\beta = 0^\circ$, Chord (C) = 9.375 inches

Point No.	X / C	Y / C (Windward)	Y / C (Leeward)
1	0.4717	0.121	0.121
2	0.5121	0.108	0.108
3	0.5391	0.081	0.081
4	0.5660	0.081	0.081
5	0.5930	0.108	0.108
6	0.6469	0.162	0.162
7	0.7008	0.216	0.215
8	0.7547	0.215	0.215
9	0.7817	0.215	0.215

Table 99 : Beginning of fillet vortex core trajectory of the diamond-fillet model .
 $\alpha = 20^\circ$, $\beta = 5^\circ$, Chord (C) = 9.375 inches

Point No.	X / C	Y / C (Windward)	Y / C (Leeward)
1	0.4717	0.121	0.121
2	0.5121	0.108	0.121
3	0.5391	0.081	0.108
4	0.5930	0.081	0.121
5	0.6469	0.054	0.175
6	0.7008	0.067	0.189
7	0.7547		0.189
8	0.8086		0.175
9	0.8625		0.189

Table 100 : Beginning of fillet vortex core trajectory of the diamond-fillet model .
 $\alpha = 20^\circ$, $\beta = 10^\circ$, Chord (C) = 9.375 inches

Point No.	X / C	Y / C (Windward)	Y / C (Leeward)
1	0.4717	0.121	0.121
2	0.5121	0.108	0.135
3	0.5391	0.081	0.121
4	0.5660	0.054	0.108
5	0.5930	0.054	0.135
6	0.6469	0.040	0.175
7	0.7008		0.202
8	0.7547		0.229
9	0.8086		0.216
10	0.8625		0.243
11	0.9164		0.270

Table 101 : Beginning of fillet vortex core trajectory of the diamond-fillet model .
 $\alpha = 20^\circ$, $\beta = 15^\circ$, Chord (C) = 9.375 inches

Point No.	X / C	Y / C (Windward)	Y / C (Leeward)
1	0.4717	0.121	0.121
2	0.5121	0.094	0.148
3	0.5391	0.081	0.148
4	0.5930	0.067	0.135
5	0.6469		0.175
6	0.7008		0.175
7	0.7547		0.243
8	0.8086		0.275
9	0.8625		0.296
10	0.9164		0.296
11	0.9704		0.350

Table 102 : Beginning of fillet vortex core trajectory of the diamond-fillet model .
 $\alpha = 25^\circ$, $\beta = 0^\circ$, Chord (C) = 9.375 inches

Point No.	X / C	Y / C (Windward)	Y / C (Leeward)
1	0.4717	0.121	0.121
2	0.5121	0.135	0.135
3	0.5391	0.135	0.135
4	0.5930	0.135	0.135
5	0.6469	0.108	0.108
6	0.7008	0.108	0.108

Table 103 : Beginning of fillet vortex core trajectory of the diamond-fillet model .
 $\alpha = 25^\circ$, $\beta = 5^\circ$, Chord (C) = 9.375 inches

Point No.	X / C	Y / C (Windward)	Y / C (Leeward)
1	0.4717	0.121	0.121
2	0.5121	0.108	0.135
3	0.5391	0.108	0.121
4	0.5930	0.108	0.094
5	0.6469	0.081	0.108
6	0.7008		0.162
7	0.7278		0.215

Table 104 : Beginning of fillet vortex core trajectory of the diamond-fillet model .
 $\alpha = 25^\circ$, $\beta = 10^\circ$, Chord (C) = 9.375 inches

Point No.	X / C	Y / C (Windward)	Y / C (Leeward)
1	0.4717	0.121	0.121
2	0.5121	0.108	0.135
3	0.5391	0.094	0.135
4	0.5930	0.081	0.148
5	0.6469		0.135
6	0.7008		0.189
7	0.7547		0.215
8	0.8086		0.215
9	0.8356		0.243

Table 105 : Beginning of fillet vortex core trajectory of the diamond-fillet model .
 $\alpha = 25^\circ$, $\beta = 15^\circ$, Chord (C) = 9.375 inches

Point No.	X / C	Y / C (Windward)	Y / C (Leeward)
1	0.4717	0.121	0.121
2	0.5121	0.108	0.148
3	0.5391	0.081	0.162
4	0.5660	0.081	0.148
5	0.6469		0.162
6	0.7008		0.175
7	0.7547		0.215
8	0.8086		0.243
9	0.8625		0.270
10	0.8895		0.297

Table 106 : Beginning of fillet vortex core trajectory of the diamond-fillet model .
 $\alpha = 30^\circ$, $\beta = 0^\circ$, Chord (C) = 9.375 inches

Point No.	X / C	Y / C (Windward)	Y / C (Leeward)
1	0.4717	0.121	0.121
2	0.5121	0.108	0.135
3	0.5391	0.135	0.135

Table 107 : Beginning of fillet vortex core trajectory of the diamond-fillet model .
 $\alpha = 30^\circ$, $\beta = 5^\circ$, Chord (C) = 9.375 inches

Point No.	X / C	Y / C (Windward)	Y / C (Leeward)
1	0.4717	0.121	0.121
2	0.4852	0.108	0.135
3	0.5121		0.148
4	0.5391		0.162
5	0.5930		0.189

Table 108 : Beginning of fillet vortex core trajectory of the diamond-fillet model .
 $\alpha = 30^\circ$, $\beta = 10^\circ$, Chord (C) = 9.375 inches

Point No.	X / C	Y / C (Windward)	Y / C (Leeward)
1	0.4717	0.121	0.121
2	0.4852		0.162
3	0.5391		0.189
4	0.5930		0.202
5	0.6469		0.216

Table 109 : Beginning of fillet vortex core trajectory of the diamond-fillet model .
 $\alpha = 30^\circ$, $\beta = 15^\circ$, Chord (C) = 9.375 inches

Point No.	X / C	Y / C (Windward)	Y / C (Leeward)
1	0.4717	0.121	0.121
2	0.4852		0.175
3	0.5391		0.216
4	0.5930		0.216
5	0.6469		0.229
6	0.6739		0.243

Table 110 : End of fillet vortex core trajectory of the diamond-fillet model .
 $\alpha = 10^\circ$, $\beta = 0^\circ$, Chord (C) = 9.375 inches

Point No.	X / C	Y / C (Windward)	Y / C (Leeward)
1	0.5795	0.175	0.175
2	0.5930	0.189	0.189
3	0.6469	0.162	0.162
4	0.7008	0.135	0.135
5	0.7547	0.148	0.148
6	0.8086	0.175	0.189
7	0.8356	0.215	0.215

Table 111 : End of fillet vortex core trajectory of the diamond-fillet model .
 $\alpha = 10^\circ$, $\beta = 5^\circ$, Chord (C) = 9.375 inches

Point No.	X / C	Y / C (Windward)	Y / C (Leeward)
1	0.5795	0.175	0.175
2	0.5930	0.167	0.175
3	0.6469	0.140	0.151
4	0.7008	0.116	0.162
5	0.7547	0.102	0.221
6	0.7817	0.108	0.256
7	0.8086	0.113	0.297
8	0.8625		0.323
9	0.9164		0.297

Table 112 : End of fillet vortex core trajectory of the diamond-fillet model .
 $\alpha = 10^\circ$, $\beta = 10^\circ$, Chord (C) = 9.375 inches

Point No.	X / C	Y / C (Windward)	Y / C (Leeward)
1	0.5795	0.175	0.175
2	0.5930	0.175	0.175
3	0.6469	0.148	0.167
4	0.7008	0.135	0.194
5	0.7278	0.135	0.202
6	0.7547	0.148	0.243
7	0.7817	0.148	0.297
8	0.8086		0.323
9	0.8625		0.323
10	0.9164		0.323
11	0.9704		0.350

Table 113 : End of fillet vortex core trajectory of the diamond-fillet model .
 $\alpha = 10^\circ$, $\beta = 15^\circ$, Chord (C) = 9.375 inches

Point No.	X / C	Y / C (Windward)	Y / C (Leeward)
1	0.5795	0.175	0.175
2	0.5930	0.183	0.189
3	0.6469	0.162	0.178
4	0.6739	0.148	0.183
5	0.7008		0.189
6	0.7547		0.243
7	0.8086		0.297
8	0.8625		0.377
9	0.9164		0.404
10	0.9704		0.431
11	1.0000		0.445

Table 114 : End of fillet vortex core trajectory of the diamond-fillet model .
 $\alpha = 15^\circ$, $\beta = 0^\circ$, Chord (C) = 9.375 inches

Point No.	X / C	Y / C (Windward)	Y / C (Leeward)
1	0.5795	0.175	0.175
2	0.5930	0.162	0.162
3	0.6469	0.121	0.121
4	0.7008	0.108	0.108
5	0.7278	0.113	0.108
6	0.7547	0.108	0.121
7	0.7817	0.135	0.135
8	0.8086	0.162	0.162

Table 115: End of fillet vortex core trajectory of the diamond-fillet model .
 $\alpha = 15^\circ$, $\beta = 5^\circ$, Chord (C) = 9.375 inches

Point No.	X / C	Y / C (Windward)	Y / C (Leeward)
1	0.5795	0.175	0.175
2	0.5930	0.189	0.167
3	0.6200	0.183	0.156
4	0.6469	0.175	0.162
5	0.6739	0.170	0.162
6	0.7008	0.170	0.162
7	0.7547		0.175
8	0.8086		0.189
9	0.8625		0.216
10	0.9164		0.256
11	0.9434		0.283

Table 116 : End of fillet vortex core trajectory of the diamond-fillet model .
 $\alpha = 15^\circ$, $\beta = 10^\circ$, Chord (C) = 9.375 inches

Point No.	X / C	Y / C (Windward)	Y / C (Leeward)
1	0.5795	0.175	0.175
2	0.5930	0.189	0.162
3	0.6200	0.175	0.156
4	0.6469	0.162	0.162
5	0.7008		0.175
6	0.7547		0.202
7	0.8086		0.243
8	0.8625		0.283
9	0.9164		0.323
10	0.9704		0.377

Table 117 : End of fillet vortex core trajectory of the diamond-fillet model.
 $\alpha = 15^\circ$, $\beta = 15^\circ$, Chord (C) = 9.375 inches

Point No.	X / C	Y / C (Windward)	Y / C (Leeward)
1	0.5795	0.175	0.175
2	0.5930	0.189	0.175
3	0.6200	0.162	0.175
4	0.6469		0.189
5	0.7008		0.202
6	0.7547		0.221
7	0.8086		0.297
8	0.8625		0.364
9	0.9164		0.418
10	0.9704		0.458
11	1.0000		0.458

Table 118 : End of fillet vortex core trajectory of the diamond-fillet model .
 $\alpha = 20^\circ$, $\beta = 0^\circ$, Chord (C) = 9.375 inches

Point No.	X / C	Y / C (Windward)	Y / C (Leeward)
1	0.5795	0.175	0.175
2	0.5930	0.162	0.162
3	0.6469	0.135	0.135
4	0.6739	0.121	0.121
5	0.7008	0.135	0.135
6	0.7547	0.162	0.162

Table 119 : End of fillet vortex core trajectory of the diamond-fillet model .
 $\alpha = 20^\circ$, $\beta = 5^\circ$, Chord (C) = 9.375 inches

Point No.	X / C	Y / C (Windward)	Y / C (Leeward)
1	0.5795	0.175	0.175
2	0.5930	0.156	0.162
3	0.6200	0.135	0.162
4	0.6469	0.121	0.135
5	0.6739	0.116	0.148
6	0.7008		0.148
7	0.7547		0.189
8	0.8086		0.216
9	0.8356		0.270

Table 120 : End of fillet vortex core trajectory of the diamond-fillet model .
 $\alpha = 20^\circ$, $\beta = 10^\circ$, Chord (C) = 9.375 inches

Point No.	X / C	Y / C (Windward)	Y / C (Leeward)
1	0.5795	0.175	0.175
2	0.5930	0.151	0.189
3	0.6200	0.130	0.189
4	0.6469		0.189
5	0.7008		0.202
6	0.7547		0.202
7	0.8086		0.243
8	0.8356		0.297
9	0.8625		0.323

Table 121 : End of fillet vortex core trajectory of the diamond-fillet model .
 $\alpha = 20^\circ$, $\beta = 15^\circ$, Chord (C) = 9.375 inches

Point No.	X / C	Y / C (Windward)	Y / C (Leeward)
1	0.5795	0.175	0.175
2	0.5930	0.175	0.189
3	0.6469		0.189
4	0.7008		0.215
5	0.7547		0.229
6	0.8086		0.270
7	0.8625		0.337
8	0.9164		0.377

Table 122 : End of fillet vortex core trajectory of the diamond-fillet model .
 $\alpha = 25^\circ$, $\beta = 0^\circ$, Chord (C) = 9.375 inches

Point No.	X / C	Y / C (Windward)	Y / C (Leeward)
1	0.5795	0.175	0.175
2	0.5930		

Table 123 : End of fillet vortex core trajectory of the diamond-fillet model.
 $\alpha = 25^\circ$, $\beta = 5^\circ$, Chord (C) = 9.375 inches

Point No.	X / C	Y / C (Windward)	Y / C (Leeward)
1	0.5795	0.175	0.175
2	0.5930		0.189
3	0.6200		0.202
4	0.6469		0.229
5	0.6739		0.270

Table 124 : End of fillet vortex core trajectory of the diamond-fillet model .
 $\alpha = 25^\circ$, $\beta = 10^\circ$, Chord (C) = 9.375 inches

Point No.	X / C	Y / C (Windward)	Y / C (Leeward)
1	0.5795	0.175	0.175
2	0.5930		0.189
3	0.6469		0.243
4	0.7008		0.283
5	0.7547		0.310
6	0.8086		0.324

Table 125 : End of fillet vortex core trajectory of the diamond-fillet model .
 $\alpha = 25^\circ$, $\beta = 15^\circ$, Chord (C) = 9.375 inches

Point No.	X / C	Y / C (Windward)	Y / C (Leeward)
1	0.5795	0.175	0.175
2	0.5930		0.215
3	0.6469		0.256
4	0.7008		0.283
5	0.7547		0.350
6	0.8086		0.350
7	0.8625		0.364
8	0.9146		0.377

APPENDIX B

Photographs and plots (Figures 15 - 93)

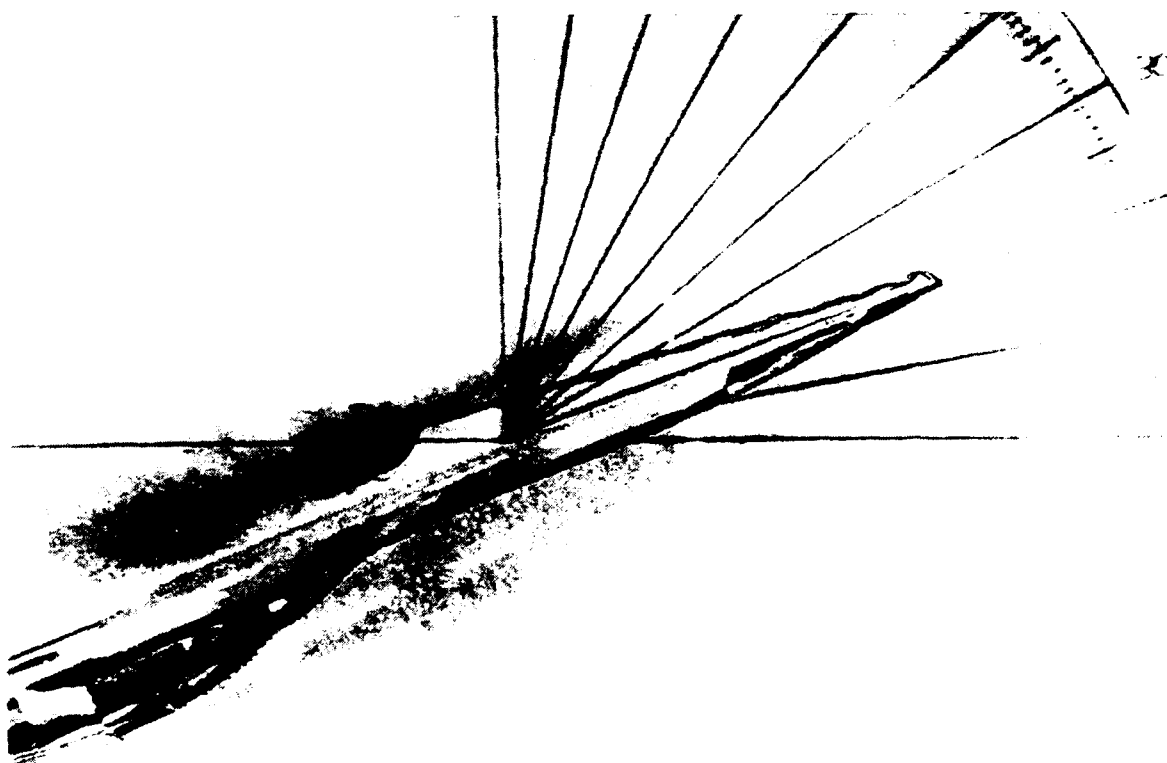
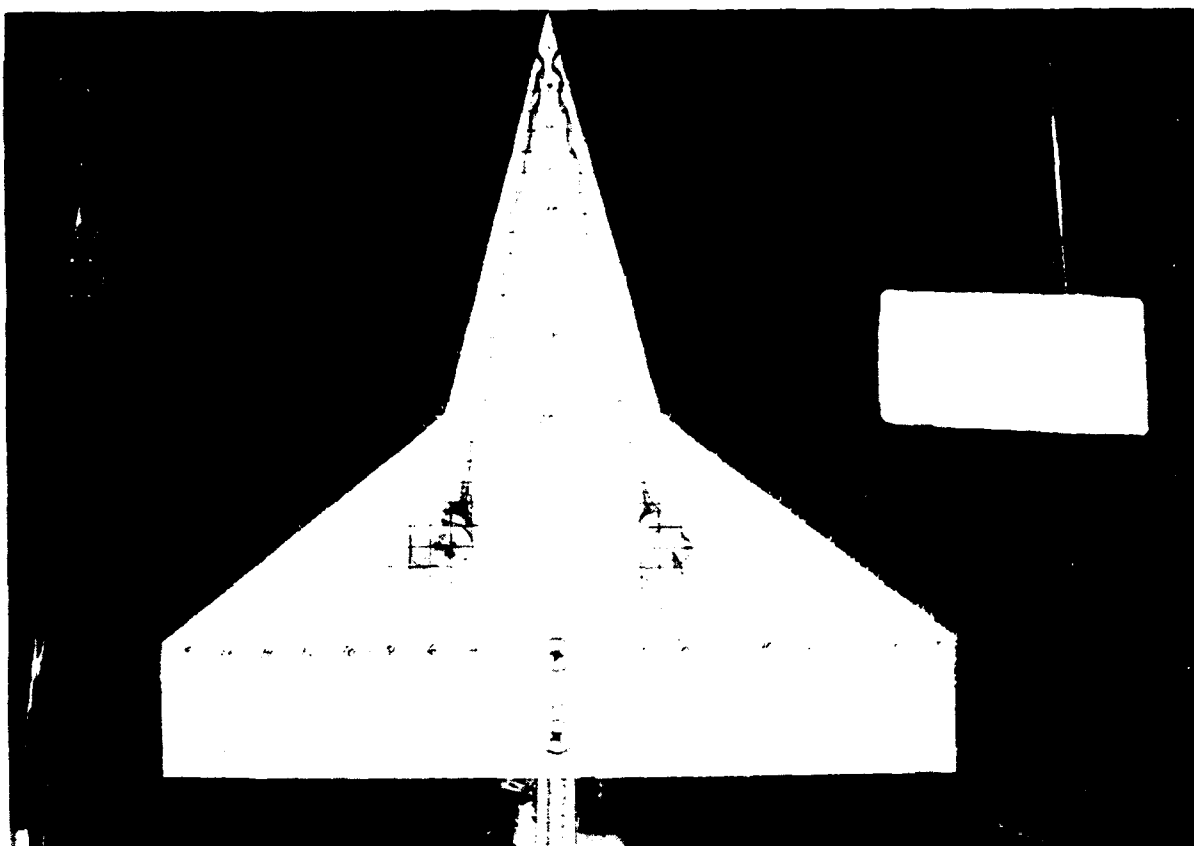


Figure 15 : Baseline model strake vortex , $\alpha=20^\circ$, $\beta=0^\circ$.

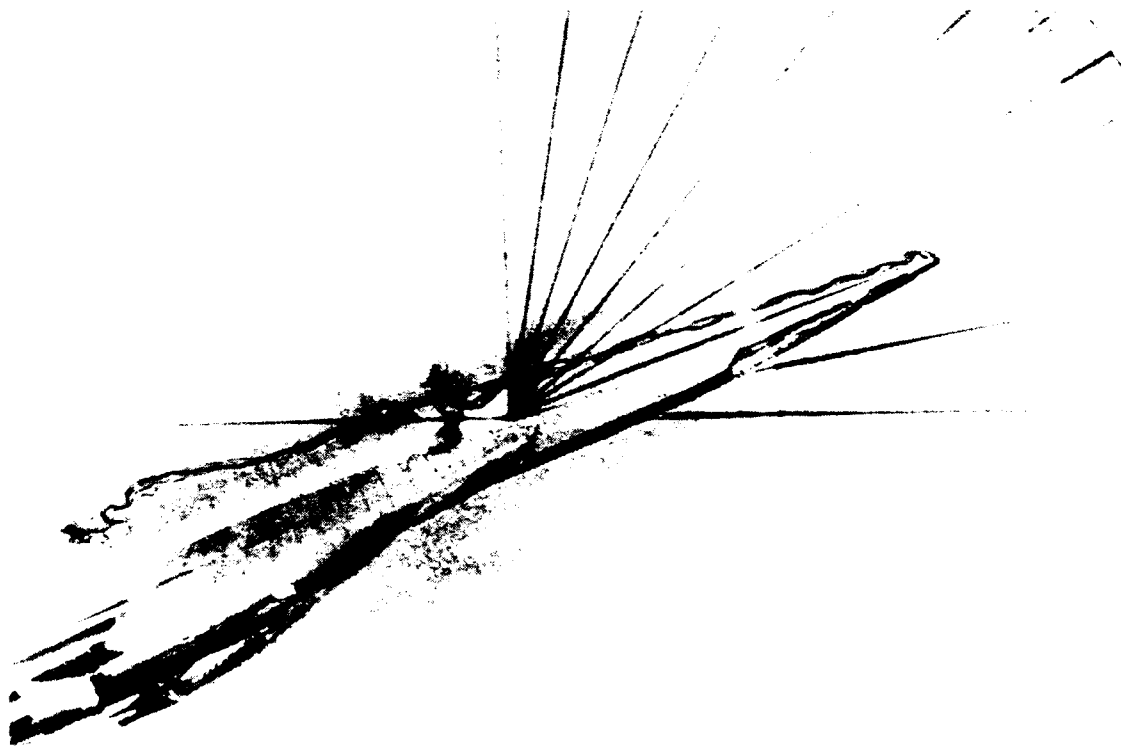
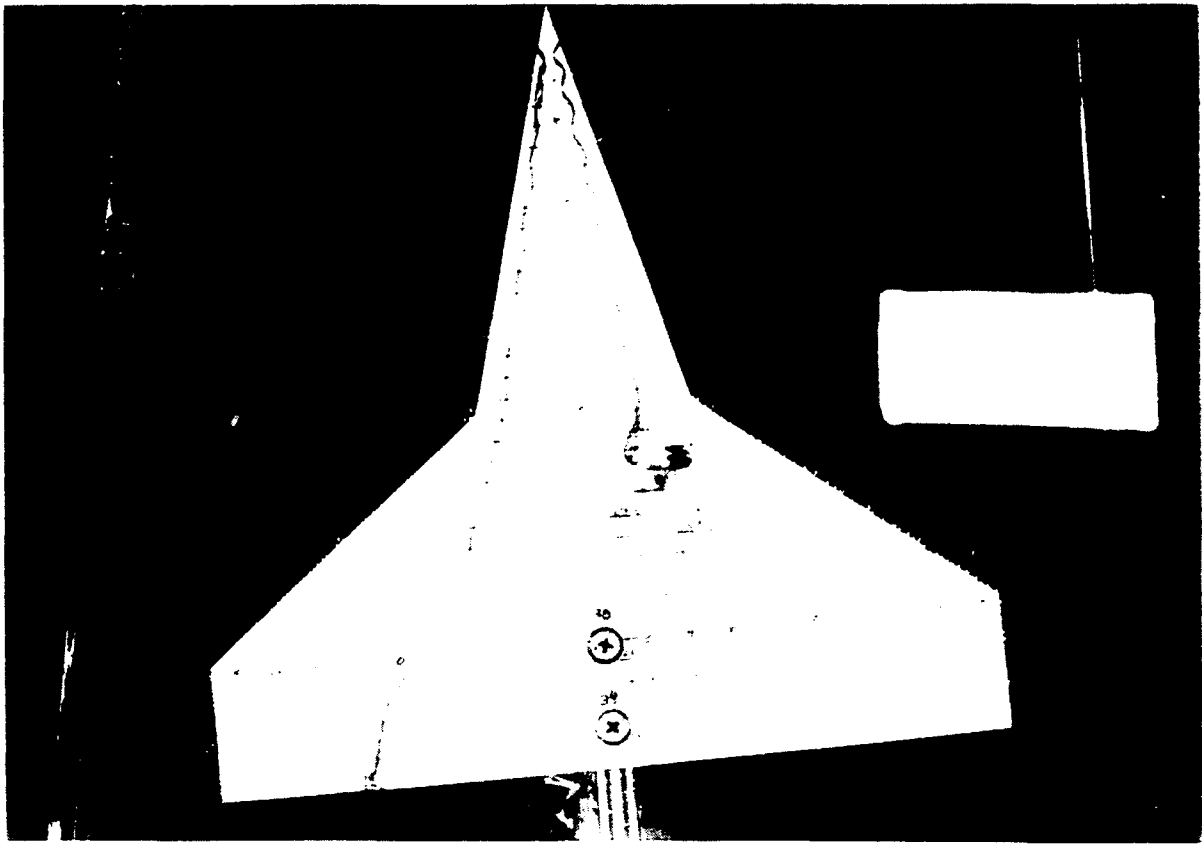


Figure 16 : Baseline model strake vortex , $\alpha=20^\circ$, $\beta=5^\circ$.

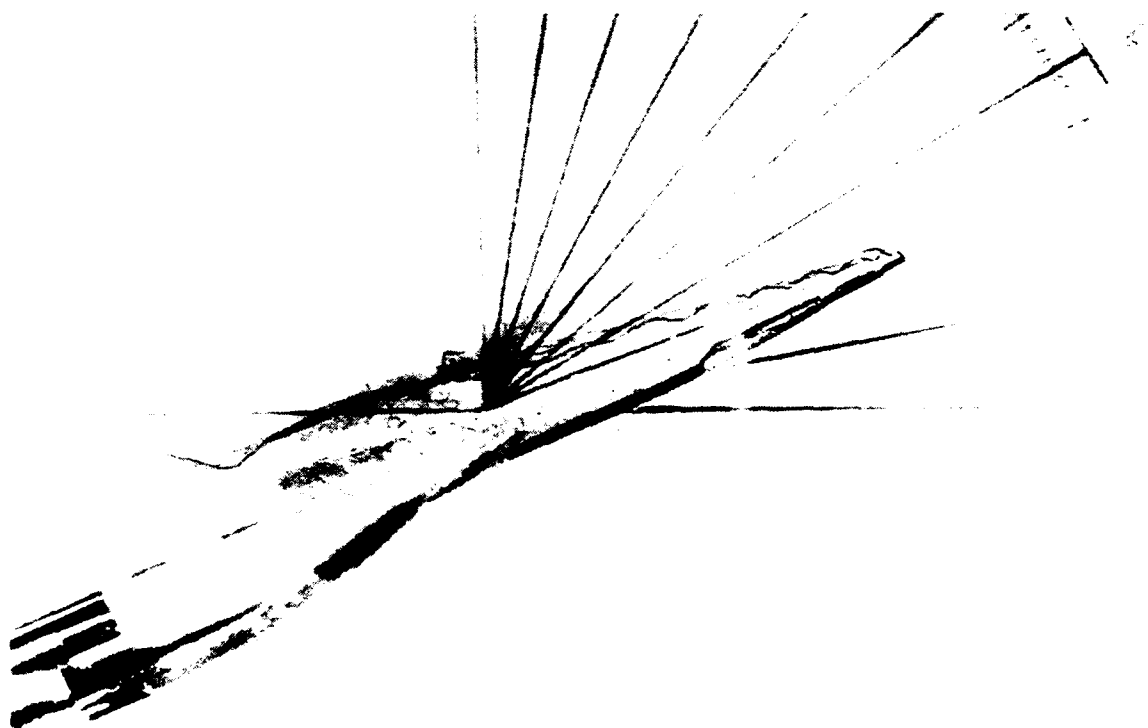
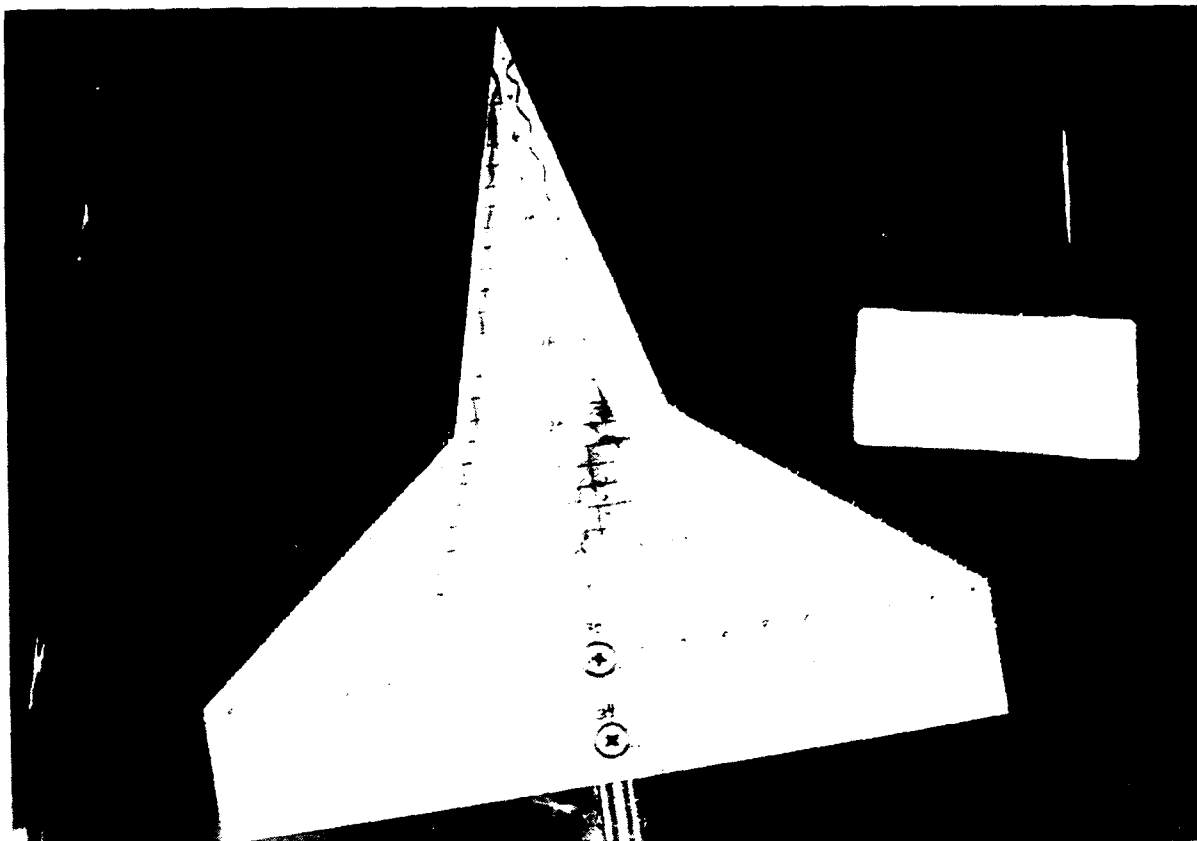


Figure 17 : Baseline model strake vortex , $\alpha=20^\circ$, $\beta=10^\circ$.

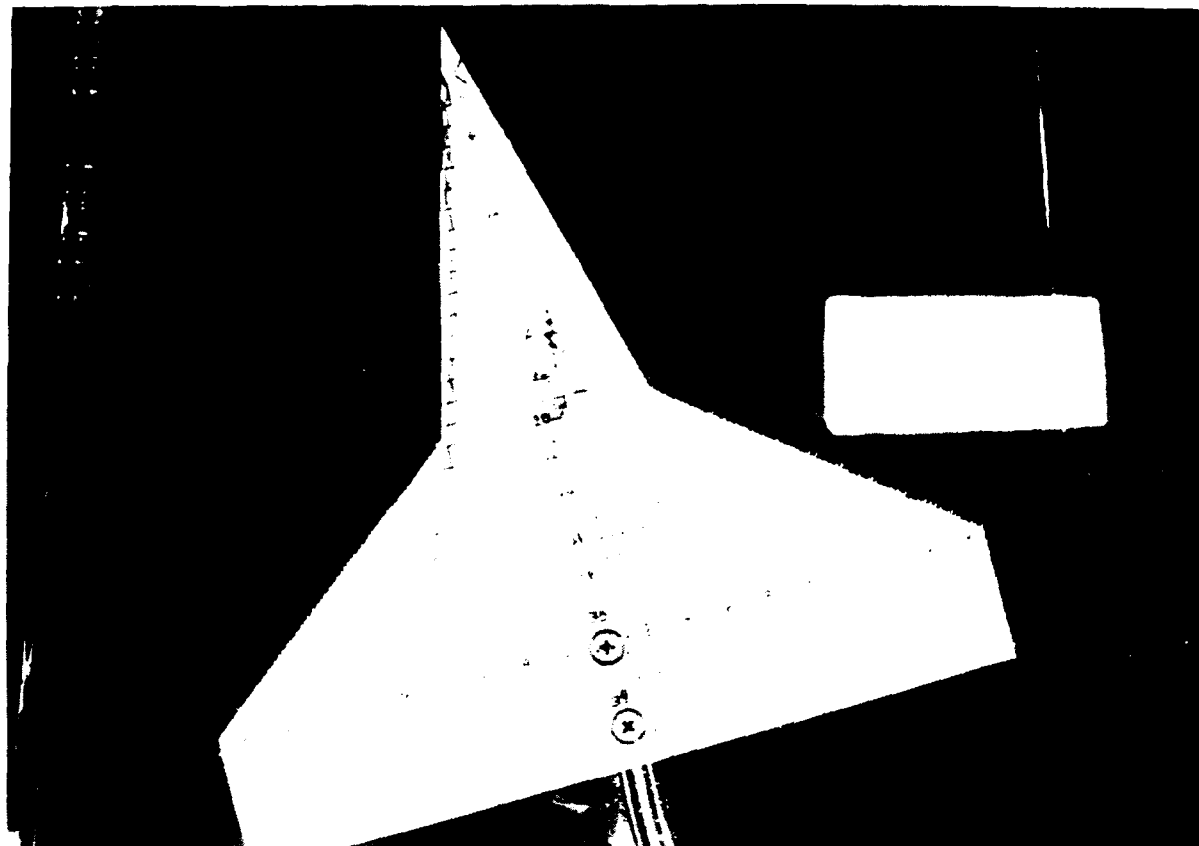


Figure 18 : Baseline model strake vortex , $\alpha=20^\circ$, $\beta=15^\circ$.

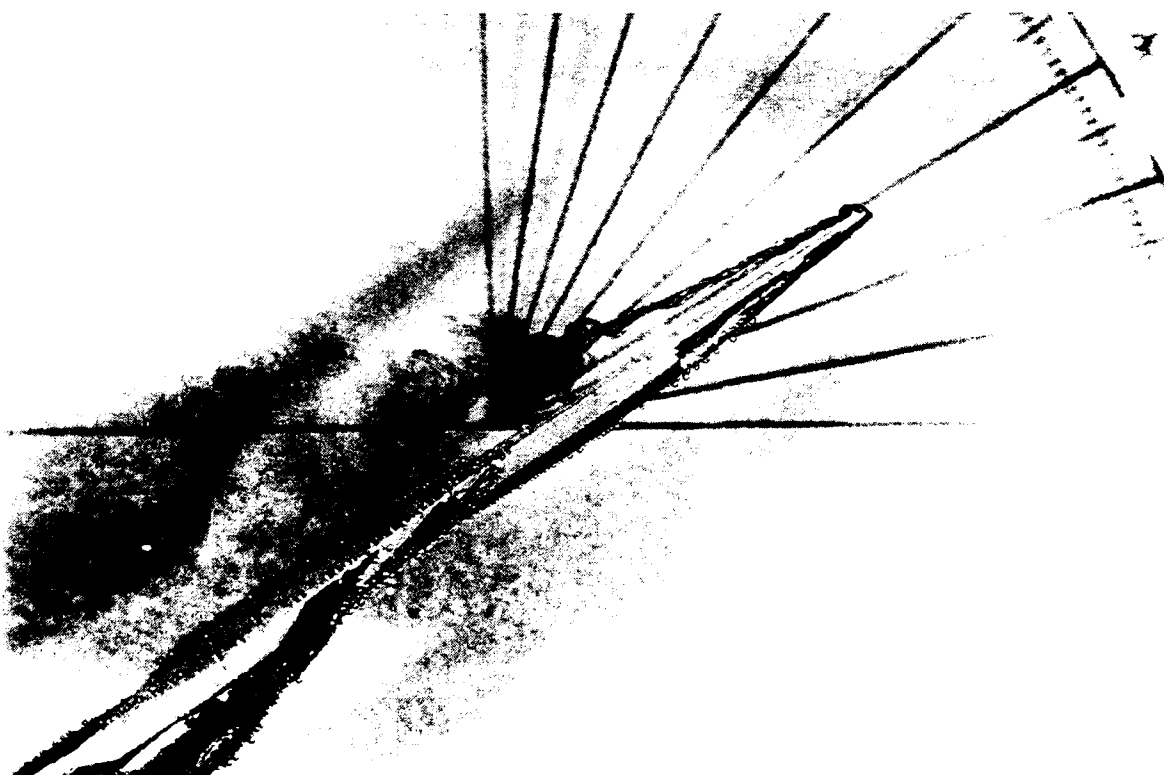
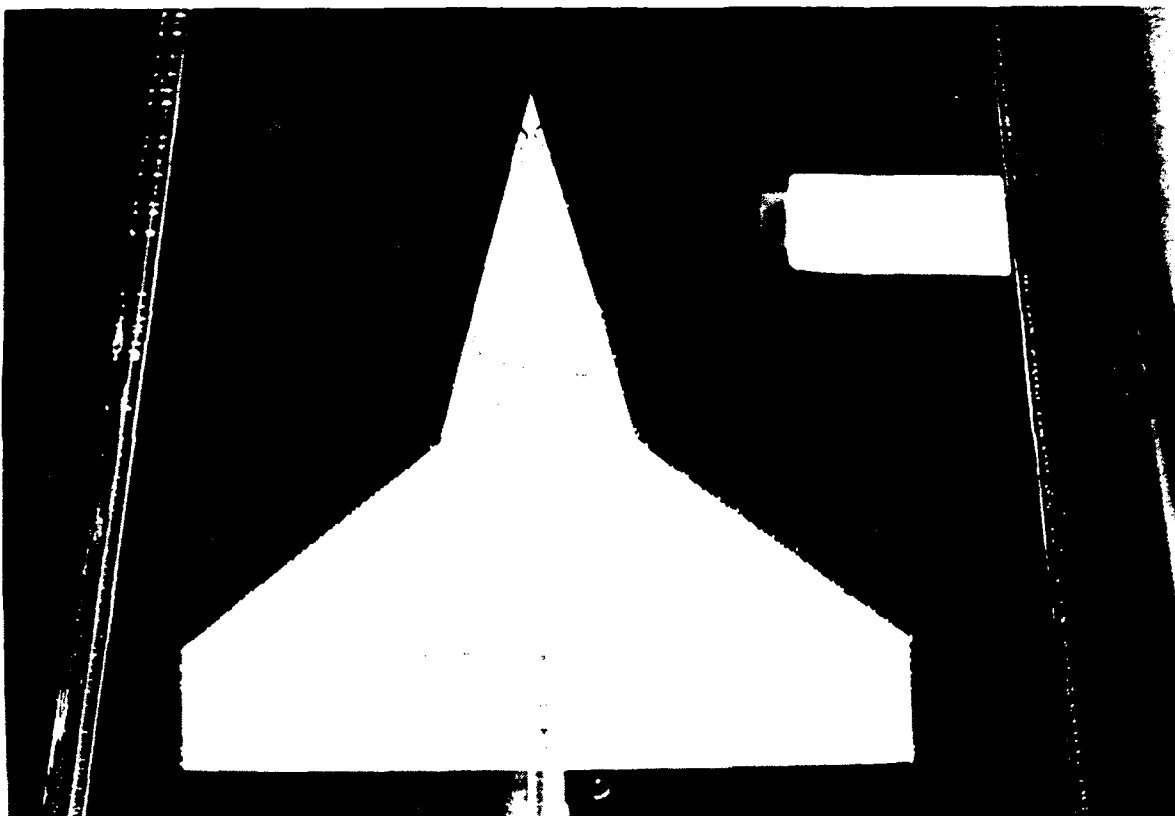


Figure 19 : Baseline model strake vortex , $\alpha=30^\circ$, $\beta=0^\circ$.

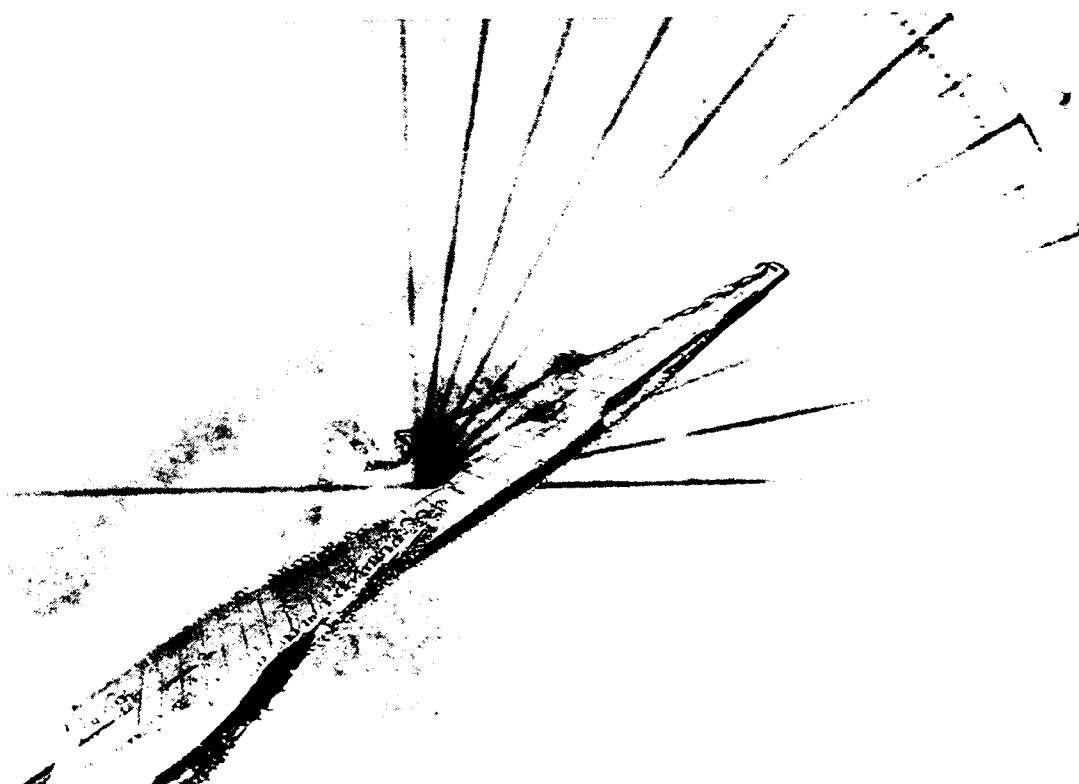
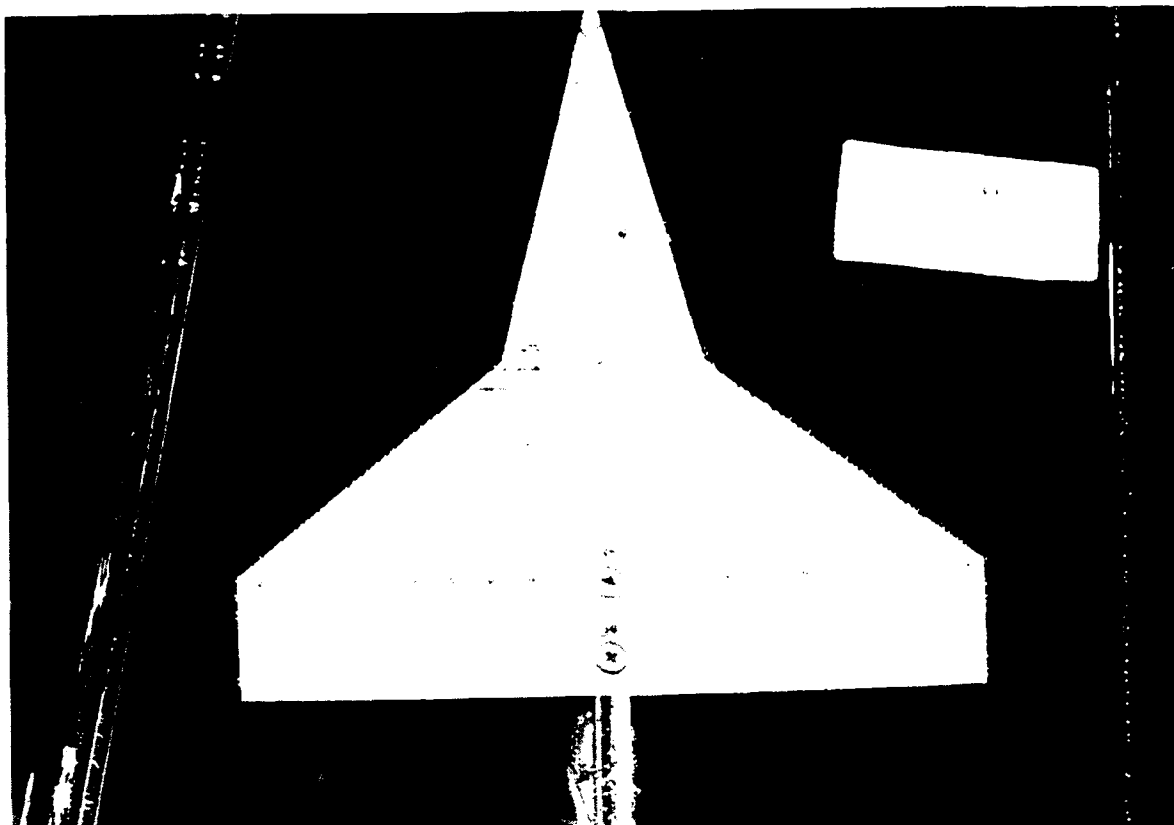


Figure 20 : Baseline model strake vortex , $\alpha=30^\circ$, $\beta=5^\circ$.

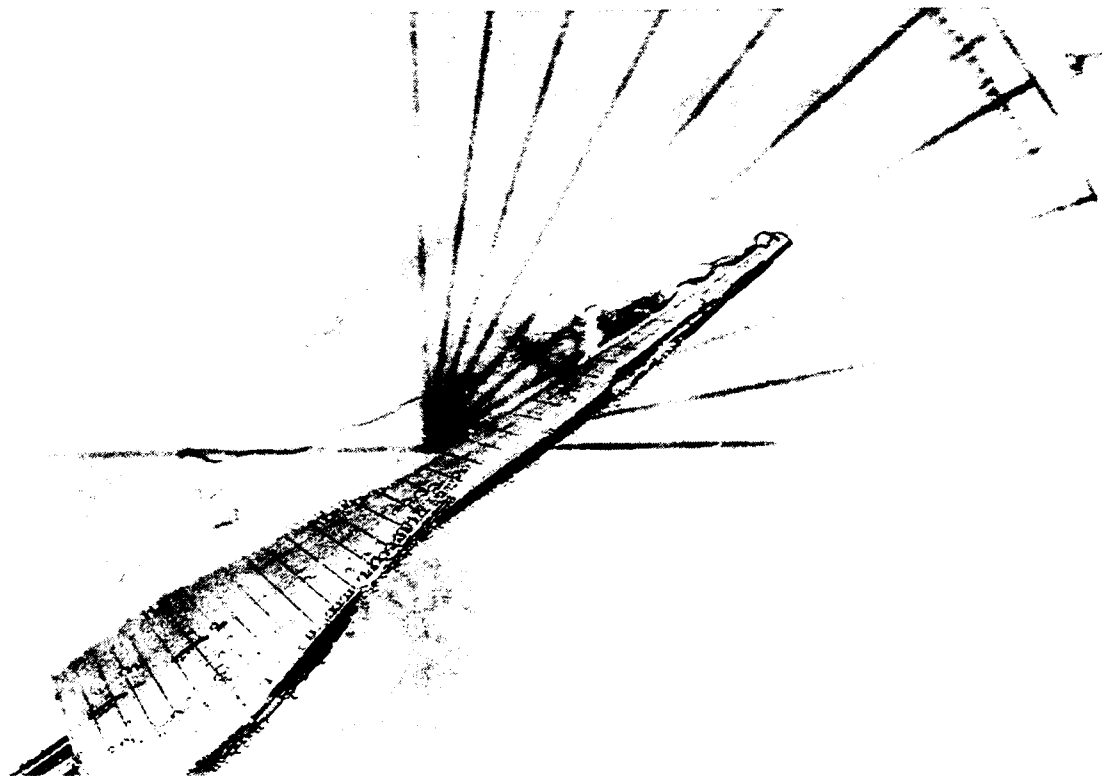
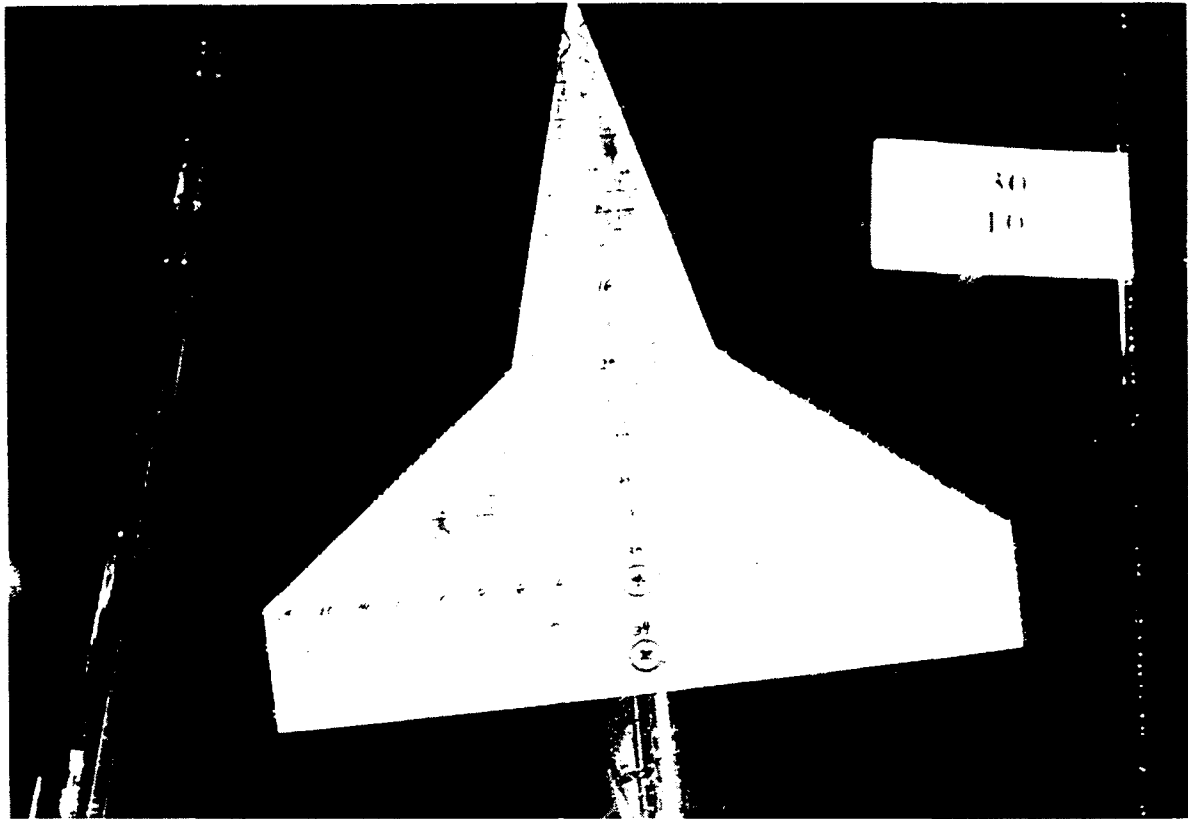


Figure 21 : Baseline model strake vortex , $\alpha=30^\circ$, $\beta=10^\circ$.

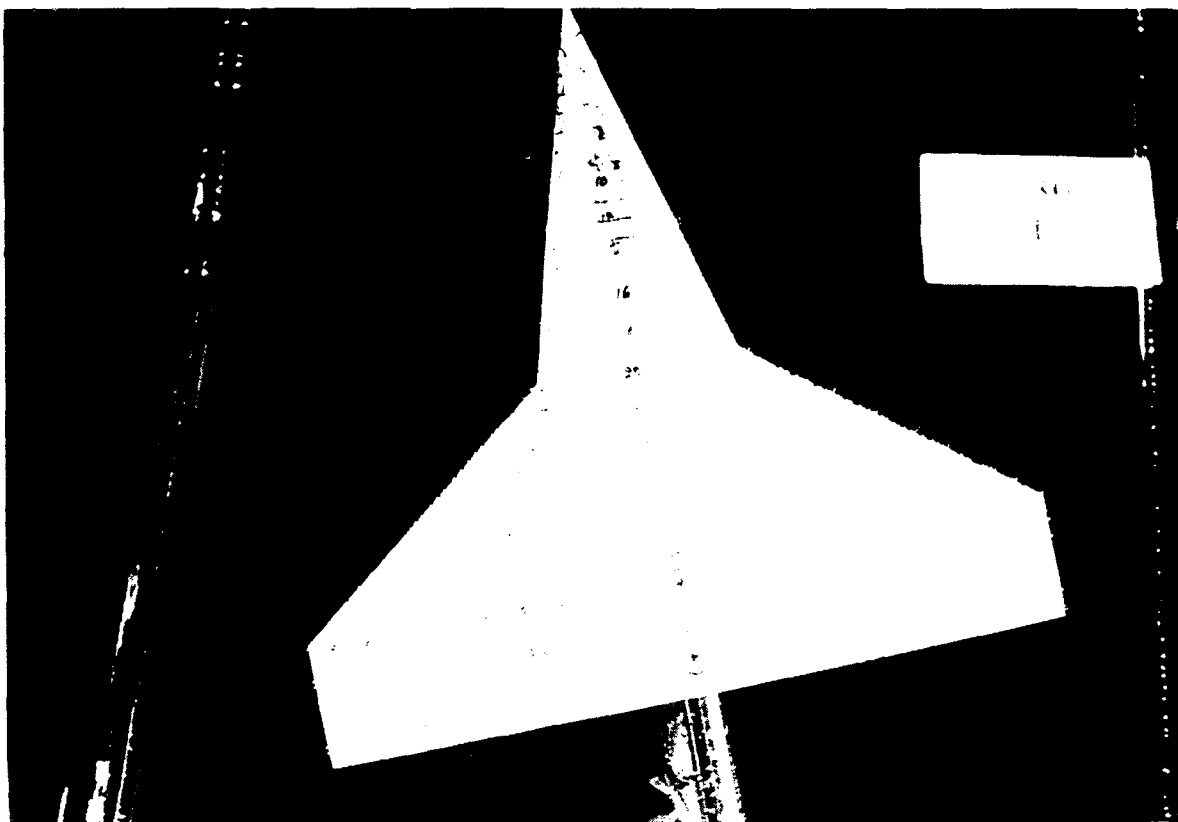


Figure 22 : Baseline model strake vortex , $\alpha=30^\circ$, $\beta=15^\circ$.

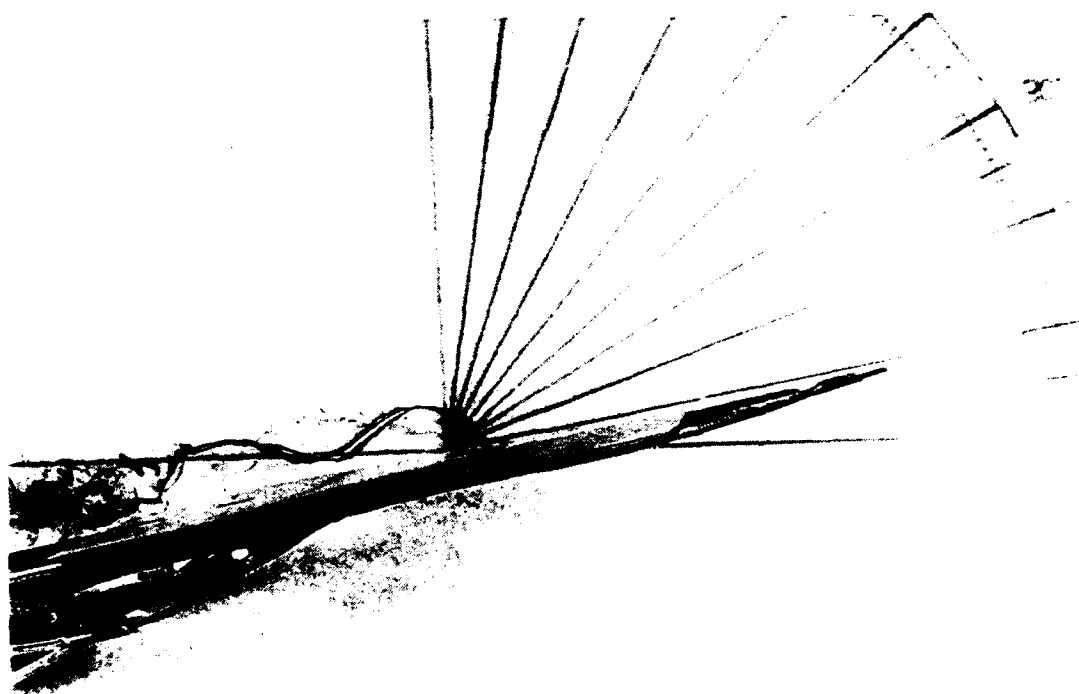
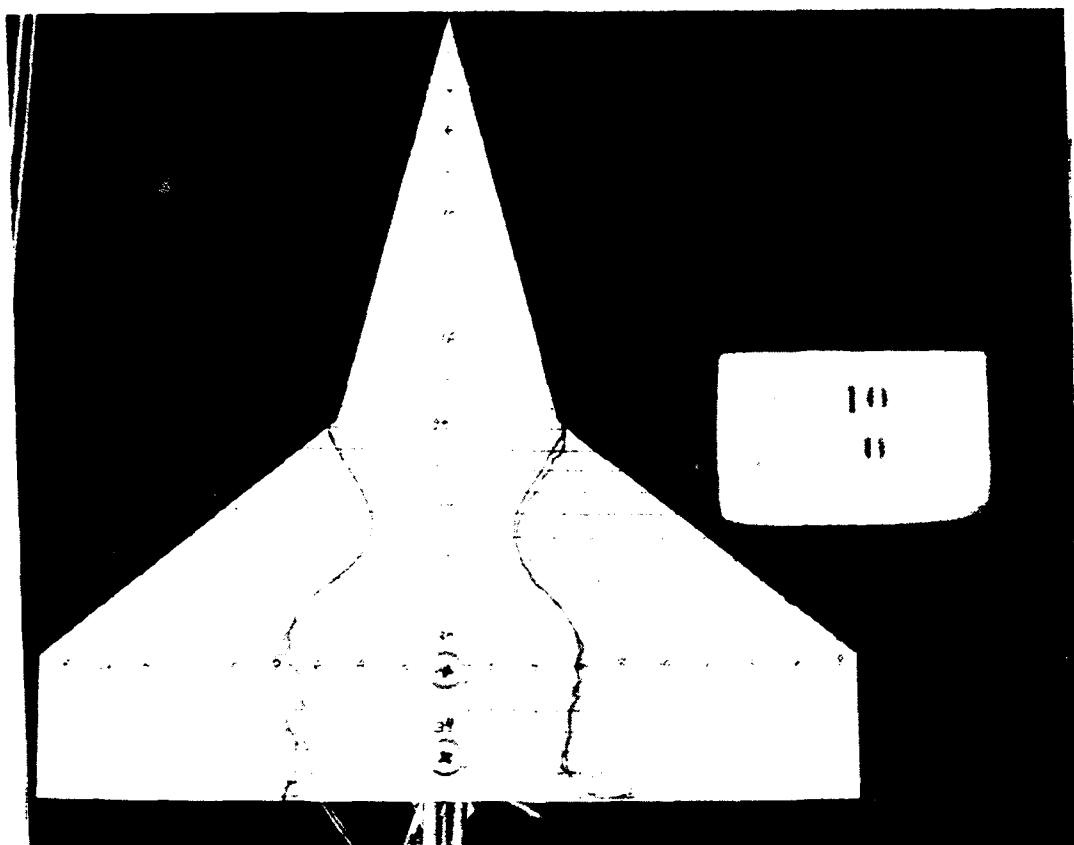


Figure 23 : Baseline model wing vortex , $\alpha=10^\circ$, $\beta=0^\circ$.

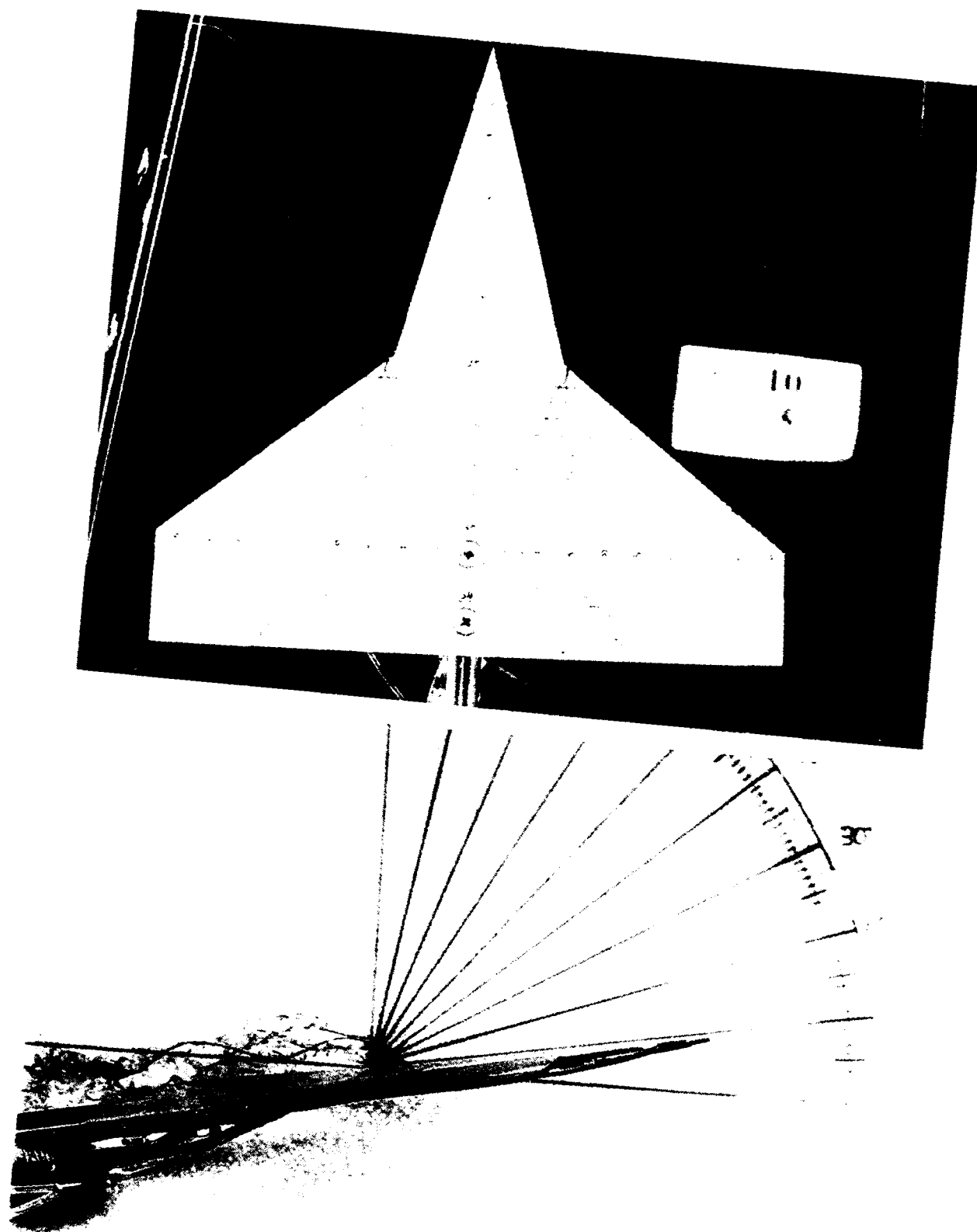


Figure 24 : Baseline model wing vortex , $\alpha=10^\circ$, $\beta=5^\circ$.

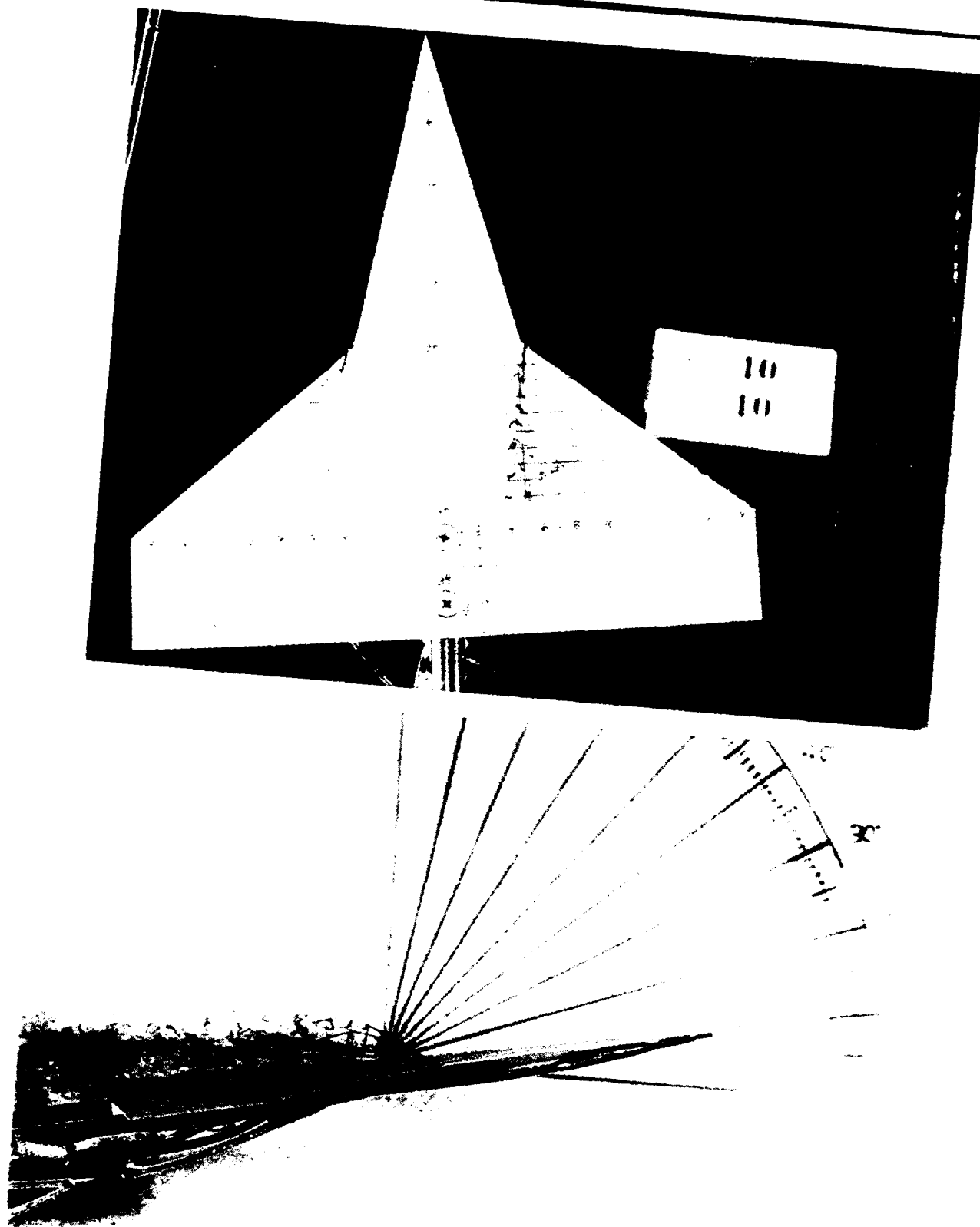


Figure 25 : Baseline model wing vortex , $\alpha=10^\circ$, $\beta=10^\circ$.

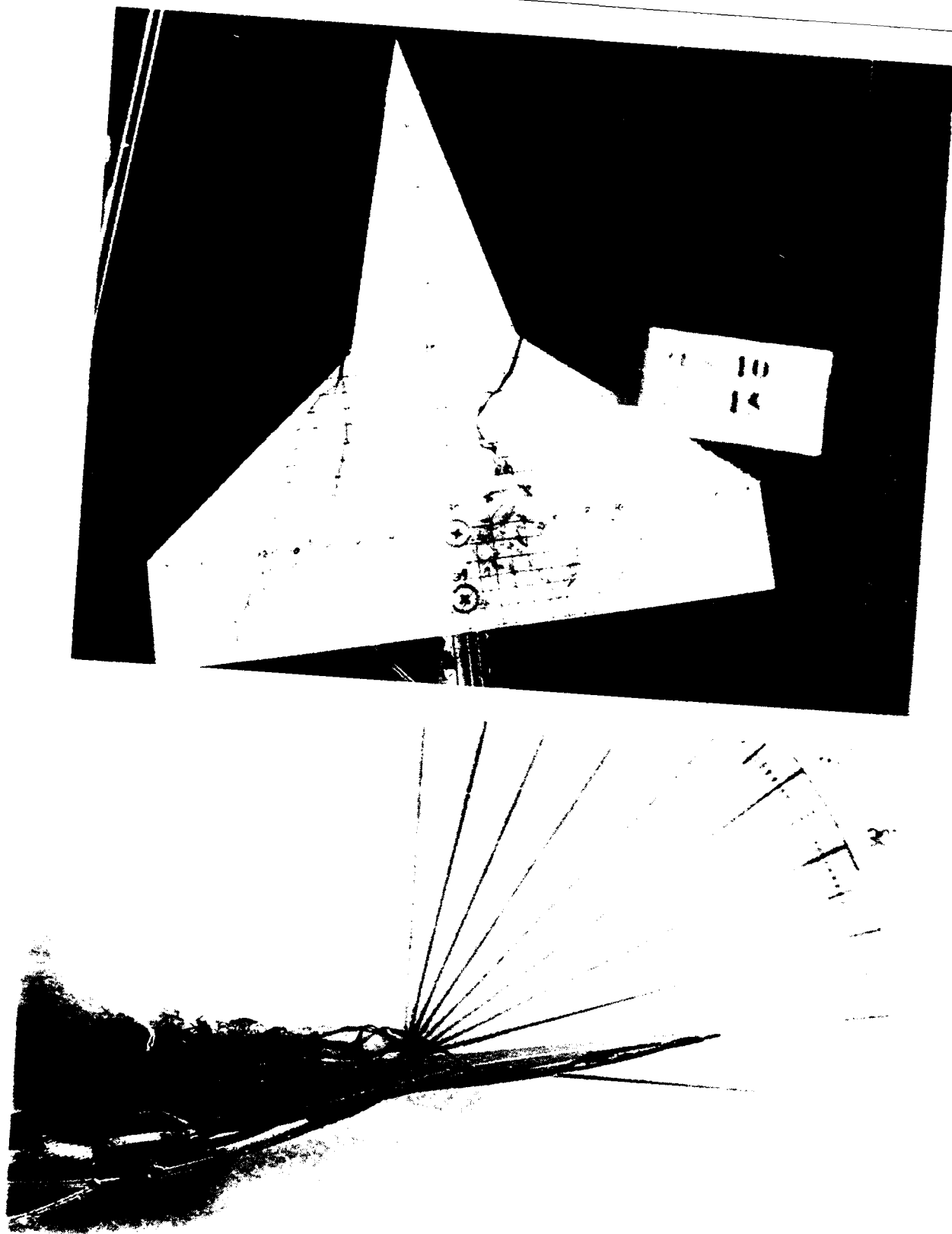


Figure 26 : Baseline model wing vortex , $\alpha=10^\circ$, $\beta=15^\circ$.

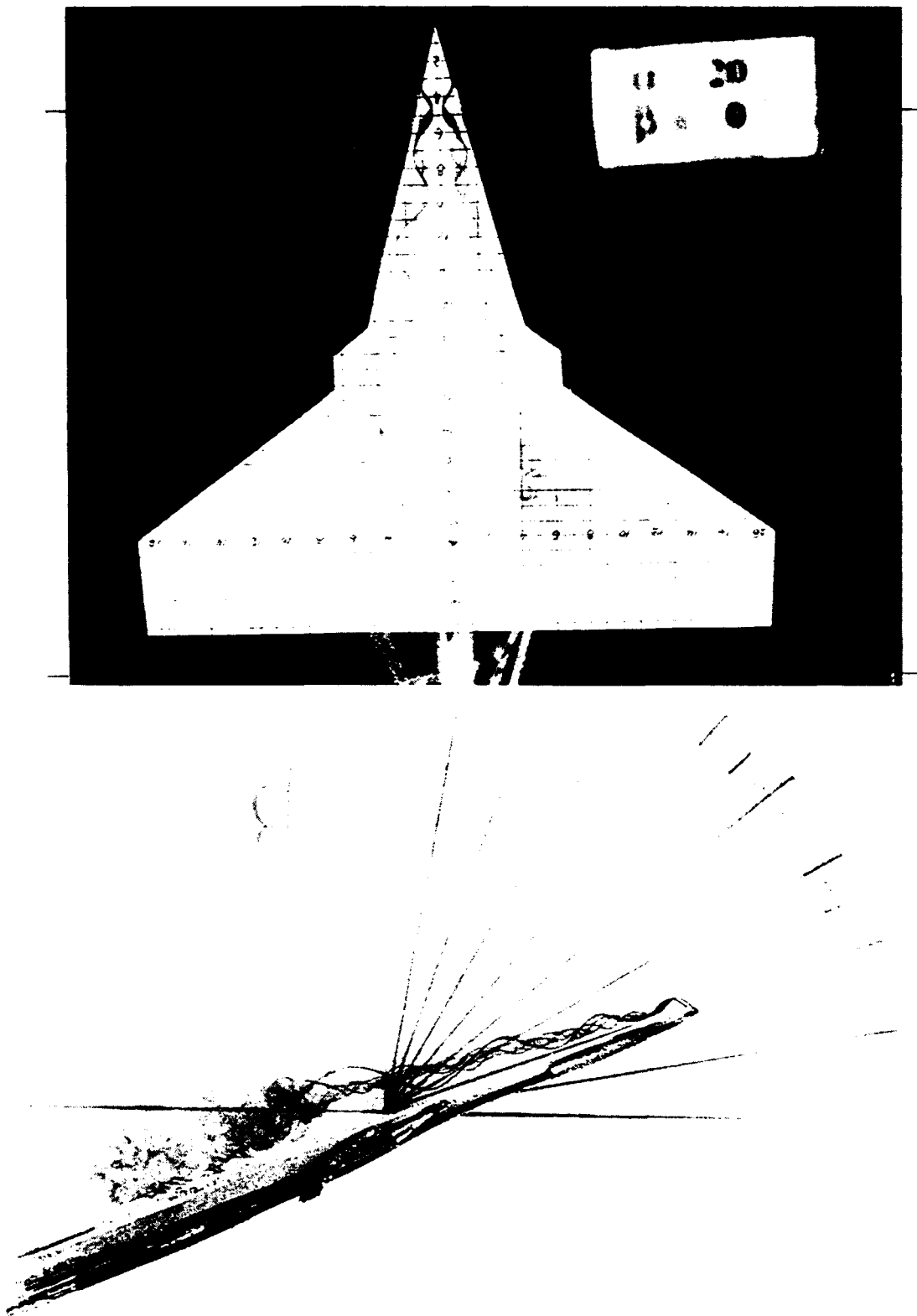


Figure 27 : Diamond-fillet model strake vortex , $\alpha=20^\circ$, $\beta=0^\circ$.

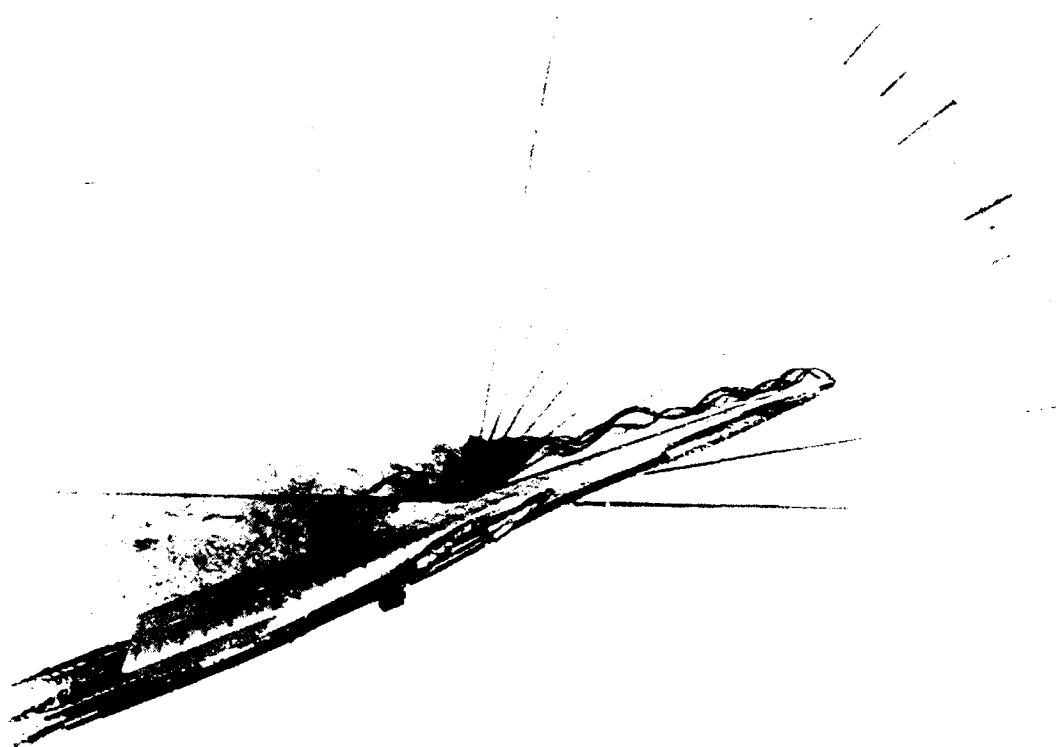
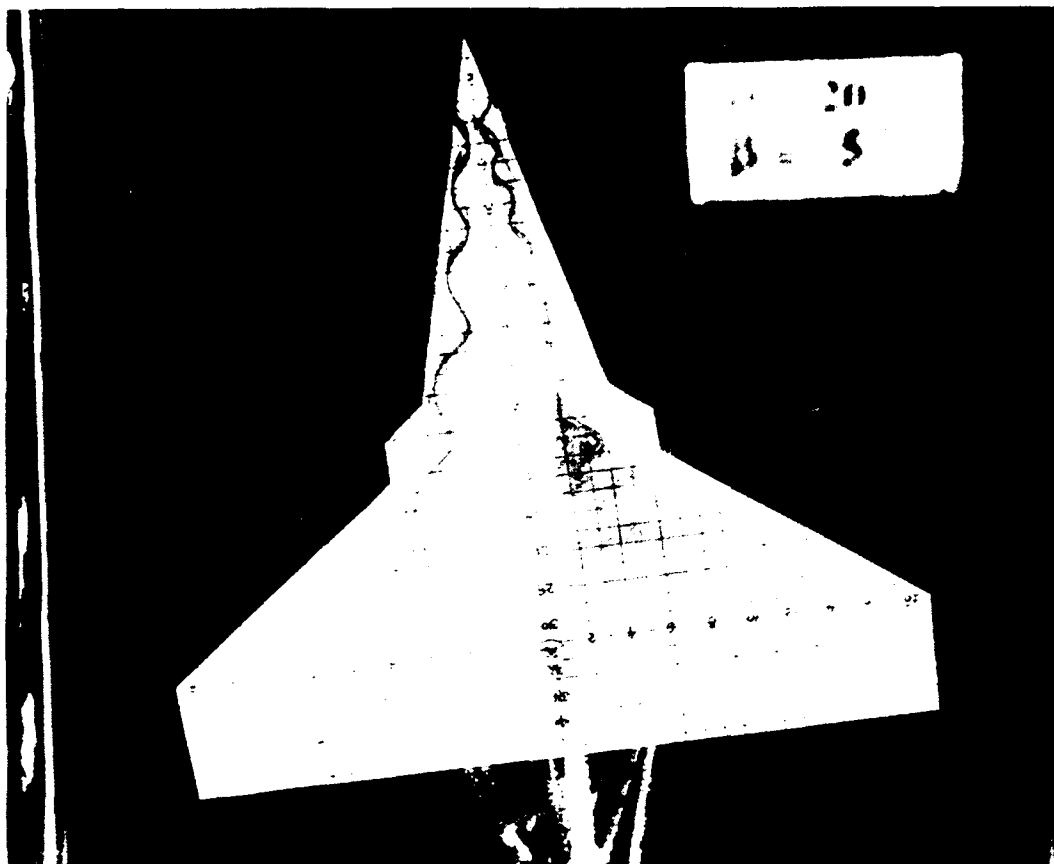


Figure 28 : Diamond-fillet model strake vortex , $\alpha=20^\circ$, $\beta=5^\circ$.

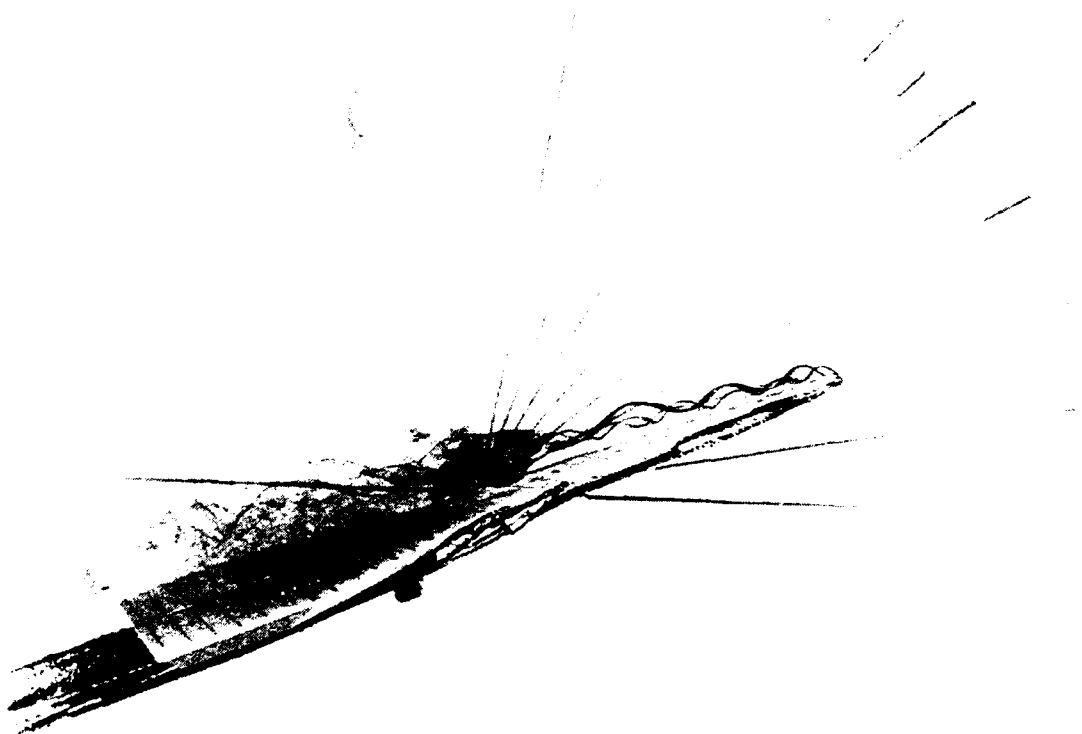
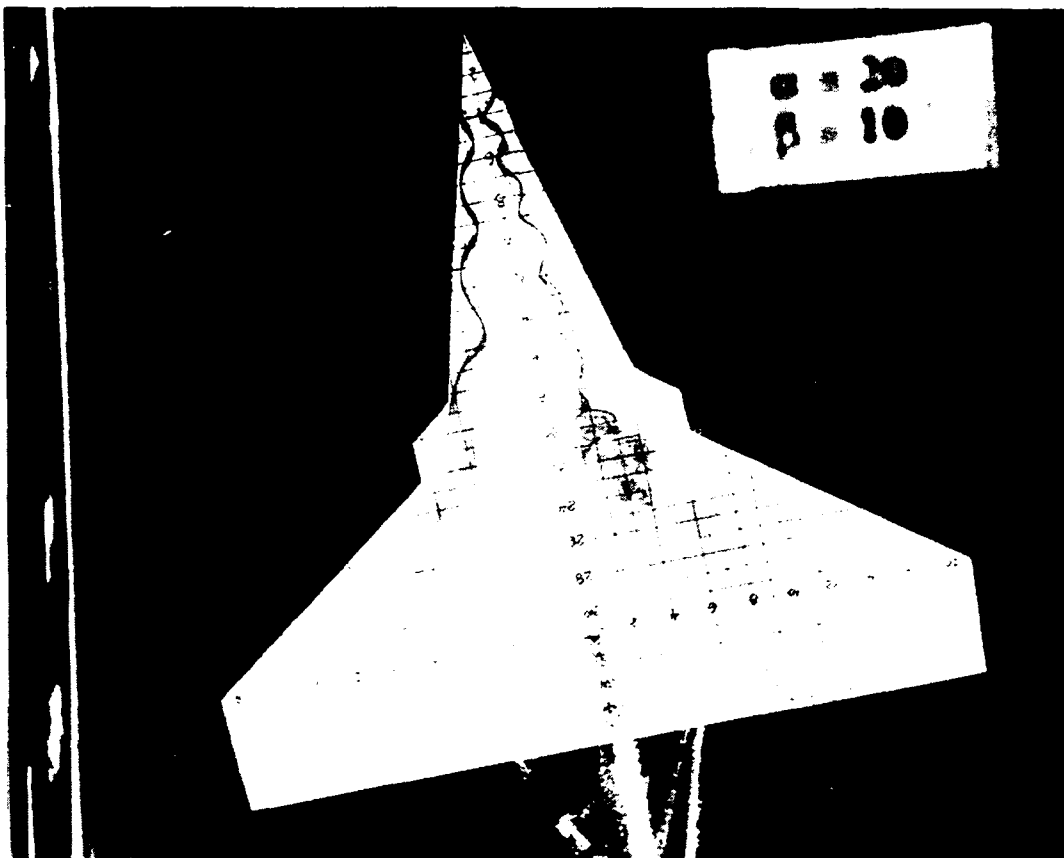


Figure 29 : Diamond-fillet model strake vortex , $\alpha=20^\circ$, $\beta=10^\circ$.

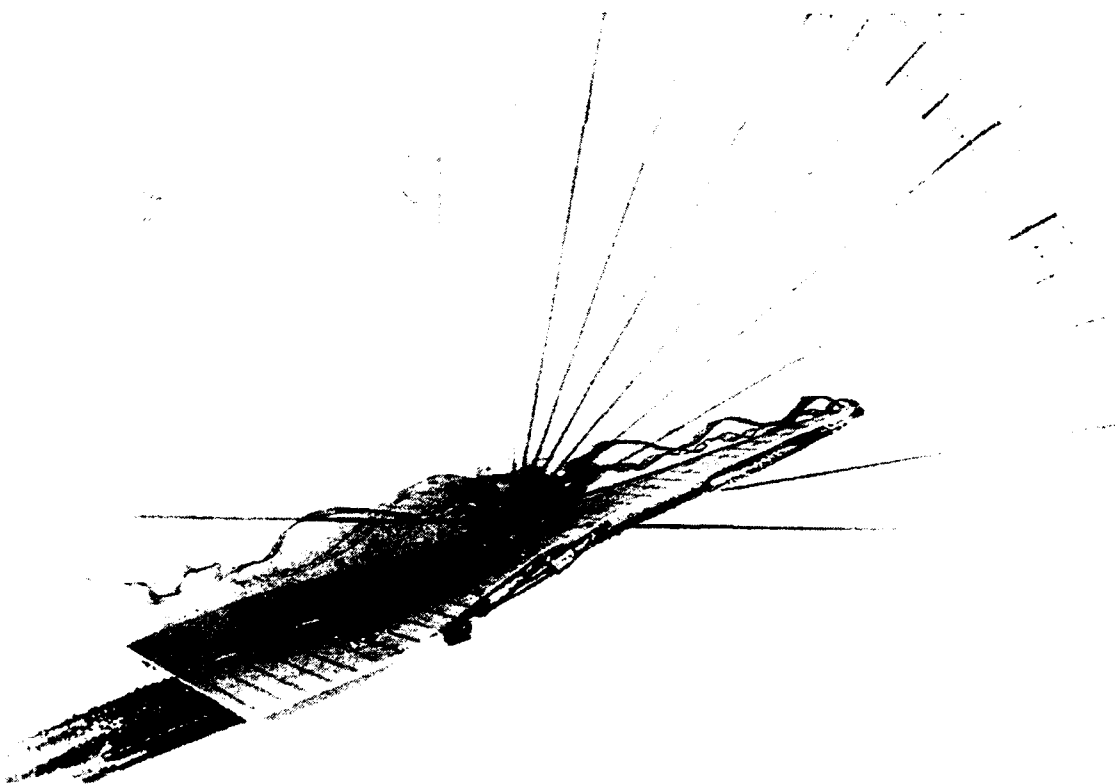
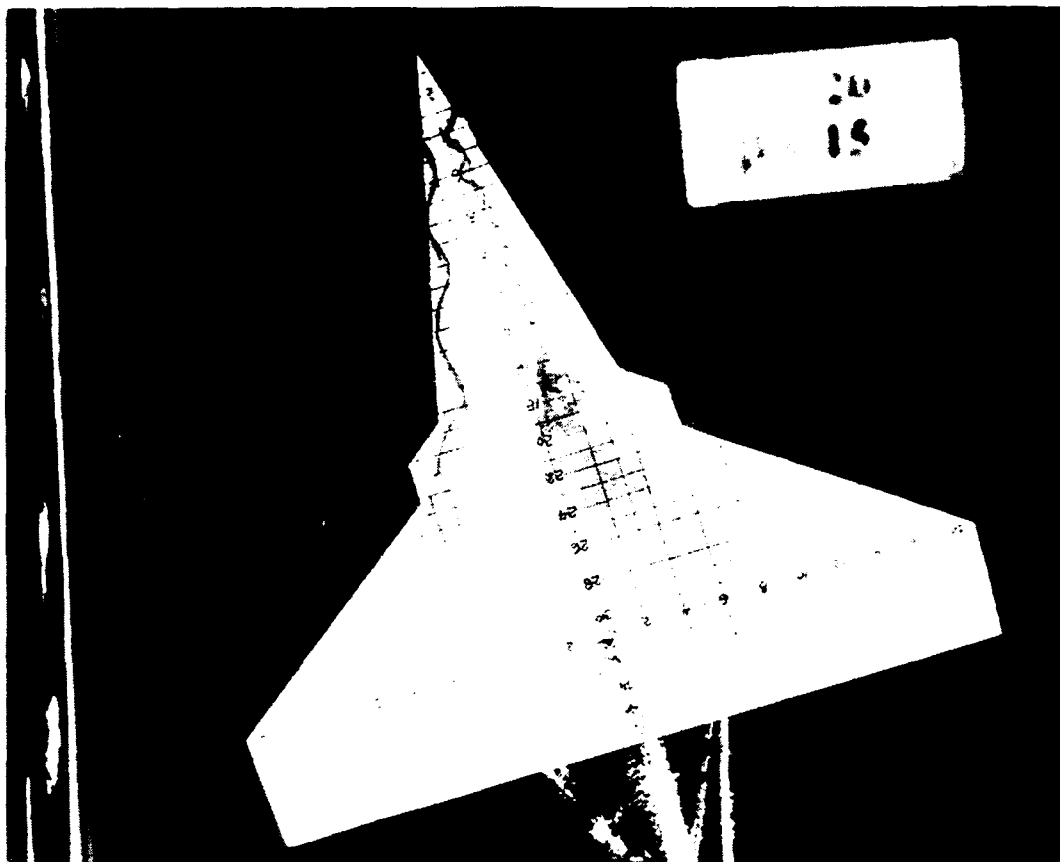


Figure 30 : Diamond-fillet model strake vortex , $\alpha=20^\circ$, $\beta=15^\circ$.

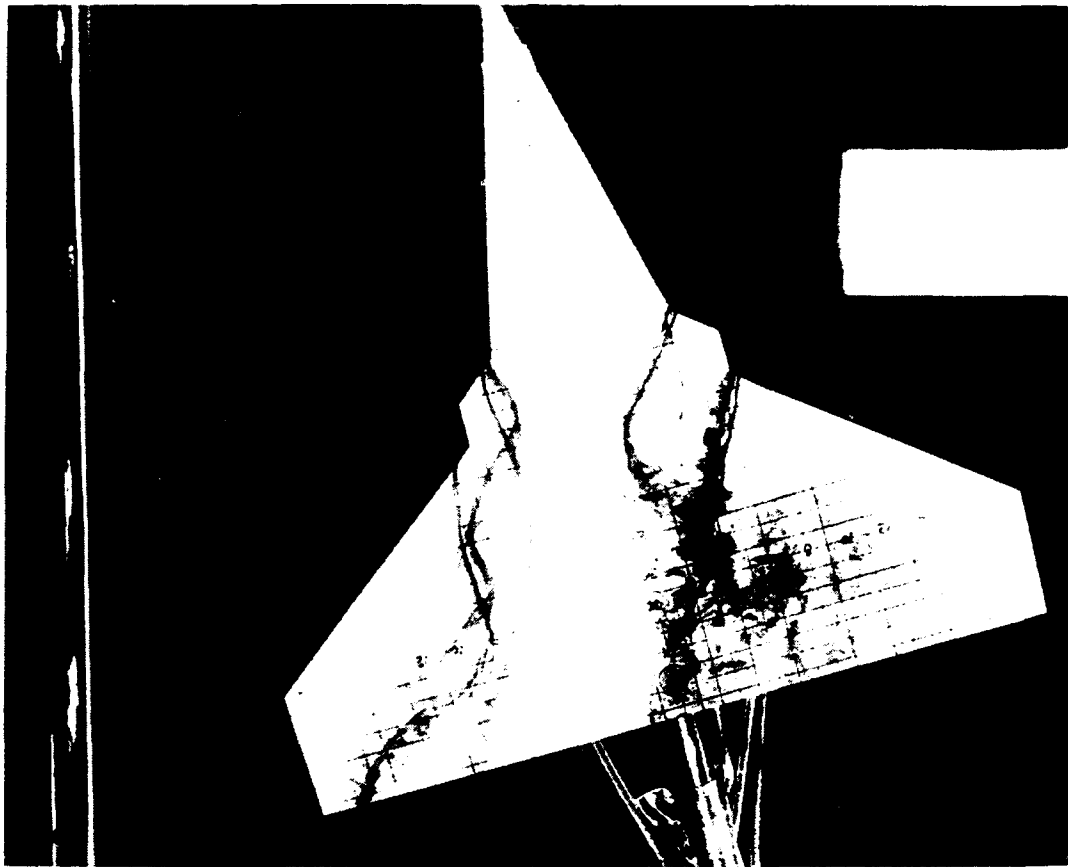


Figure 30A : Diamond-fillet model fillet vortex , $\alpha=10^\circ$, $\beta=15^\circ$.

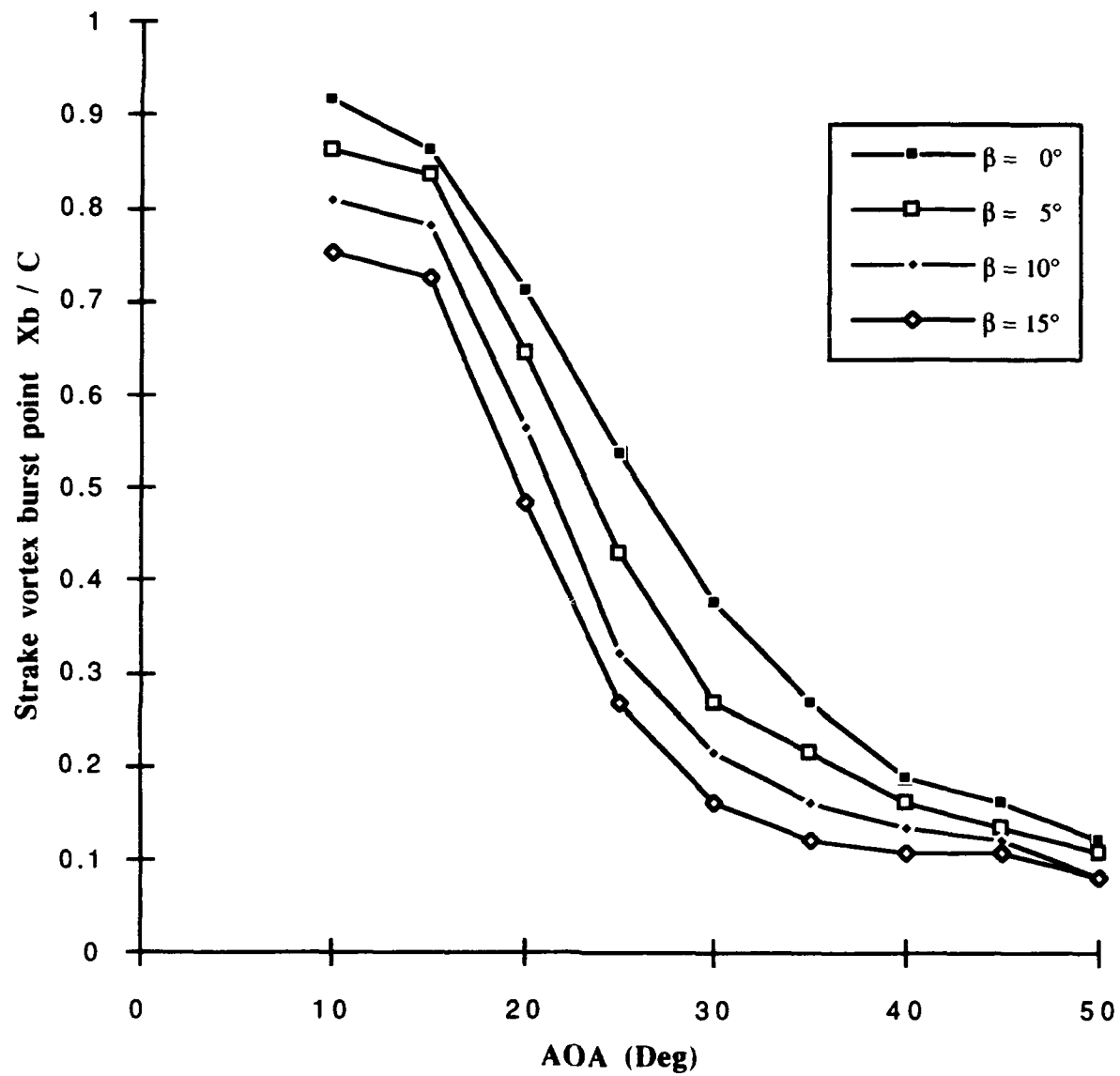


Figure 31 : Baseline model strake vortex burst point (Windward side)

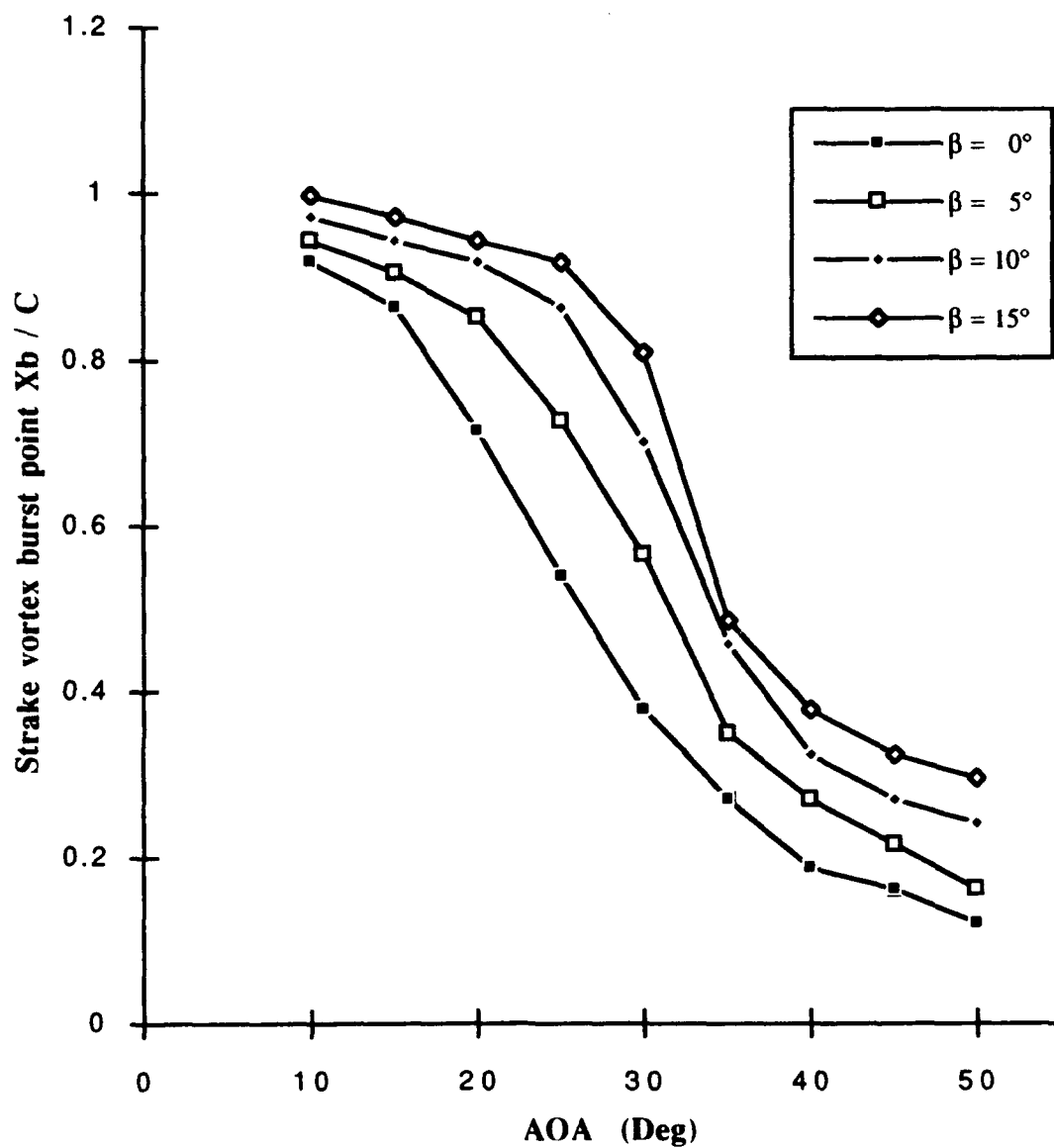


Figure 32 : Baseline model strake vortex burst point (Leeward side)

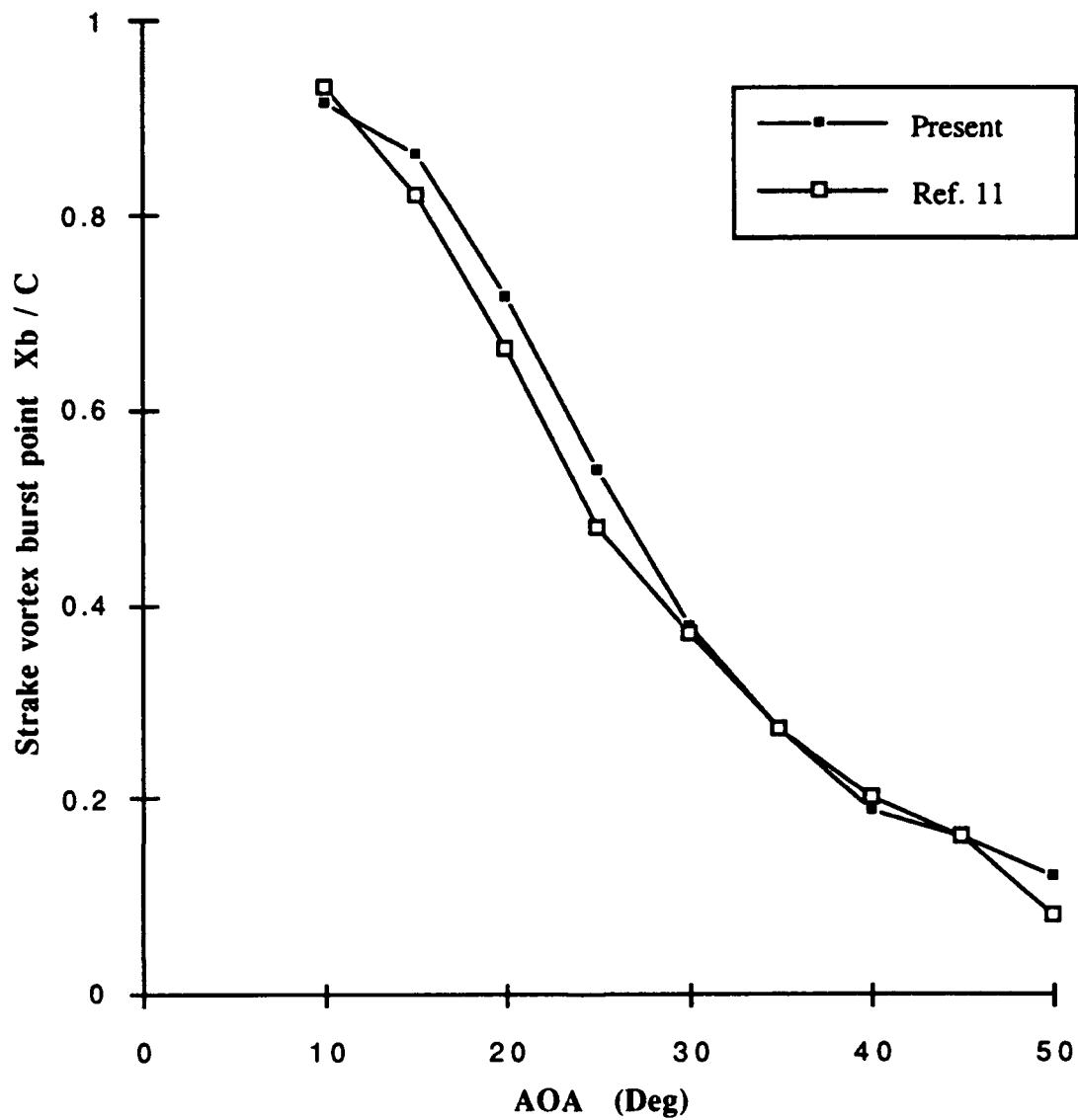


Figure 33 : Baseline model strake vortex burst point data comparison

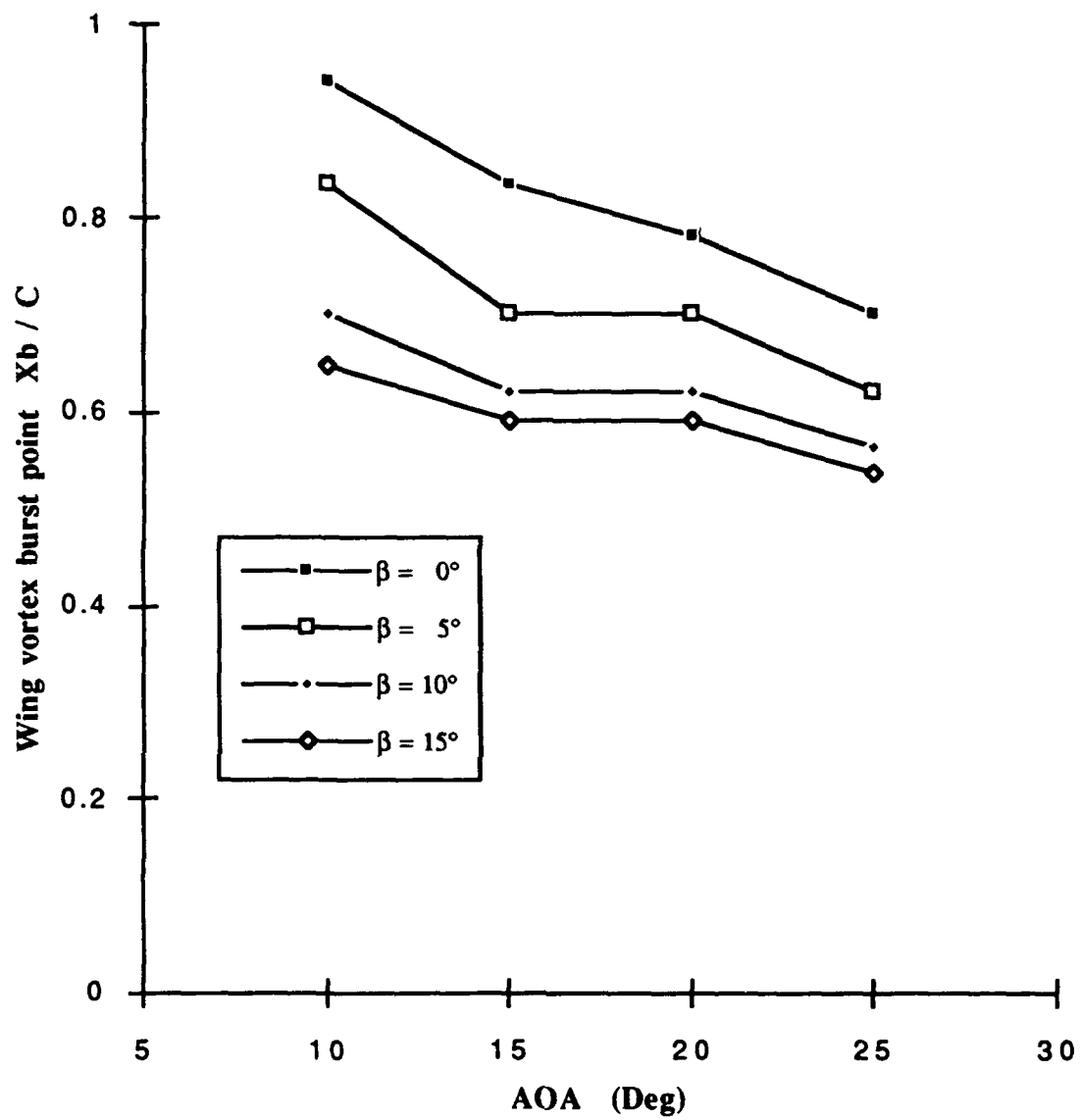


Figure 34 : Baseline model wing vortex burst point (Windward side)

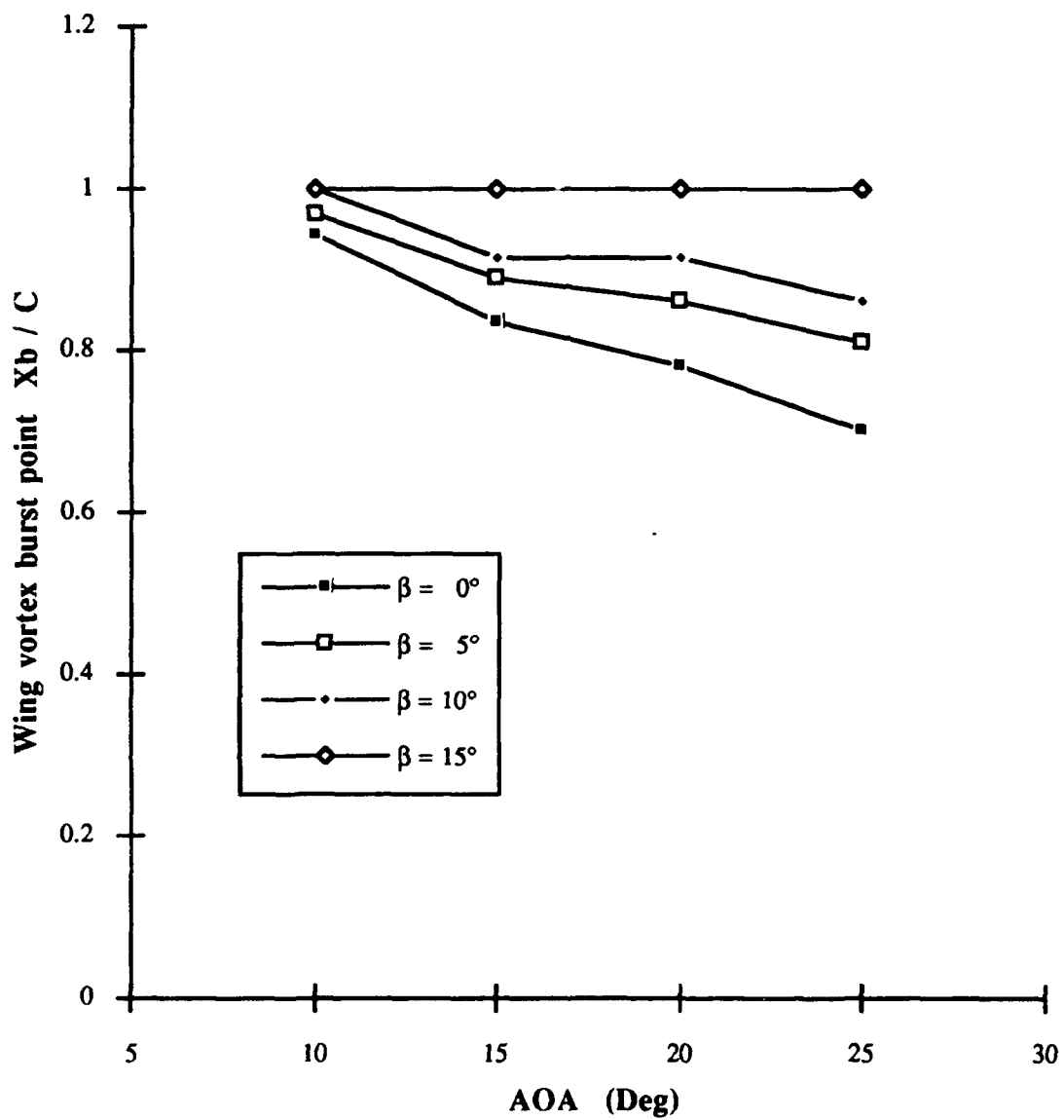


Figure 35 : Baseline model wing vortex burst point (Leeward side)

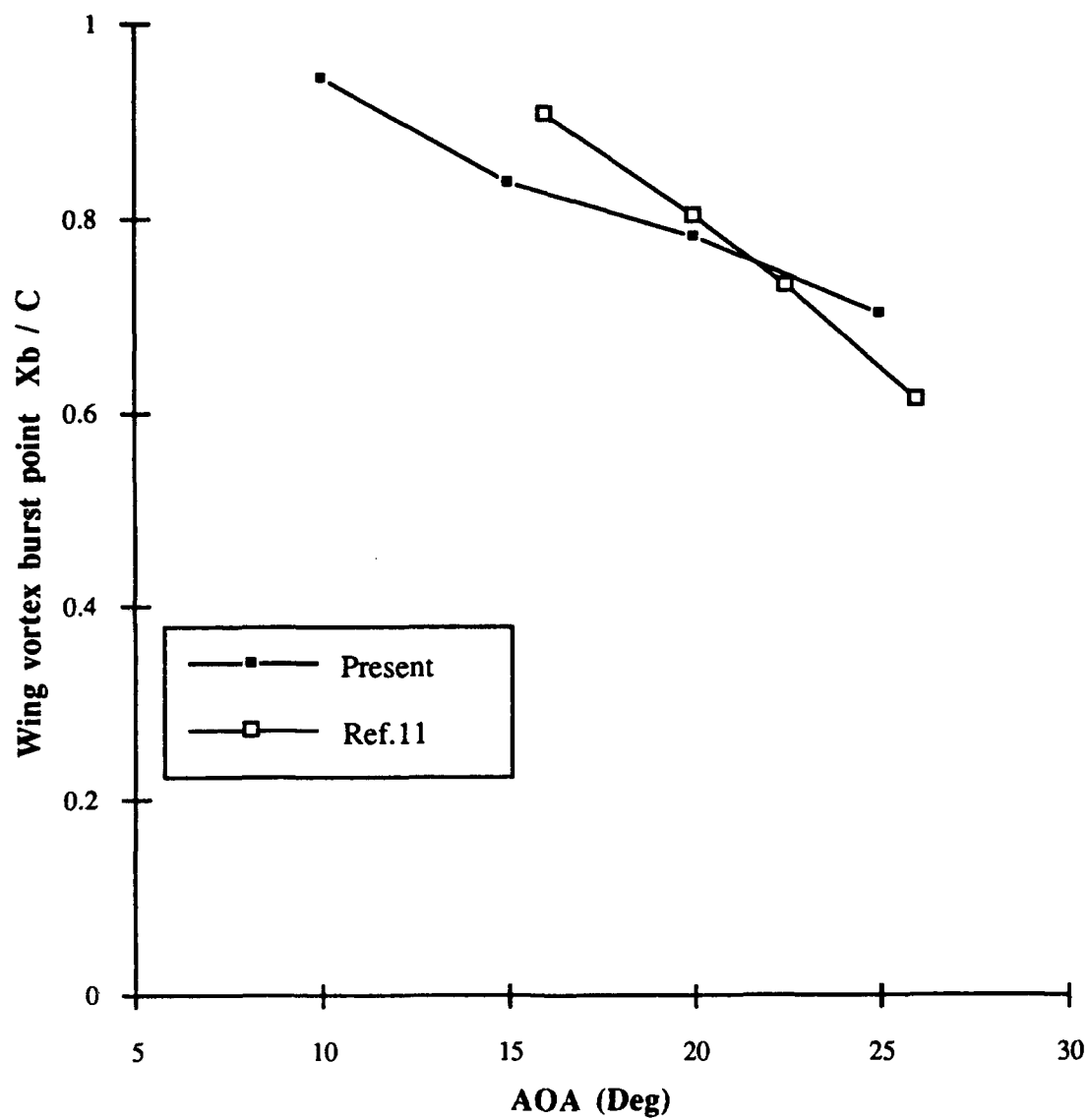


Figure 36 : Baseline model wing vortex burst point data comparison (AOS=0)

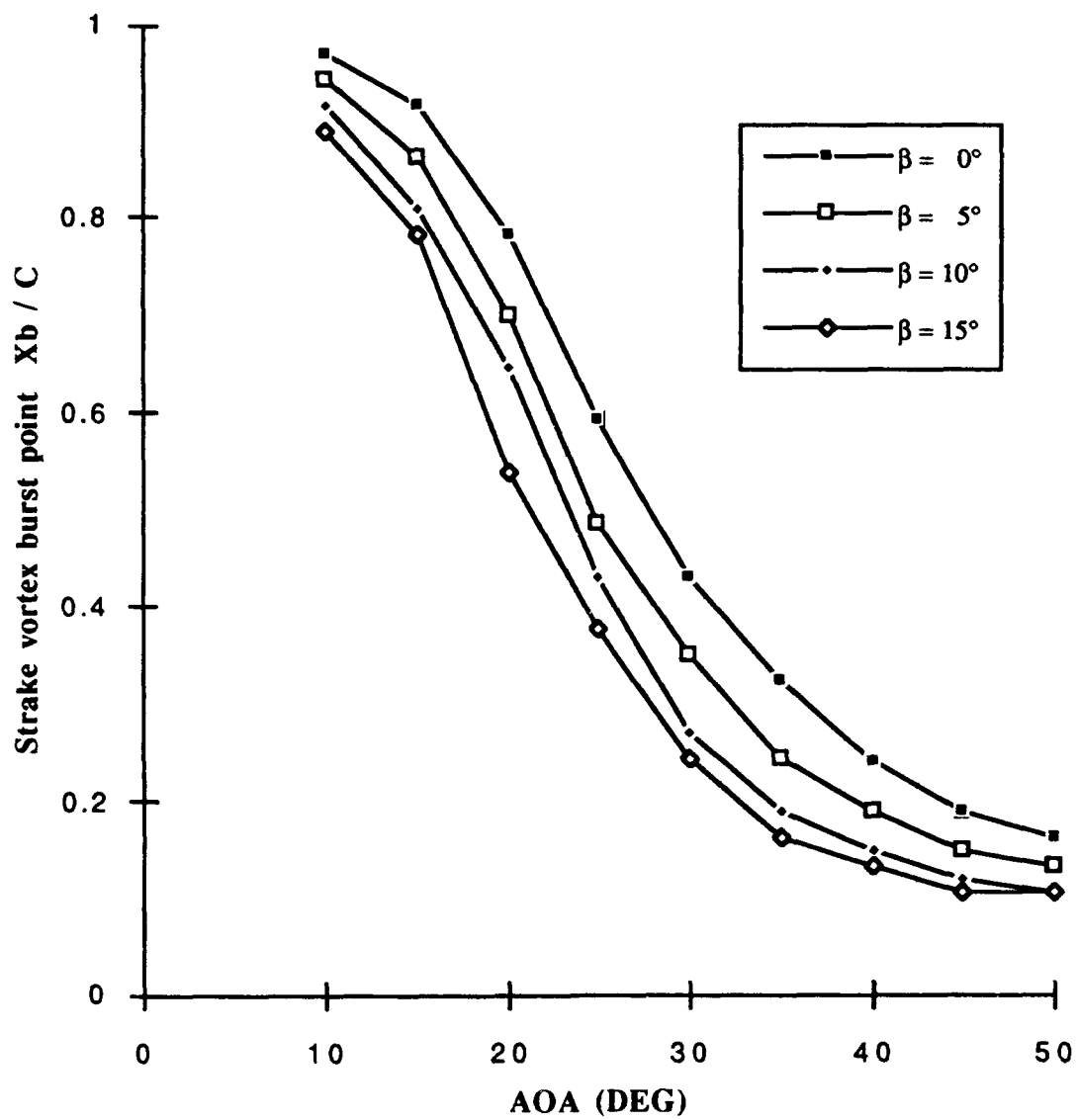


Figure 37 : Diamond-fillet model strake vortex burst point (Windward side)

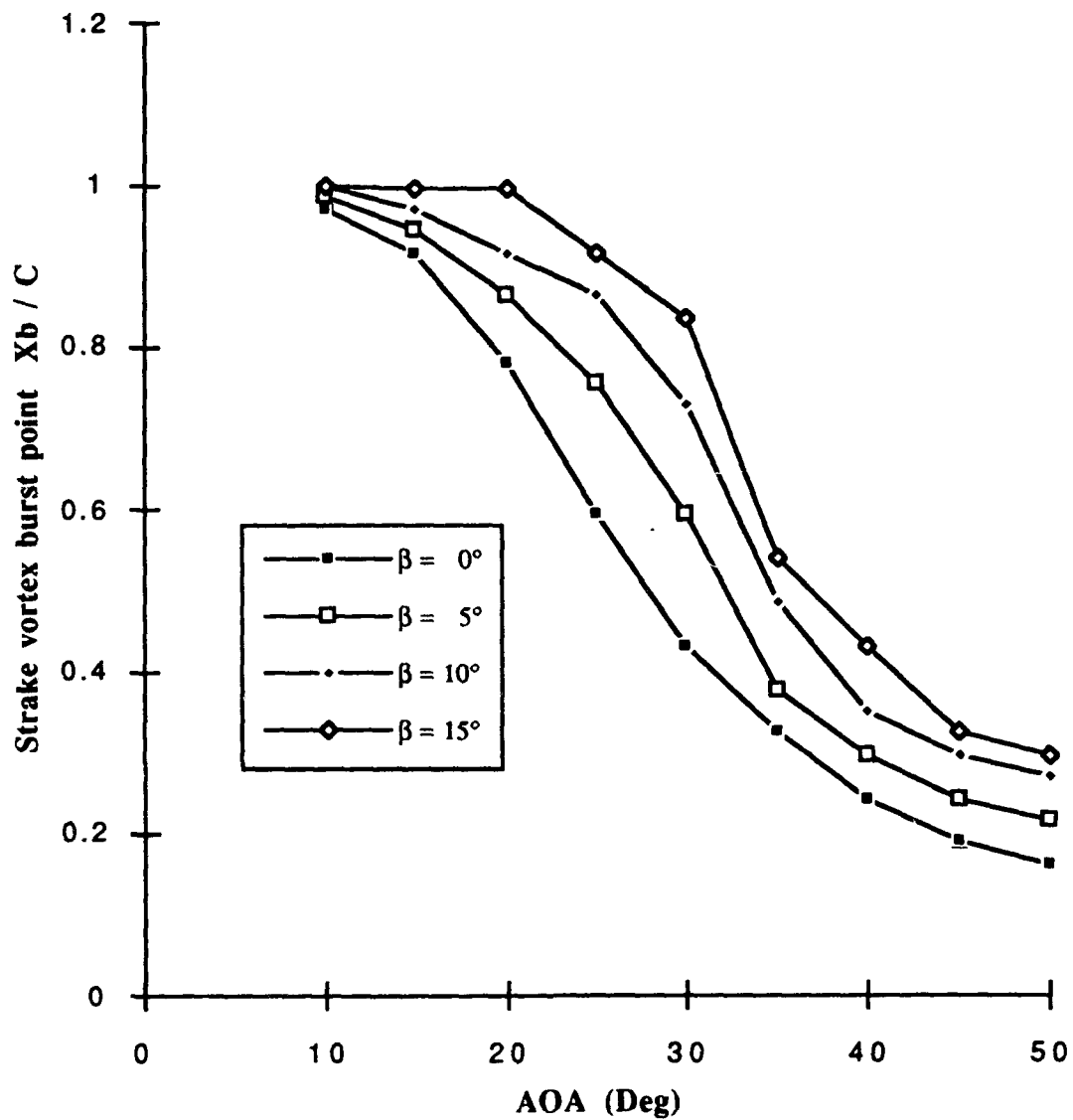


Figure 38 : Diamond-fillet model strake vortex burst point (Leeward side)

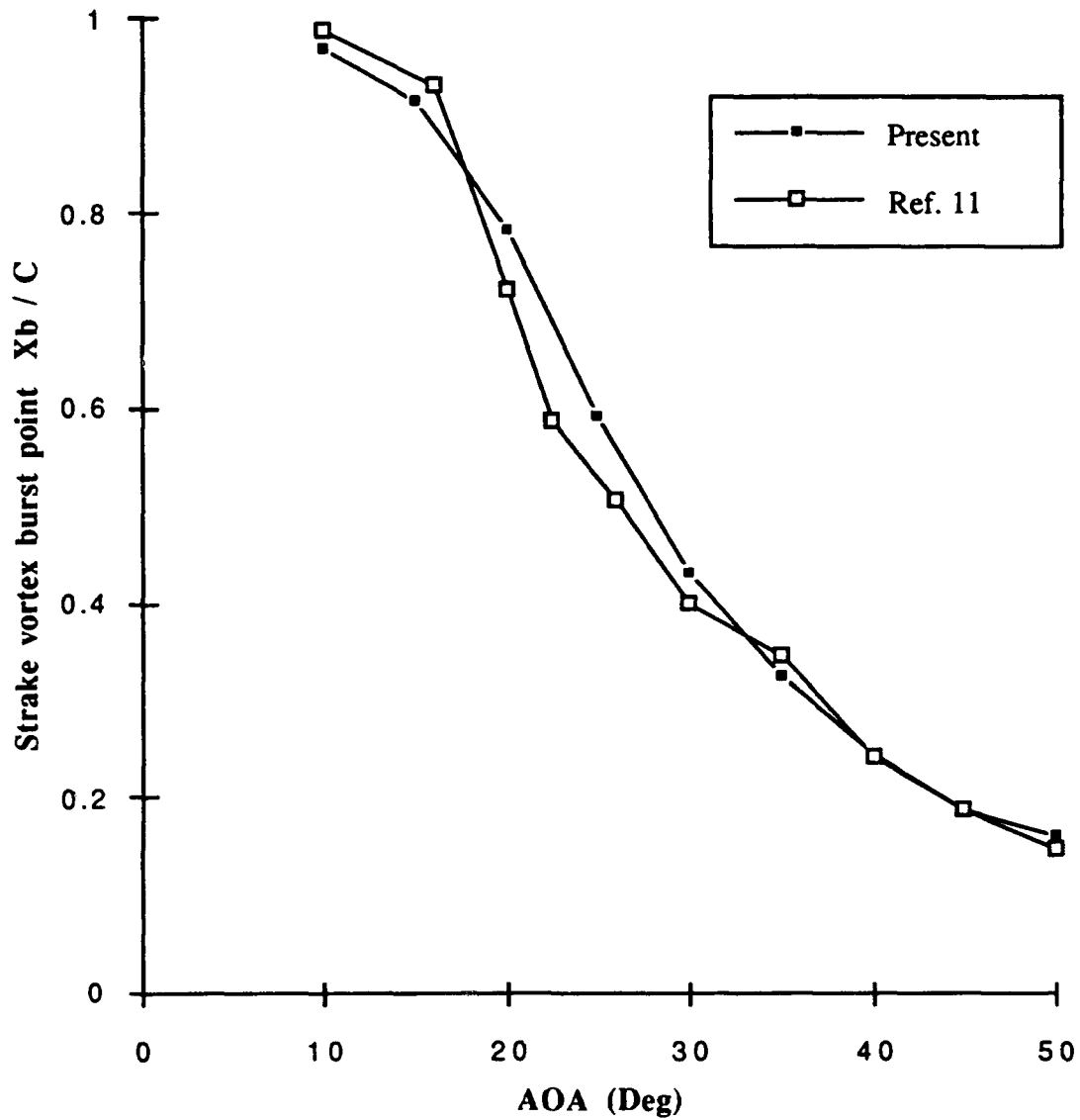


Figure 39 : Diamond-fillet model strake vortex burst point data comparison

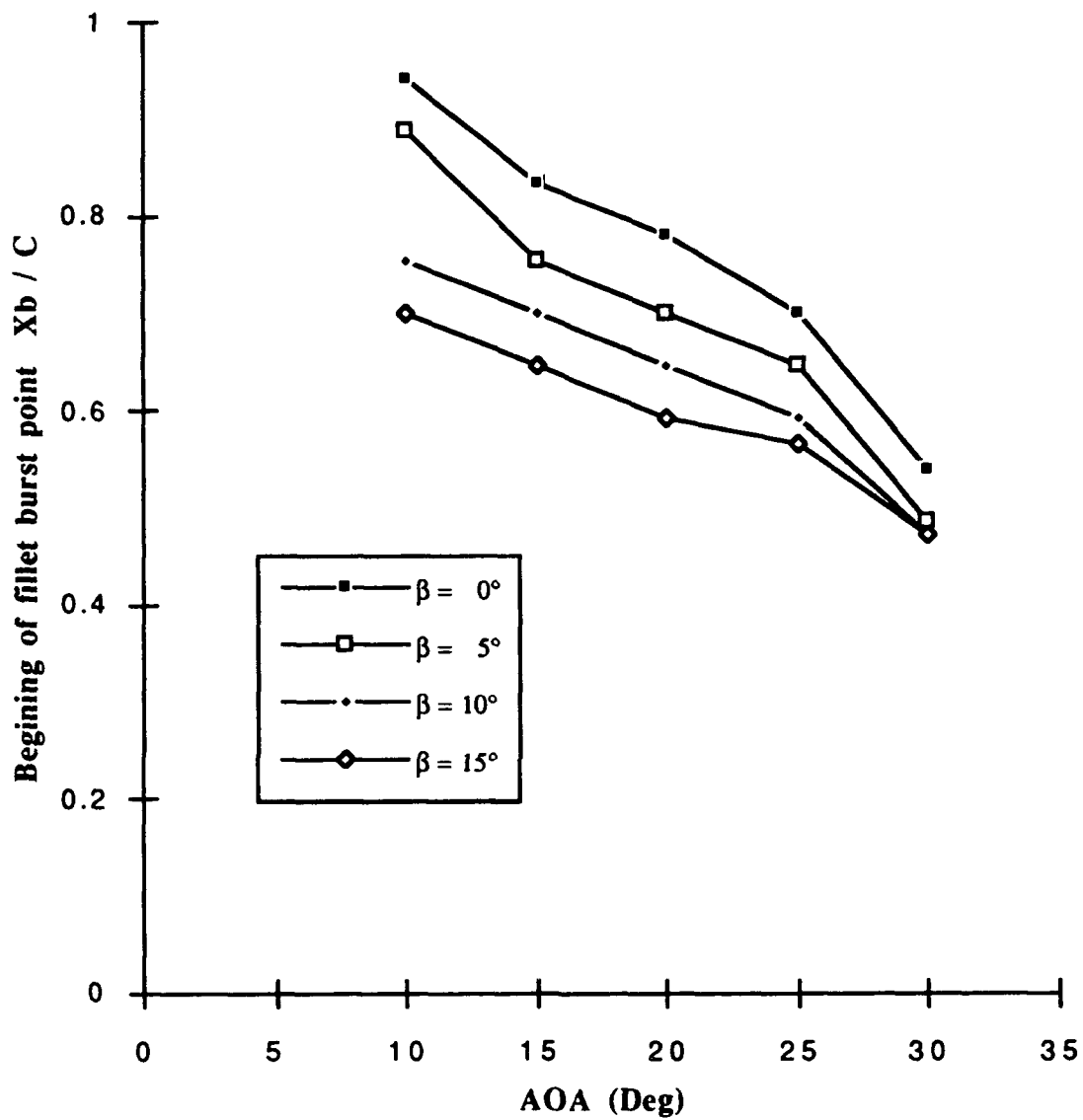


Figure 40 : Diamond-fillet model beginning-of-fillet vortex burst point (Windward side)

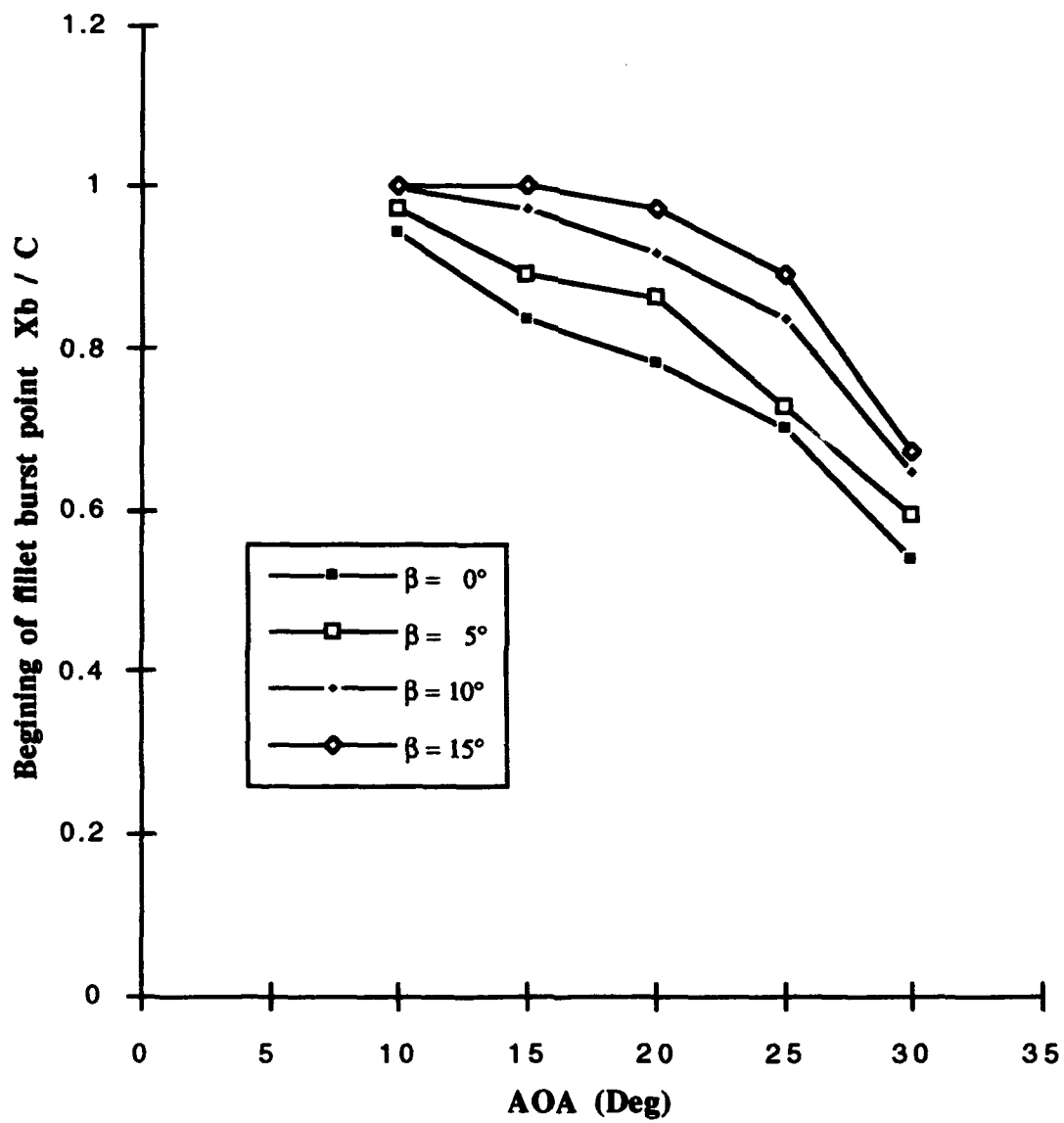


Figure 41 : Diamond-fillet model beginning-of-fillet vortex burst point (Leeward side)

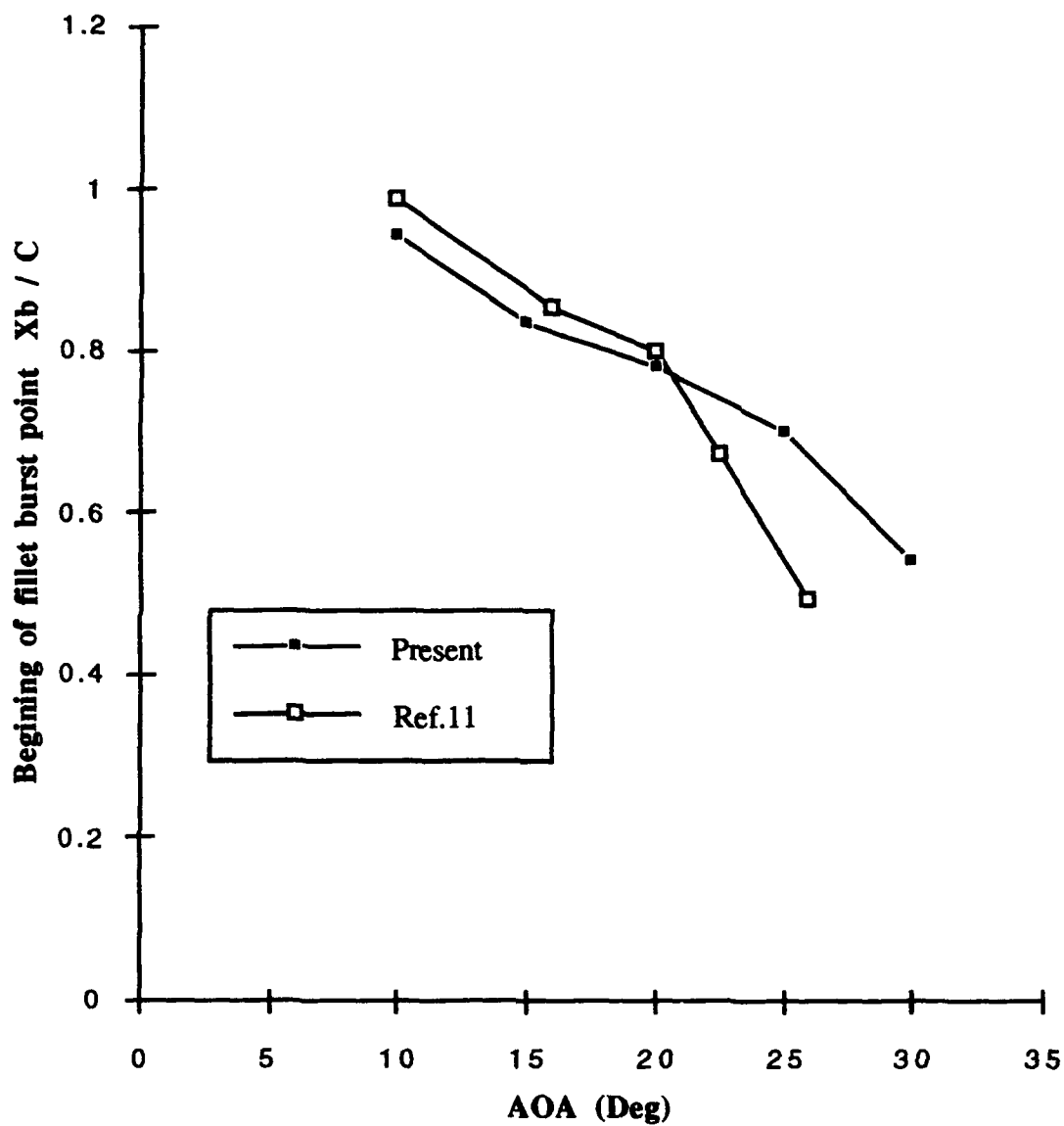


Figure 42 : Diamond -fillet model beginning-of-fillet vortex burst point data comparison

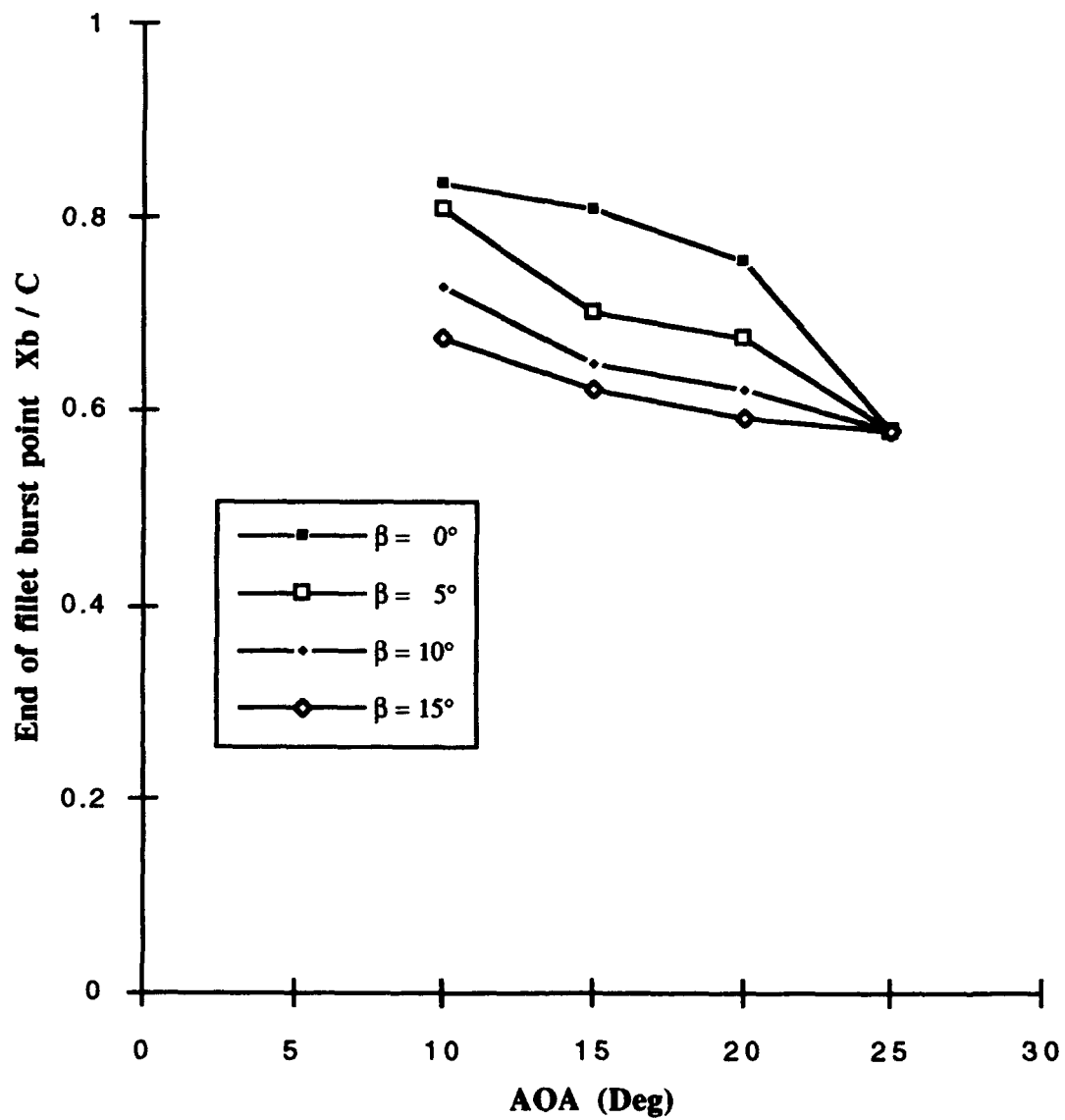


Figure 43 : Diamond-fillet model end-of-fillet vortex burst point (Windward side)

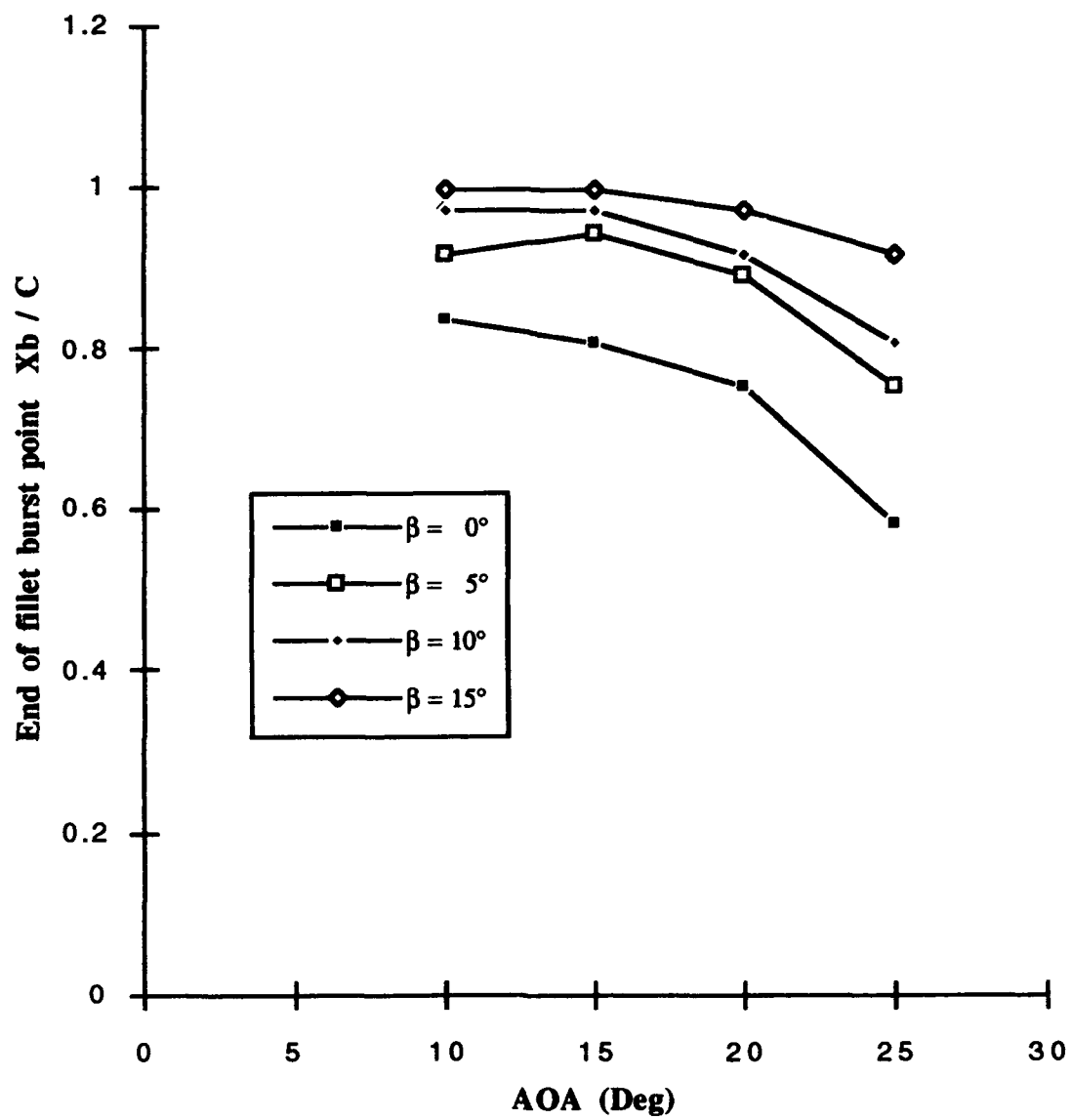


Figure 44 : Diamond-fillet model end-of-fillet vortex burst point (Leeward side)

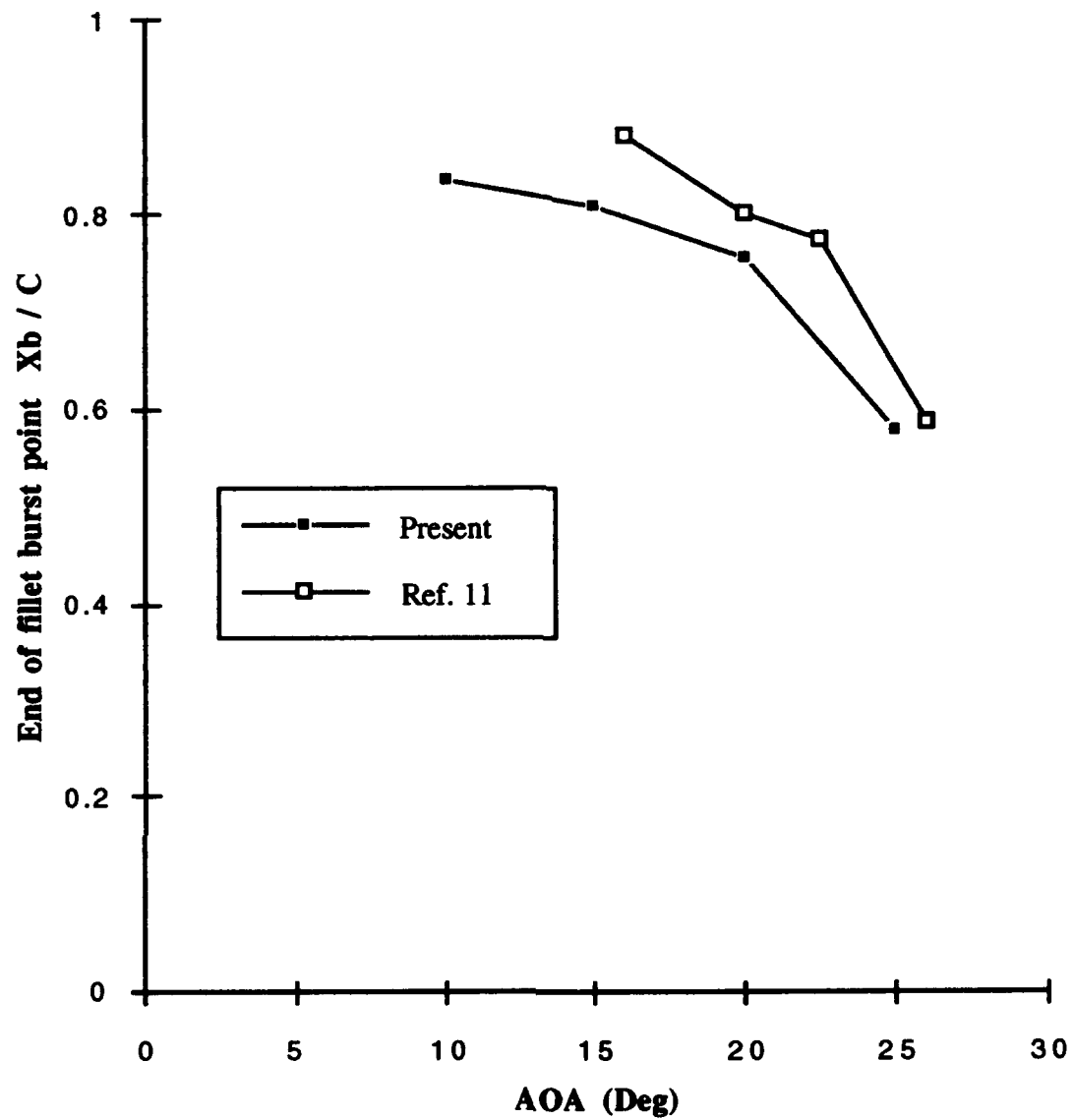


Figure 45 : Diamond-fillet model end-of-fillet vortex burst point data comparison

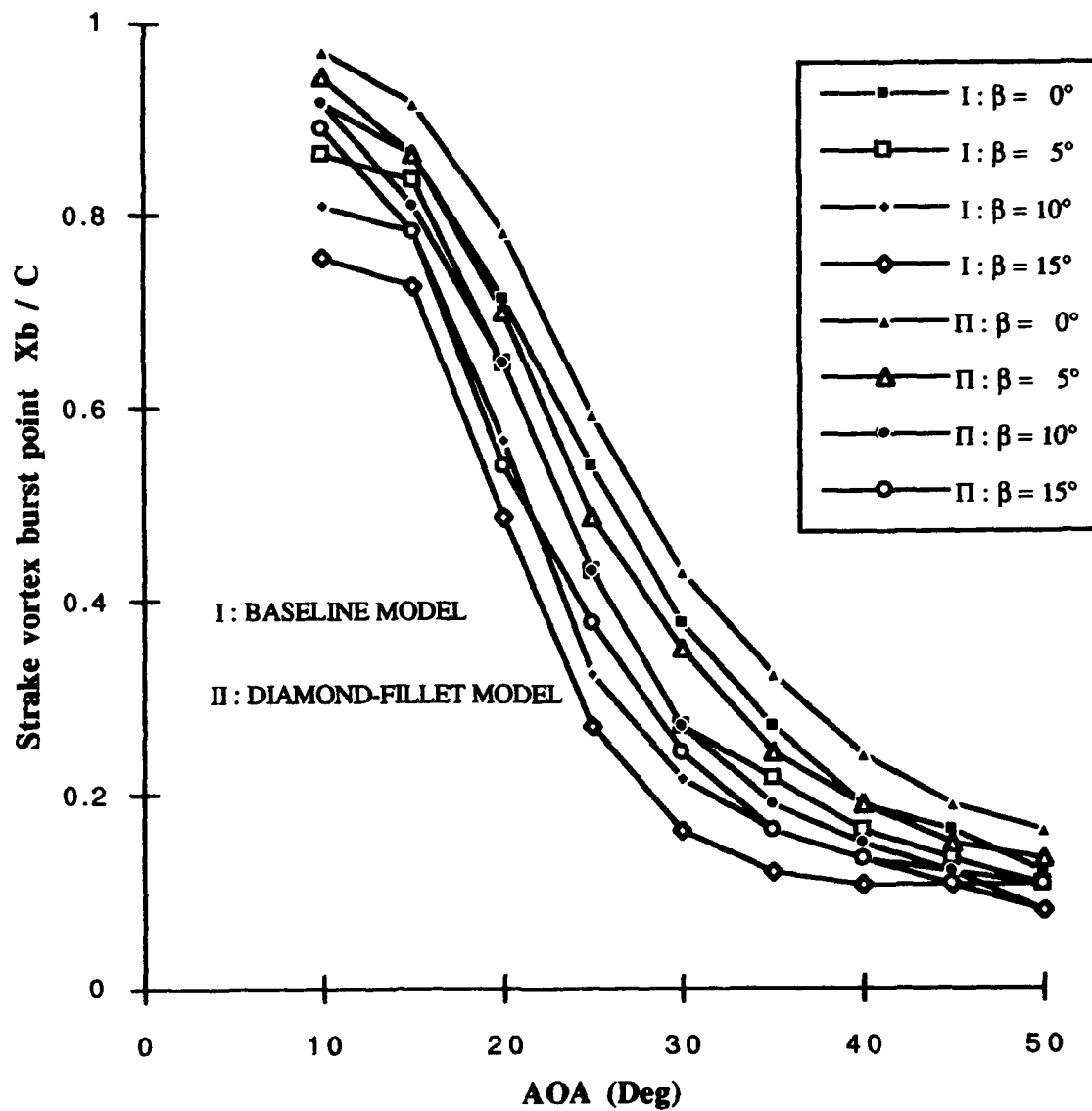


Figure 46 : Strake vortex burst point data comparison for two models (Windward side)

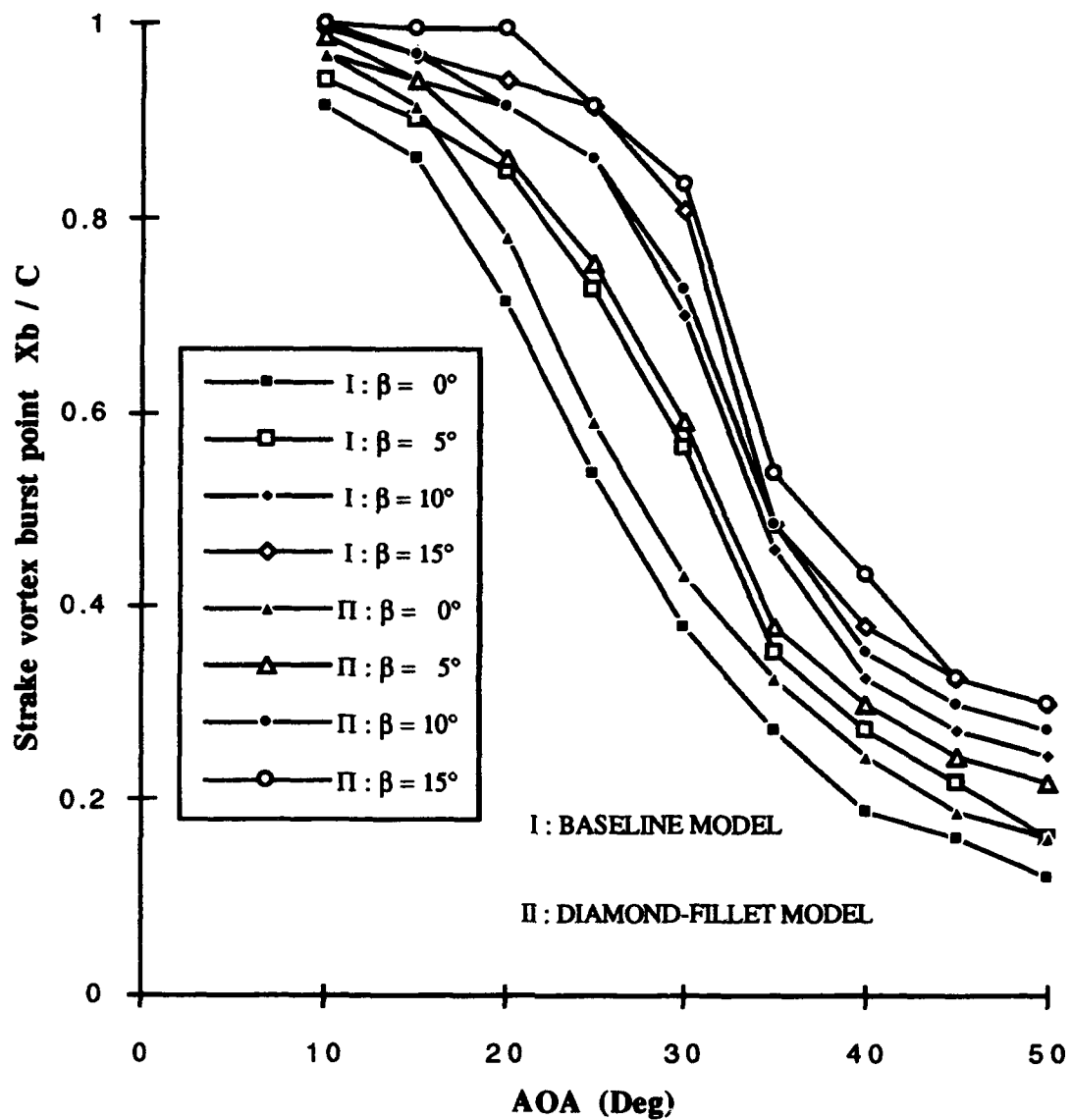


Figure 47 : Strake vortex burst point data comparison for two models (Leeward side)

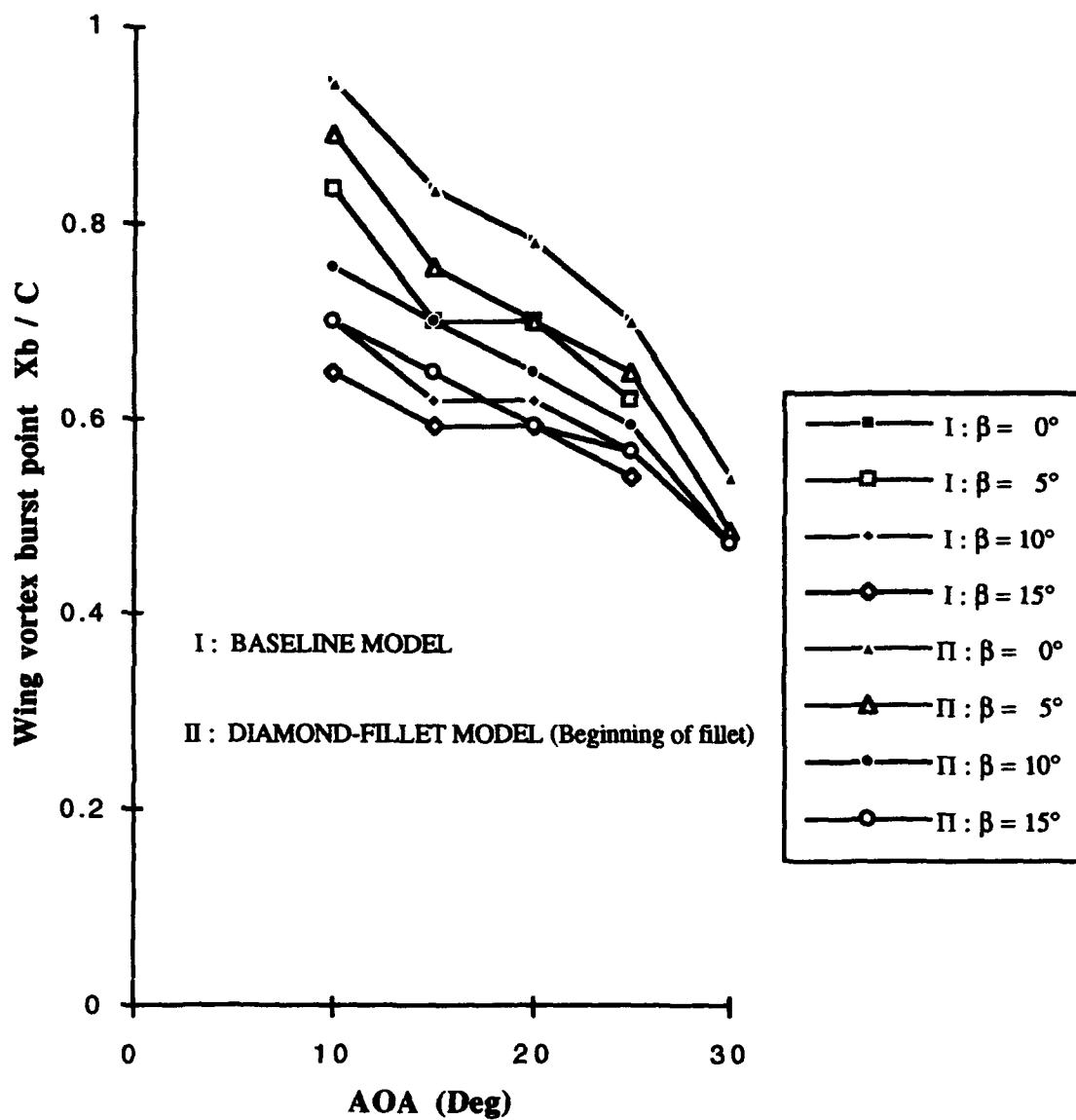


Figure 48 : Wing vortex burst point data comparison for two models (Windward side)I

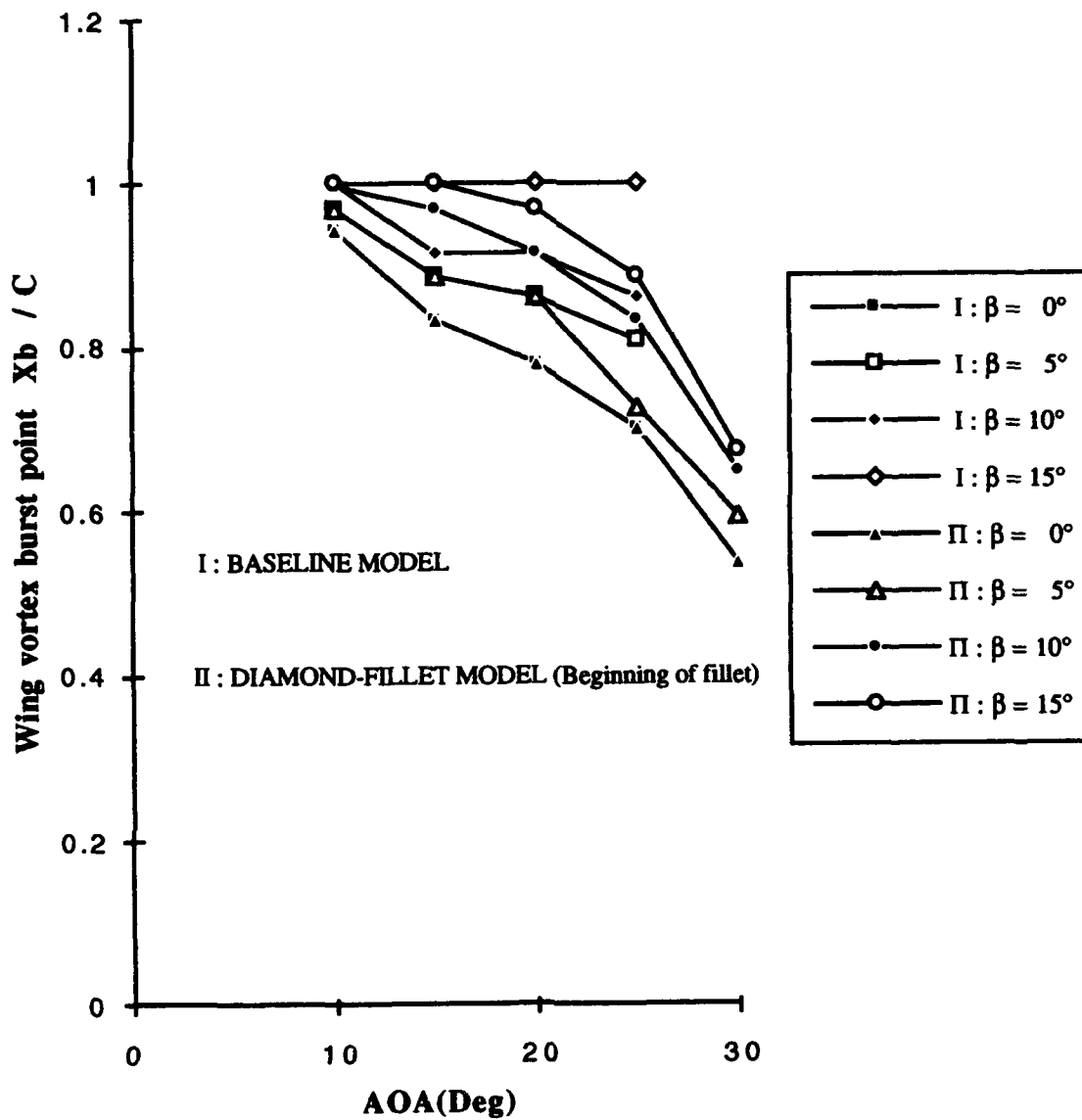


Figure 49 : Wing vortex burst point data comparison for two models (Leeward side)I

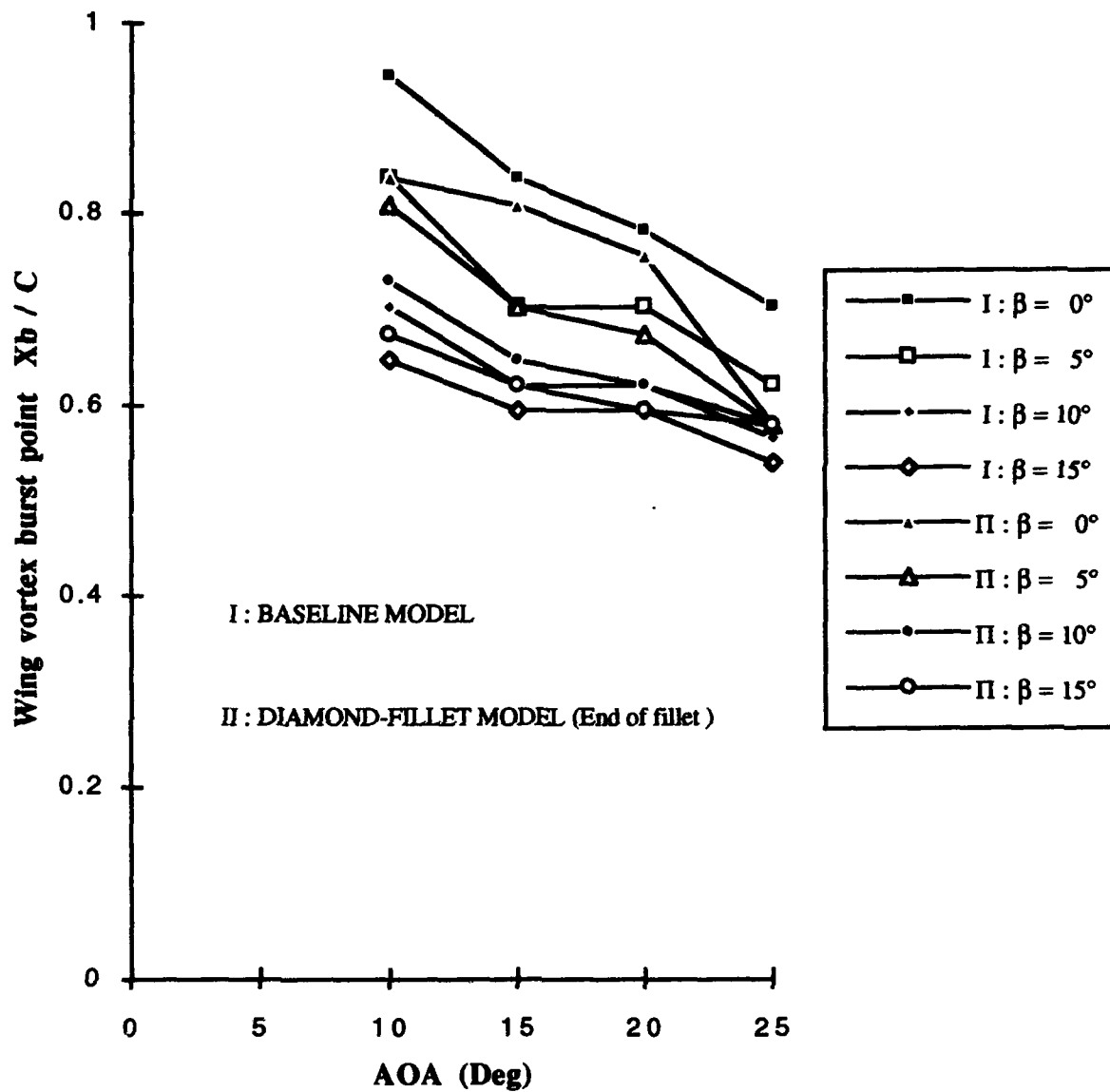


Figure 50 : Wing vortex burst point data comparison for two models (Windward side) II

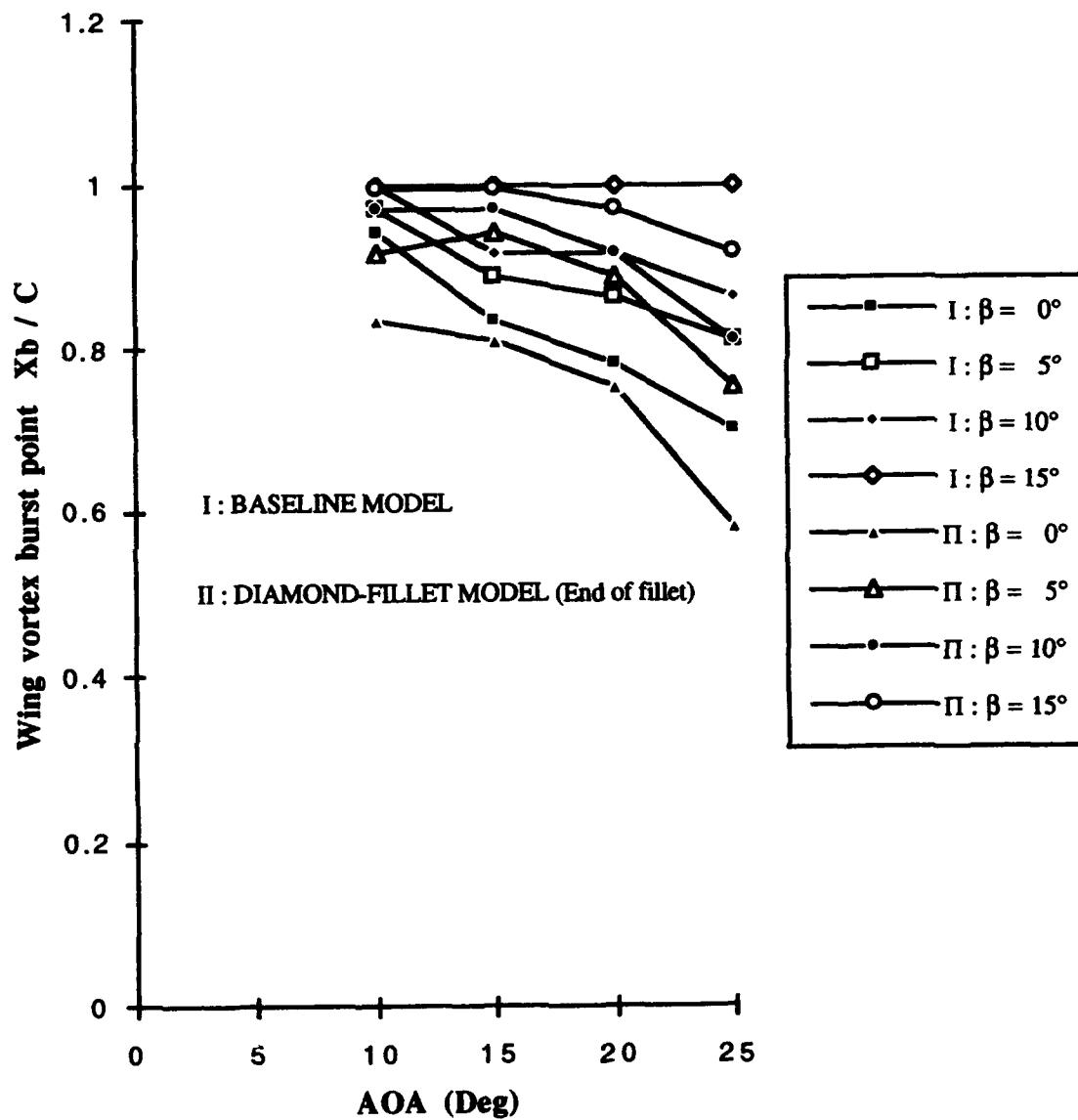


Figure 51 : Wing vortex burst point data comparison for two models
(Leeward side) II

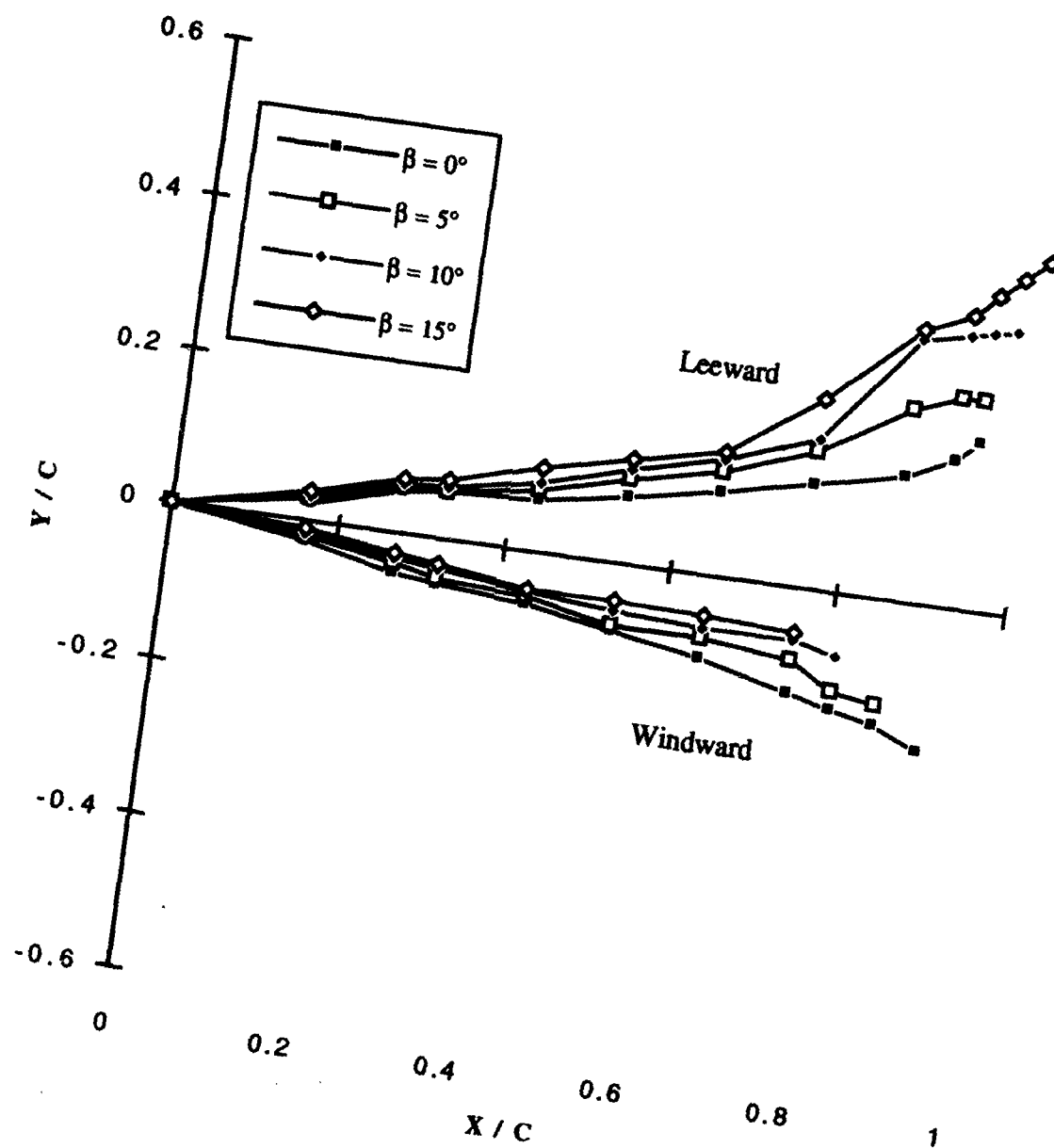


Figure 52 : Baseline model strake vortex core trajectory (AOA=10°)

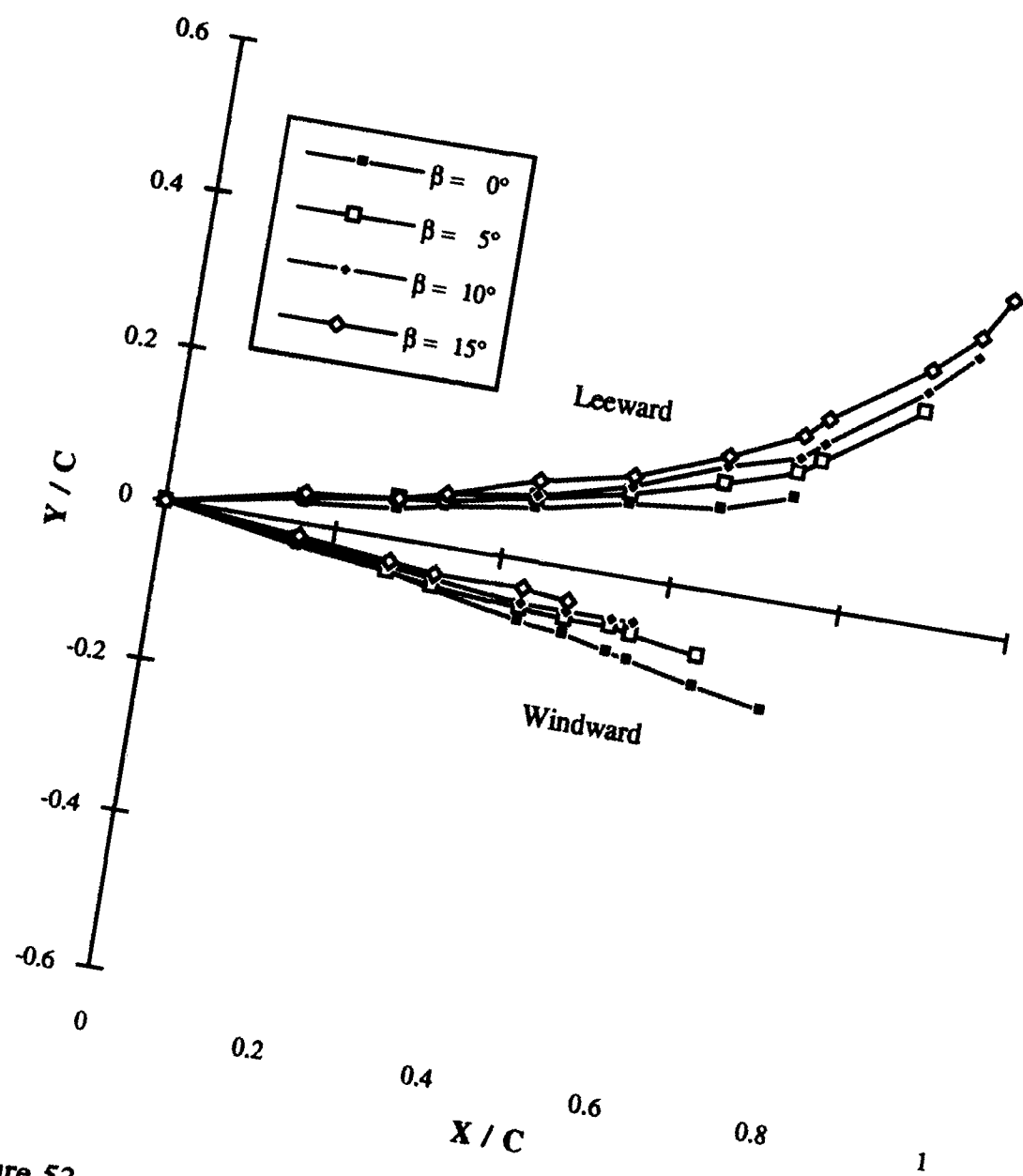


Figure 53 : Baseline model strake vortex core trajectory (AOA=20°)

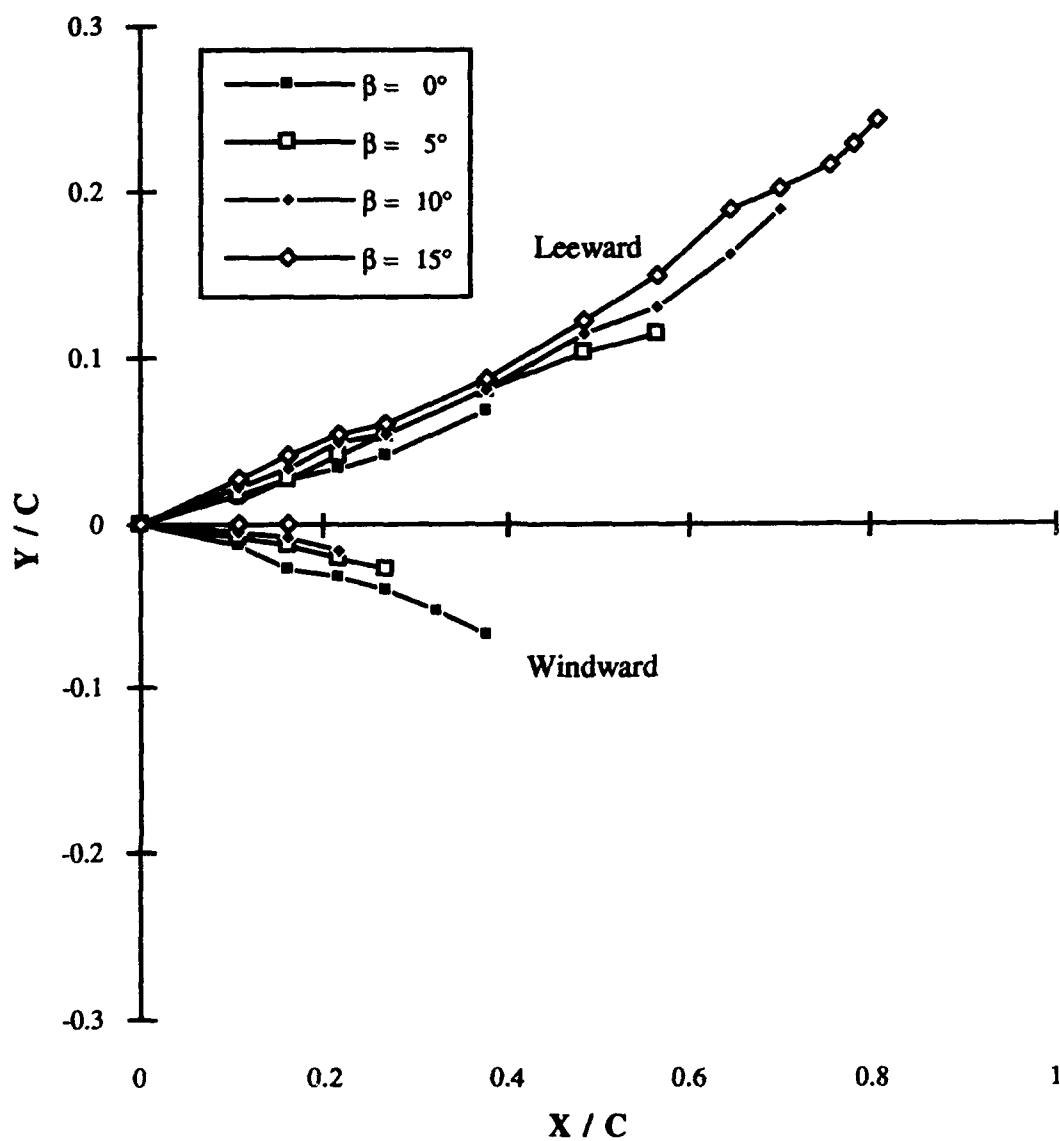


Figure 54 : Baseline model strake vortex core trajectory (AOA=30°)

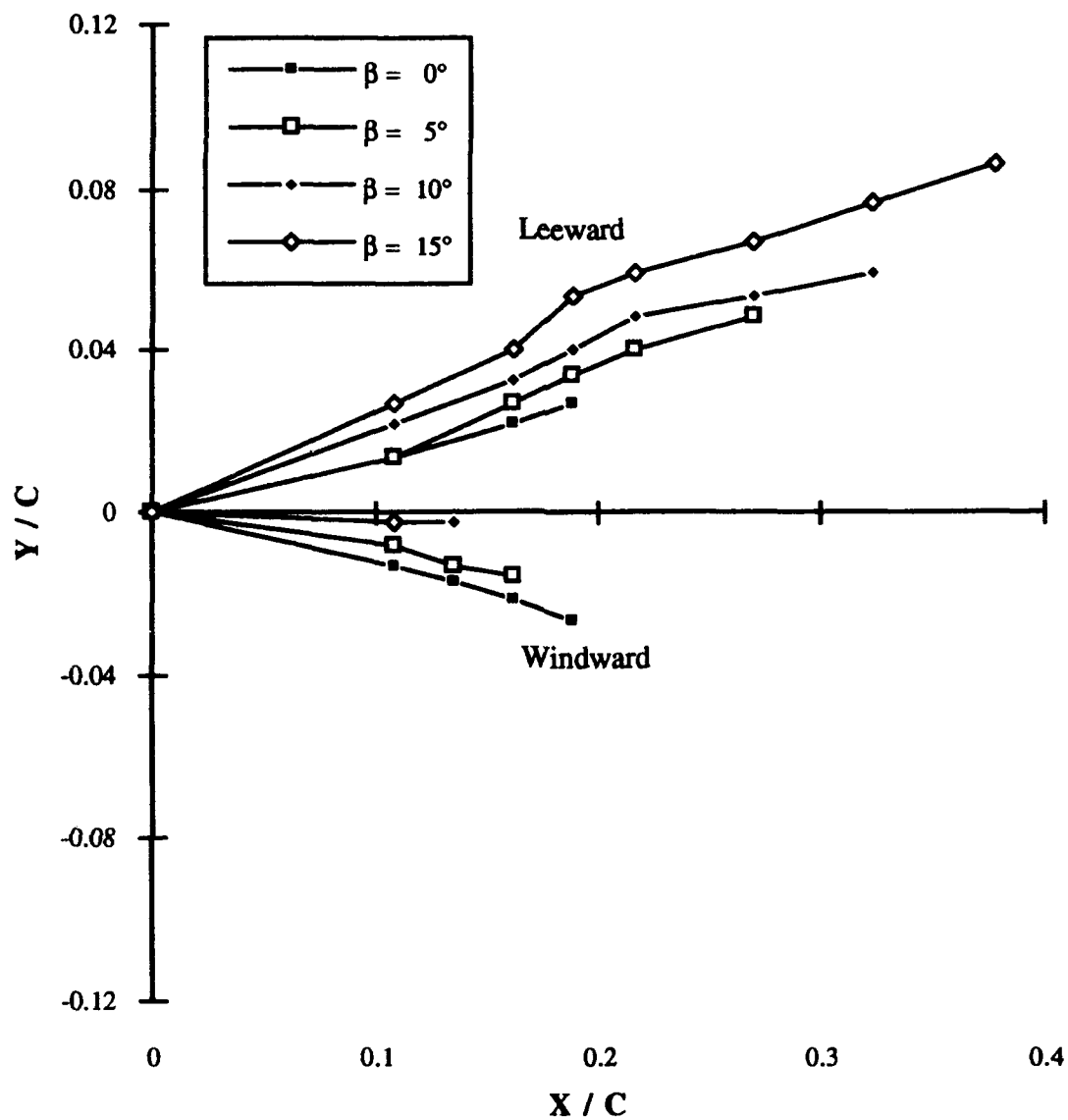


Figure 55 : Baseline model strake vortex core trajectory (AOA=40°)

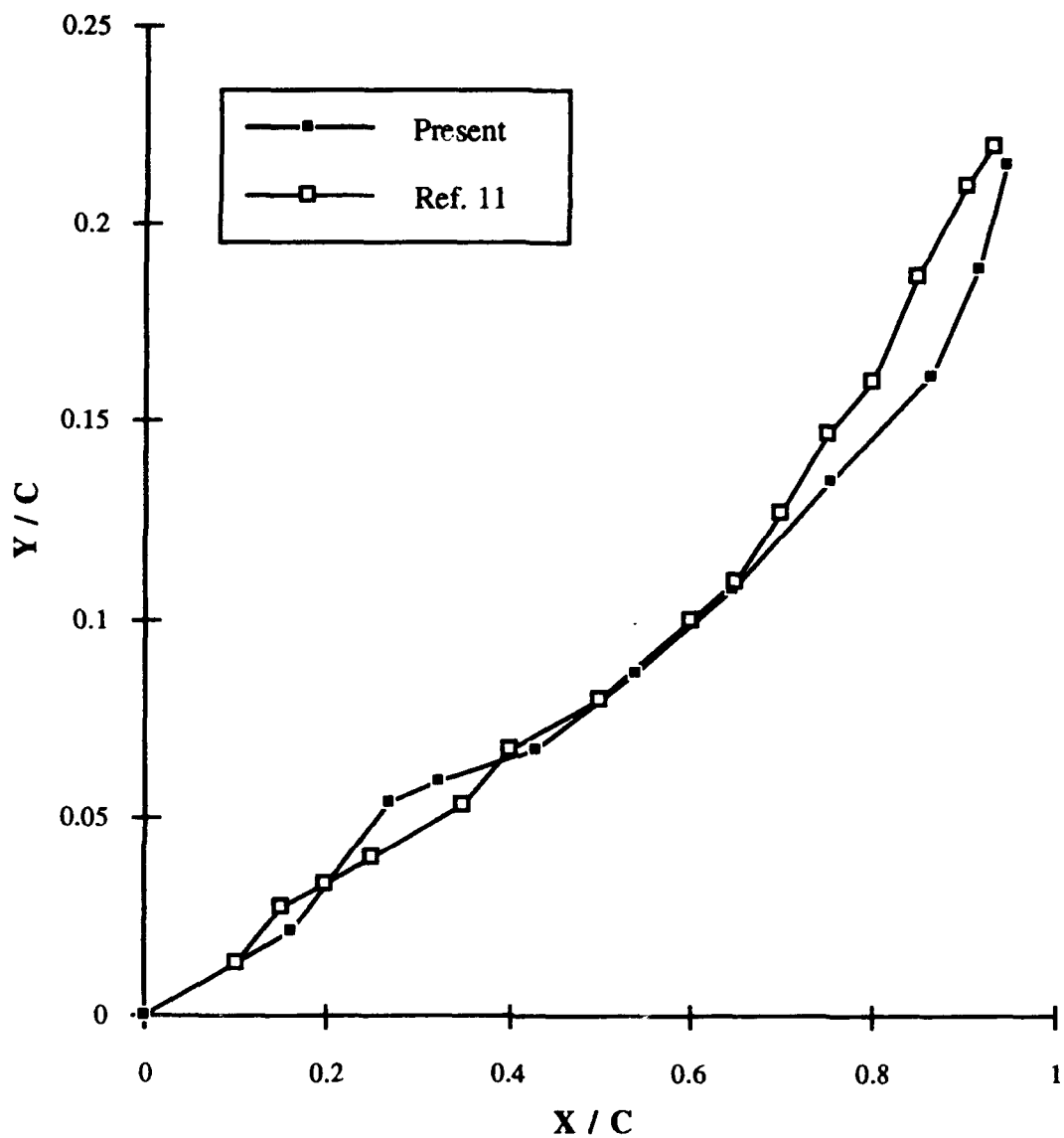


Figure 56 : Baseline model stroke vortex core trajectory data comparison
($AOA=10^\circ, AOS=0^\circ$)

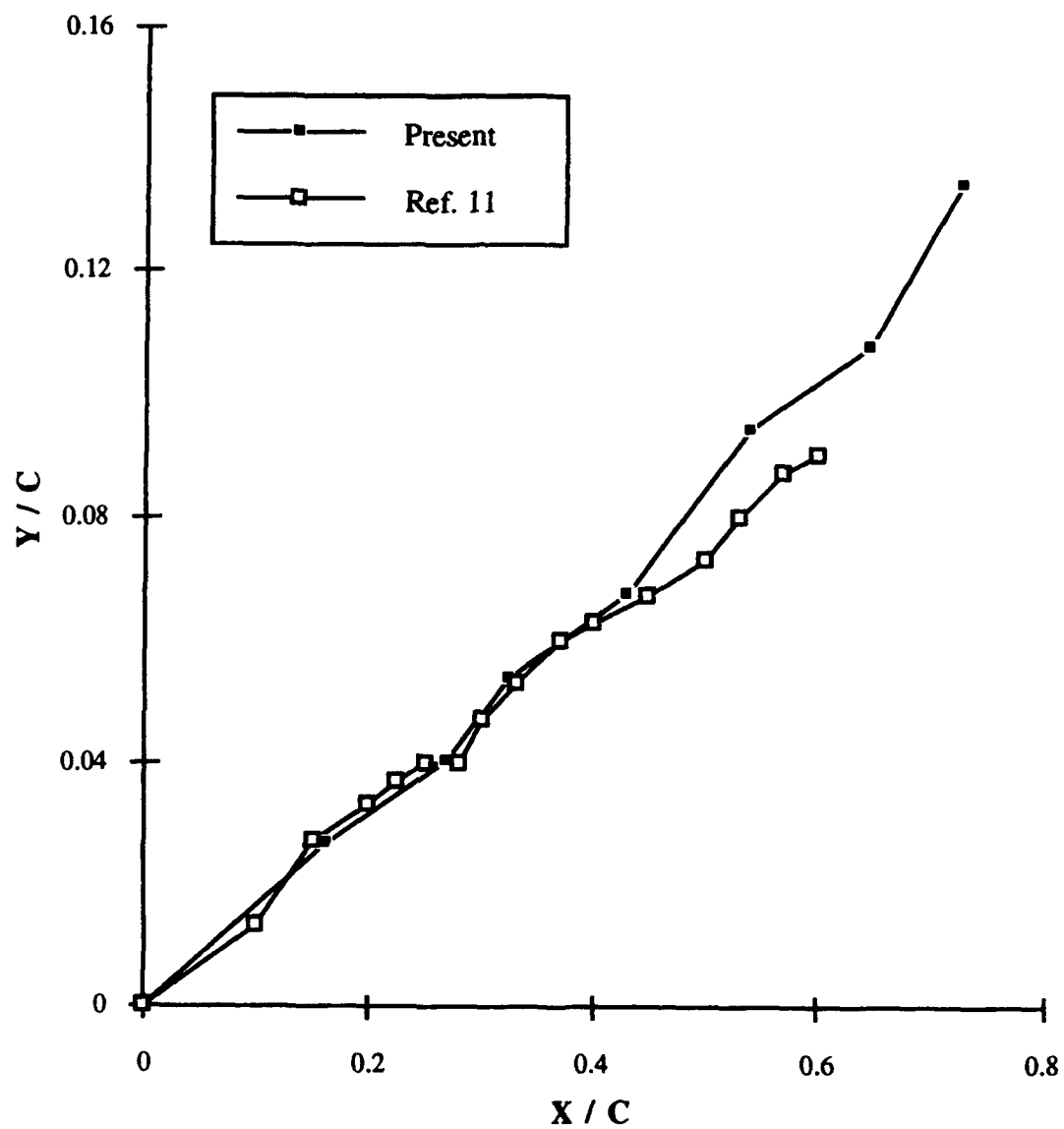


Figure 57 : Baseline model stroke vortex core trajectory data comparison
($AOA=20^\circ, AOS=0^\circ$)

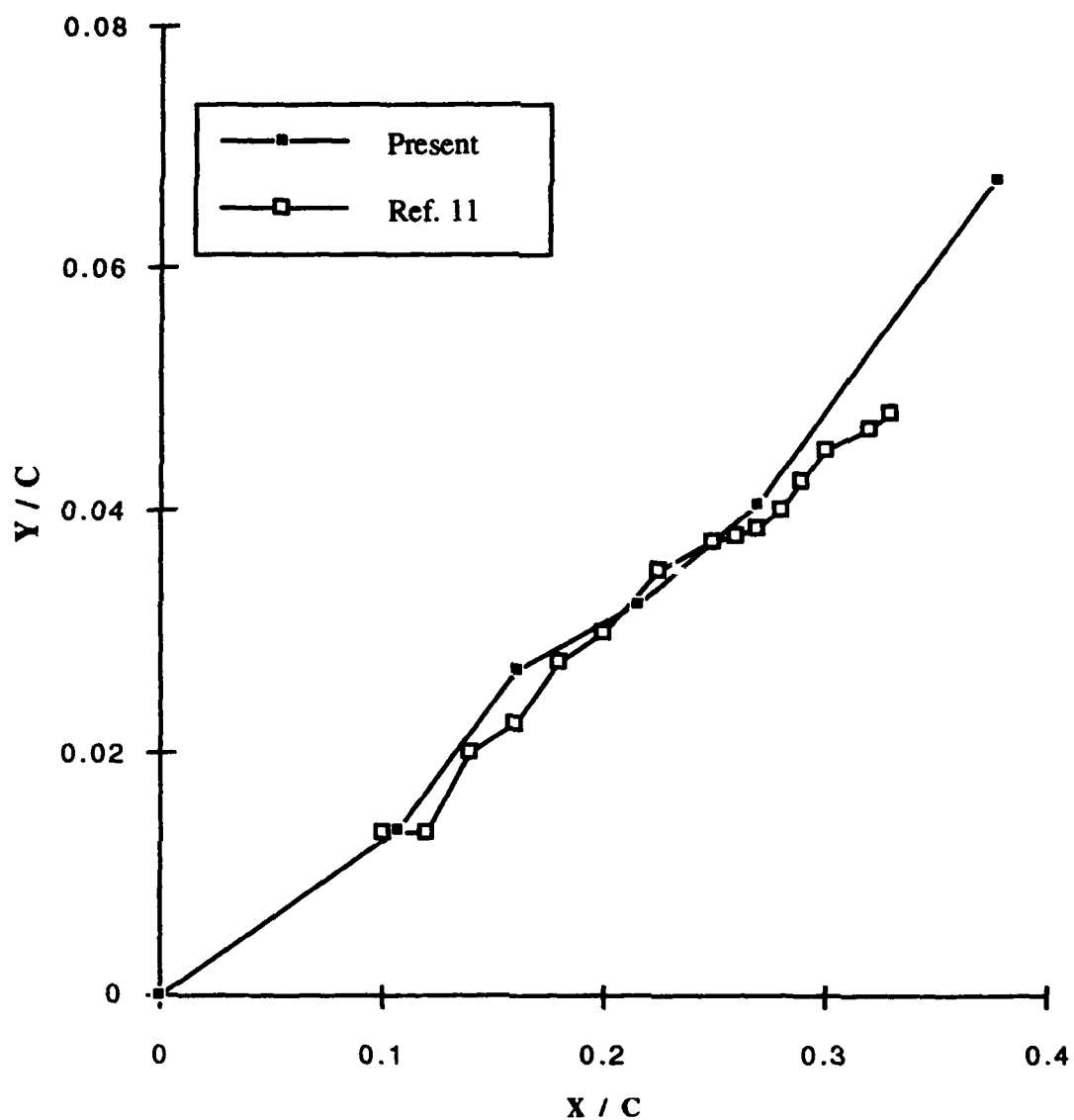


Figure 58 : Baseline model strake vortex core trajectory data comparison
(AOA =30°,AOS=0°)

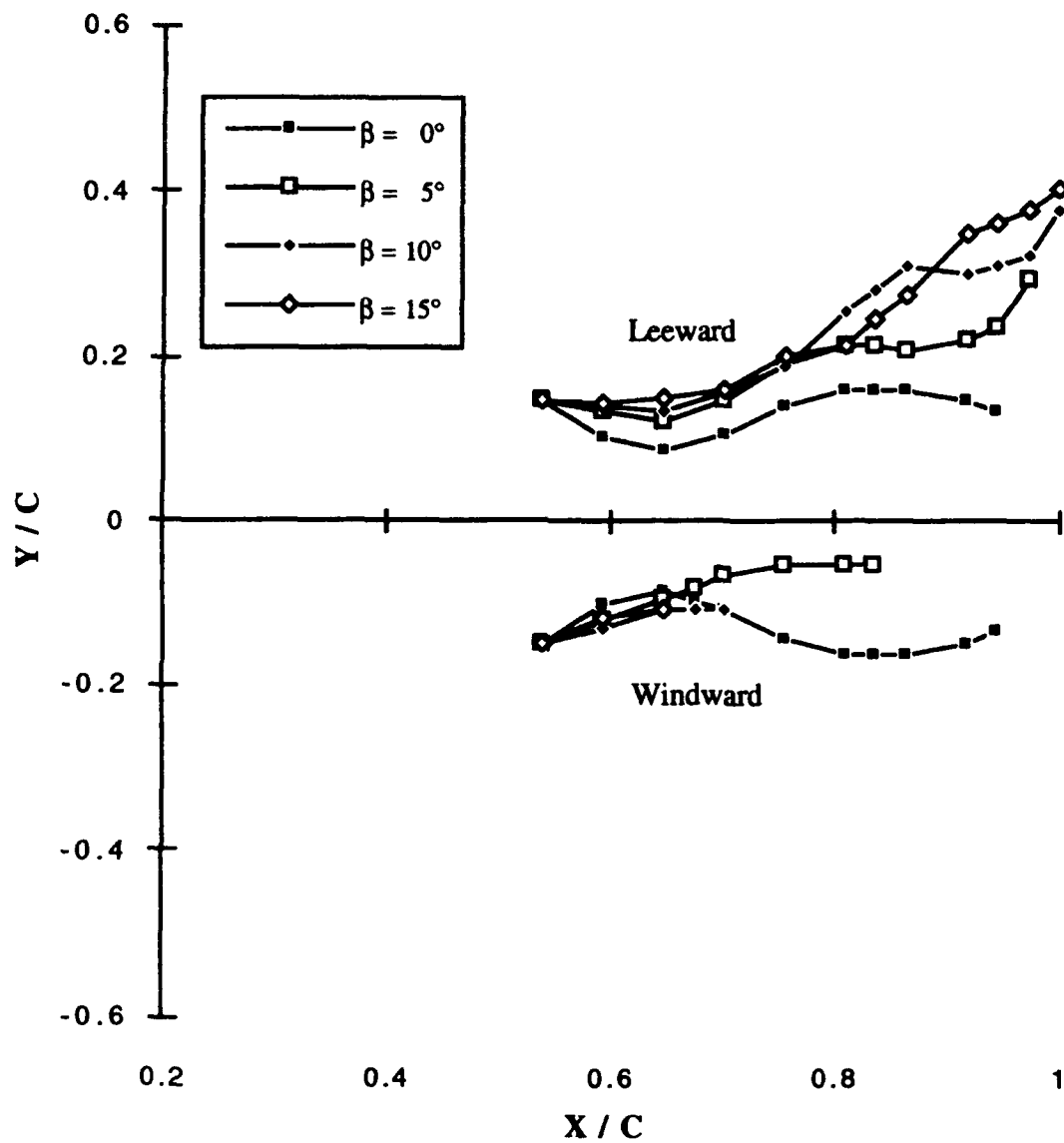


Figure 59 : Baseline model wing vortex core trajectory (AOA=10°)

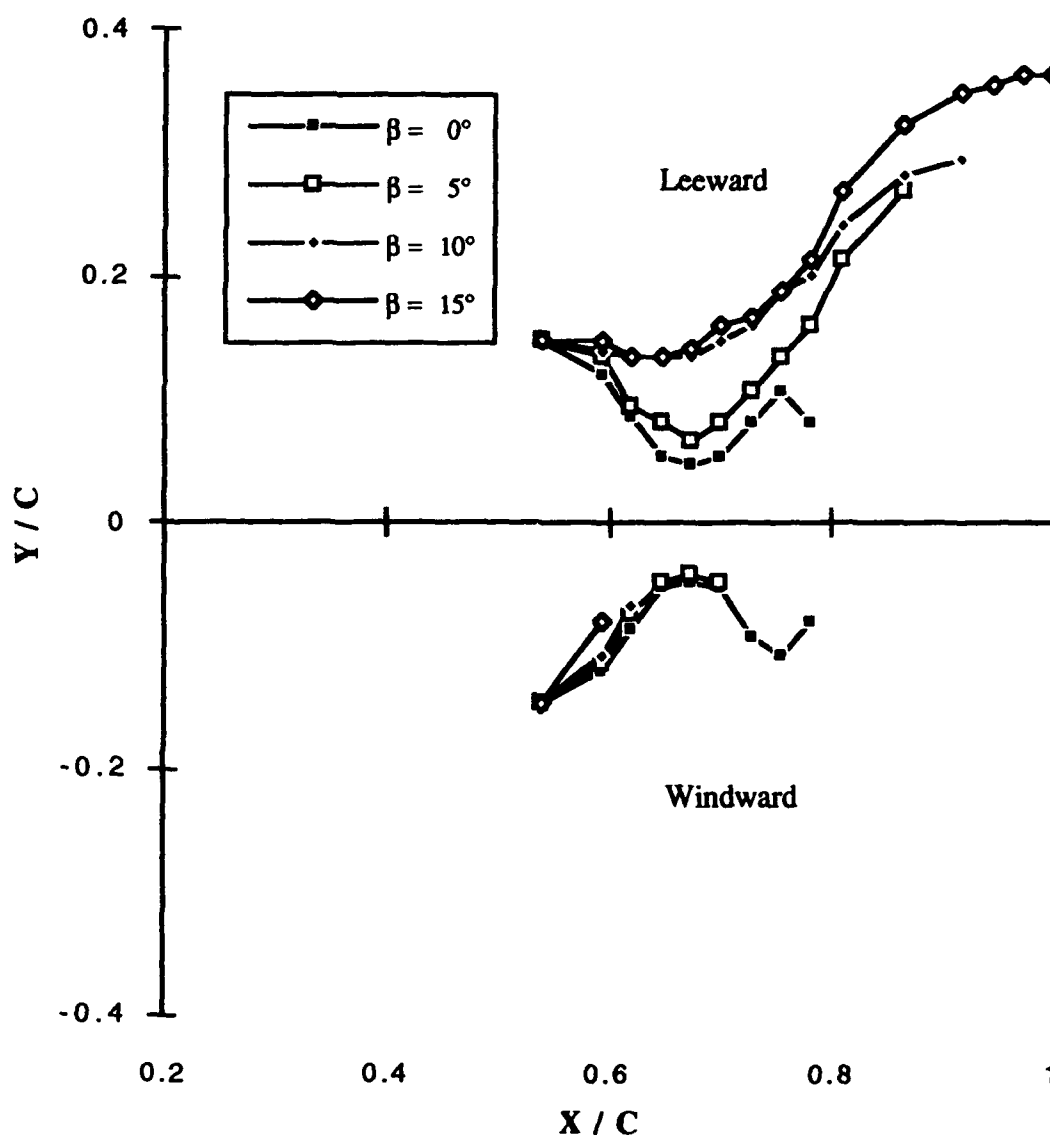


Figure 60 : Baseline model wing vortex core trajectory (AOA=20°)

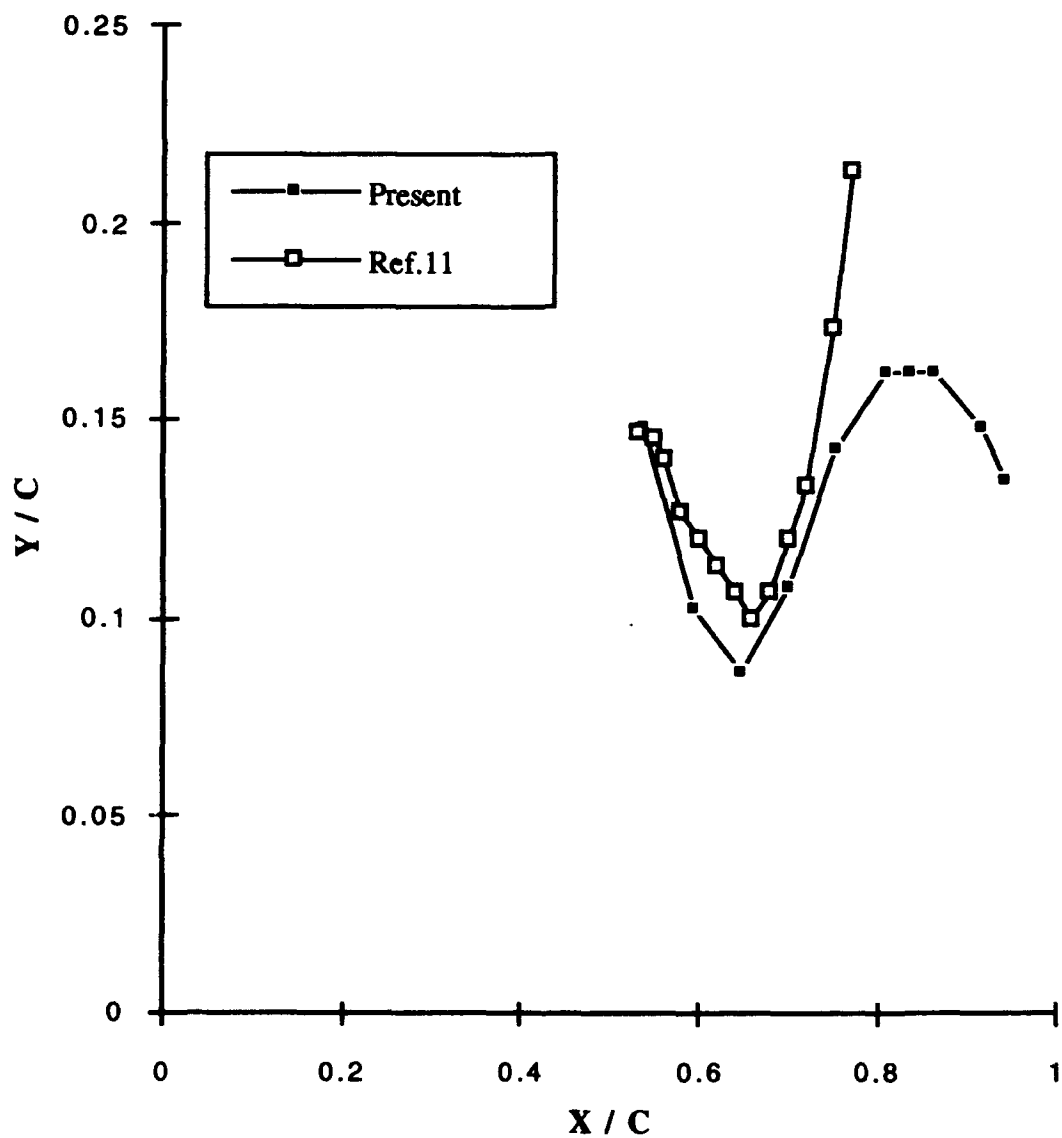


Figure 61 : Baseline model wing vortex core trajectory data comparison
(AOA=10°, AOS=0°)

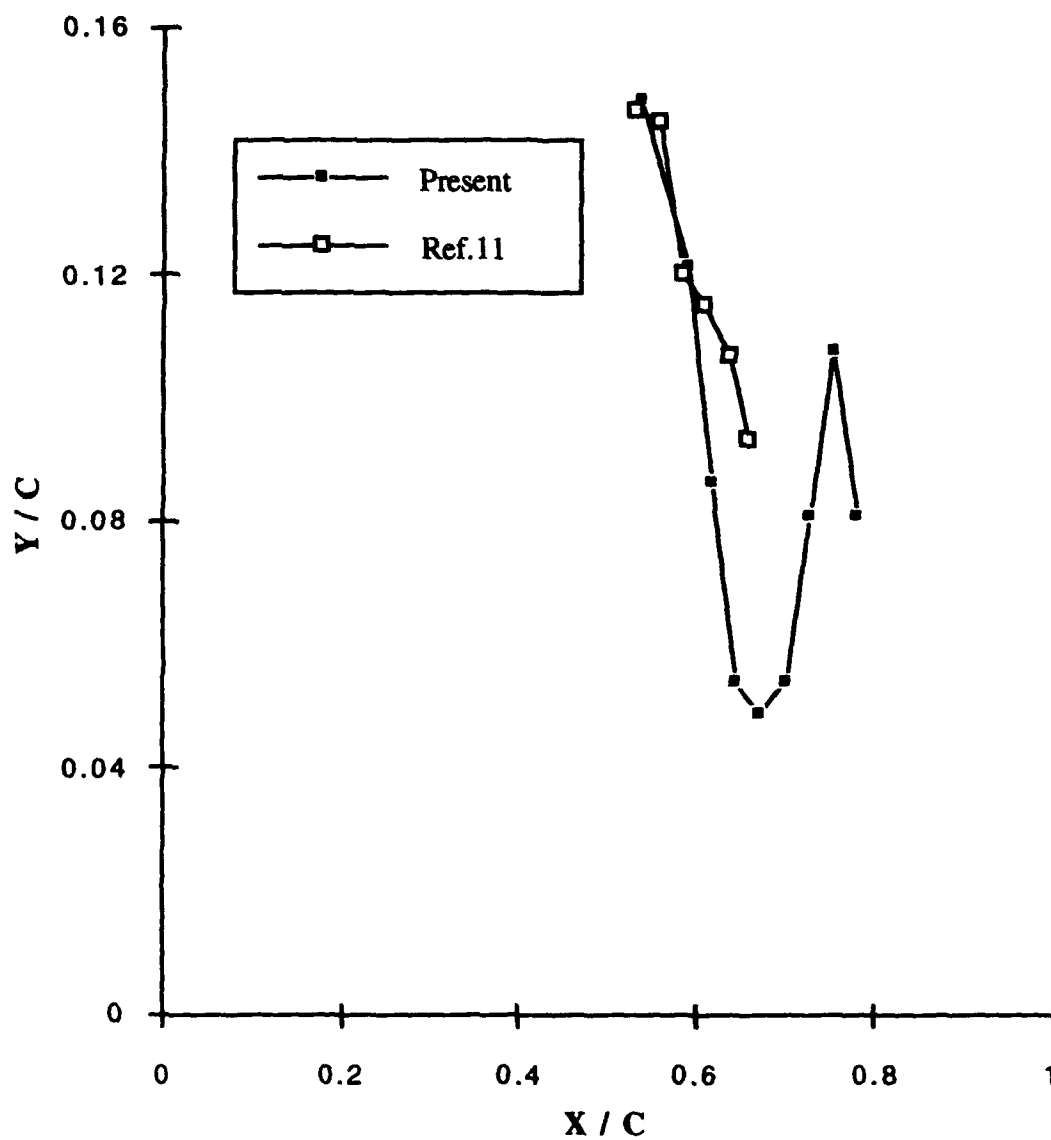


Figure 62 : Baseline model wing vortex core trajectory data comparison
($AOA=20^\circ$, $AOS=0^\circ$.)

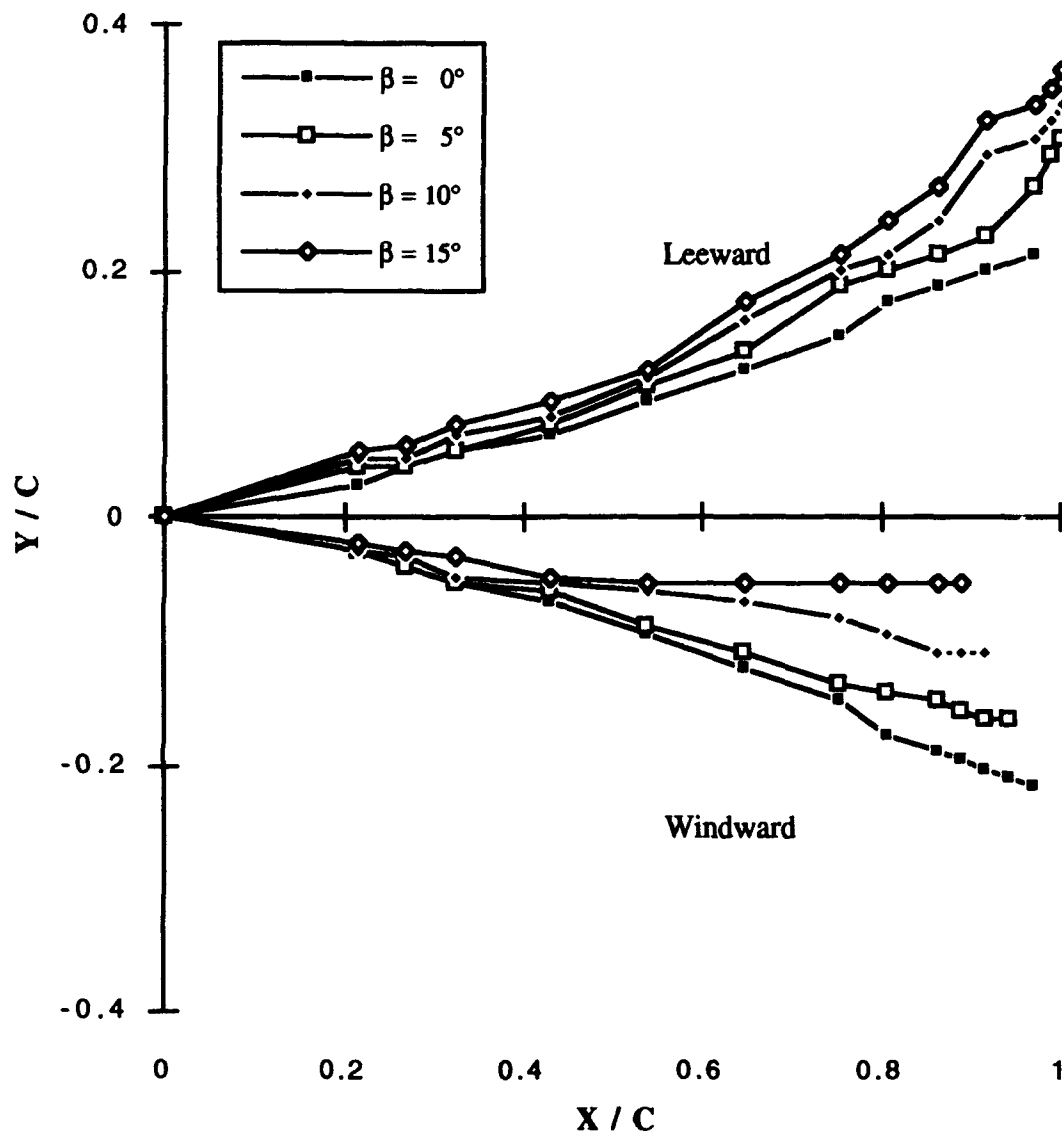


Figure 63 : Diamond-fillet model strake vortex core trajectory (AOA=10°)

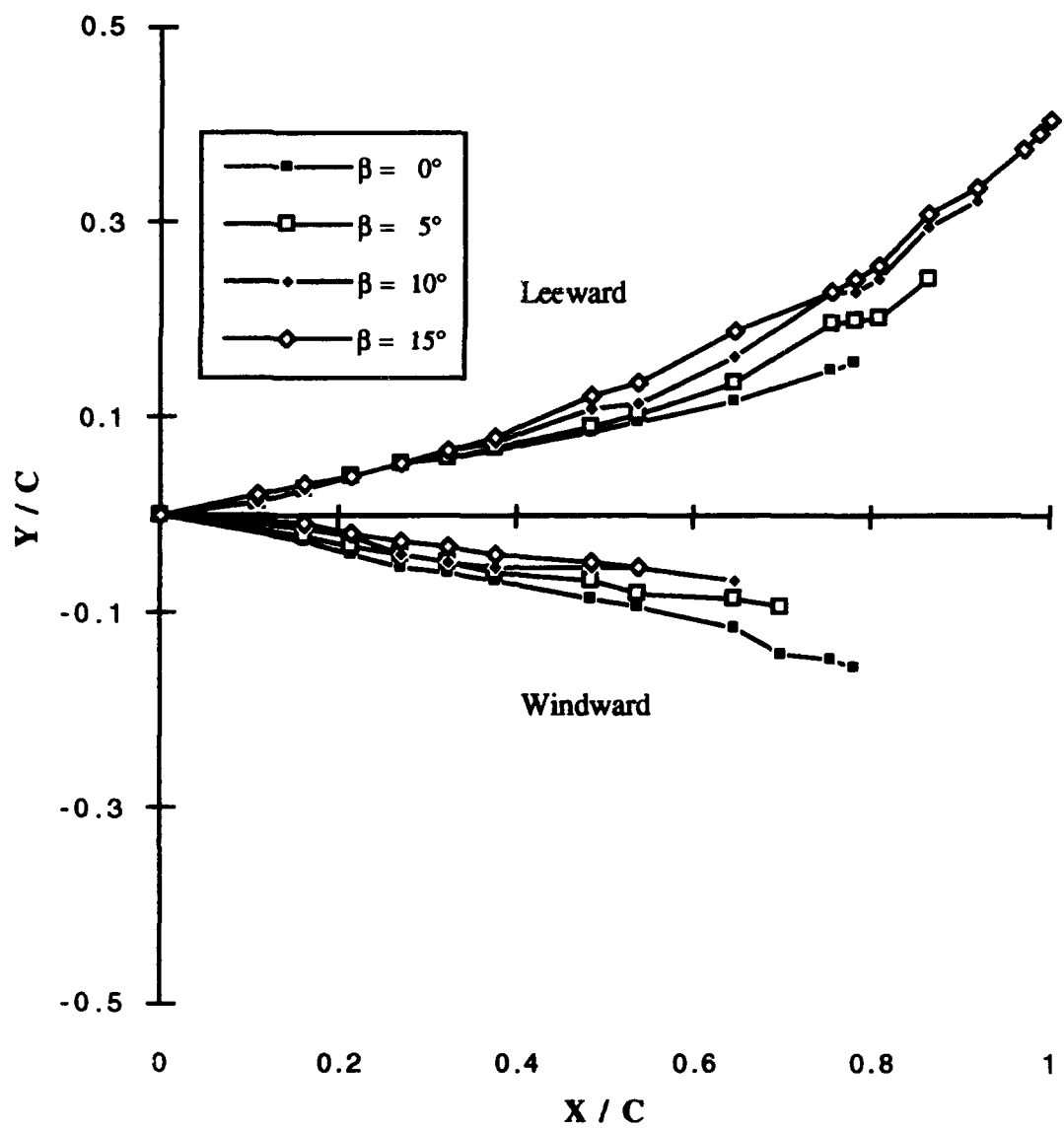


Figure 64 : Diamond-fillet model strake vortex core trajectory ($AOA=20^\circ$)

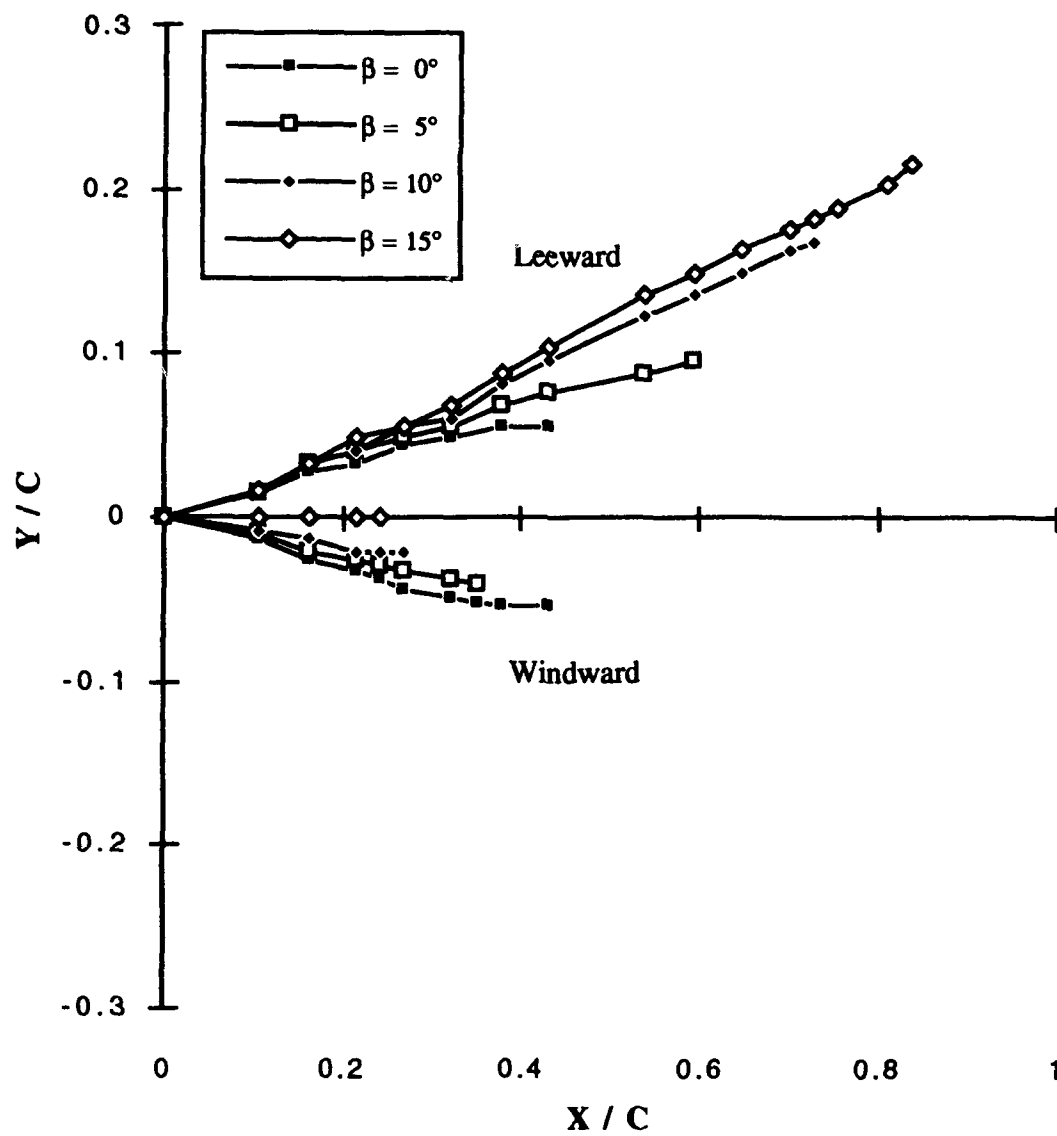


Figure 65 : Diamond-fillet model strake vortex core trajectory (AOA=30°)

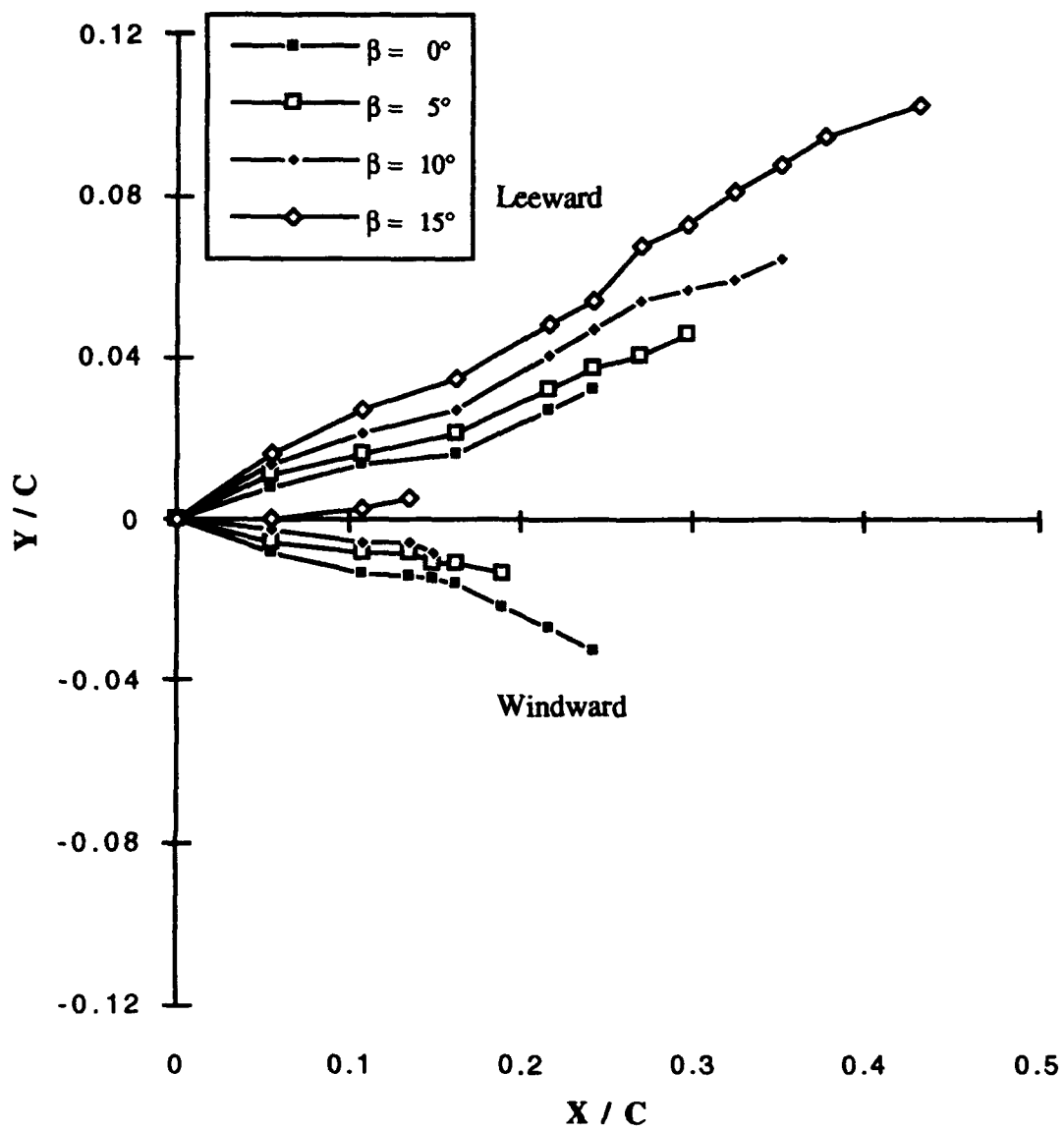


Figure 66 : Diamond-fillet model strake vortex core trajectory (AOA=40°)

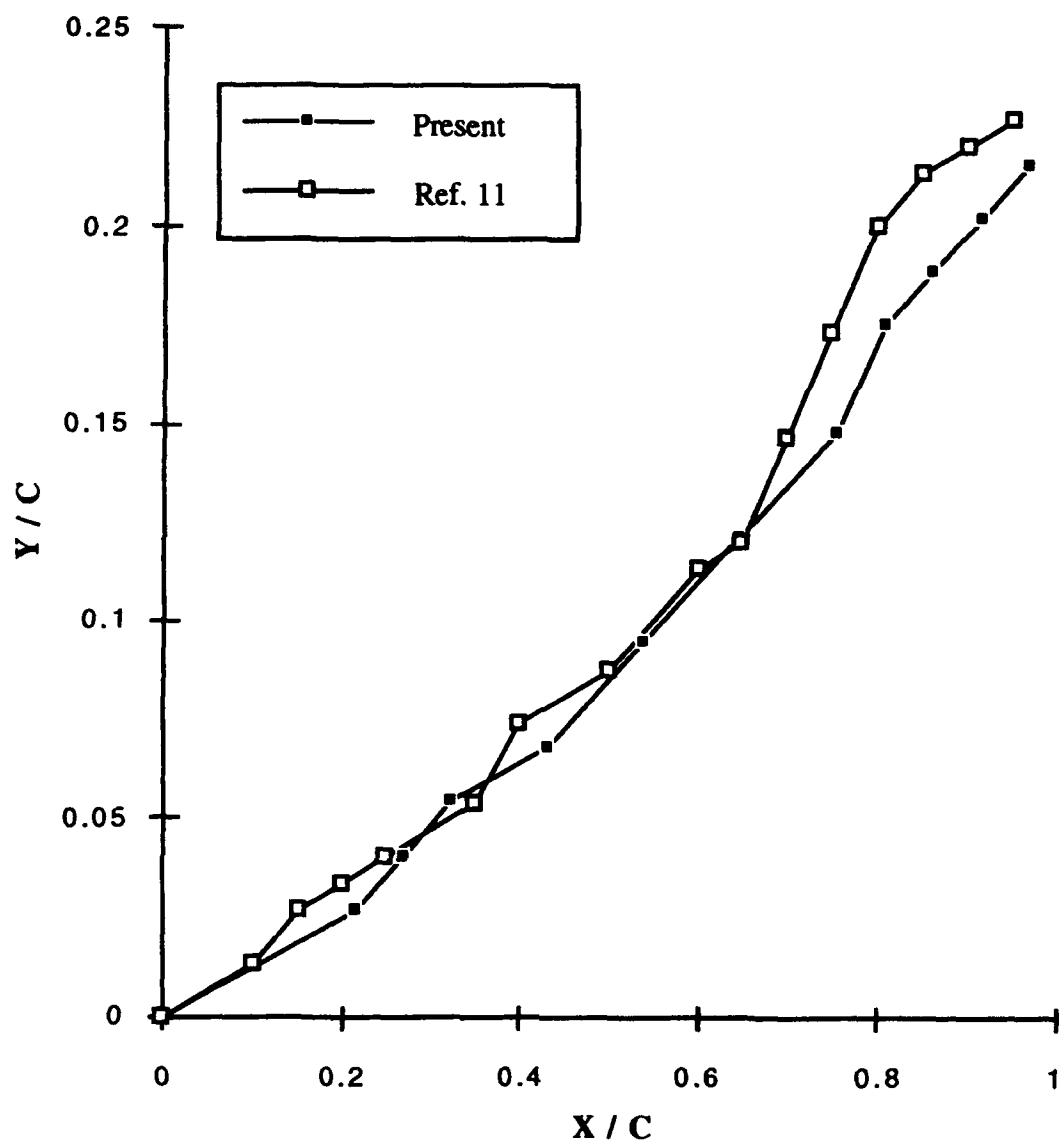


Figure 67 : Diamond-fillet model strake vortex core trajectory data comparison
($AOA=10^\circ, AOS=0^\circ$)

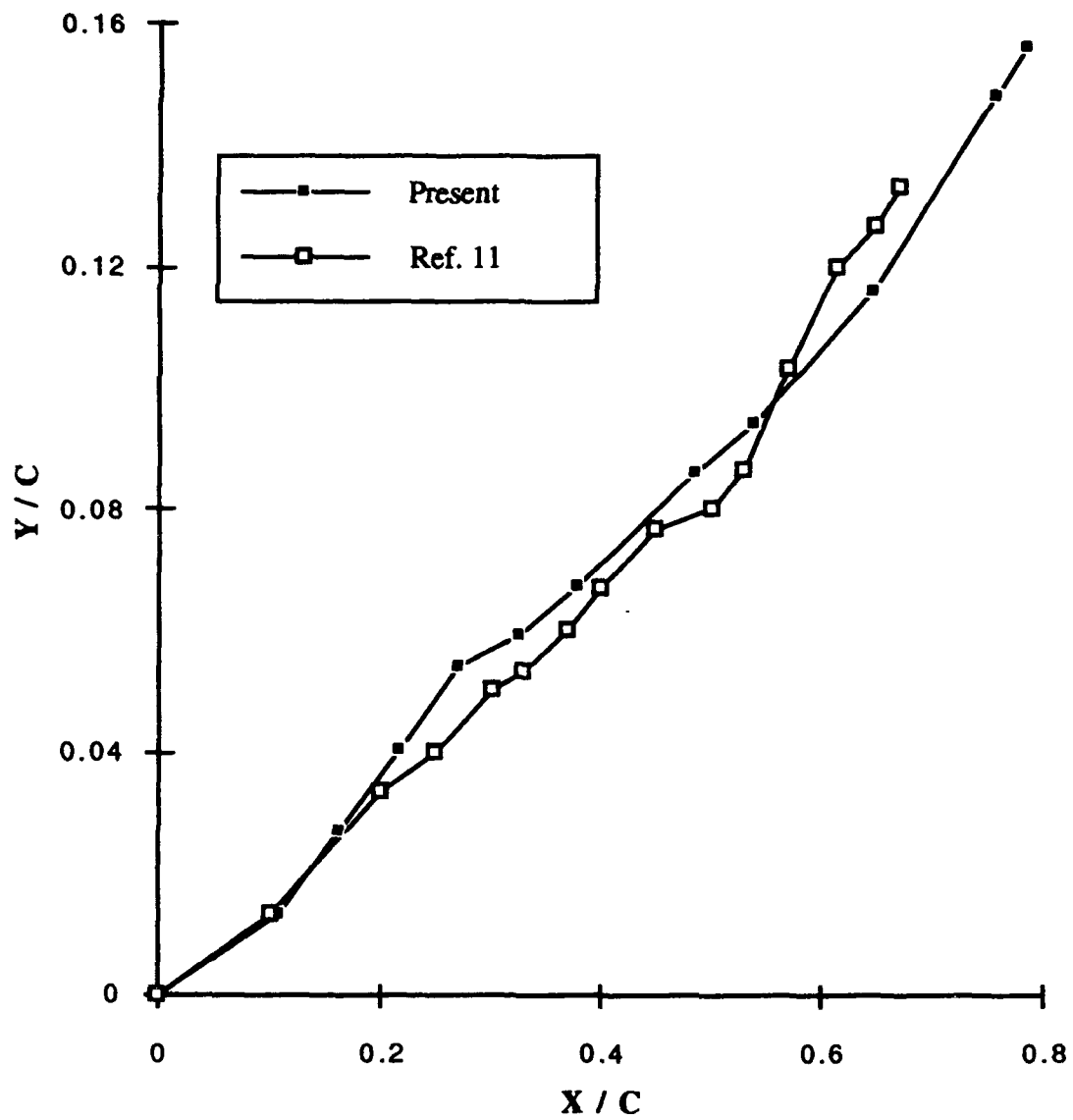


Figure 68 : Diamond-fillet model strake vortex core trajectory data comparison .
(AOA=20°, AOS=0°)

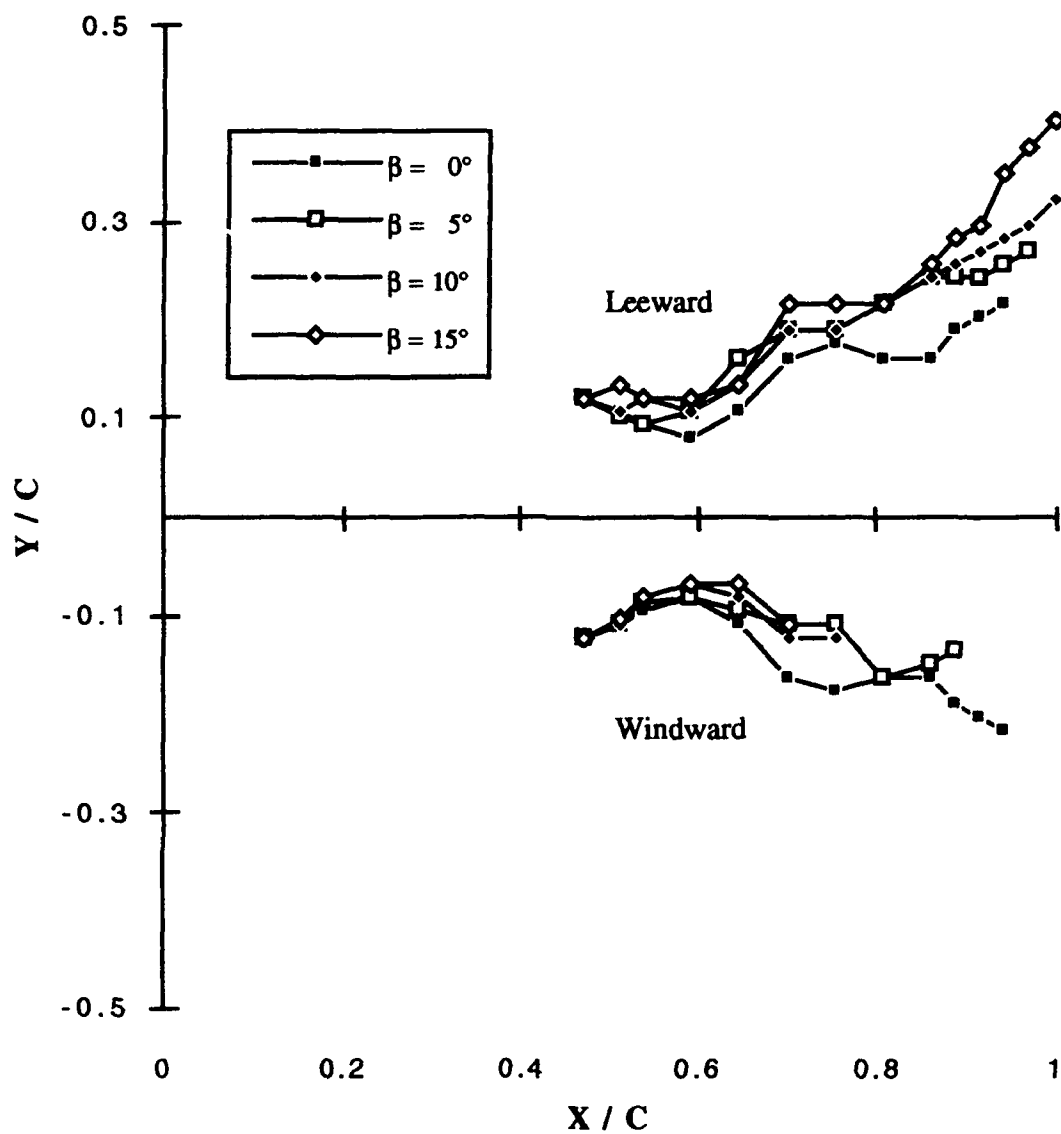


Figure 69 : Diamond-fillet model beginning-of-fillet vortex core trajectory (AOA=10°)

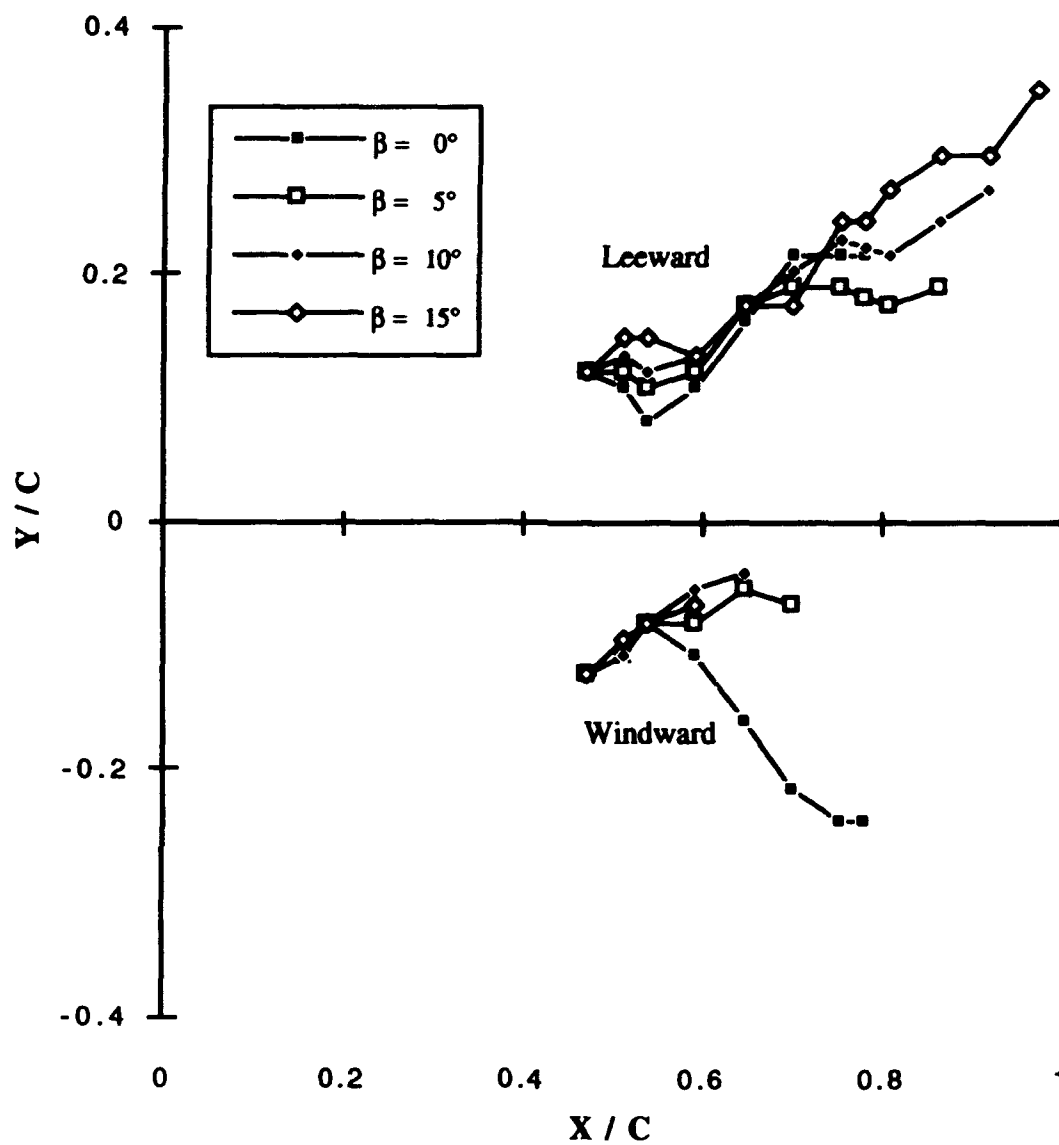


Figure 70 : Diamond-fillet model beginning-of-fillet vortex core trajectory (AOA=20°)

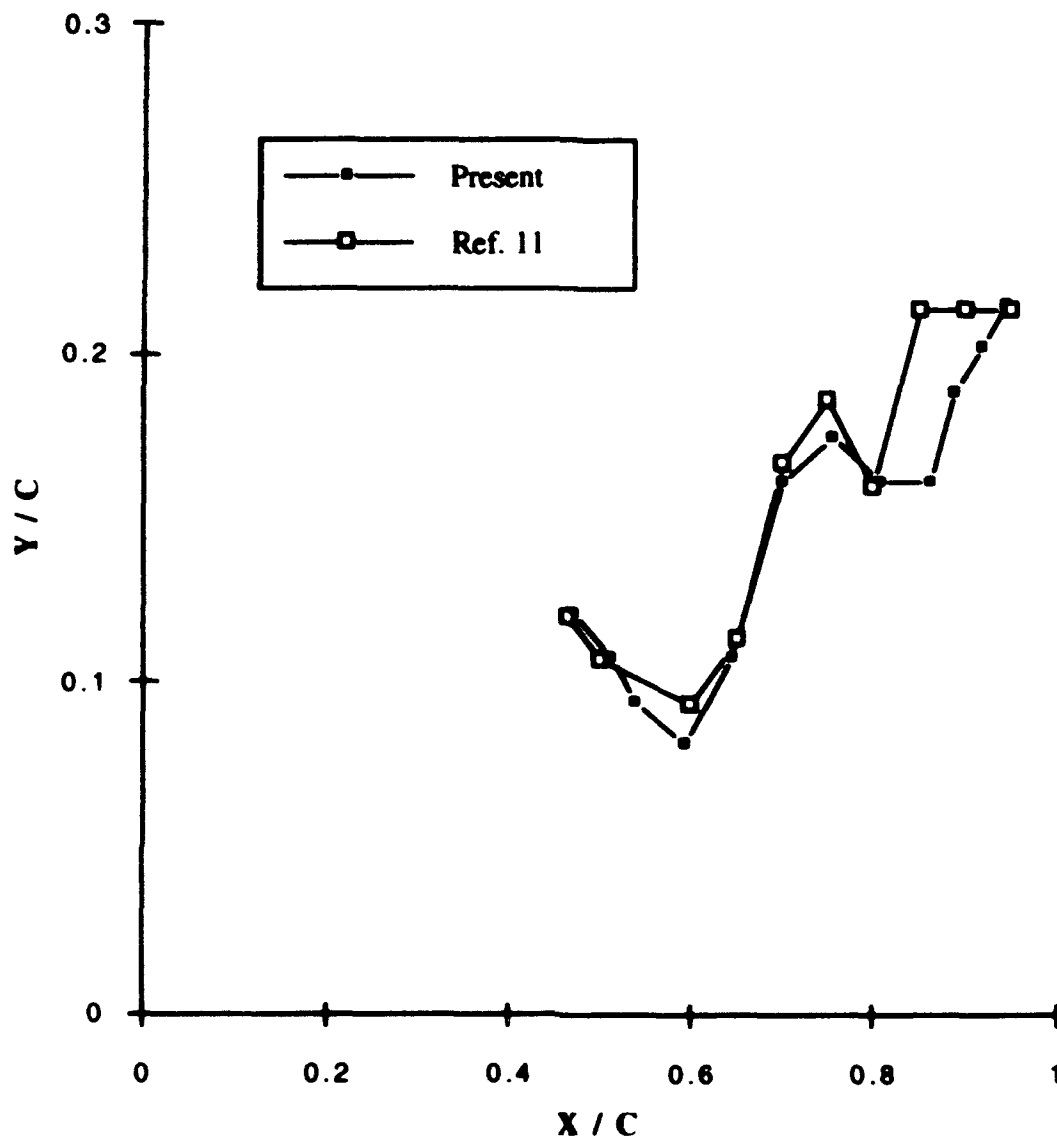


Figure 71 : Diamond-fillet model begining-of-fillet vortex core trajectory data comparison (AOA=10°, AOS=0°)

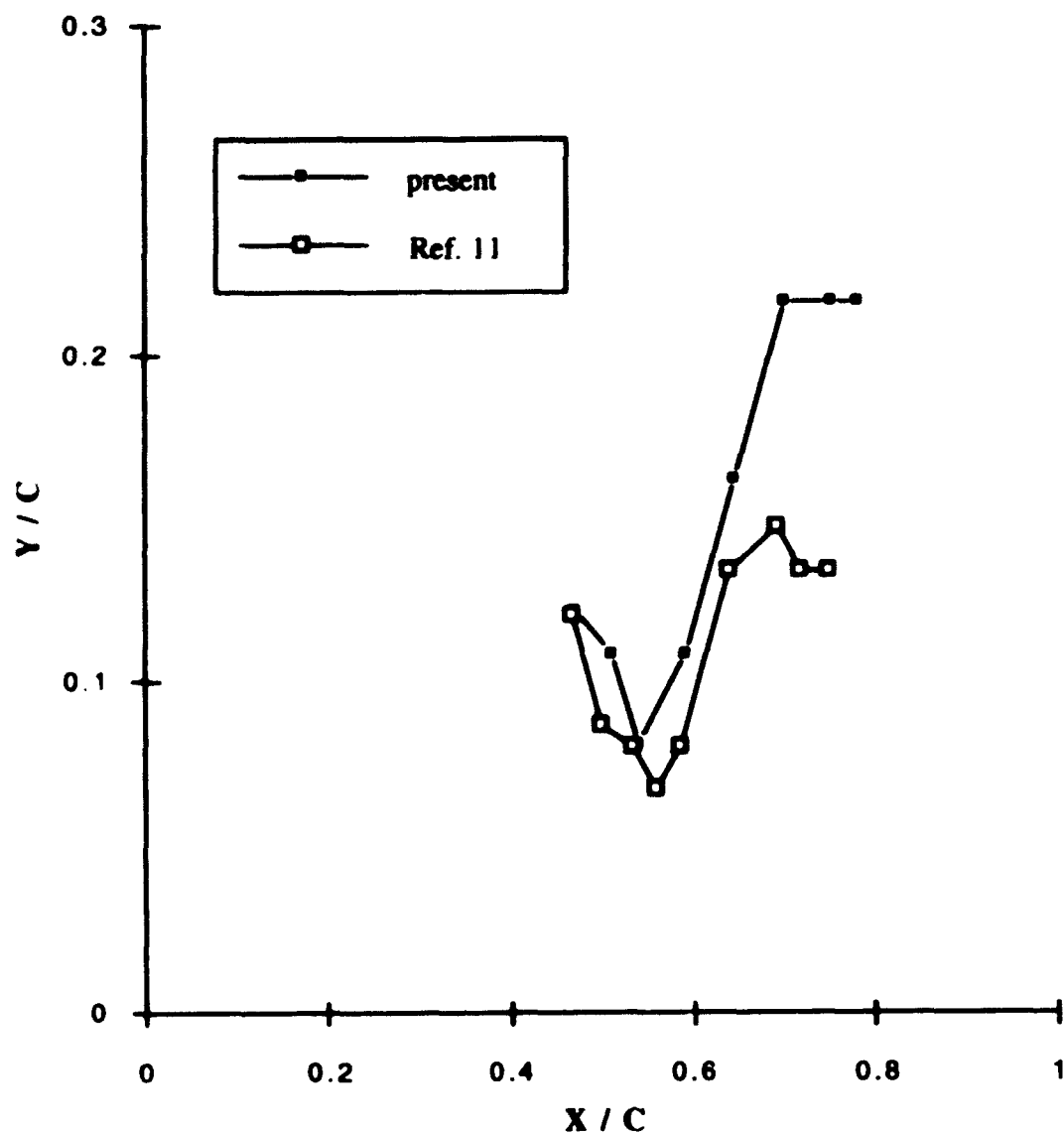


Figure 72 : Diamond-fillet model beginning-of-fillet vortex core trajectory data comparison (AOA=20°, AOS=0°)

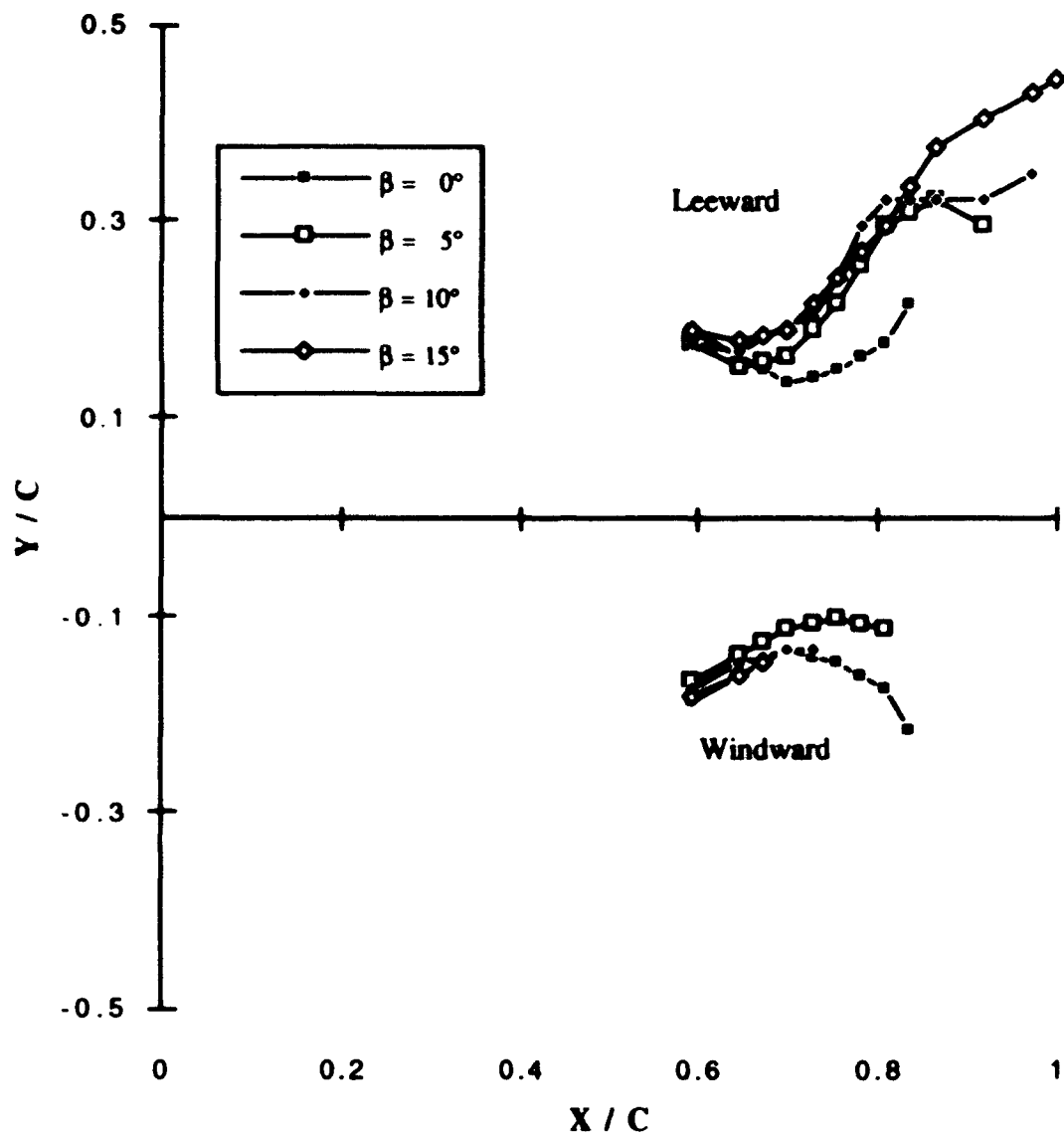


Figure 73 : Diamond-fillet model end-of-fillet vortex core trajectory (AOA=10°)

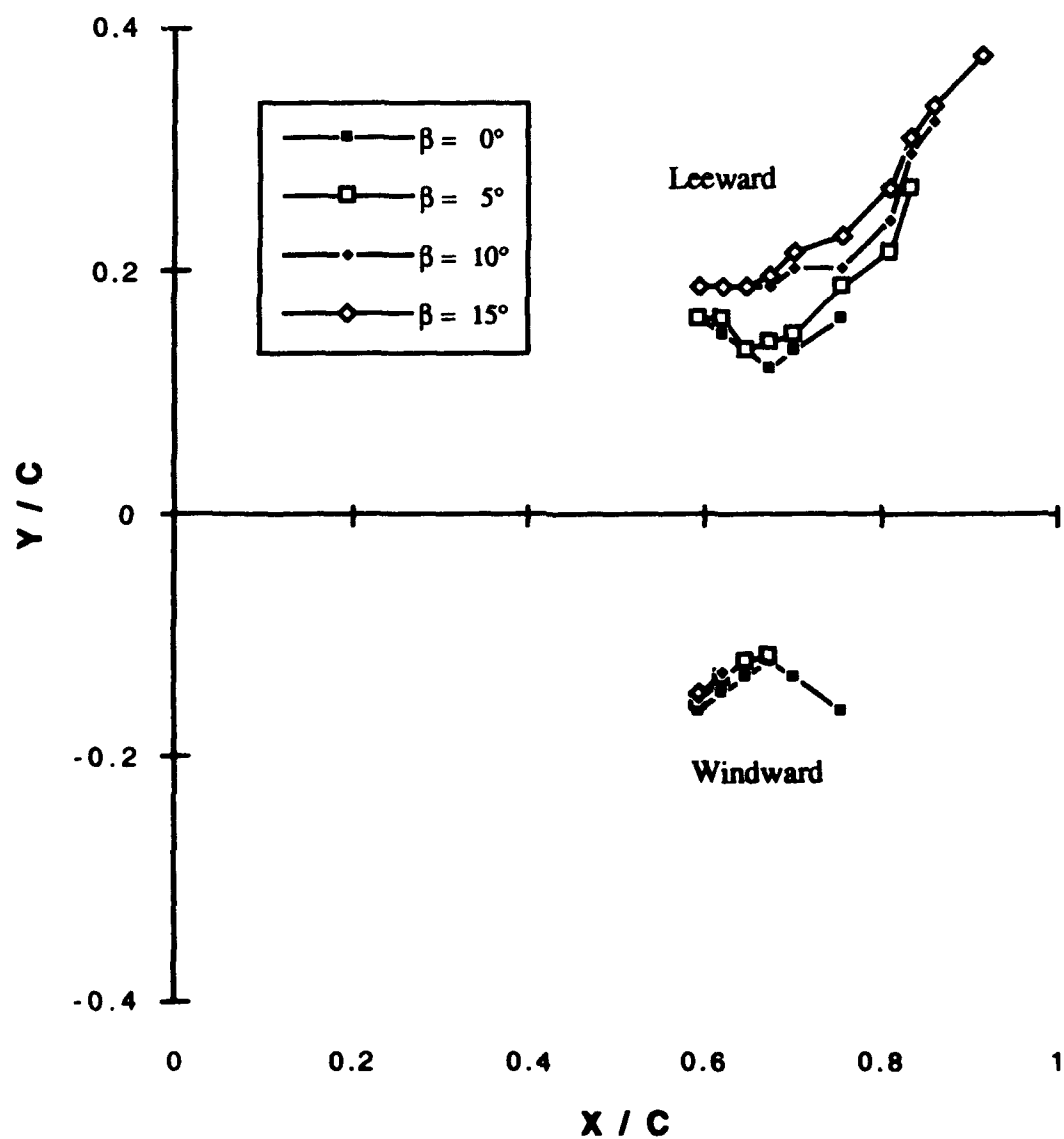


Figure 74 : Diamond-fillet model end-of-fillet vortex core trajectory (AOA=20°)

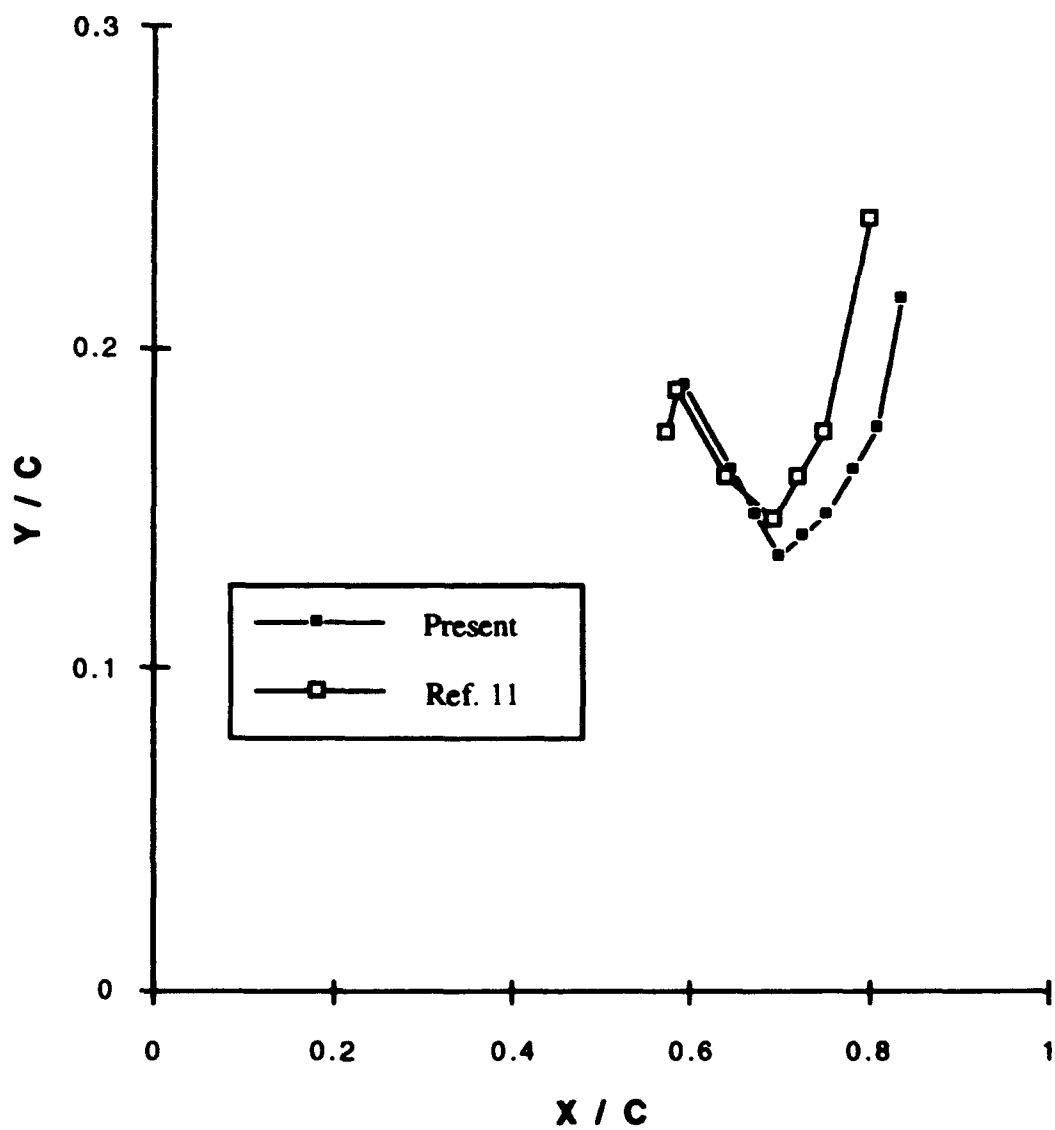


Figure 75 : Diamond-fillet model end-of-fillet vortex core trajectory data comparison ($AOA=10^\circ$, $AOS=0^\circ$)

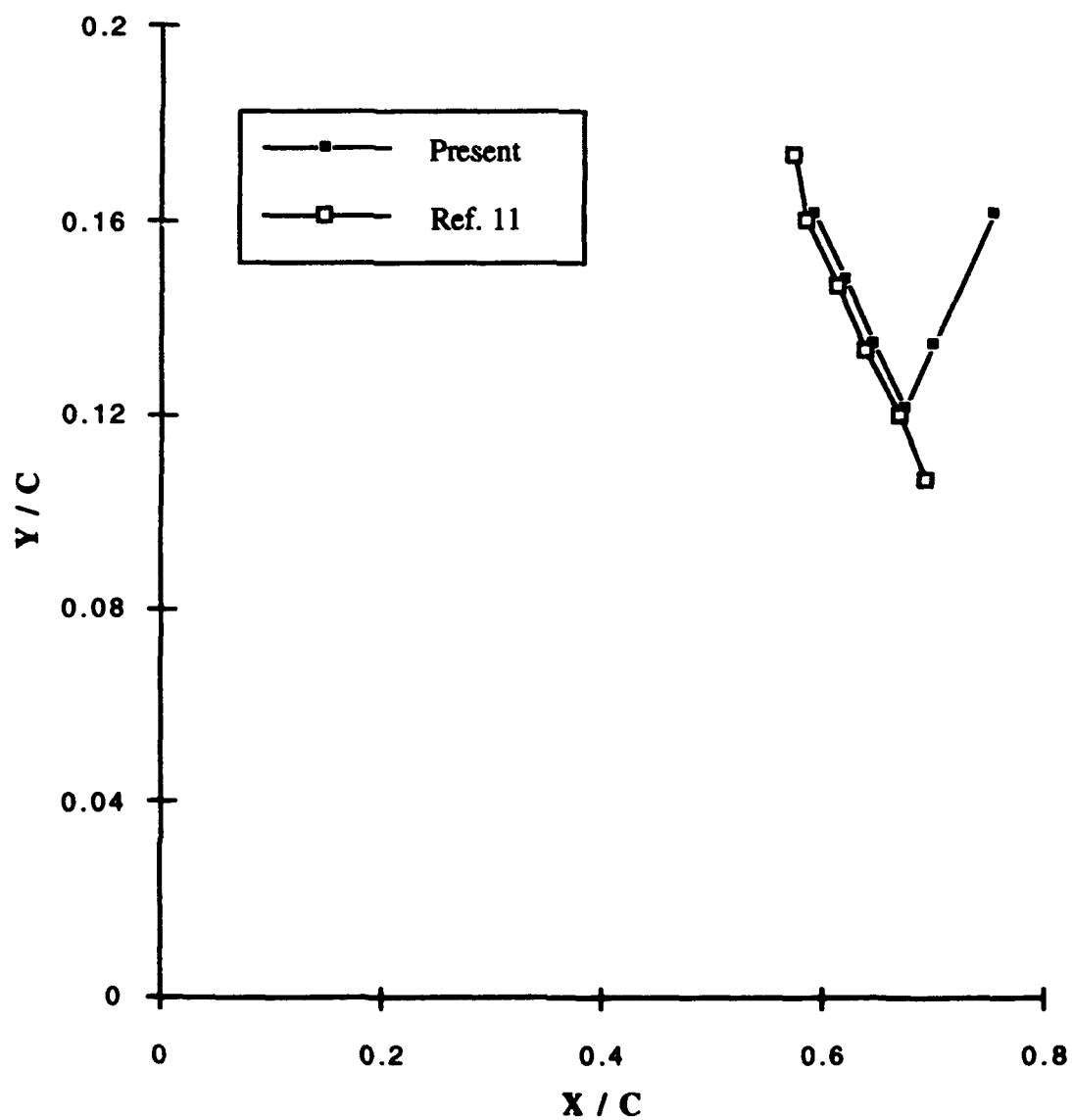


Figure 76 : Diamond-fillet model end-of-fillet vortex core trajectory data comparison ($AOA=20^\circ$, $AOS=0^\circ$)

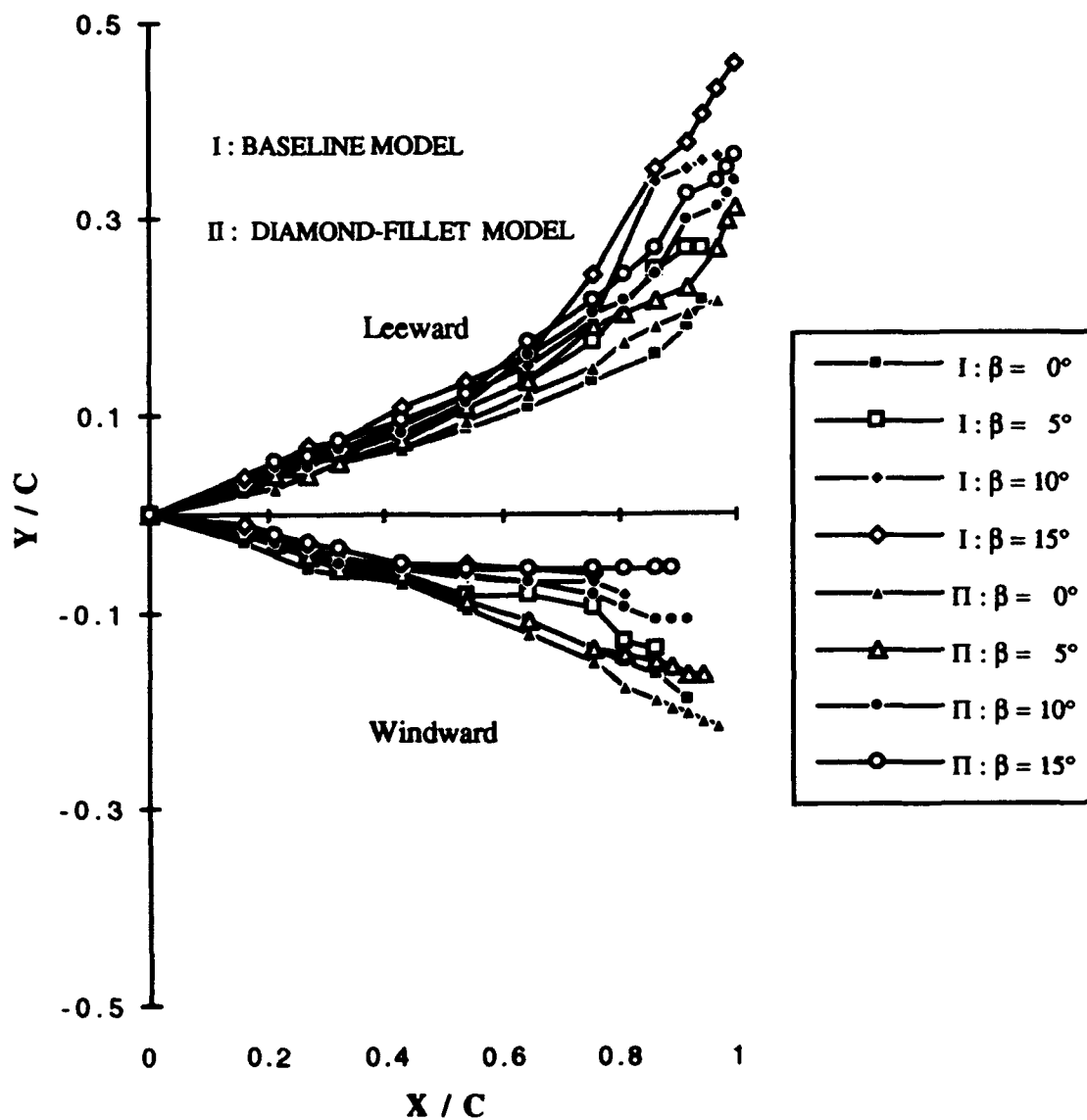


Figure 77 : Strake vortex core trajectory data comparison for two models (AOA=10°)

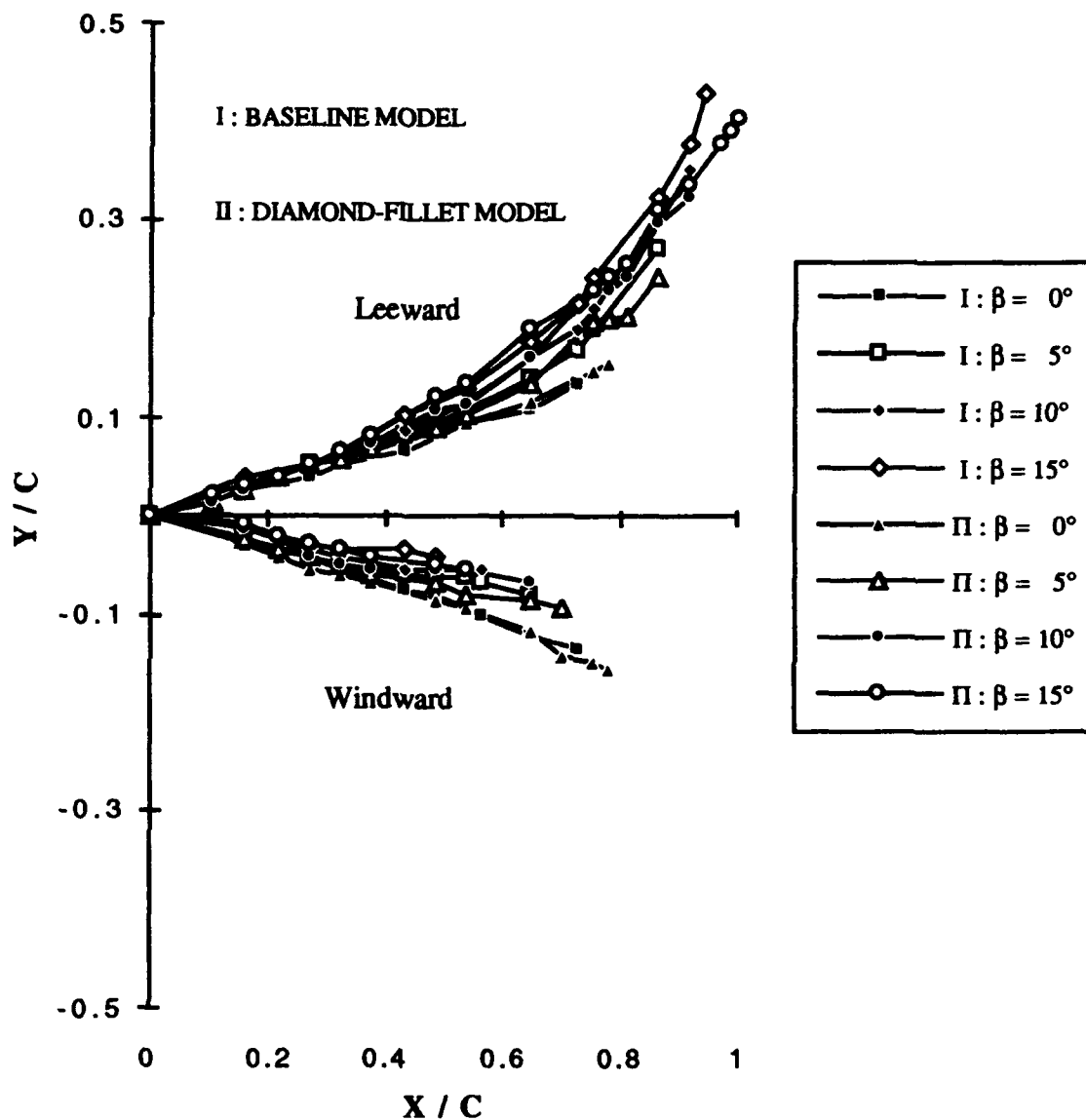


Figure 78 : Strake vortex core trajectory data comparison for two models (AOA \approx 20°)

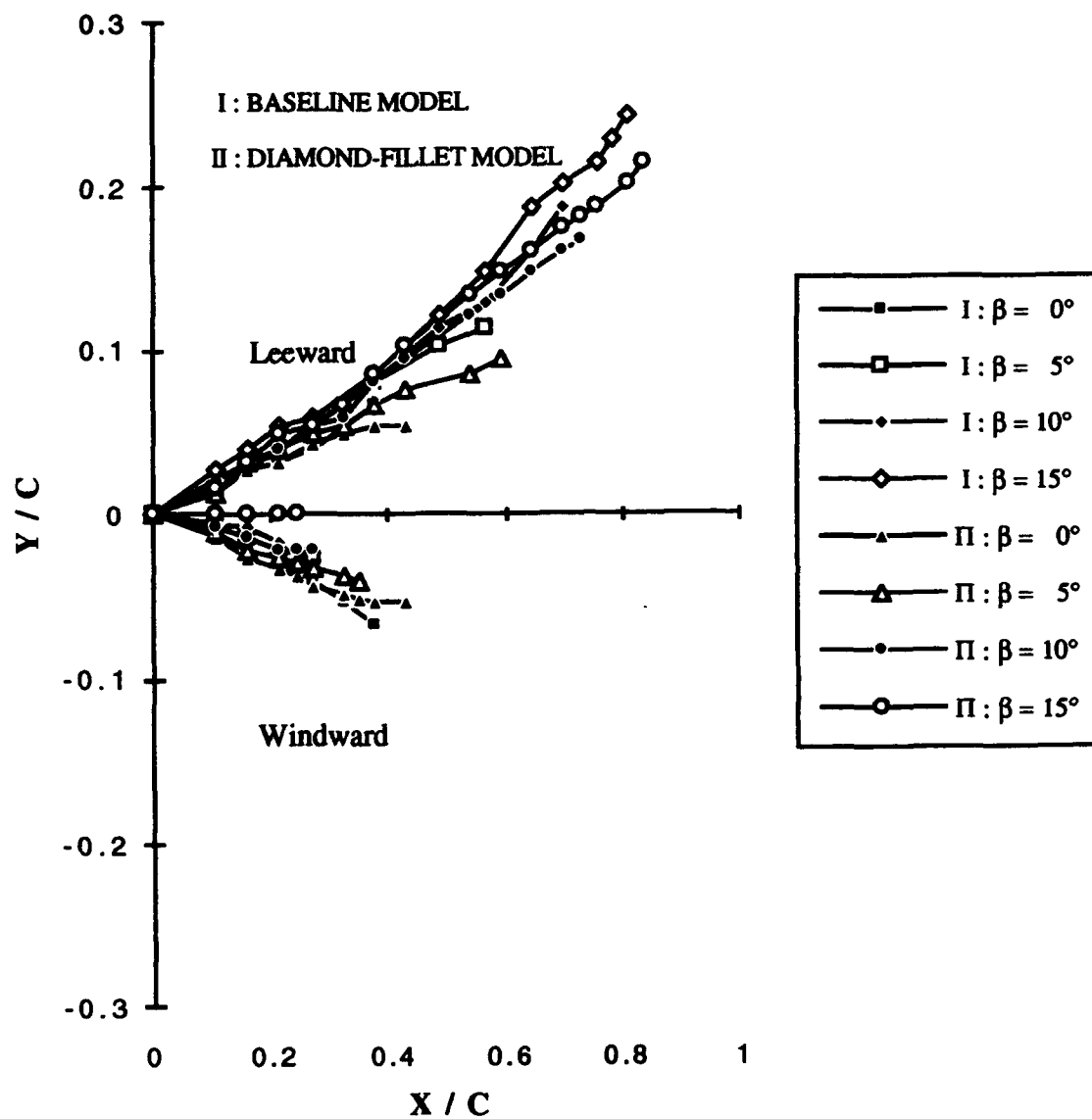


Figure 79 : Strake vortex core trajectory data comparison for two models (AOA=30°)

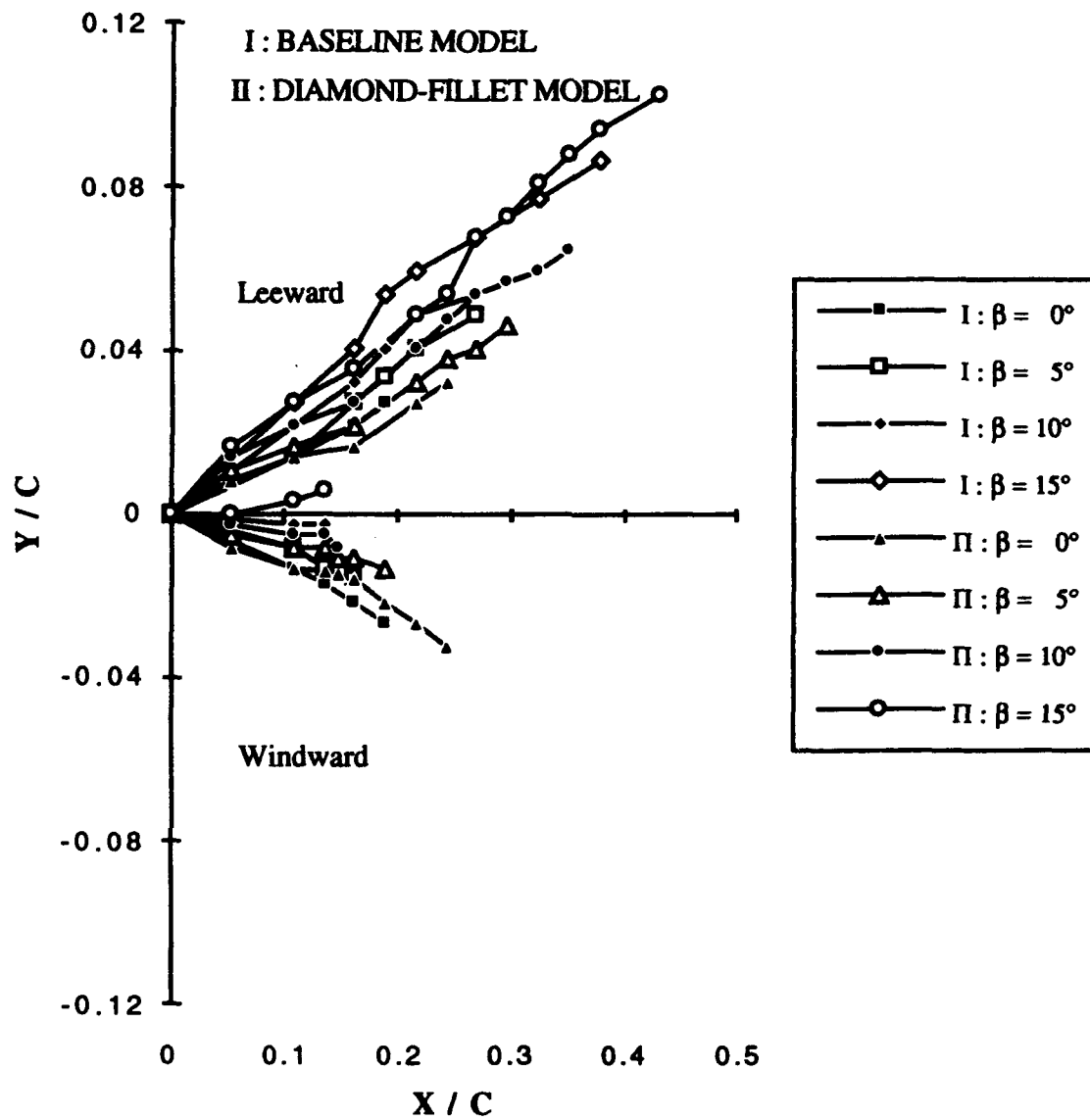


Figure 80 : Strake vortex core trajectory data comparison for two models (AOA=40°)

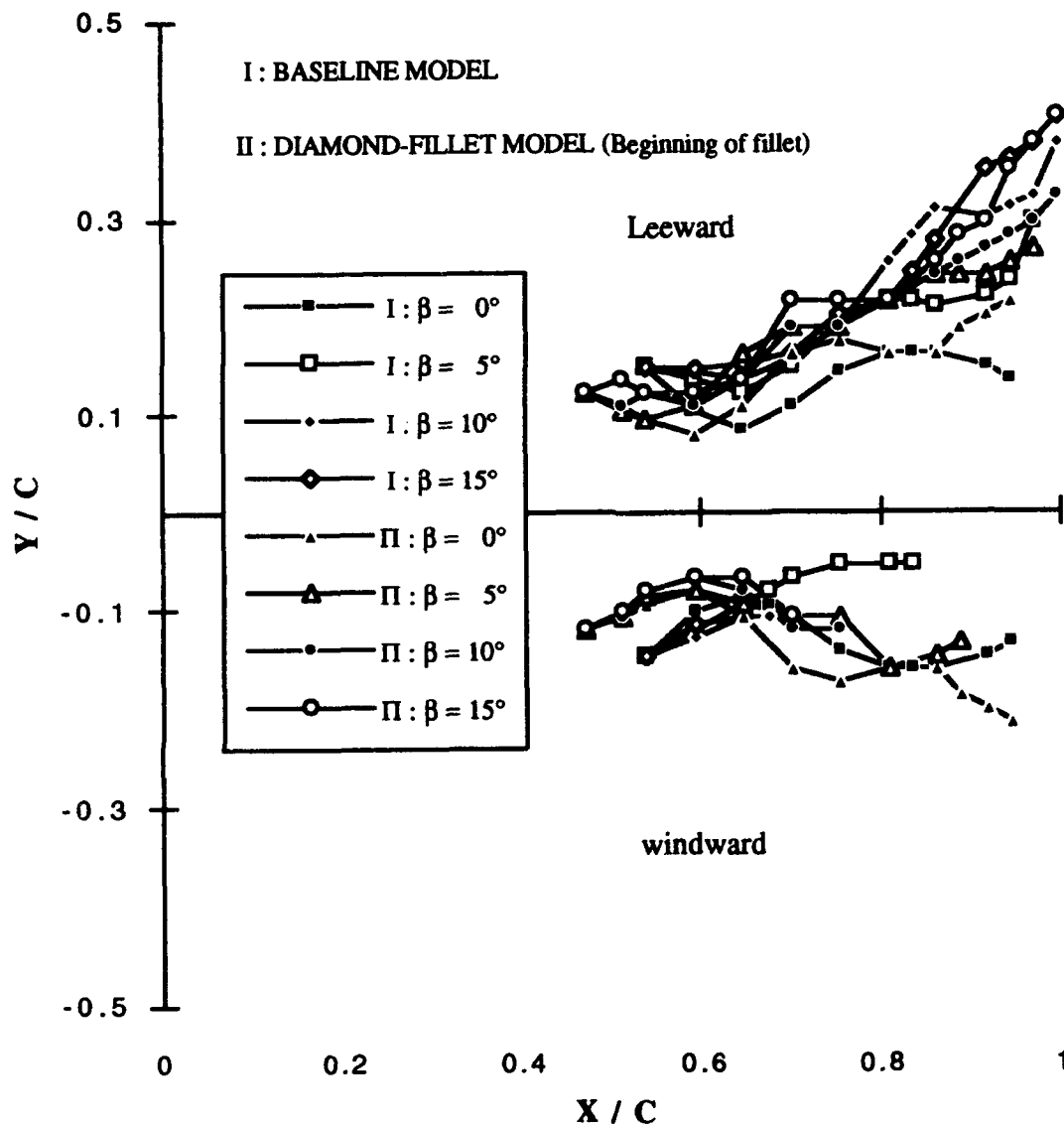


Figure 81 : Wing vortex core trajectory data comparison for two models (AOA=10°) I

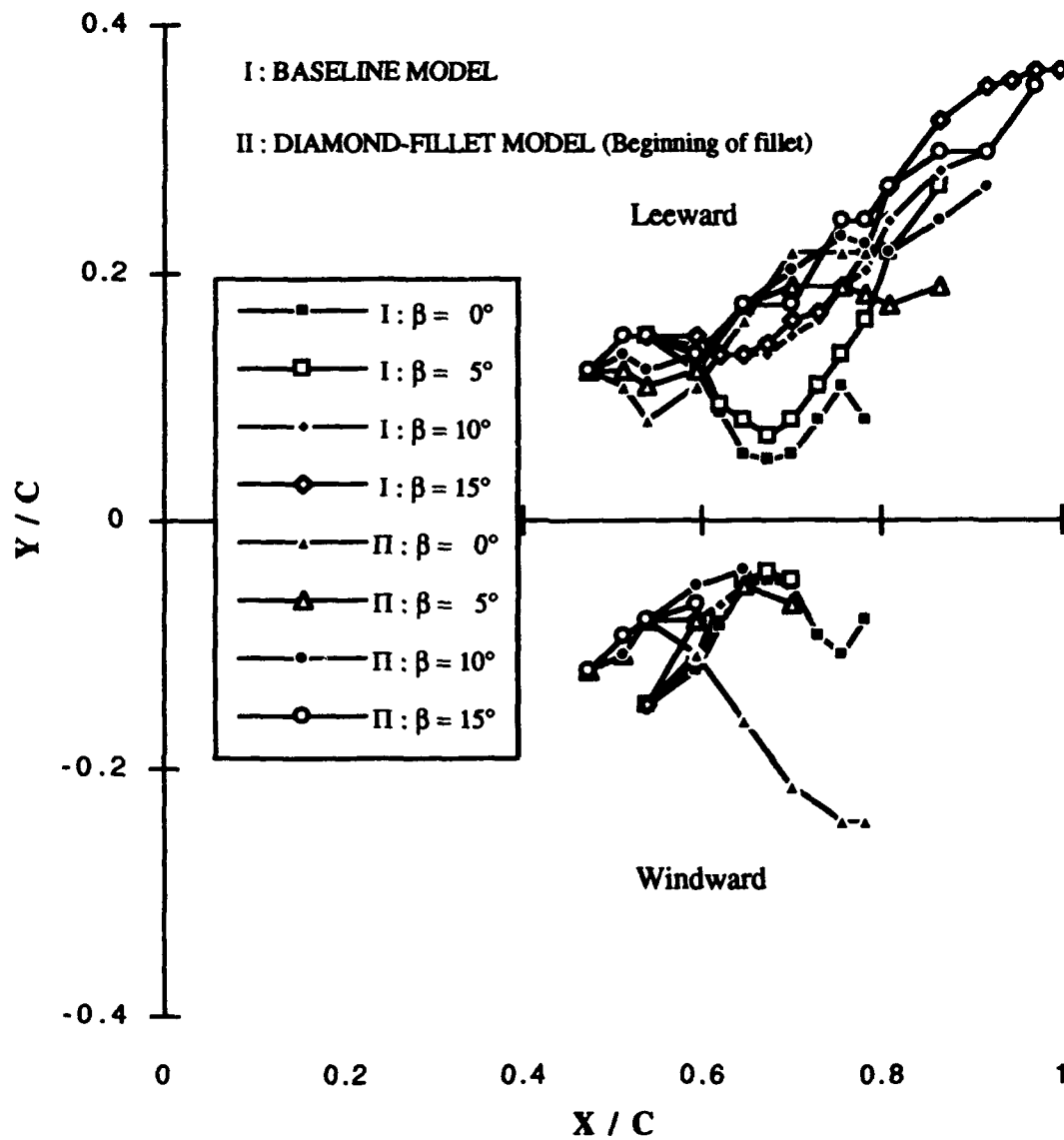


Figure 82 : Wing vortex core trajectory data comparison for two models (AOA=20°)I

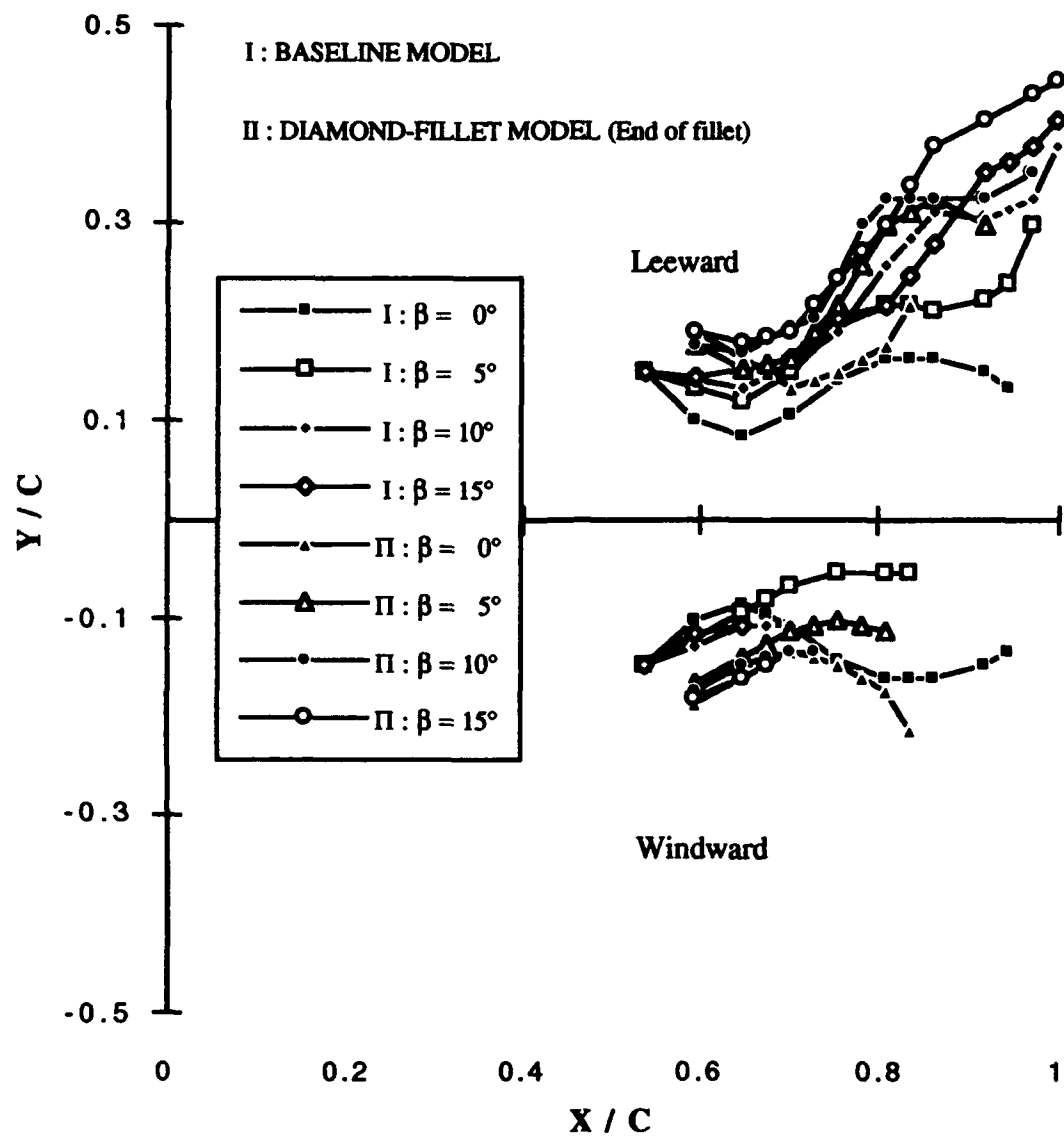


Figure 83 : Wing vortex core trajectory data comparison for two models
($\text{AOA} = 10^\circ$)

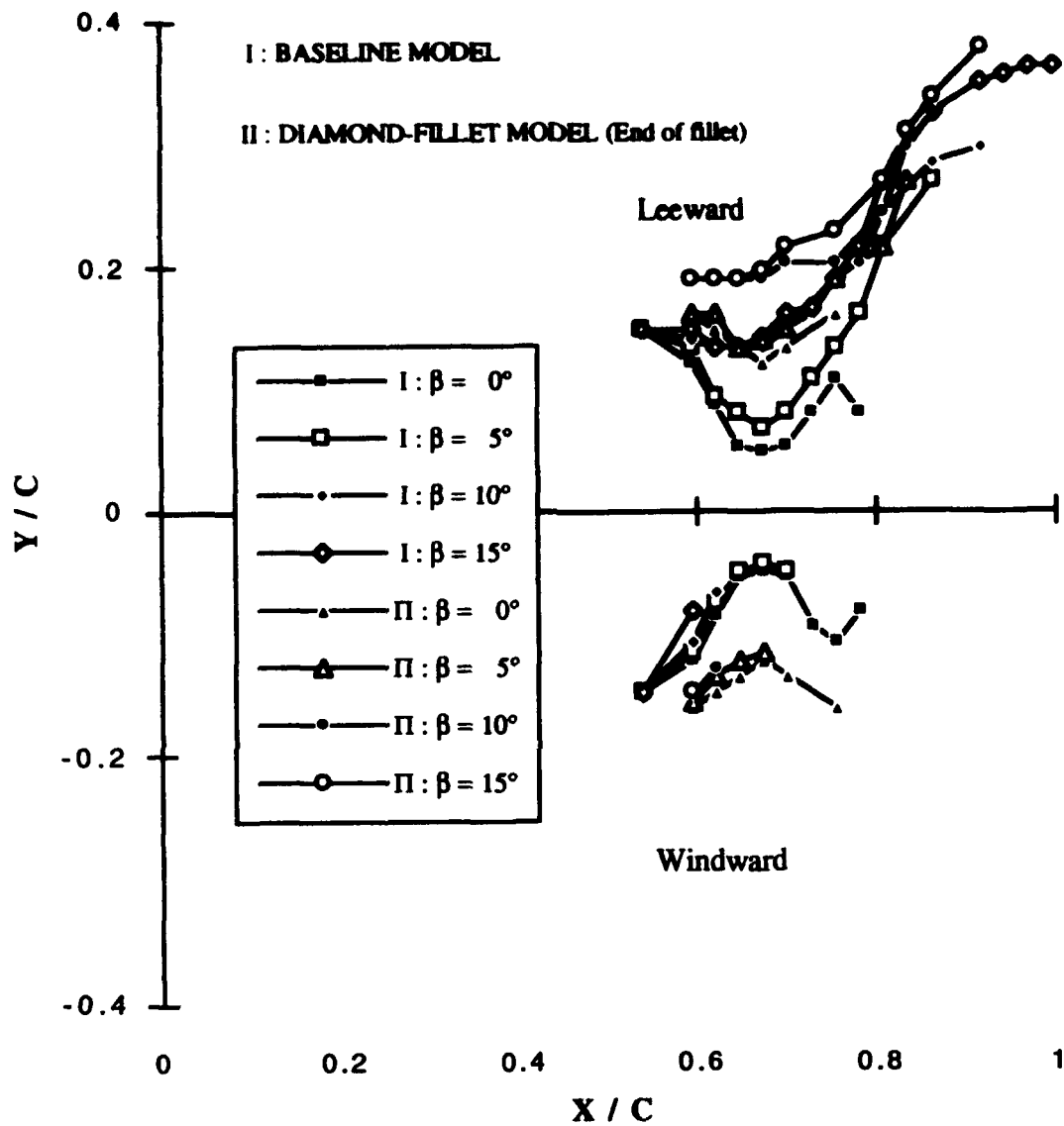


Figure 84 : Wing vortex core trajectory data comparison for two models (AOA=20°)II

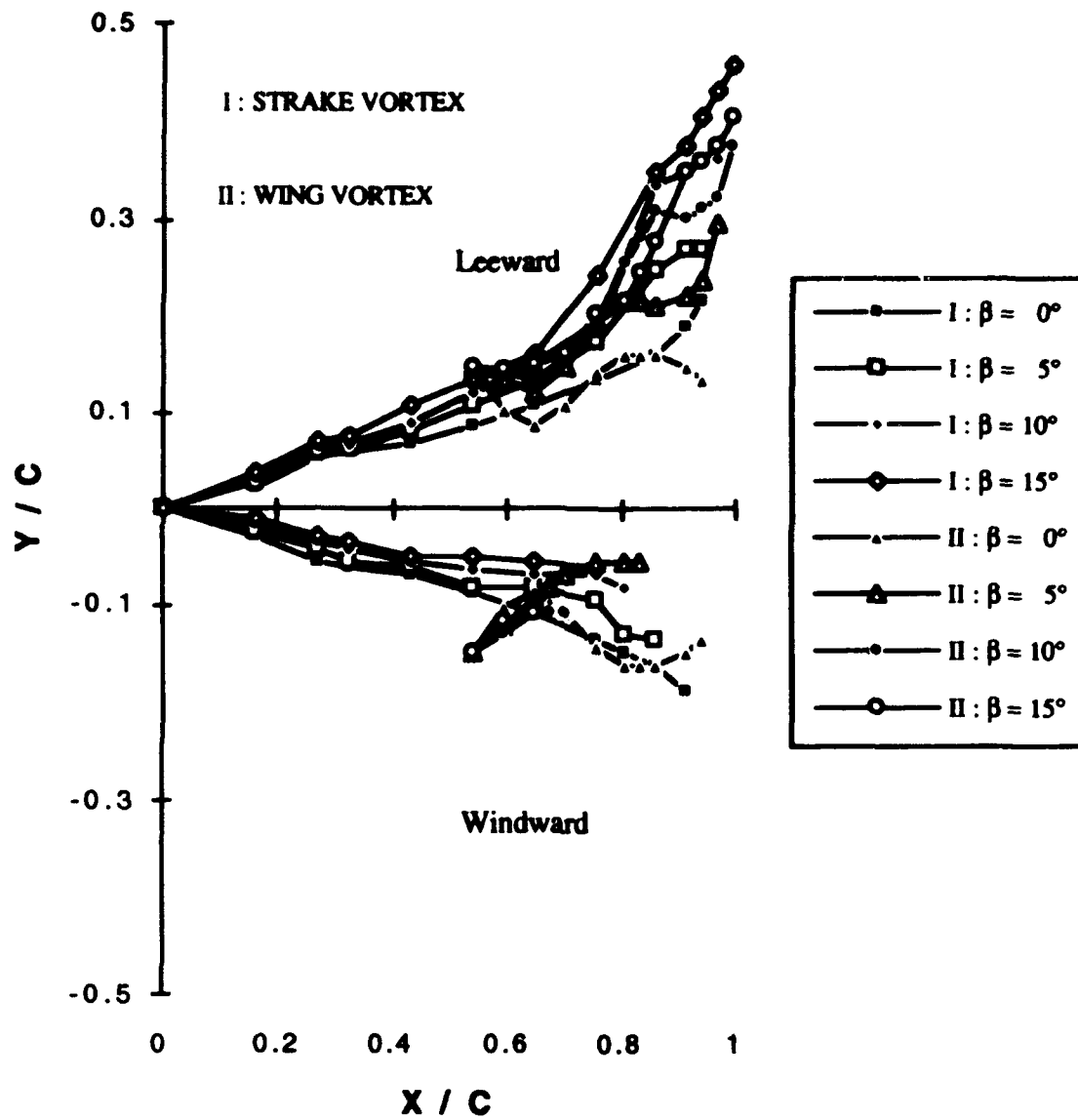


Figure 85 : Baseline model vortex core trajectories for different sideslip angles (AOA=10°)

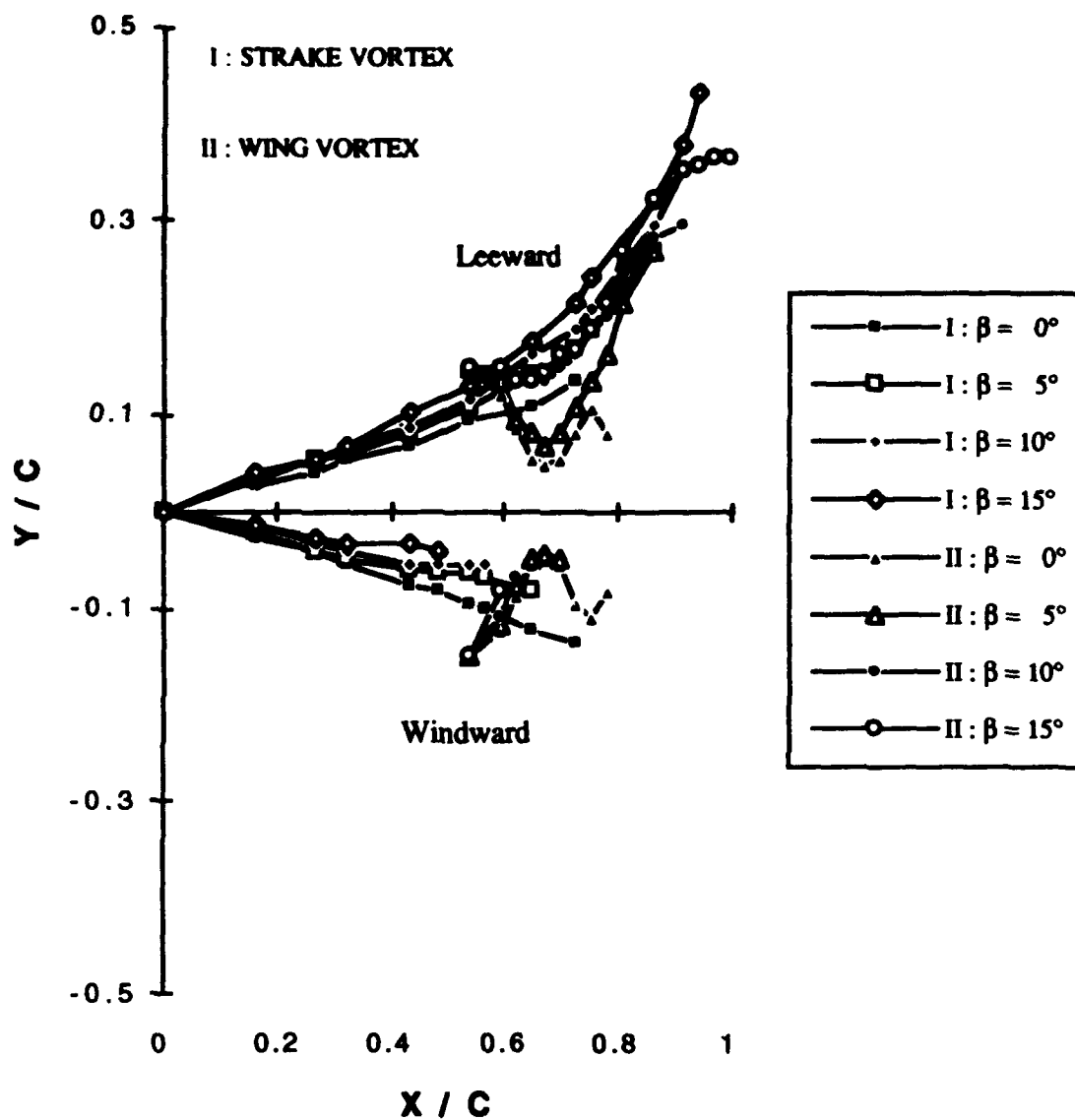


Figure 86 : Baseline model vortex core trajectories for different sideslip angles (AOA=20°)

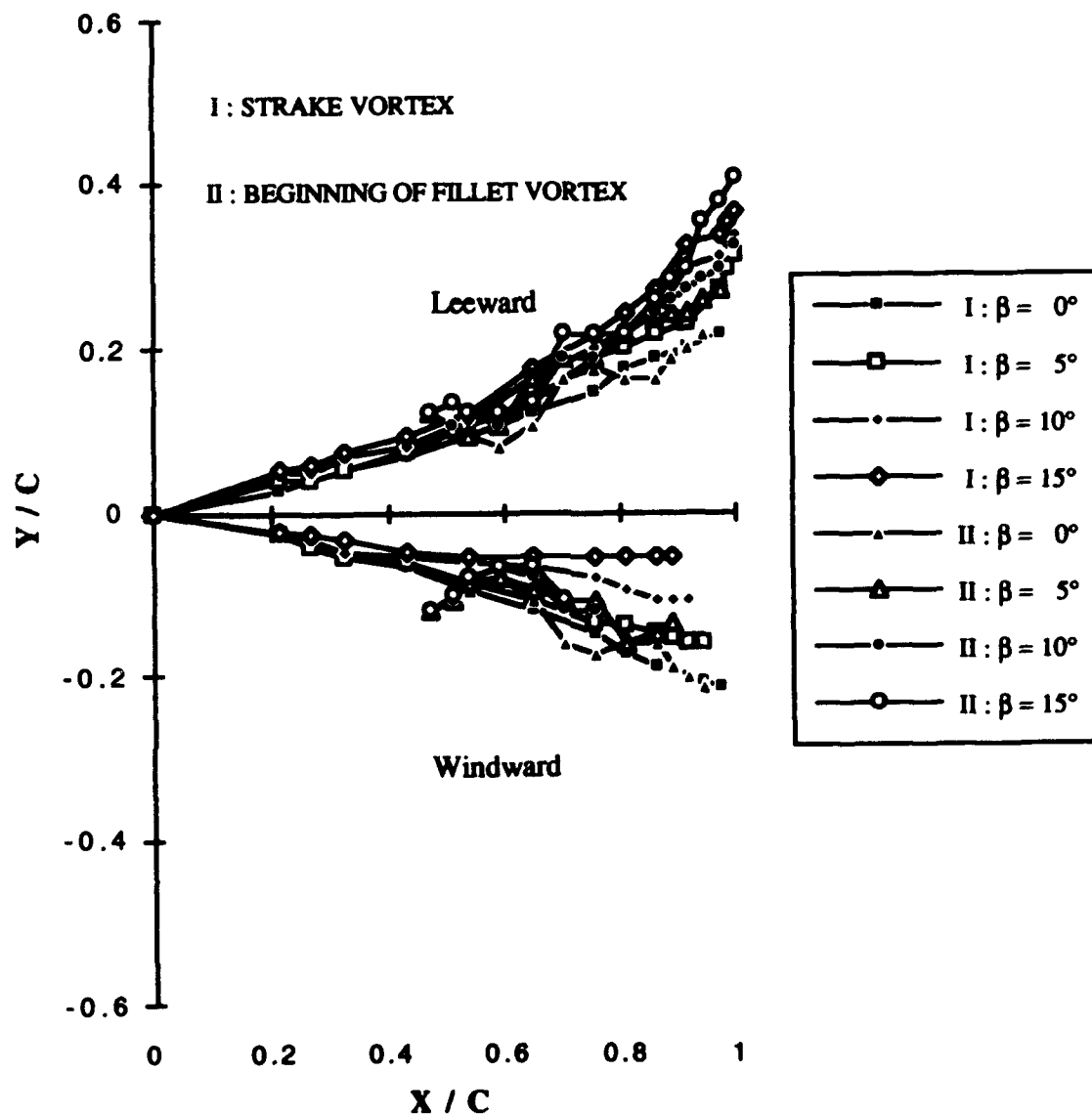


Figure 87 : Diamond-fillet model vortex core trajectories for different sideslip angles (AOA=10°) I

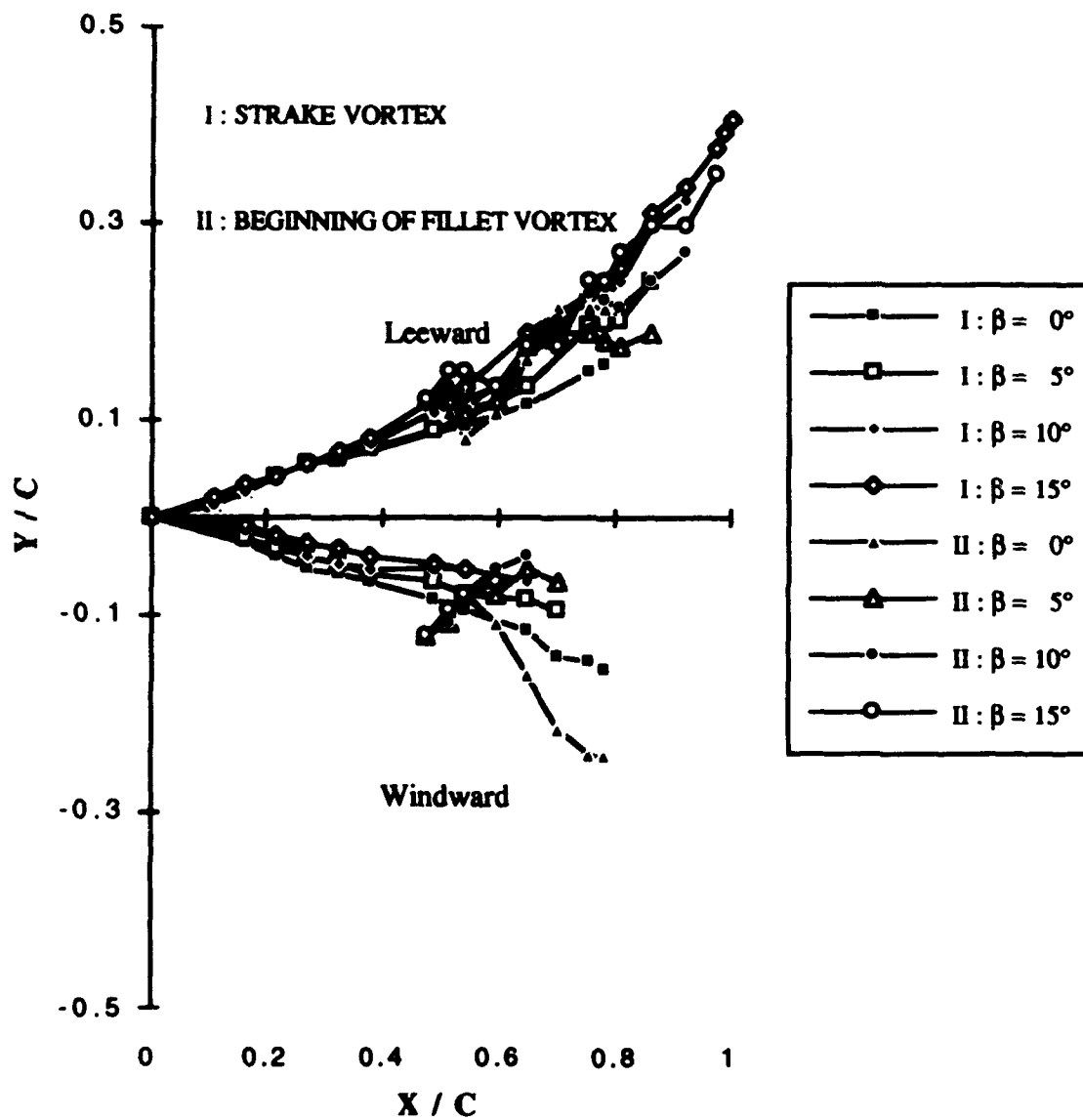


Figure 88 : Diamond-fillet model vortex core trajectories for different sideslip angles (AOA=20°) I

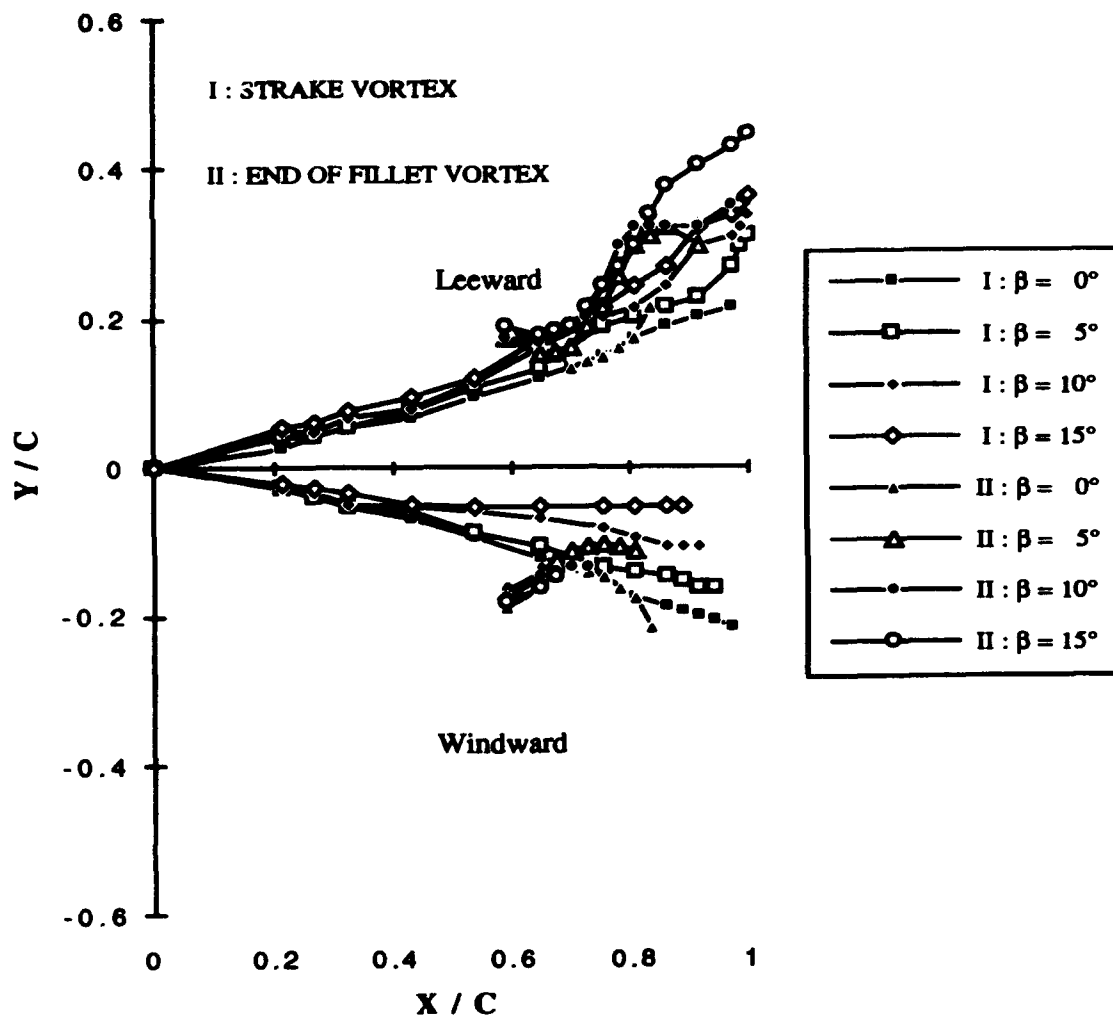


Figure 89 : Diamond-fillet model vortex core trajectories for different sideslip angles (AOA=10°) II

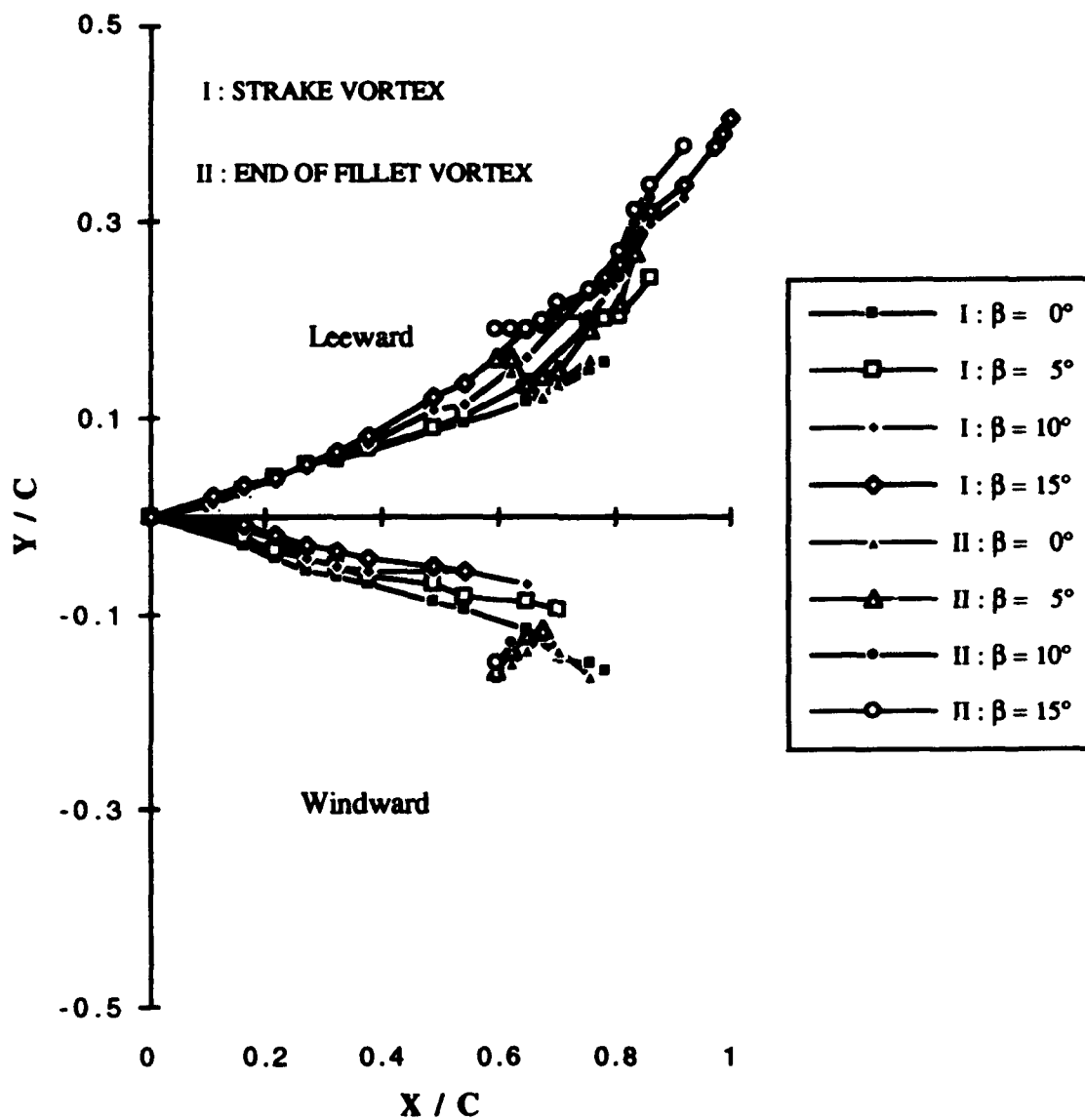


Figure 90 : Diamond-fillet model vortex core trajectories for different sideslip angles ($AOA=20^\circ$) II

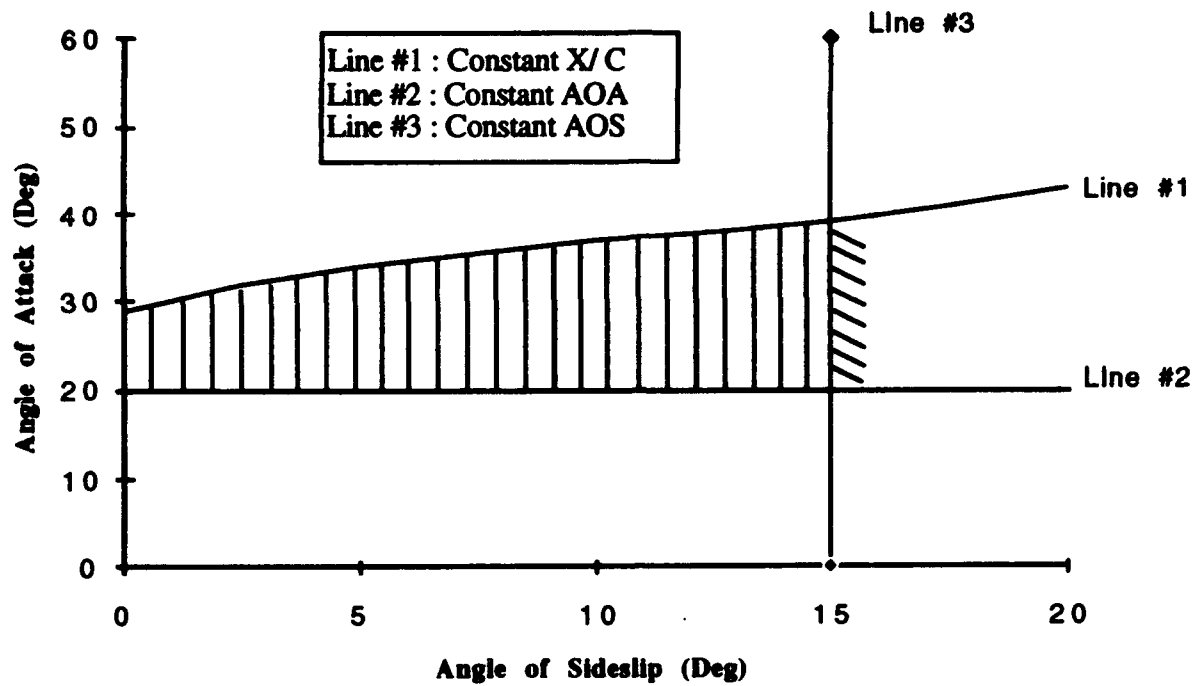


Figure 91 : Baseline model operational envelope

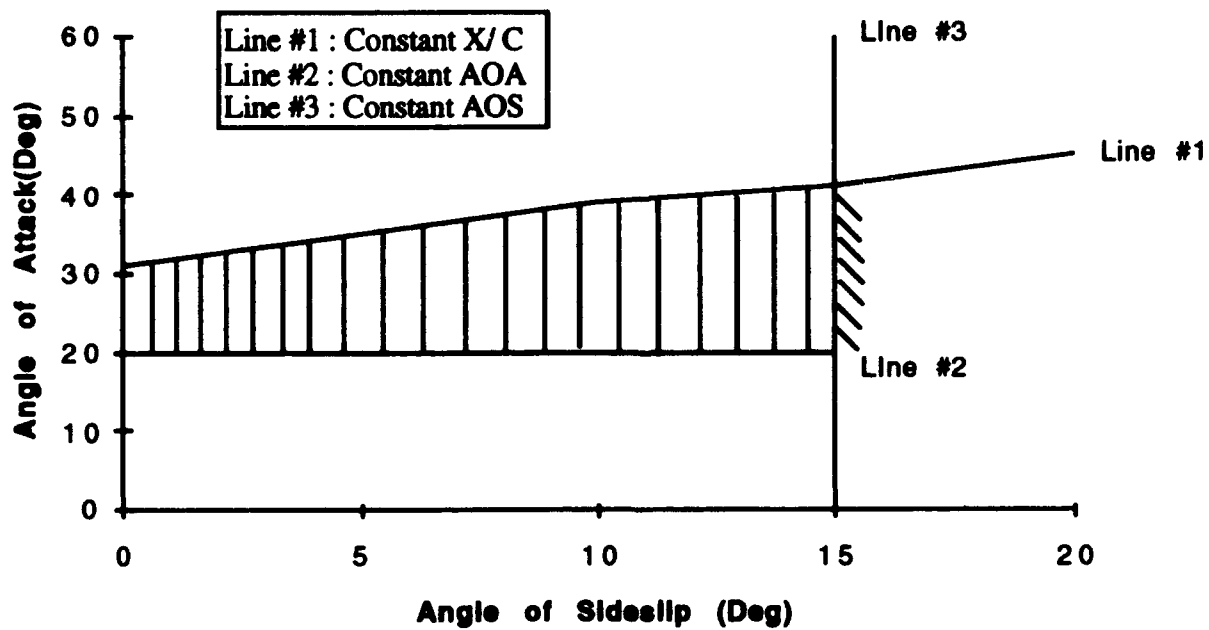


Figure 92 : Diamond-fillet model operational envelope

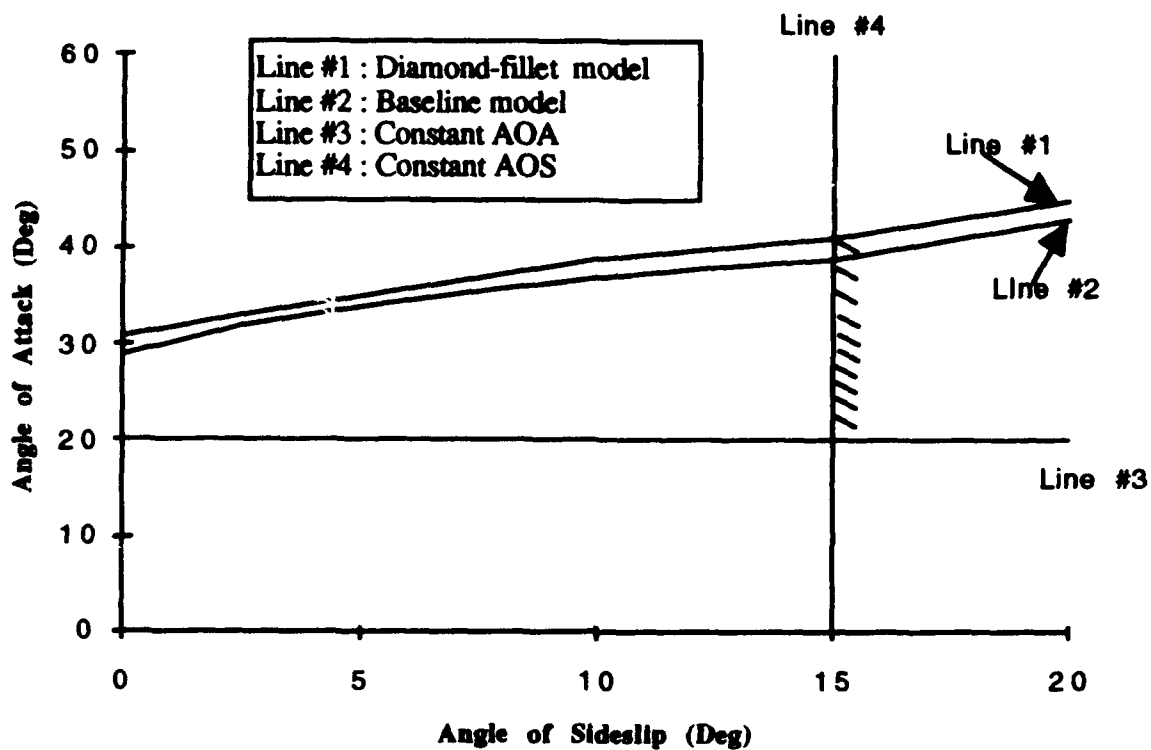


Figure 93 : Operational envelope comparison.

INITIAL DISTRIBUTION LIST

	No. Copies
1. Defense Technical Information Center Cameron Station Alexandria, VA 22304-6145	2
2. Library, Code 52 Naval Postgraduate School Monterey, CA 93943 - 5000	2
3. Chairman, Code AA/Co Naval Postgraduate School Monterey, CA 93943-5000	1
4. Professor S. K. Hebbbar, Code AA/Hb Naval Postgraduate School Monterey, CA 93943-5000	5
5. Professor M. F. Platzner, Code AA/Pl Naval Postgraduate School Monterey, CA 93943-5000	2
6. AIDC library P. O Box 90008 - 1, Taichung, Taiwan R. O. C	1
7. Library, Chinese Air Force Academy P. O Box 90277, Kangshan, Kaohsiung, Taiwan R. O. C	1
8. LT. COL. Chen, Shih - Chang P. O Box 90277 - 23, Kangshan, Kaohsiung, Taiwan R. O. C	1

9. LT. COL. Chang, Wen - Huan
P. O Box 90008 - 12 - 4, Taichung, Taiwan,
R. O. C 3
10. Mr. Marvin Walters
Naval Air Warfare Center / Aircraft Division
Street Rd., Warminster, PA 18974-5000 1
11. Michael J. Harris
Aircraft Division Code AIR-913
Naval Air System Command
Washington, D. C., 20361-9320 1
12. Mr. Steve Kern
Naval Air Warfare Center / Aircraft Division
Street Rd. Warminster, PA 18974-5000 1